STUDIES OF THE GROWTH AND STRUCTURE OF THIN CRYSTALS OF ALKALI HALIDES.

by

JAN MUHAMMAD

A Thesis submitted for the
Degree of Doctor of Philosophy
in the University of London.

Department of Physics,
Royal Holloway College.

July, 1984.

TO FARHAN ANJAM.

(ABSTRACT)

Studies of the Growth and Structure of Thin Crystals of Alkali Halides.

Existing techniques have been reviewed for the production of thin electron-transparent films of alkali halides for study by electron microscopy and a new technique has been developed.

A novel apparatus has been designed and built by means of which samples prepared from the vapour phase in high vacuum may be transported to, and examined in an electron microscope without exposure to the atmosphere. Special specimen holders and a couple of heaters have been designed so that the effects of varying temperatures on the growth and subsequent behaviour of alkali halide crystals may be studied. Other factors examined are the pressure during growth, the effects of atmospheric moisture after growth and the electron irradiation in the electron microscope. The surface of the alkali halide crystals have been examined by decoration with evaporated gold and subsequent examination in the electron microscope and their crystallographic structures investigated by electron diffraction. Thicknesses of the crystals have been measured by extinction contour technique.

The principal materials studied are CsBr, CsCl, CsF and CsI, as over growth on electron-transparent crystals of CsI and on two different types of mica: muscovite and biotite. These are the first studies of alkali halides on CsI and on biotite.

The main results of investigations are:

1. CsI may be prepared as a flat, electron-transparent single crystal suitable for electron microscopic studies in situ.

2. Small crystallites are produced by vapour deposition of alkali halides in the early stages and after exposure to the atmosphere large single crystals are formed.

3. CsBr, CsCl, CsF and CsI grow epitaxially on CsI at room temperature.

4. CsF may grow in bcc form in thin layers in certain circumstances, instead of the usual fcc form in bulk.

5. No significant difference was observed in the growth of alkali halides on muscovite and biotite.

CONTENTS

CHAPTER TWO (continued)

CHAPTER THREE

INSTRUMENTATION

CHAPTER FOUR

NUCLEATION AND GROWTH OF THIN LAYERS OF ALKALI HALIDES ON CARBON.

CHAPTER FOUR (continued)

CHAPTER FIVE.

NUCLEATION AND GROWTH OF ALKALI HALIDES ON CsI SUBSTRATES

CHAPTER SIX

NUCLEATION AND GROWTH OF ALKALI HALIDES FROM THE VAPOUR PHASE AND SOLUTION ON SUBSTRATES OF MICA

CHAPTER SIX (continued)

Chapter One

INTRODUCTION

The most commonly used process that leads to the growth of thin monocrystalline films is based on the phenomenon of epitaxy. The word epitaxy comes from the Greek 'epi'+'taxis' , the former meaning outer, upon or attached to, and the latter meaning arrangement or order. Thus, epitaxy is the growth of a crystalline layer on a single crytalline substrate where the atoms in the growing layer mimic the arrangement of the substrate.

1.1 Historical Review of Epitaxy.

Although the major interest in the study of epitaxy has existed only 30 years, the subject originated as a laboratory study about 150 years ago. Mineralogists noticed first that two crystal species sometimes grew together with some definite and unique orientation relationship, as revealed by their external forms. This led to attempts to reproduce the effect artificially, during crystal growth from solution. According to Pashley (1975) the first recorded successful attempt was reported by Frankenheim (1837), who demonstrated the now well-known case of the parallel oriented growth of sodium nitrate on calcite,and the first systematic studies were caried out by Barker (1906, 1907 and 1908) who studied, among other things, the growth of alkali halides upon each other. He

found that epitaxy occurred with some combinations, and not others. At that time growth from solution was the only readily available technique for preparing samples and the orientation of crystals was determined by optical microscopy. Nevertheless, Barker was able to deduce that epitaxy was more likely to occur if the molecular volumes of the two intergrowing alkali halides were nearly equal (i.e., low misfit).

In 1912, with the discovery of X-ray diffraction, the knowledge of internal crystal structure began to develop very rapidly. Royer (1928) carried out extensive and systematic studies of a wide variety of overgrowths, and introduced the term epitaxy. He put forward some rules of epitaxy, the most important of which was that oriented growth occurs only when it involves the parallelism of two lattice planes that have networks identical or quasi-identical form and of closely similar spacings. The experiments indicated that epitaxy occurs only if the misfit is no more than about 15% . The misfit was defined as 100(b-a)/a, where a and b are the corresponding network spacings in the substrate and overgrowth, respectively. A survey of the very extensively studies that have been made of epitaxy of crystals grown from solutin has been given by Neuhaus (1950, 1951) and Seifert (1953).

The first major advance resulted from the application of electron diffracction, which was discovered by Davisson and Germer (1927) and Thomson and Reid (1927). Davisson and Germer used electrons of only a few tens of electron volts in energy, and thus initiated the technique

of LEED (low energy electron diffraction). Thomson and Reid used electrons of a few thousand, or tens of thousands of electron volts in energy, and initiated the technique of HEED (high energy electron diffracction). At the time, HEED was by for the more practical technique because it would work satisfactorily with quite a poor vacuum (10^{-4} bar), whereas LEED required a much higher vacuum (10^{-9} bar) which could be obtained only with great difficulty. Thus from about 1930, HEED began to be applied to the study of epitaxy, and this involved reflection diffraction (RHEED) as well as transmission through thin films. The electron diffraction permits the examination of extremely thin layers of overgrowths prepared by a variety of methods, and orientation can be determined from internal crystal structure rather than external morphology. As a result, the years 1930—1950 saw a steady increase in the number of observed cases of epitaxy, and the variety of growth techniques, especially vacuum evaporation, electrodeposition, and chemical growth. A useful survey and compilation of data is given by van der Merwe (1949). A review of the electron diffraction studies has been given by Pashley (1956).

Up to the late 1920s, specimen preparation and handling techniques had not been developed for thin crystal films for transmission studies of epitaxy, and the reflection technique proved to be more appropriate. The first use of RHEED was by Nishikawa and Kikuchi (1928), who obtained patterns from calcite. The first reported applications of RHEED to the study of epitaxy were carried

out in the early 1930s, and the technique was firmly established by the middle 1930s. An important concept was introduced by Finch and Quarrell (1933 and 1934) as a result of studying the growth of zinc oxide on zinc. They conclude that the initial growth layer was strained so that its spacing matched that of the substrate (i.e., a forced zero misfit). They termed this phenomenon "basal plane pseudomorphism", now commonly known simply as "pseudomorphism". Other examples included the growth of tetragonal aluminium (normally cubic) on sputtered platinum layers (Finch and Quarrell, 1933) and electrodeposited nickel and cobalt on copper crystals, (Cochrane, 1936). Shishakov (1952) and Pashley (1956), both claimed that the claim of pseudomorphic aluminium was based upon a misinterpretation of diffraction patterns, and Newman (1956) cast serious doubts on the Cochrane (1936) evidence for pseudomorphic nickel and cobalt. The theoretical model for epitaxy put forward by Frank and van der Merwe (1949 a, b, c) was based on the formation of pseudomorphic monolayers, and their calculations appeared to define the conditions under which such monolayers would form. However, Smollett and Blackman (1951) criticized some of their conclusions on the grounds that the monolayers would not always be stable.

It was Lassen (1934) who first demonstrated that silver deposited on the cleavage face of rock salt crystal could be oriented, and Lassen and Bruck (1935) who showed that heating the substrate during deposition resulted in improved epitaxy. Bruck (1936) showed that orientation of

a number of metals deposited on rock salt is markedly dependent upon substrate temperature. He first introduced the term "epitaxial temperature". Above this temperature, good epitaxy was obtained, whereas below it there was at least some poorly or randomly oriented deposit. The concept of epitaxial temperature has had a major influence on subsequent work, and many workers have obtained a similar kind of dependence of epitaxy upon temperature, for a variety of deposits. There is considerable disagreement between the values of epitaxial temperature that are observed. It seems clear that there is no unique and sharply defined critical temperature, and that other deposition variables can have an important influence. One first demonstrated by Shirai (1939) is that preheating of the substrate has a cleaning effect, which can lead to a lowering of the epitaxial temperature.

During the first 25 years of the application of HEED and RHEED, many cases of epitaxy were established, many involving misfits considerably in excess of 15%. These have been classified and tabulated by Pashley (1956). The most important evidence was obtained by Schulz (1951a and 1952) who showed that parallel orientation occurs for a wide range of alkali halides deposited, by vacuum evaporation, onto the cleavage surface of several alkali halides. The misfit cover a more or less continuous range from -39% (LiF on KBr) to +90% (CsI on LiF). Similarly, Schulz (1951a) showed that the alkali halides are also oriented onto a mica cleavage surface, over a misfit range of zero (RbI) to -27% (KF). It had been

realized for many years that RHEED was a very sensitive technique. Schulz (1951 and (1952) demonstrated for the first time that deposits of no more than 0.1 nm or 0.2 nm thickness could give observable patterns. Quantitative studies by Newman and Pashley (1955), in which deposit thicknesses were measured by radioactive tracer techniques, showed that the limit of detection by RHEED was below 0.1 nm in favourable cases. Thus RHEED could be used to study of the first atomic monolayer. Shulz (1951a,b and 1952) was able to show that many alkali halide deposits on mica, or on other alkali halides, consist of three-dimensional crystallites from the earliest observable stage of growth. Newman and Pashley (1955) showed quite conclusively that three-dimensional crystallites form well before there is even enough deposit present to form a single monolayer covering the substrate surface (e.g., for copper deposited on silver). These and many other experiments demonstrated quite clearly that the initial stages of growth consisted of three-dimensional nuclei, rather than monolayers, in many systems.

Although the electron microscope was already available by 1945, it was not applied to transmission studies of epitaxial layers until the mid 1950s. This was mainly due to the lack of suitable specimen preparation and handling techniques. The emergence of the first high-performance electron microscopes in 1954 heralded a period of rapid development of the application of transmission electron microscopy (TEM), particularly for the direct observation of crystalline specimens. Bulk samples

of metals were thinned chemically, or electrochemically, and this revealed that considerable structural detail could be obtained. At about the same time, self-supporting epitaxial layers of metals were detached from their substrate to provide specimens that were very well suited for direct examination. Also, much thinner deposits were detached on carbon-supporting films to reveal the structure of initial deposits. By means of the TEM technique, it was possible to obtained a wealth of new information on the nucleation, growth and structure of thin films. There was the possibility of obtaining important crystallographic information, both as a result of carrying out electron diffraction analysis inside the electron microscope and because diffraction contrast on the microscope image revealed crystallographic features such as grain boundaries, twinned structures, and lattice defects such as dislocations and stacking faults. The technique became even more powerful when a thin film substrate was employed (e.g.,molybdenite or mica) so that the crystallographic analysis could be carried out on the substrate and deposit while they were still in contact. Thus the period 1955—1965 saw a major breakthrough by a rapidly growing number of workers employing the transmission electron microscope to study thin epitaxial deposits. Reviews of the electron microscope work on epitaxy have been given by Pashley (1965) and Matthews (1967).

The pioneering work of Hirsch and his collaborators (1956) established that TEM studies of thin crystalline specimens could reveal lattice imperfections

(dislocations and stacking faults) present in the films by means of diffraction contrast. Similar studies of epitaxial films of metals revealed that numerous lattice imperfactions were commonly present in such specimens (Pashley, 1959b; Matthews, 1959; Bassett et al., 1959; and Phillips, 1960). Some of the initial interest centered on obtaining information on the geometrical properties of these imperfactions, and the technique of moiré patterns from overlapping crystals was employed for this purpose by several workers such as Hashimoto and Uyeda (1957), Pashley et al. (1957) and Bassett et al. (1958). The moire fringe patterns can be regarded as magnified projection images of the individual crystal lattices, and dislocations are revealed as terminating fringes (Bassett et al., 1958). The TEM provided, in conjunction with selected area diffraction and dark field imaging, precise crystallographic evidence on individual defects, such as Burgers vectors of dislocations, displacement vectors of stacking faults, and the crystallographic indices of the planes of planar defects. Analysis of this kind immediately led to attempts to understand how lattice defects were introduced into epitaxial films during their growth. The TEM technique was also applied to the study of the structure and defects in deposited semiconductor layers on semiconductor substrates. A detailed study and analysis of these defects was made by Booker (1964). These studies were important because of the need to reduce the numbers of imperfections in order to obtain semiconductor devices with adequate properties.

Much improved and commercially available systems for producing ultrahigh vacua started to have an impact in early 1960s, providing both a means of preparing specimens under very much cleaner conditions and a "new" technique for structural studies. LEED equipment, as it is known today, depended on these new UHV techniques as well as the introduction of the technique of post acceleration of the diffracted electrons to provide a visible pattern on a fluorescent screen (Scheibner et al., 1960). LEED is a very sensitive technique that allows layers of much less than one monolayer to be analyzed, and hence it has been very valuable in providing evidence on surface cleanness, as well as on the very initial stages of growth of deposits. HEED and RHEED have also gained from the advent of UHV techniques, and they are also very sensitive; there are good reasons why LEED and RHEED should be used simultaneously (Pashley, 1970). By measuring the energy of the Auger electrons that are emitted under low-energy electron bombardment in the case of LEED, providing the facilities of chemical analysis (Harris, 1968 a, b; Palmberg et al., 1967 a, b). In the case of RHEED, this is done by measuring the wavelengths of the characteristic X-rays emitted under high-energy electron bombardment (Sewell and Cohen, 1967).

1.2 The Modes of Growth and Dominant Factors in Epitaxy

The amount of data on epitaxy that has been

accumulated during this century is now very considerable, covering orientation relationships for a wide variety of substrates, deposits and growth conditions, as well as structural information at various stages. As each new technique has provided new and important information, it has also served to demonstrate the enormous complexity of the problem. As a result, it can be seen now more clearly what is needed of a realistic theoretical model, but it can also be seen that the formulation of such a model is likely to be very difficult task. From the earliest days the workers in the field of epitaxy, have been concerned with two main problems:

(i) The mechanism of the formation and growth of the film, the mode of growth.
(ii) The factor or factors inducing epitaxial growth.

Until 1950 one mode was conceived for the growth of the film, and that had been proposed by Finch and Quarrell (1933). According to this mechanism the growth of a film occurs layer by layer and the lattice spacings of the early layers vary in order to match with the lattice of the substrate, therefore for several layers near the substrate surface there is no fixed parameter. This effect was termed pseudomophism. Frank and van der Merwe (1949 a, b, c) introduced the concept of misfit dislocations at the interface between the substrate and deposit, as part of their theoretical model for epitaxial monolayers discussed

in the previous section. This mode of growth is termed as the Frank-van der Merwe mode. The experimental results obtained from RHEED by Shulz (1951 a, 1952) and Newman and Pashley (1955) showed that epitaxial growth often occurs without the formation of monolayers. The diffraction patterns revealed that growth occurred, in many cases, in the form of isolated three-dimensional nuclei in the early stages, and that continuity was achieved when the isolated nuclei coalesce. This is called the Volmer-Weber mode. Another mode of growth is Stranski-Krastanov mode which is an intermediate case, in that layer growth is followed by island growth. The growth mechanism in these modes is shown schematicaly in Fig. 1.1.

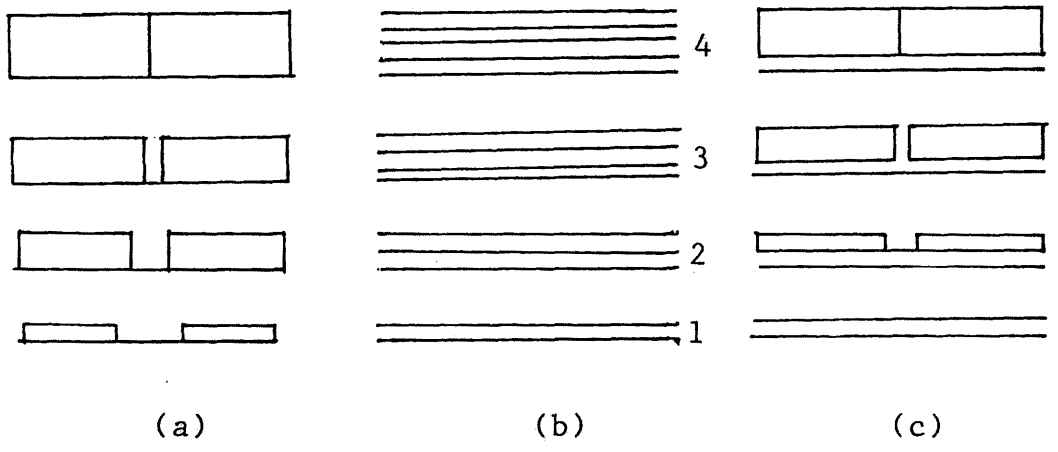

Fig. 1.1 The three growth mechanism, after Bauer (1958). (a) Volmer-Weber mode, (b) Frank-Van der Merwe layer growth mechanism, (c) Stranski-Krastanov mode

The fundamental reasons for these growth modes, and how these depends on temperature, growth rate, impurity effect, etc., is of course a large and continuing field of study. However, Bauer (1958 a) has classified the various growth modes in terms of the surface and interface energies of the deposit and substrate as:

(a) When the surface energy of the deposit material is greater than that of the substrate, three dimensional nuclei are formed, in th Volmer-Weber mode.

(b) When the surface energy of the deposit is less than that of the substrate, layer-by-layer growth occurs in Frank-Van der Merwe mode.

(c) A special case of (b) that arises when there is high strain energy in the deposit film, that leads to the nucleation of three dimensional nuclei on top of an initial monolayer and termed the Stranski-Krastanov mode.

Bauer and Poppa (1972) studied the growth of Au and Ag on different substrates such as LiF, NaCl, KCl, MgO, PbS, PbTe, Si, Cu and W, and observed the three described modes. For example, according to these authors, an Ag film on the substrates of LiF, W and Si (Ag/LiF(100), Ag/W(110) and Ag/Si(111) grows in the Volmer-Weber, Frank-Van der Merwe and Stranski-Krastanov modes respectively. Also, Honjo and his co-workers (1977) made in situ observations at very high vacuum, 10^{-11} bar- 10^{-14}

bar, and demonstrated many examples of the Volmer-Weber and Frank-Van der Merwe modes. High resolution electron microscopy has thus played a leading part in establishing the existence of these modes of growth, but the stated mechanisms or the mechanism of epitaxy is still the subject of some controversy.

As stated in previous section Royer (1928) suggested that epitaxy occurs only if the misfit is not more than 15%. Although later numerous examples showed that epitaxy with quite large misfits was possible (Schulz, 1951 a, and 1952), the geometrical approach was so attractive that many workers devised various models to interpret the epitaxial growth of different materials with large misfit by the concept of low misfit requirement. Among these models the ideas of pseudomorphism and misfit dislocation received considerable attention. In this model if the natural misfit is zero, or if the actual misfit is zero because of the occurrence of pseudomorphism, there will be no dislocations (assuming perfact alignment between substrate and deposit). However, if there is some misfit this can be accommodated by the incorporation of an appropriate array of dislocations, or dislocations with significant edge components. In a series of elegant experiments, Matthews and co-workers showed, by depositing thin metal layers on thin metal single-crystal film substrates, that the density of interface dislocation structures depends on deposit thickness. For a case of low natural misfit (say less than few percent), no misfit dislocations could be detected for low deposit thicknesses

(say a few tens of a nm), and as the deposit thickness increased misfit dislocations were generated. This was observed for both continuous monolayer-type deposits (Jesser and Matthews, 1967) and island-type deposits (Jesser and Matthews, 1968).

Honjo (1976) and Honjo et al. (1977), in a series of in situ experiments, have observed pseudomorphic layers in the deposit-substrate systems of noble metals (Au, Ag, Pb), and PbS, PbSe, PbTe... . According of these authors, in the latter systems the misfit dislocations appear in complete agreement with the Frank-Van der Merwe model. The pseudomorphism model was applied by Cabrera (1964) to explain epitaxy in the Volmer-Weber mode, but a series of in situ experiments which have been carried out for this purpose, with high resolution TEM, have not shown pseudomorphism or misfit dislocations. In their recent works Takayangi, Yagi and Honjo (1978), have studied the nucleation and growth of a number of different materials on MgO. The experiments were carried out in very clean conditions. The substrate was produced inside the microscope by an electron-flashing technique, (Honjo and Yagi, 1969), and the deposition and observation conducted at pressure less than 10^{-11} bar. Their results show a connection between the lattice spacings of the overgrowth and the substrate, and the orientation of the overgrowth. They concluded that for the systems of deposit-substrate which have lattice parameter ratio, $\rho=a_d/a_s$, (d for deposit and s for substrate), near to 1, the parallel, P, orientation occurs, that is, (001)[100]d//(001)[100]s.

For systems with ρ near $\sqrt{2}$ the (001)[110]d//(001)[100]s orientation, R, is dominant and so on. From their results it could be concluded that alkali halides have a strong tendency towards the P orientation.

The bcc lattices of iron and chromium are practically identical, with lattice parameters of 0.2886 and 0.2875 nm repectively, their orientations on the substrates of NaCl are not the same. The iron appears in three orientations, namely:

(R) (001)[100]d//(001)[110]s

(P) (001)[100]d//(001)[100]s

(S) (111)[112]d//(001)[110]s,

while the chromium deposits appear only with the R orientation. Pynko and Lyudvik (1975), in a number of experiments on the vacuum cleaved rock salt, under clean conditions, have confirmed the earlier results. These authors have reasoned that the difference in orientations is due to the difference between the heats of formation of $FeCl_2$ and $FeCl_3$, -15.3 KCal mol^{-1},on the one hand and the heats of formation of $CrCl_2$ and $CrCl_3$, -40.1 KCal mol^{-1}, on the other hand. In the first case formation of $FeCl_2$ and $FeCl_3$leads to three different orientations while in the second case mainly $CrCl_3$ is formed, which leads to single orientation. Therefore, it seems the chemical reactions

---

The sign[ ] stands for a particular direction.

have a major role to play. It should be noted that any chemical reaction that leads to epitaxy necessarily occurs at definite sites which form a network on the surface of the substrate. In many cases such a network may end up with an orientation which is consistent with the geometrical approach. There are also numerous reports which show that the irradiation of the substrate before or during the deposition by electrons, ions, or X-rays improves the epitaxy considerably (Green, 1973). This may indicate that chemical reactions are an important factor in epitaxy.

A rather different approch to explain the epitaxy has been introduced by Distler and his co-workers. They have reported extensive experimental evidence that oriented nuclei can form on top of a continuous amorphous layer deposited on a single crystal substrate. For example, Distler et al. (1968a) obtained well-oriented nuclei of lead sulphide on rock salt cleavage surfaces with intermediate carbon layers up to 15 nm in thickness. In some cases, epitaxy occurs with intermediate amorphous layers of up to 150 nm in thickness. The observed cases include lead sulfide on mica (Distler and Kobzareva, 1966), gold on rock salt (Gerasimov and Distler, (1968), and cadmium sulfide on rock salt (Distler et al., 1968b). These results are interpreted in terms of the effect of long-range forces arising from some kind of active centers, such as lattices of point defects which produce electrical microfields, which are supposed to be responsible for epitaxy. In another work it has been shown that when a triglycine sulphate crystal is decorated with

AgCl, a network-like deposit is formed. Almost the same pattern of deposits are obtained when the substrate is covered with an amorphous film of selenium (Distler, 1975). But the subject rapidly aroused considerable controversy both from the validity of the experimental observations and from the interpretation of the effect. Chopra (1969) failed to observe the effect, but other workers (e.g., Barna et al., 1969) have supported, at least in part, the findings reported by Distler and his co-workers. It is also evident that this model cannot explain the epitaxy of the Frank-Van der Merwe mode. Furthermore, chemical reaction at atomic level cannot be ignored.

From the above considerations of the models of epitaxy and the experimental evidence, it is concluded that at present the mechanism of epitaxy is not fully understood, but it seems likely that several factors such as chemical reaction, lattice fitting, surface energy and defects are involved in epitaxial growth. It can also be said that for each deposit-substrate system one or two of these factors may be more important and may have varying effect at different stages of growth. The strengths of these factors can be varied by different treatments: substrate heating, irradiation, exposure to particular vapour (postnucleation growth and recrystallization), etc.

At the present, there is no single model that can give a satisfactory explanation of epitaxy for all systems. Moreover one cannot be sure that any single model will be the ultimate answer for any one system. It is suggested that instead of the in-depth studies of a very restricted

number of systems, a more balanced and meaningful picture seems more likely to emerge from studies of a broader range of substrate-deposit combinations.

1.3 The Influence of Surface Topography on Epitaxy.

The concept of lattice misfit between the substrate and the deposit implies knowledge of the actual crystal planes in contact. It is normally assumed that these are the planes parallel to the macroscopic surface of the substrate. Although this is probably true when cleavage surfaces can be used as substrates, the extent to which cleavage surfaces can be used is very limited and other methods of surface preparation must be employed. The disadvantages of cleavage surfaces for certain experiments will be discussed in chapter 2.

The use of metallic substrates has always been very desirable, and the specimen preparation techniques especially difficult. If the flat surfaces are prepared by grinding and polishing single crystals of metal, the worked surface layer must be removed. Chemical or electrolytic methods of removal commonly leave a matt surface that is rough on an atomic scale, and these are not very convenient as substrates. Further, electropolished surfaces were generally found to be geometrically complex, leading to complex arrangements of overgrowth orientations. Because of the difficulties of preparing flat surfaces on macroscopic crystals, single-crystal films prepared by epitaxy have been used as a substrates for further epitaxial growth (e.g., Newman and Pashley, 1955; Pashley, 1959a).

Many workers have used electron-transparent monocrystalline substrates in the studies of thin films (Pashley et al., 1964; and Pashley, 1970). This kind of studies has revealed many interesting and important features of the early stages of the growth. For example the liquid-like coalescence of metal clusters, change of orientation of the nuclei, migration of grain boundaries out of the composite islands, have been revealed by in situ observations. Thin crystals of mica, MoS and MgO have been used frequently in these kind of experiments. Although halides have been used extensively as bulk substrates, electron-trasparent crystals of alkali halides have rarely been used as substrates. In situ studies of overgrowth on an electron-transparent monocrystalline substrate have advantages, but there are , however, a number of practical problems, such as the limitation of the space inside the microscope, contamination, reaction of the deposit materials with the internal parts of the microscope, and restricted facilities for treatment of the deposit during or after the deposition. The major problem with monocrystalline electron transparent substrates is their preparation. Usually it is not easy to prepare good quality substrates, and the preparation methods are either tedious or the resulting substrates are of poor quality. The importance of electron-transparent substrates, existing techniques for their preparation and their advantages and disadvantages will be discussed in detail in chapter 2.

1.4 Introduction to the Present Work.

One striking fact that emerges from a close study of the literature is the very high proportion of publications devoted to the studies of the growth of metals (predominantly fcc metals) on alkali halide cleavage surfaces (predominantly sodium chloride). This seems to have come about because of the considerable experimental convenience of these systems. To understand the factors which dominate epitaxial growth, it seems necessary to use more substrate-deposit systems.

Electron-transparent substrates are very useful in the studies of nucleation and growth, because they make in situ studies possible and they avoid many of the problems of using the bulk substrate, but in situ studies have their own problems. A film can be deposited in a conventional deposition unit and then transferred to the electron microscope for observation, but if the deposited materials are hygroscopic and react with the atmosphere, studies of early stages of nucleation are difficult.

Having in mind these points, the present work has been carried out with four main objectives:

1. To use materials as substrates which have not been used before.
2. To produce monocrystalline electron transparent substrates.
3. To design and construct a device for transporting a specimen from a vacuum evaporating system to the

electron microscope without exposure to the atmosphere.

4. To study films of materials that react with the atmosphere and have not been used extensively before, by means of the transporting device and electron transparent substrates.

The main topics of the work are as follows:

Chapter 2 - The importance of the electron transparent substrate has been discussed and the existing techniques of producing alkali halide electron transparent foils have been reviewed. A recent technique is modified: the substrate crystals are formed inside the holes of a perforated carbon support film, so that each crystal has two free faces for deposition and study. The mechanism of formation of crystals from solution has been reviewed and the important factors involved in the formation of the crystals inside the holes has been suggested.

The study of the effect of electron irradiation and defect-formation has been discussed. The thickness of these crystals, inside the holes, has been measured by a new technique. These crystals have been decorated by gold to study the surfaces, and the material with most flat surface has been chosen for epitaxial growth studies of other materials on it.

Chapter 3 - A description, with all the technical details, of a chamber which has been designed and constructed to transport the specimen from a vacuum deposition unit into the electron microscope has been given. Another intermediate chamber has been designed and

constructed to fix the transport chamber on the deposition system. The detail of the operation of the transport chamber and the pressure inside the chamber, when it is isolated from vacuum system, as a function of time, has been given. Two special heaters which have been constructed and used, are described.

The camera constant and its variation with objective lens current have been measured. A curve is drawn between the camera constant and objective lens current and used in the determination of d-spacings of lattice planes from diffraction patterns.

Chapter 4 - Old and new theories of nucleation and growth have been discussed. The sequence of the growth of thin continuous films has been summarised. The technique of preparation of thin continuous uniform carbon films for use as substrates, has been described. The nucleation of five different alkali halides, on carbon substrate, from the vapour phase has been studied by transmission electron microscopy, and the sizes of smallest stable nuclei has been investigated. The structure of thin evaporated films and their recrystallisation after atmospheric exposure have been discussed. The effects of water vapour on thin deposits have been studied.

Chapter 5 - The lattice structure of the substrate CsI has been discussed and the transmission electron microscope studies of the growth of caesium halides on substrates of CsI, from vapour phase have been made. The orientation of the overgrowth has been determined by electron diffraction. The effect of the atmosphere on thin

deposits after evaporation has been discussed and it has been shown that CsI displays poor epitaxy from the vapour and good epitaxy from solution. The growth of an fcc lattice structure (CsF) on bcc lattice structure substrates has been studied and it has been concluded that the lattice structure of the overgrown material has been changed. The models of orientations and a possible model of morphological change has been given.

Chapter 6 - In this chapter the previous work on studies of the epitaxial growth of alkali halides on the substrates of mica by electron diffraction and electron microscopy has been reviewed. The structures of four different kind of micas have been studied by electron diffraction. Two different kinds of micas have been chosen as substrates and their surfaces have been studied by gold decoration. The nucleation and growth of halides of caesium, from vapour and solution, have been studied by transmission electron microscopy. The orientations of alkali halides with respect to the atomic arrangement of the mica surface have been discussed. The effect of heating before deposition has been studied and the recrystallisation process after atmospheric exposure have been discussed.

References

BARKER,T.V. (1906). J. Chem. Soc. Trans. 89, 1120.

BARKER,T.V. (1907). Mineral. Mag. 14, 235.

BARKER,T.V. (1908). Z. Kristallogr. 45, 1.

BARNA,A., BARNA,P.B., and POCZA,J.F. (1969). Thin Solid Films 4, R32.

BASSETT,G.A., MENTER,J.W., and PASHLEY,D.W. (1958). Proc. Roy. Soc. A 246, 345.

BASSETT,G.A., MENTER,J.W., and PASHLEY,D.W. (1959). In "Structure and Properties of Thin Films" (Neugebauer, Newkirk, and Vermilyea, eds.), p. 11 Wiley, New York.

BAUER,E. (1958a). Z. Kristallogr. 110, 372.

BAUER,E., and POPPA,H. (1972). Thin Solid Films 12, 167.

BOOKER,G.R. (1964). Discuss. Faraday Soc. NO. 38, 298.

BRUCK,L.(1936). Ann. Phys. Leipzig 26, 233.

CABRERA,N. (1964). Surface Sci. 2, 320.

CHOPRA,K.L. (1969). J. Appl. Phys. 40, 906.

COCHRANE,W. (1936). Proc.Phys. Soc. 48, 723.

DAVISSON,C., and GERMER,L.H. (1927). Phys. Rev. 30, 707.

DISTLER,G.I., and KOBZAREVA,S.A. (1966). Proc. Int. Congr. Electron Microsc., 6th, Kyoto, 1966 p. 493. Maruzen, Tokyo.

DISTLER,G.I., KOBZAREVA,S.A., and GERASIMOV,Y.M. (1968a) J. Crystal Growth 2, 45.

DISTLER,G.I., GERASIMOV,Y.M., KOBZAREVA,S.A.,MOSKIN,V.V. and SHENYAVSKAYA,L.A. (1968b). Proc. Eur. Reg. Conf. Electron Microsc., 4th, Rome, 1968 p.517. Tipographia Poliglotta Vaticana, Rome.

DISTLER,G.I. (1975). Third Int. Conf. on Thin Films, Budapest, Hungary, Paper 2.02.

FINCH,G.I., and QUARRELL,A.G. (1933). Proc. Roy. Soc. A 141, 398.

FINCH,G.I., and QUARRELL,A.G. (1934). Proc. Roy. Soc. A 46, 148.

FRANK,F.C., and van der MERWE,J.H. (1949a). Proc. Roy. Soc. A 198, 205.

FRANK,F.C., and van der MERWE,J.H. (1949b). Proc. Roy. Soc. A 198, 216.

FRANK,F.C., and van der MERWE,J.H. (1949c). Proc. Roy. Soc., A 200, 125.

FRANKENHEIM,M.L. (1836). Ann. Phys. 37, 516.

GERASSIMMOV,Y.M., and DISTLER,G.I. (1968). Naturwiss.55, 132.

GREEN,A.K. (1973). NASA, CR-2234.

HARRIS,L.A. (1968a). J. Appl. Phys. 39, 1419.

HARRIS,L.A. (1968b). J. Appl. Phys. 39, 1428.

HASHIMOTO,H., and UYEDA,R. (1957). Acta. Cryst. 10, 143.

HIRSCH,P.B., HORNE,P.B., and WHELAN,M.J. (1956). Phil1. Mag. 1, 677.

HONJO,G., and YAGI,K. (1969). J. Vac. Sci. Technol. 6, 567.

HONJO,G. (1976). Thin Solid Films 32, 143.

HONJO,G., TAKAYANGI,K., KOBAYASHI,K., and YAGI,K. (1977) J. of Crystal Growth 42, 98.

JESSER,W.A., and MATTHEWS,J.W. (1967). Phil. Mag. 15, 1097.

JESSER,W.A., and MATTHEWS,J.W. (1968). Phil. Mag. 17, 597.

LASSEN,H. (1934). Phys. Z. 35, 172.

LASSEN,H., and BRUCK,L.(1935). Ann. Phys. 22, 65.

MATTHEWS,J.W. (1959). Phil. Mag. 4, 1017.

MATTHEWS,J.W. (1967). Phys. Thin Films 4, 137.

NEUHAS,A. (1950-51). Forstschr. Mineral. 29-30, 136.

NEWMAN,R.C. (1956). Proc. Phys. Soc. B69, 432.

NEWMAN,R.C., and PASHLEY,D.W. (1955). Phil. Mag. 46, 917.

NISHIKAWA,S., and KIKUCHI,S. (1928). Nature (London) 121, 1019.

PALMBERG,P.W., RHODIN,T.N., and TODD,C.J. (1967a). Appl. Phys. Lett. 10, 122.

PALMBERG,P.W., RHODIN,T.N., and TODD,C.J. (1967b). Appl. Phys. Lett. 11, 33.

PASHLEY D.W. (1956). Advan. Phys. 5, 173.

PASHLEY,D.W., MENTER,J.W., and BASSETT,G.A. (1957). Nature (London), 179, 752.

PASHLEY,D.W. (1959a). Phil. Mag. 4, 316.

PASHLEY,D.W. (1959b). Phil. Mag. 4, 324.

PASHLEY,D.W. (1965). Advan. Phys. 14, 327.

PASHLEY,D.W. (1970). Recent Progr. Surface Sci. 3, 23.

PASHLEY,D.W., STOWELL,M.J., JACOBS,M.H., and LAW,T.J. (1964). Phil. Mag. 10, 127.

PASHLEY,D.W. (1975). In "Epitaxial Growth" (Matthews ed.) p.1. Academic Press, New York.

PHILLIPS,V.A. (1960). Phil. Mag. 5, 571.

PYNKO,V.G., and LYUDVIK,E.Z.R. (1975). Third Int. Conf. on Thin Films, Paper 1.25, Budapest, Hungary.

ROYER,L. (1928). Bull. Soc. Fr. Mineral. Crist. 51, 7.

SCHEIBNER,E.J., GERMER,L.H., and HARTMAN,C.D. (1960). Rev. Sci. Instrum. 31, 112.

SCHULZ,L.G. (1951a). Acta Cryst. 4, 483.

SCHULZ,L.G. (1951b). Acta Cryst. 4, 487.

SCHULZ,L.G. (1952). Acta Cryst. 5, 130.

SEIFERT,H. (1953). In "Structure and Properties of Solid Surfaces" (Gomer and Smith eds.), p. 218. Chicago Univ. Press, Chicago, Illinois.

SEWELL,P.B., and COHEN,M. (1967). Appl. Phys. Lett. 11, 298.

SHIRAI,S. (1939). Proc. Phys.-Math. Soc. Japan 21, 800.

SHISHAKOV,N.A. (1952). Zh. Eksper. Teor. Fiz. 22, 241.

SMOLLETT,M., and BLACKMAN,M. (1951). Proc. Phys. Soc. A 64, 683.

TAKAYANAGI,K., YAGI,K., and HONJO,G. (1978). Thin Solid Films 48, 137.

THOMSON,G.P., and REID,A. (1927). Nature (London), 119, 80.

Van der MERWE,J.H. (1949). Discuss. Faraday Soc. No. 5, 201.

Chapter Two

PREPARATION OF ELECTRON TRANSPARENT SUBSTRATES OF ALKALI HALIDES.

2.1 Introduction.

The most important basic requisite for transmission electron microscopical studies of the nucleation and growth of a material from the vapour phase, is a suitable substrate. The substrate materials usually used for nucleation studies are non-metallic. Sometimes the substrate materials are semiconducting, but usually they will be insulating materials, owing to the need for a low free energy of the surface if three-dimensional nucleation is to occur (Bauer, 1958).

For epitaxial films the nature and the structure of the substrate is, of course, an essential part of the whole subject and numerous individual combinations of substrate and overgrowth are possible. Most important is the preparation of the substrate surface since it is here that the film-substrate interaction occurs. Ideally the surface should be extremely smooth, flat and free from contamination. The method of prepration depends on the particular substrate material. The importance of the detailed structure of the substrate surface has been shown in the studies of Sella and Trillat (1964), Ino et al. (1964) and Matthews and Grunbaum (1965).

2.2 Preparation of the Substrate surface.

The following substrate surfaces are usually used for nucleation and growth studies:

1. Cleavage surface of a single crystal:- This is the nearest approach to an ideal smooth surface. However, such a surface has a stepped structure, the region between the steps having areas flat on an atomic scale. The (100) cleavage surface of an alkali halide, especially rock salt, is by far the most commonly used substrate. The (100) cleavage surface of MgO is also used. Orientations other than (100) can be obtained by choosing suitable single crystal material, for example the cleavage faces of CaF and ZnS are (111) and (110) respectively. A wide range of orientations can be obtained by cutting a single crystal parallel to the desired crystallographic planes.

Some substrate crystals can be cleaved in the vacuum chamber so that the newly created surface is immediately exposed to the previously established vapour stream. This method was introduced by Walton et al. (1963) and extensively used for the deposition of metal films on alkali halides. Green et al. (1969) and (1970) used cleaved alkali halide substrates for studying the growth mechanism in epitaxial films.

2. Surface of an epitaxial grown film:- An epitaxial film may be used as a substrate for thin film growth. It is essential to examine the surface structure of the film, since it is usually rough on an atomic scale. This has been demonstrated by Pashley (1959) for silver films grown

on mica by vacuum evaporation. Thin epitaxial layers of alkali halides are evaporated at room temperature on to air-cleavage mica and subsequently serve as substrates for the metal deposition. The epitaxial intermediate layers then permit easy detachment of the epitaxial metal films by floating them off in water. Au, Ni, Cu, and Ag continuous epitaxial films of good quality and in (111) orientation have been prepared successfully in this way.

3. Mechanically polished single crystal surface:- This involves the preparation of single crystal surface with any desired crystallographic orientation by lapping and mechanical polishing, usually followed by chemical etching. A surface prepared by this technique usually has well-developed facets. It should be noted that film growth occurs on such facets, and this will complicate the nucleation and growth.

Brockway and Marcus (1963) have demonstrated a technique that reduces the damage and steps on a cleavage surface. It involves polishing the crystal surface with moist polishing cloth or paper, followed by a quick rinse in water and methonal. Methods of preparing clean surfaces have been reviewed by Roberts (1963) and Moll (1963).

2.3 The Importance of The Electron Transparent Substrate.

The substrates discussed in the previous section have been used to condense metal films, and after deposition the overgrowth is usually coverd by evaporated low-density suport films of carbon or SiO. The substrate

is then dissolved in a suitable solvent and only the overgrowth is examined in the transmission electron microscope. These amorphous support films have excellent stability under intense electron irradiation but do actually exhibit appreciable phase contrast eigenstructure at the highest magnifications and sometimes obscure the original fine structure of the deposit (Jaeger et al., 1969; Bachmann and Hilbrand, 1966). Single-crystal support films offer the advantage of lower phase contrast background structures although they are more difficult to prepare.

The possibility of separating the substrate and overgrowth is basically determined by the different chemical activities of substrate and overgrowth materials. As very small amounts of deposit material are usually involved, especially when studying the very early stages of film growth, and chemical reaction rates are quite different with very small single-crystalline particals, this can lead to problems. Such small deposit particles can also be lost during the dissolution of the substrate material by mechanical stripping action during the detachment process. It is not easy to grow alkali halide thin films from vapour phase on a bulk substrate and strip it off.

Some of the major disadvantages of investigating the ovegrowth only can be eliminated by not detaching the deposit film from its substrate. To examine the substrate and overgrowth simultaneously imposes new substrate material requirements of electron transparency and good

stability under the imaging electron beam. It also has the advantage that itshould be possible to assess, most directly, epitaxial relationships between substrate and overgrowth. The requirement for transmission electron microscopy inspection of substrate and overgrowth defines the class of substrate materials suitable for this approach. It is necessary, of course, to be able to thin the material sufficiently either before or after depositing the overgrowth film. Since the application of transmission electron microscopy to the study of matter, numbers of thin foil producing techniques have been developed.

In general the substrate should have these properties that are necessary for the studies of the nucleation and growth of materials:

1. The substrate should be reasonably transparent to electrons for the study of early stages of nucleation.

2. The substrate should be large enough in order to have areas not being influenced by the boundaries of the substrate.

3. The surface of the substrate should be similar to the surface of the conventional bulk crystalline substrates, as for as surface features are concerned.

4. The most important property which is vital for the transparent substrates: the experimental results should be similar to the results obtained on the bulk substrates of the same materials with the similar crystallographic feature.

5. It is also important that technique to produce such

substrate should not too complicated and time consuming.

6. The out come of the technique should be reasonably reproducible.

2.4 Recent Techniques Producing Transparent Substrates.

The following techniques have been used to produce thin foils of alkali halides for electron microscopical studies:

1. Rapid vacuum-drying technique: a very dilute(0.5% to 2% w/v) solution of alkali halide is put on the surface of a very thin amorphous support film of carbon or Cr_2O_3 and then it is dried rapidly in vacuum. Crystals with various sizes and thicknesses are formed. Some of them are electron-transparent and used as substrate. This technique was used first by Hibi and Yada (1960) to prepare KCl transparent single crystals from solution.

The crystals formed with this technique are shown in Fig. 2.1 and 2.2. A tiny droplet of 5% w/v solution of KCl was put on a 5 nm thick continuous carbon support film on a specimen grid. The grid was transferred to the electron microscope specimen chamber which was then evacuated. The resulting large crystals were thick and opaque to the electron but smaller crystals were sufficiently transparent. These crystals have one free face and can be used for further growth studies but as they are formed on support film, its surface condition can effect the crystals and their surfaces.

Fig. 2.1 (a).

Fig. 2.1 (b).

Fig. 2.1 (a) and (b):- KCl crystals on continuous carbon support films.

3000nm

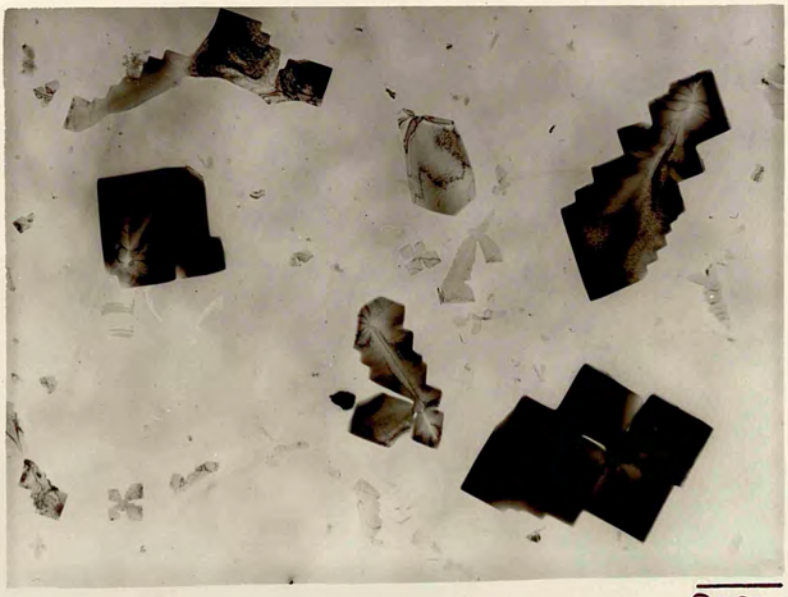

3000nm

Fig. 2.2 (a).

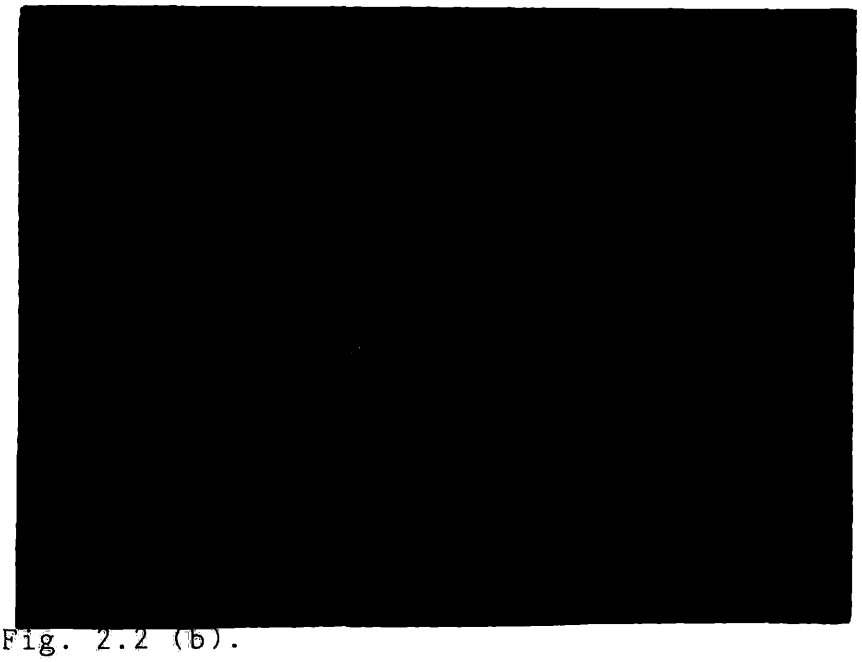

Fig. 2.2 (b).

Fig. 2.2 KCl crystals on continuous carbon support film (a) micrograph, (b) diffraction pattern of a [001] single crystal.

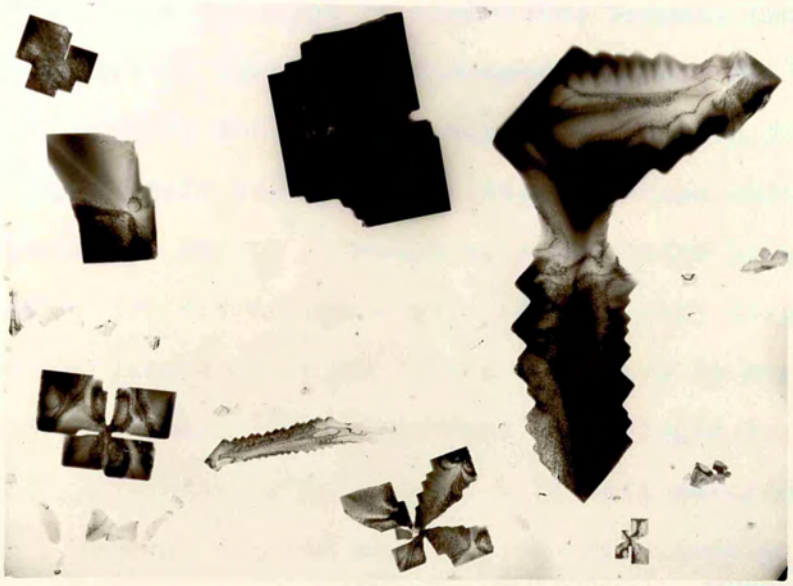
3000 nm

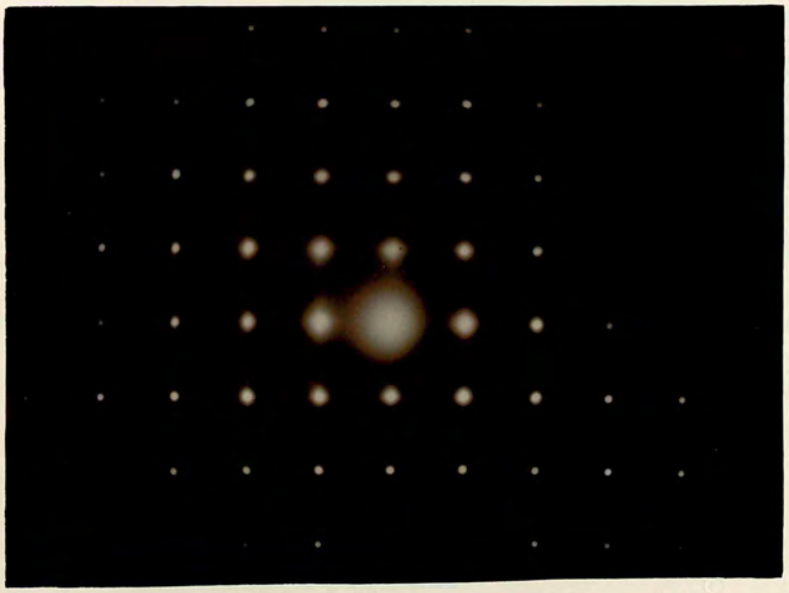

2. The sandwich technique: In this technique a layer of alkali halide solution is sandwiched between two planes. When the water of the solution evaporates thin foil of the material suitable for electron microscopy can be found. Mollenstedt, Graff and Speidel (1962) produced thin monocrystals of KCl by sandwiching a saturated solution of KCl between two microscope slides covered with carbon films.The crystallization had been initiated by cooling the sandwich. Demny (1965) produced thin single crystals of NaCl by sandwiching a layer of 0.1% salt solution between a carbon film and an electron microscope grid with carbon support film on it.

The foils obtained by this method are usually coverd with carbon from both sides, the energy states could be considerably different from the energy states of the foils with free faces. This can be effect the behaviour of the crystals in the electron microscopic investigation, and therefore, they can not be used as crystalline substrates.

3. The dissolving technique: In this method water or a mixture of water and alcohol is used to thin the material. Heydenreich (1969) has given a list of the workers who have used this technique to produce thin foils of alkali halides. The substances that have been used by these workers are mainly KCl and NaCl. Izumi (1969) used 0.2 mm thin cleaved plates of KCl and NaCl from bulk single crystals, then the plates are thinned in an aqueous alcohal mixture and dried quickly between the two sheets of filter paper.

These crystals have free faces but the surfaces could be quite uneven due to chemical etching and the drying with filter paper. Also the surfaces of the crystals are bound to be contaminated in the foregoing treatment: they do not seem to be suitable substrates.

4. The electron beam flashing thinning technique: This technique involves bulk single crystals which are cleaved into plates of tenths of a millimeter thick, then further thinned by a mixture of water and alcohol down to 2 to 10 microns. A slice so prepared is transfered into the electron microscope and observed at low magnification, the intensity of the electron beam is increased abruptly and parts of the surface layers of the slice are detached, leaving thin transparent areas. Yagi and Honjo (1964) have produced electron transparent crystals by this method and used them to grow epitaxial films of gold from the vapour phase.

The appropriate intensity of electron beam varies from slice to slice depending on the size and thickness of the slice, so it is very difficult to find an appropriate intensity for every slice. This technique is tedious and time-consuming and it is not easy to produce a large number of adequate substrates for a long series of experiments. The detached chips, from the slice, are so small that they resemble the evaporation of substance, leaving the surface of the remaining transparent slice uneven. Thick chips might be shattered into large numbers of pieces, spread around and contaminate the substrate as well as the electron microscope. However, when a limited

number of in situ nucleation experiments and observations is required, these substrates are ideal, especially because their surfaces are fresh like vacuum cleaved bulk substrates.

5. The oblique cleaving technique: Miller and Hoffman (1968) developed this technique, in which a rectangular prism of approximately 2x4x15 mm bounded by $\{100\}$ planes of a salt crystal is cleaved in a direction which makes an angle of roughly 30° with the long axis of the prism. Salt does not cleave in such direction easily, number of flakes are produced from the cleaved surface. These flakes are transferred on to a microscope grid, with carbon support film on it, by a very fine tungsten wires brush. Some of these flakes are transparent or have transparent parts to be used as substrate.

Since the flakes are not treated by water or aqueous alcohol they could be considerably free from contamination. They are directly cut from the bulk crystal and show the same behaviour as the bulk substrate, provided the likely mechanical demage that can develop during the cleaving process can be ignored. On the average only few flakes can be found on each grid which are adequate as a substrate and they can be lost easily in the process of transferring them from the microscope to the vacuum system and back. The reproducibility is not very good.

6. The evaporating thinning technique : By sublimation from bulk material in vacuum, it is possible to thin a crystal. In this technique, a disc of the crystal

is prepared and its edges are firmly covered by a metal frame, to prevent easy sublimation from the edges. The crystal is then heated in vacuo and the evaporation process is observed by an optical microscope. As soon as a small hole appears in the crystal the process is stopped. By stopping the process at the right time, an electron--transparent wedge-shaped foil can be obtained. Although this technique can give very clean and possibly smooth electron transparent foils, the foils are of doubtful value as ideal substrates. Since the process of evaporation must be stopped quickly at the right time, gradual cooling of the foil is not easy. This quenching can produce defects in the foil which might affect the nucleation process.

7. Growth of crystals from solution on perforated carbon support film: This technique was developed by Tavassoli (1978) from the method described by Kay (1967) and Meek (1970) for producing perforated carbon support films. In this method 4 cc distilled water is added to 100 cc solution of 1% formvar in equal parts of ethylene dichloride and dioxane. A microscope slide is dipped in this solution and then allow to dry thoroughly, first in a jar containing some ethylene dichloride and then in a dust-free place. The formvar film is stripped off and floated on distilled water. This perforated formvar film is transferred on 10 to 20 electron microscope grids by the method given by Meek (1970). After coating with a 15 to 20 nm carbon film, the formvar is dissolved in the vapour of

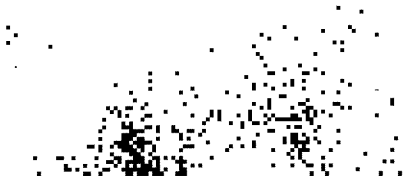

ethylene dichloride. Some grids have numerous holes of 10 μ to 20 μ diameter. A drop of 20% salt solution in distilled water is put on the grid and drained gently from the beneath of the grid by a filter paper. A large number of crystals are formed inside the holes of carbon film. Single crystals of NaCl, KCl and KBr are produced which are wholly or partially electron-transparent. The crystals prepared this way have two free faces which are adequate substrates for studies of nucleation and growth of metals or other alkali halides.

The reproducibility of this method is good but it takes a much longer time to prepare the perforated carbon film. The dried formvar film adheres to the glass slide so firmly that it is often not easy to strip off and float on the water surface. The average hole diameter does not appear to be reproducibly related to the quantity of water added to the formvar solution.

2.5 The Development in Producing Transparent Substrates.

This new method based on the use of an emulsion made with formvar solution and glycerol. After casting on glass, the film is steamed. The proportion of the glycerol controle the size of the holes which range from 0.25 μ to 25 μ diameter. The relationship between hole size and glycerol content is indicated in table 2.1. This method according to Kay (1967) has been suggested by Harris (1962).

Table 2.1

Relationship of hole size to glycerol content for perforated film.

formvar solution (parts)	glycerol (parts)	max. hole diam. (μ)
8	1	25
16	1	14
32	1	7
120	1	4

The detail of the procedure is as follows: A 1% w/v solution of formvar in ethylene dichloride is prepared, a quantity of glycerol (determined from table 2.1) is added and mixture is shaken well to form an emulsion. A microscope slide is dipped into the mixture, drained vertically and then dried in a dust-free place for 10 minutes. The film is exposed to a jet of steam for 1 minute and floated on to the surface of distilled water in a bowl. After putting 10 to 15 electron microscope grids on to the film, it is picked up with a dry glass slide in such a way that the grids are sandwiched between the formvar film and the slide. These grids with the perforated formvar film are then covered with a deposit of 20 nm of carbon and the formvar film is dissolved by putting the grids in the vapour of ethylene dichloride for 2 to 3 hours. Finally the suitable grids with large numbers

of holes are selected and kept in a clean container. Although the method looks time-consuming, it should be appreciated that since the grids with perforated carbon film do not deteriorate a large quantity of grids for a series of experiments can be made in one operation. This method of producing perforated carbon film is more reliable than given in the last paragraph of previous section.

A grid coated with perforated carbon is held horizontally by a pair of tweezers, a drop of 10% salt solution in distilled water is put on the grid by a very fine dropper. The drop is then drained gently from the beneath of the grid by a clean filter paper. The grids so prepared, are kept in a clean container and can be observed immediately. The size of the drop should be smaller than the diameter of the grid to avoid the grid to stick to the tweesers and it is better to use a second pair of tweezers to transfer the grid in to the container.

2.6 Observations and Discussion

The electron microscopical observation shows that large number of crystals are formed inside the holes of carbon film, (Fig. 2.3, 2.4 and 2.5). In the case of KCl, NaCl and KBr, large crystals are formed only inside the holes and some of them have some parts on the support film. A few number of smal crystals are observed around some of the holes. Thus it seems that the holes are the preferred sites for crystallization. The crystals appear

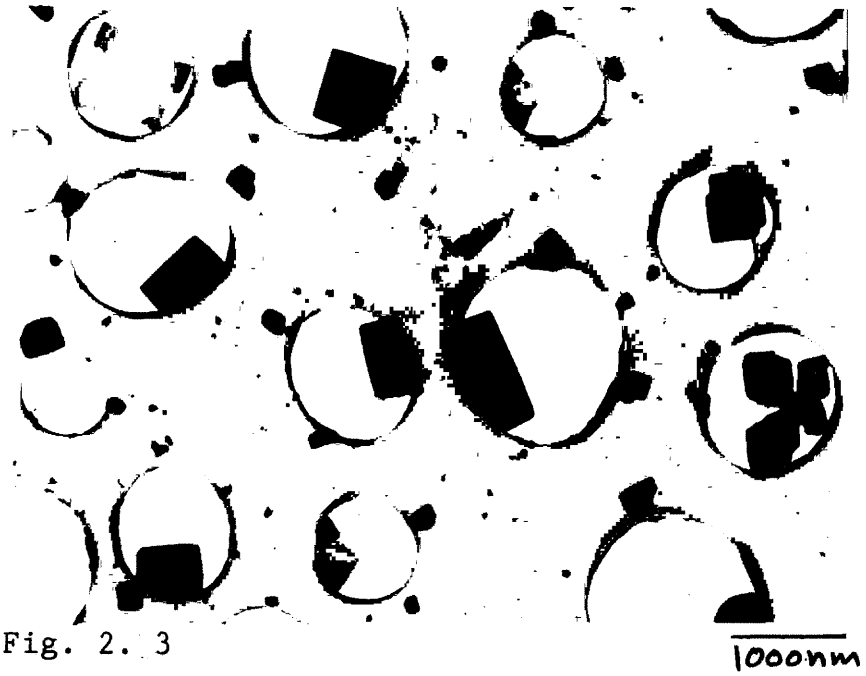

Fig. 2.3

Fig. 2.4

Fig. 2.3. KCl crystals in the holes of carbon film.

Fig. 2.4. NaCl crystals in the holes of carbon film.

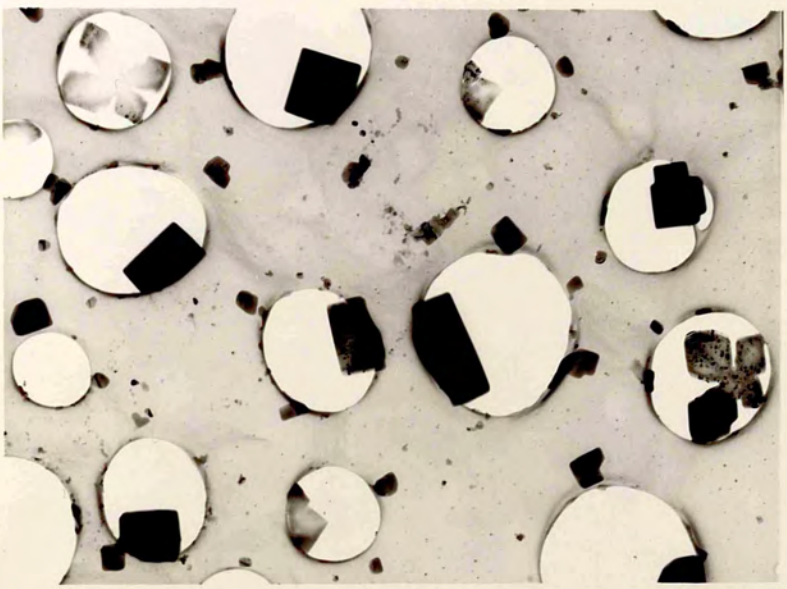

1000nm

1000nm

Fig. 2.5

Fig. 2.6

Fig. 2.5 KBr crystals in the holes of carbon film.

Fig. 2.6 KCl crystals in the holes of carbon film.

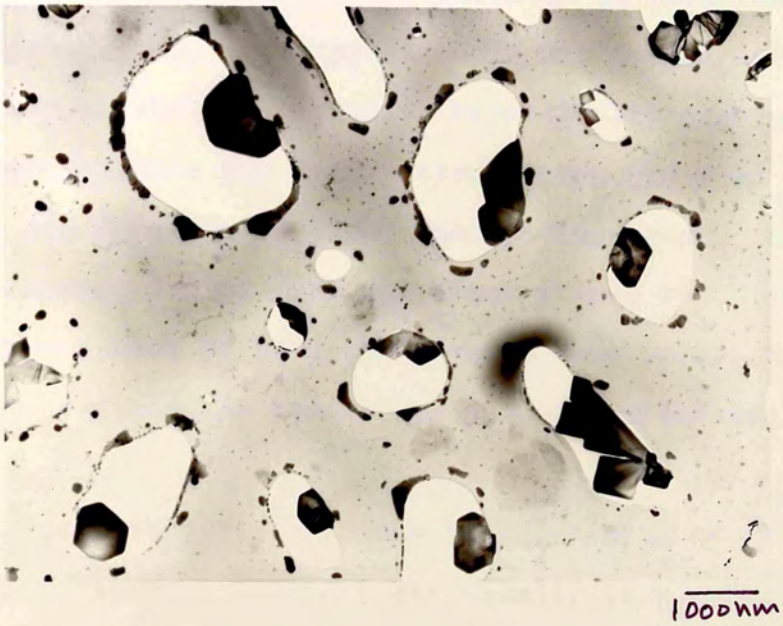
1000nm

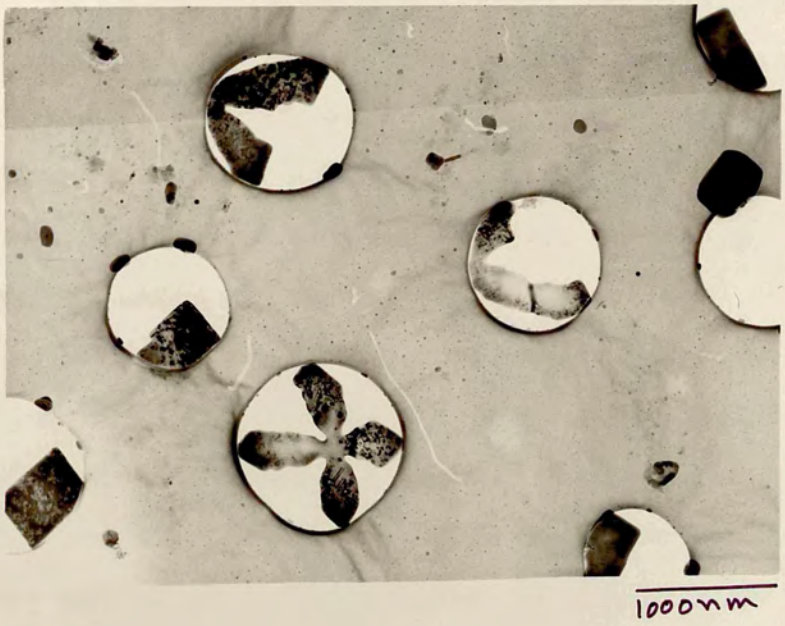
1000nm

in different shapes and sizes in holes of the same size. Mostly dark square crystals are observed in large holes. The transparency of the crystals does not depend on the size of the crystals. Very small crystals are transparent, some large crystals are fairly transparent and some small crystals are found to be dark. Usually the square-shaped crystals appear darker than the other shapes which are either transparent or have some transparent parts. For the same size crystals the transparency can be dramatically different.

The crystals are formed in holes with as little as 1% concentration, but they are usually very small at this dilution. By increasing the concentration the size and thickness of the crystals increased gradually. It is found that a concentration about 15% is adequate for KCl, NaCl and KBr to form suitable crystals. The orientation of these crystals is usually [001] normal to the plane of the holes. In the case of KCl, some crystals with [111] orientation are also observed.

The halides of caesium crystallize with a coordination number of eight (the CsCl structure), except CsF, which crystallizes wih a coordination number of six (NaCl structure), like most of the other alkali halides. CsI, CsCl and CsBr behave differently when their crystals are formed and observed in the holes of carbon support film. They usually formed dendrites: tree like growths most frequently observed in CsI (Fig. 2.7 and 2.8). They are also observed in CsBr (Fig. 2.13) and sometimes in CsCl. Crystals of CsBr and CsCl have some defects and are

easily damaged by electron bombardment, an effect which will be discussed later. The dendrites associated with very rapid growth, CsI crystals from a solution of 20% concentration are dendritic, as shown in Fig. 2.7 (a) and (b). In Fig. 2.7 (a) the crystal is entirely inside the hole, i.e., all branches seems to be connected to the edge of the hole from inside and these branches are very thick and opaque to the electron. In Fig. 2.7 (b) the branches start from some point on the carbon film and extend themselves into the holes where they broadend and become transparent. Thin and transparent dendrites are formed from 10% solution and shown in Fig. 2.8 (a) and (b). They are spread all over the perforated carbon film and the parts which come over the holes are more transparent. Some large transparent crystals of CsI are also observed (Fig. 2.9 (a) and (b)) which are suitable for use as a substrate.

The CsCl crystals are thick and dark having very small transparent areas (Fig. 2.12). They are damaged easily in the electron microscope during the examining and are therefore not suitable as substrates. CsBr behaves similarly, its crystals appearing in the form of dendrites (Fig. 2.13) with grain boundaries. Its diffraction pattern confirms a polycrystalline structure. In the case of CsF which is highly hygroscopic halide and dissolves in atmospheric humidity very rapidly, it only crystallizes inside the electron microscope. The crystals of CsF are flat but thick and do not form any particular shape (Fig. 2.14 and 2.15).

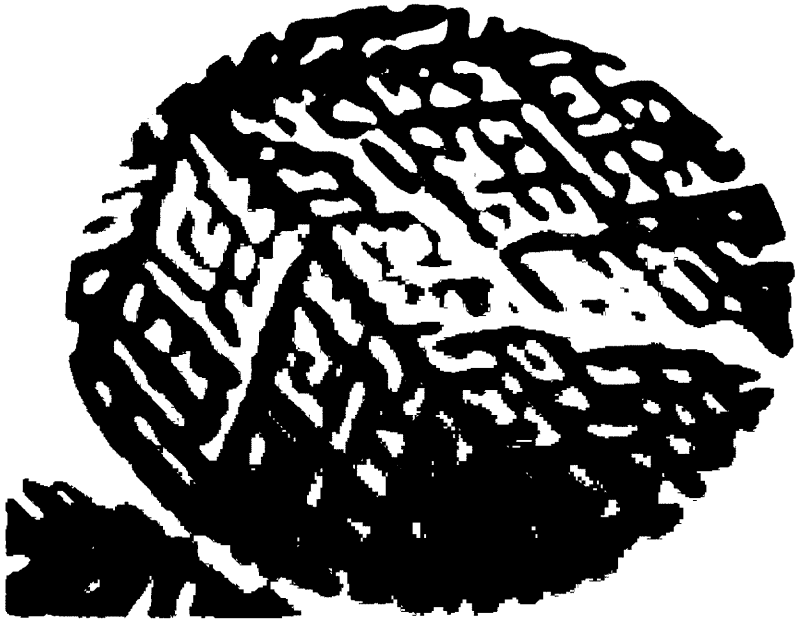

Fig. 2.7 (a)

Fig. 2.7 (b)

Fig. 2.7 (a) and (b). Dendritic crystals of CsI grown from solution in the holes of carbon film.

1000nm

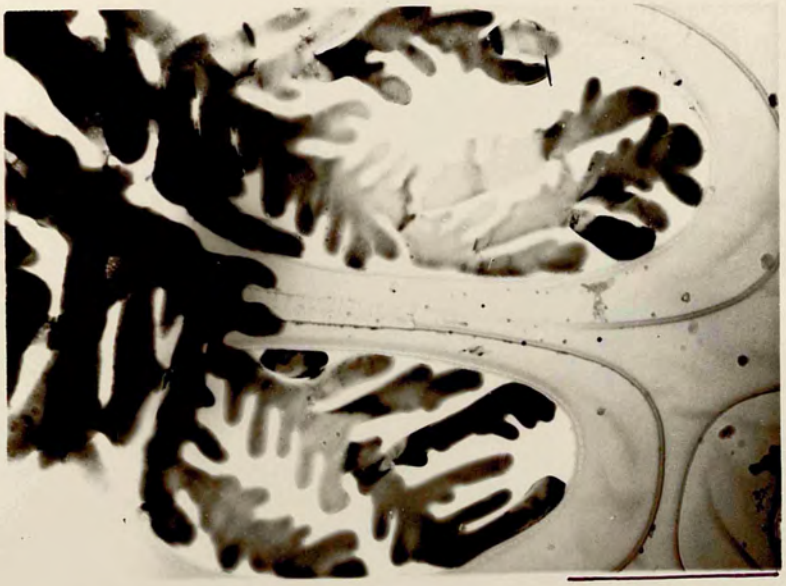

500nm

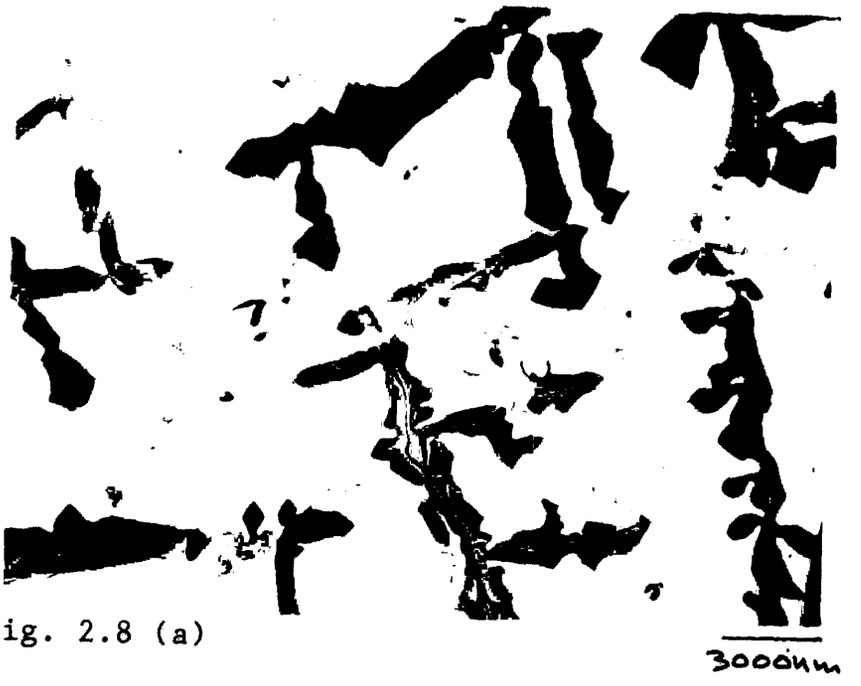

Fig. 2.8 (a)

Fig. 2.8 (b)

Fig. 2.8 (a) and (b). Dendritic growth of CsI from solution on perforated carbon support film.


3000nm


3000nm

Crystals of CsI are oriented with [111] normal to the plane of the hole as indicated by the diffraction pattern in Fig. 2.10. Some [001] and [011] orientations are also observed in large single crystals. CsCl crystals are found in [001] orientation (Fig. 2.11). The orientation of CsBr crystals is not unique as their diffraction pattern indicates a polycrystalline structure (Fig. 2.13, b). In the case of CsF, which usually crystallizes with the NaCl structure, the orientation of its crystals is found to be [011] (Fig. 2.14, b), the [111] orientation also observed in CsF crystals as shown in Fig. 2.15 (b).

2.7 The Mechanism of Formation of Crystals in Holes of Carbon Film.

Crystallization from solution has been used extensively as a method for purifying and obtaining single crystals of a variety of inorganic and organic materials. Aqueous and organic solutions have been used as solvents. In this method the liquid evaporates while the solid separates out and is potentially very useful for producing crystals of inorganic salts such as the alkali halides which are almost all soluble in water. Methods for the preparation of crystals from solution were comprehensively reviewed by Buckley in 1951 and more recently in the books of Brice (1973), Mullin (1972), Nyull (1971), Strickland-Constable (1968) and Elwell and Scheel (1975),

deal generally with growth from solution as do most of the papers at a conference (Mullin, 1976). The review by Bennema and Gilmer (1973) is concerned with the kinetics of crystal growth and many of the concepts discussed can be applied to the solution growth. Special theories describing the kinetics of crystal growth from solution have not, in general, been developed. General theories of crystal growth have usually been adopted and perhaps modified, so that they can be applied to growth from solution. The interrelations between many of the theories of crystal growth have been discussed by Bennema (1974). The growth of crystals from solution may be regarded in the same way as growth from vapour (discussed in chapter 4), the solute particles behaving in the same way as the atoms or molecules in the vapour. The deposition of a solid crystalline phase from solution can only occur if some degree of supersaturation has first been achieved in the system. In other words the attainment of supersaturated state is essentional for any crystallization operation. Generally any crystallization operation can be considered to comprise three basic steps:

1. Achieveement of supersaturation (or supercooling).
2. Formation of crystal nuclei.
3. Growth of crystal.

All three processes may be occuring simultaneously in different regions of a crystallyzation unit. Supersaturation

can be achieved either by dissolving more solute or by removing some of the solvent from the solution by evaporation. If a solution is saturated at high temperature the supersaturation can also be achieved by supercooling.

As the state of supersaturation is an essential feature of all crystallization operations. Wilhelm and Ostwald (1897) first introduced the terms 'labile' (unstable) and 'metastable' supersaturation; they referred to supersaturated solutions in which spontaneous deposition of solid phase, in the absence of solid nuclei, will or will not occur, respectively. Miers (1904), (1906), (1907) and (1927) carried out extensive research work into the relationship between supersaturation and spontaneous crystallization. He described three zones on solubility curve.

(i). The stable (unsaturated) zone where crystallization is impossible.

(ii). The metastable (supersaturated) zone, between the solubility and supersolubility zones, where spontaneous crystallization is improbable. However, if a crystal seed was placed in such a metastable solutions, growth would occur on it.

(iii). The unstable or labile (supersaturated) zone where spontaneous crystallization is probable.

Nucleation may occur spontaneously in a supersaturated solution. Exactly how a crystal nucleus is formed in a homogeneous fluid system is not known with any

degree of certainty. The probable mechanism of nucleation is as follows: Minute structures are formed, first from the collision of two molecules, then from that of a third with the pair, and so on. Short chains may be formed initially, or flat monolayers, and eventually the lattice structure builds up. The construction process, which occurs very rapidly, can only continue in local regions of very high supersaturation. The phenomenon of spontaneous nucleation can be analysed by considering various energy requirements. In this connection the theoretical and practical contributions of such workers as Gibbs (1928), Volmer (1929) and (1939), Becker and Döring (1935) and (1938) have greatly assisted understanding of the process.

Most of the micrographs in the present work show that a variety of crystals are formed inside the holes of carbon film. This leads to the assumption that when a drop of alkali halide solution is put on to a grid with a perforated carbon support film and is drained from beneath with a filter paper, a large number of small droplets are formed and captured by the holes. Due to the small volume of these droplets the water evaporates rapidly and solution becomes supersaturated. The crystal nucleus is formed somewhere in the hole and as the evaporation continues, further growth occurs until all the solid in the drop crystallizes. The holes in the carbon support film are preferred sites for formation of crystals.

To understand the mechanism of the formation of the droplets and the growth of the crystals with definite

Fig. 2.9 (a)

Fig. 2.9 (b)

Fig. 2.9 (a) and (b). Large crystals of CsI grown from solution in the holes of carbon film.


500 nm


500 nm

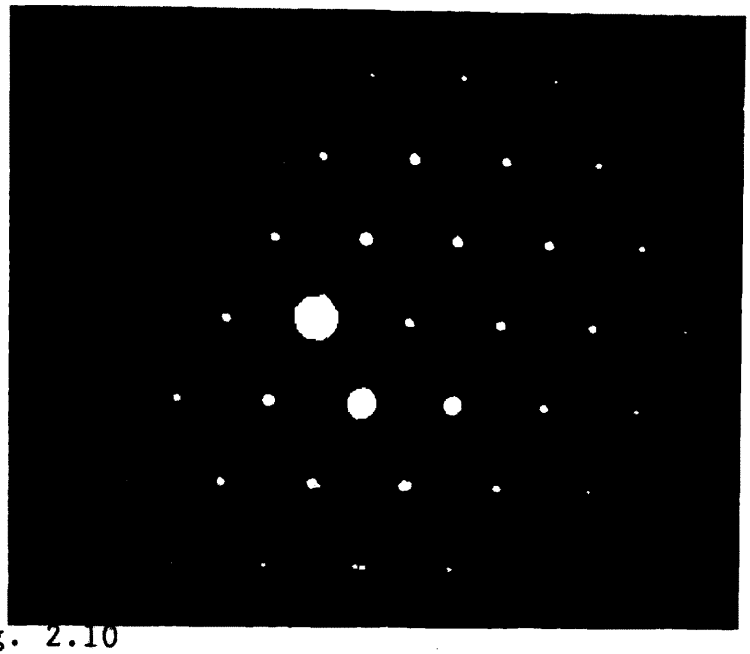

Fig. 2.10

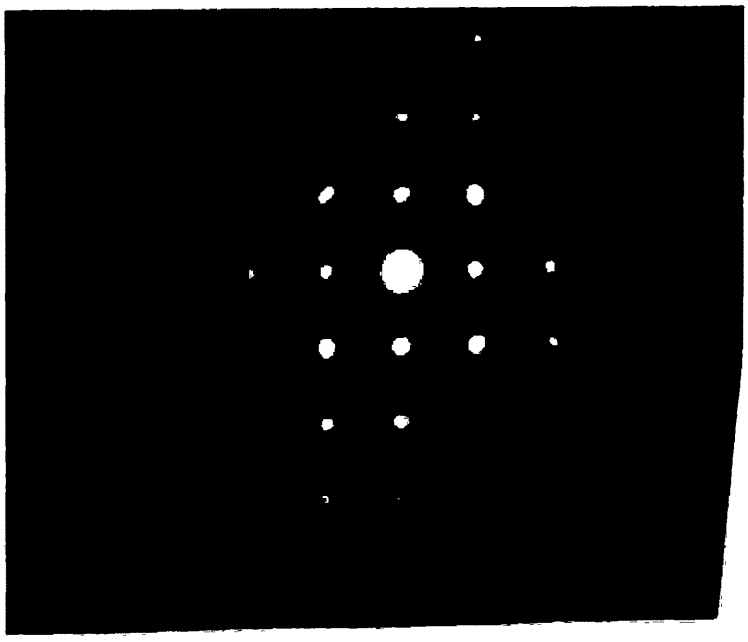

Fig. 2.11

Fig. 2.10. Single-crystal electron diffraction pattern of CsI with [111] orientation.

Fig. 2.11. Single-crystal electron diffraction pattern of CsCl with [001] orientation.

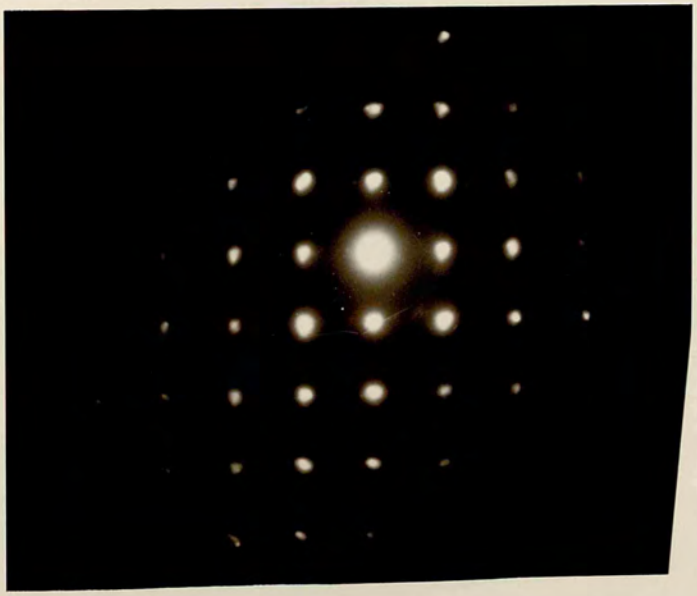

orientation, inside the holes, it is necessary to consider the important parameters which are involved. It seems, as for as the drop of solution and the support film are concerned, the surface tension of the solution and the interface energy between the drop and film are the most important parameters. The surface tension of water at room temperature (20°c) is 72.75×10^{-3} nt/m. Dissolving alkali halides in water increases the surface tension and the latter increases with the concentration. In a small droplet the surface tension produces a considerable pressure which tends to minimize the energy of the droplet by reducing its surface. If the droplet is spherical with radius R and surface tension γ, the pressure towards the centre of sphere is $2\gamma/R$. For alkali halide solution γ is about 80×10^{-3} nt/m, hence for a spherical droplet of radius 10 μ the pressure is:

$$\frac{2 \times 80 \times 10^{-3}}{10 \times 10^{-6}} = 1.6 \times 10^{4} \text{ Pa.}$$

Because of pressure of this order, it is expected that small droplet of salt solution, will be spherical, especially when the solution is a poor wetter of the substrate.

In the present work the interface energy between the alkali halide solutions and the carbon film has been studied by a simple experiment. Solution of the salt is sprayed on a glass slide coated with carbon and observed under the light microscope, separated drops with considerable heights have been observed. A drop of alkali

halide solution of diameter 3 mm or more can easily slide on the surface of glass slide coated with carbon, when the slope of the slide is more than 25 degrees. These observations show alkali halide solutions do not easily wet a microscope slide coated with carbon, i.e., the energies of the droplets are not significantly reduced by contact with the carbon support film. In particular any reduction in energy is insignificant for those droplets with considerable parts over the holes. Thus as for as the interface energy is concerned, the assumption of spherical droplets is good. If we accept the idea of spherical droplet, it is possible to evaluate the thickness of the crystals formed in the holes by considering the following points. In the present work a large number of holes of diameter less than 2 μ were observed with crystals almost entirely inside the holes and having some crystallites on the support film around the holes (Fig.2.3, 2.4, 2.5, and 2.6) Two possible configurations can be conceived for the droplets, as shown in Fig. 2.16 (a) and (b).

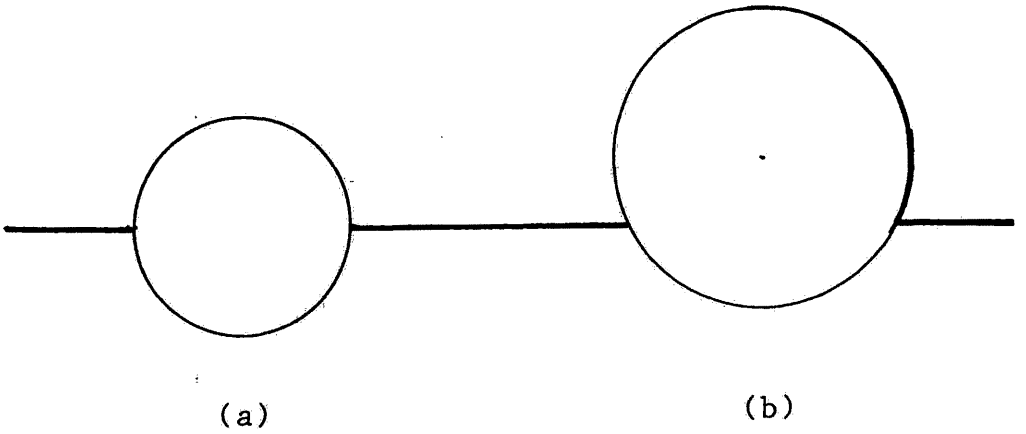

Fig. 2.16. Two different configuration of the solution droplets which could lead to crystals inside the holes, (a) no crystallite on support film, (b) with some crystallites on support film.

Fig. 2.12 (a)

Fig. 2.12 (b)

Fig. 2.12 (a) and (b). CoCl crystals in the holes of carbon film. The crystals are damaged by electron irradiation.

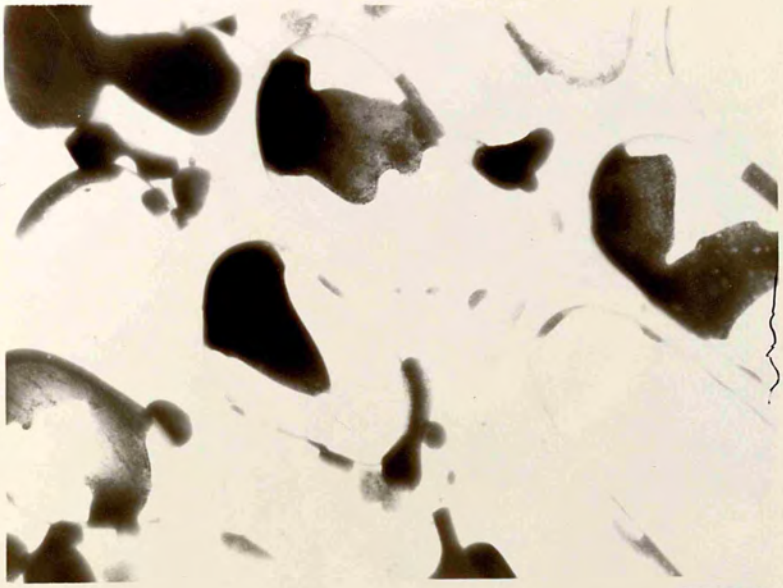
1000nm

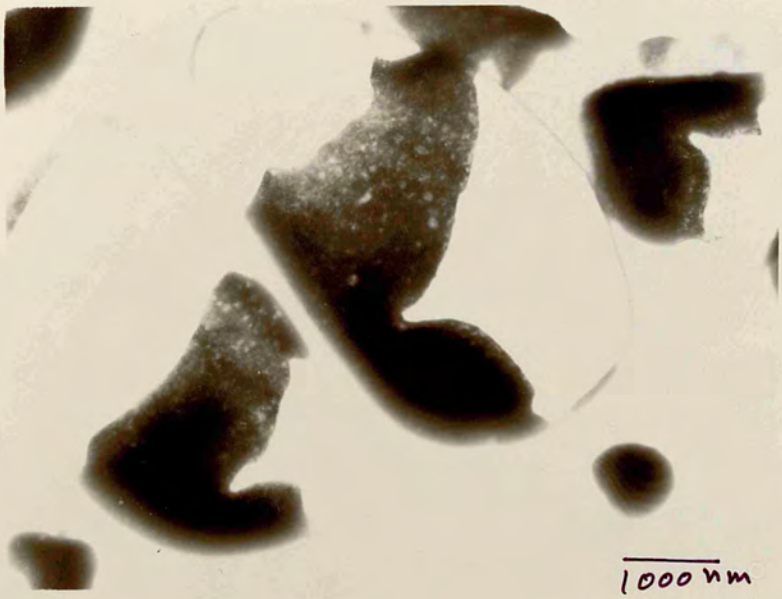
1000nm

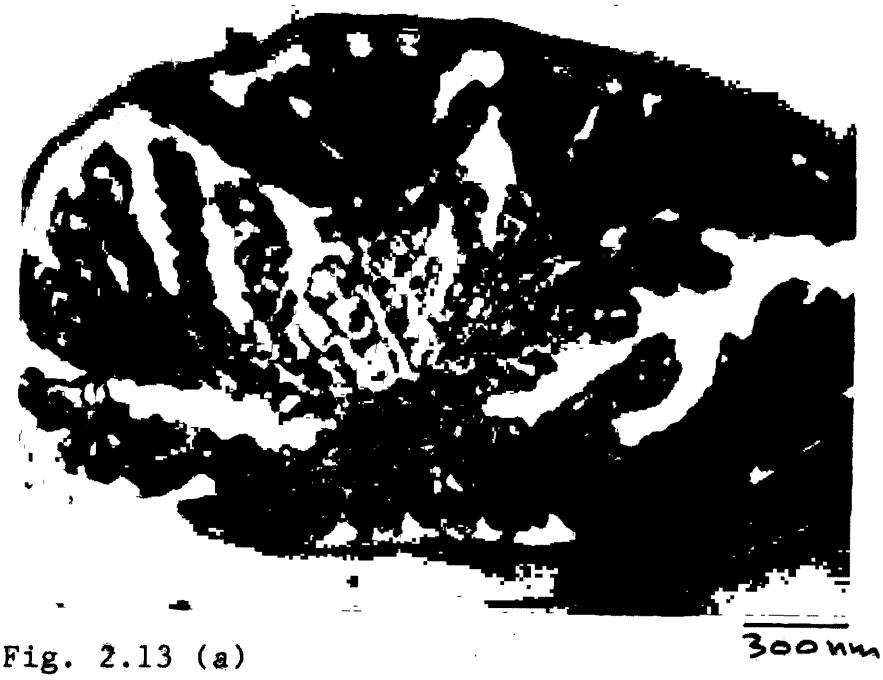

Fig. 2.13 (a)

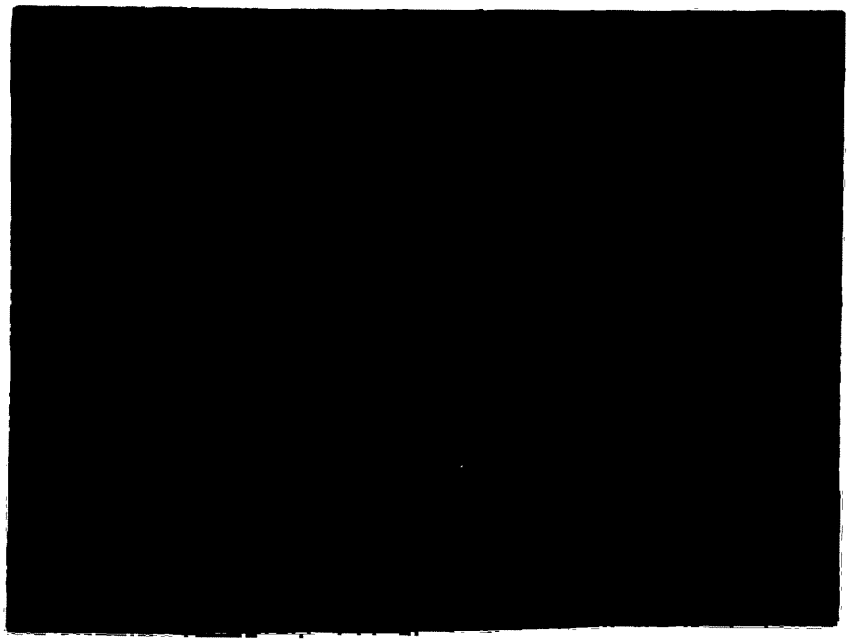

Fig. 2.13 (b)

Fig. 2.13. Dendritic crystal of CsBr in the hole of carbon film, obtained by intense electron irradiation. (a) Micrograph, (b) diffraction pattern.

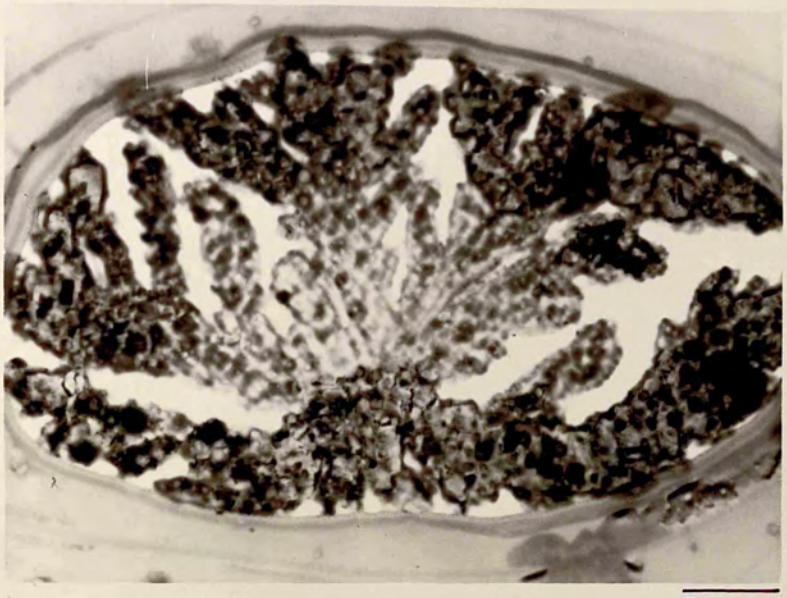

300nm

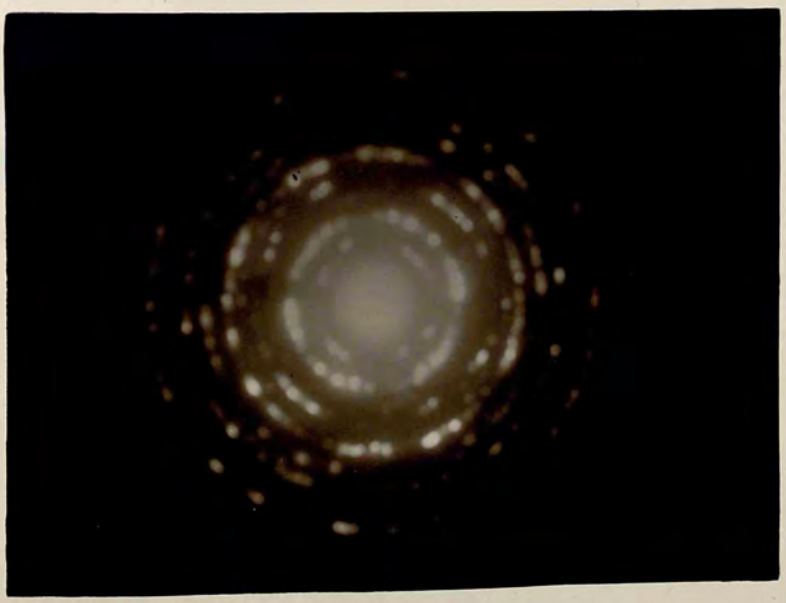

For a droplet with configuration similar to Fig. 2.16 (a) the amount of dissolved substance, m, can be obtained from

$$m = \frac{4}{3} \cdot C \pi R^3$$

where C is the concentration of the solution and R is the radius of the hole. Dividing m by the density of the substance, ρ, the volume of the crystal is found. The area of the crystal, S, can be evaluated from its micrograph. Having these data, the thickness of the crystal, t, can be obtained from:

$$t = \frac{4 \pi C R^3}{3 P S}$$

The ratio of the area of the crystal to the area of its hole $S/\pi R^2$ is not constant. For a cube-shaped thick crystal of KCl it is about 1/15 and for the transparent crystal it is less than 1/6. In a 2 μ diameter hole the thickness of a cube-shape thick crystal of KCl with $S/\pi R^2$ =1/15 and C=15% we get,

$$t = \frac{4 \times 15 \times 15 \times 2 \times 10^{-6}}{3 \times 2 \times 100} = 3 \mu$$

For a transparent crystal with $S/\pi R^2$ =1/6,

$$t = \frac{4 \times 15 \times 6 \times 2 \times 10^{-6}}{3 \times 2 \times 100} = 1.2 \mu$$

In this evolution the concentration of the prepared solution is used, while the actual concentration could be considerably higher because of evaporation of water before crystallization. The droplets with configuration similar to Fig. 2.16 (b) would give much

thicker crystals. A spherical droplet of alkali halide solution should end up almost to a cube-shaped crystal; because alkali halides have cubic crystal structure and the cube has the minimum area among all possible orthogonal prisms for a given volume. Thus the cube is the ideal shape for an alkali halide crystals as for as the energy of the crystal is concerned. According the thickness, calculated above the assumption of a spherical droplet is true only for thick cube-shaped crystals. But for the crystals with shapes other than cubic and which are also electron-transparent, the idea of spherical droplets should be abandoned.

When a drop of alkali halide solution on a grid with perforated carbon film, is drained from beneath by a filter paper the height and the size of the drop reduces very quickly. This process causes a rapid flow of the solution towards the sinking points, all over the surface of the support film. When the drop becomes thin enough it is broken by the holes into small droplets, which then are captured by them (the holes act like the roughness on a surface which can hold the droplets). Most of these droplets are not in a minimum state of enrgy as for as the surface energy is concerned. In other words a large number of droplets are not spherical or closely so. After the formation of droplets, the surface tension tends to reduce the energies of the droplets by rendering them spherical, but this process takes time and long before it happens evaporation increases the concentration of the solution

very quickly, supersaturation occurs and crystallization starts. To explain why some crystals of same size do not have the same thickness and why most of the crystals have particular orientation with respect to the holes, the following assumption is made. The droplets are not in a minimum state of energy. Each of them can be in one of the many possible states of energy and therefore droplets in the same size holes can be in the shape of lenses with different thicknesses. Thus the droplets in the same size holes can give crystals with different sizes and thicknesses. The droplet with the same diameter as the hole becomes very thin and lens-like and the droplets with greater diameters than the holes become spherical with the same diameter as the hole, so as to form a thick cube crystal.

In Fig. 2.17 some of the possible shapes for the drolets in holes of nearly the same size are shown. Droplets similar to (a) lead to a thin and flat crystals while droplets similar to (c) give thick crystals.

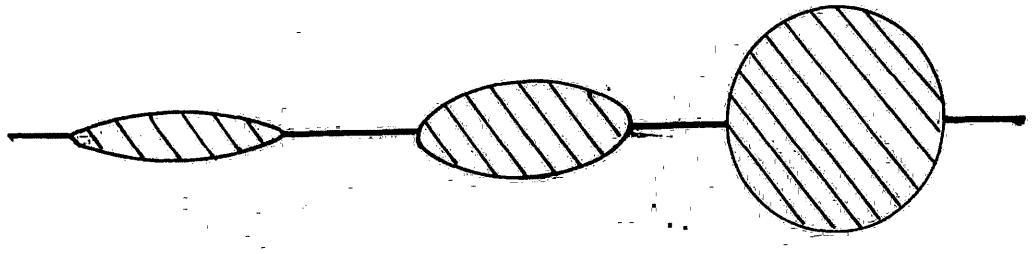

Fig. 2.17. Some of the possible profiles for the droplets captured by the holes.

For droplets sizes of the order of microns, the effect of gravity can be ignored and all diractions in a spherical droplet will be equivalent. This means a crystal grown from a spherical droplet can have any orientation with respect to the support film. In the droplets similar to (a) and (b) in Fig. 2.17 which differ considerably from sphericity, all directions are not equivalent. Therefore the crystal nuclei which appear and start crystallization can not have arbitrary position. Because the fastest way of transition from solution to crystal, for a lens-like droplet is to have the directions of the fast growth of the crystal nuclei in the plane of the droplet. It is suggested by several research workers (Brice, 1976) the directions of fast growth in KCl crystals are <110>, which have been observed in the present work.

(a)

(b)

Fig. 2.18. (a) and (b). Some of the crystals and the suggested shapes of their droplets at the beginning of crystallization.

Fig. 2.18 shows the schematic diagrams of the crystals with different shapes, which are nearly transparent and their suggested corresponding droplet shapes at the beginning of crystallization are also shown. Since the crystals are formed inside the holes, the effect of the substrate on most of these crystals is negligible. In other words the crystals are formed almost in free space and nearly have the same structural properties as a bulk crystal.

Rapid crystallization from supercooled melt, supersaturated solutions and condensed vapour frequently produces a tree-like crystal formation called dendrites. Dendrites may also be formed in chemical reactions or electrolysis. In dendritic growth the main crystal stem grows quite rapidly in a supersaturated system that has been seeded and at a later stage primary branches grow at a slower rate out of the stem at angles determined by crystal structure (often at right angle). In certain cases, small secondary branches may grow slowly out of the primaries. Fig. 2.19 shows a schematic diagram of dendritic growth. Most metals crystallize from the molten state in this manner, but because of the filling in process the final crystalline mass may show little outwards appearance of dendrites formation. The fascinating patterns of snow crystals are good examples of dendritic growth.

Several theories have been proposed to explain the formation and growth of dendrites. Some of them regard

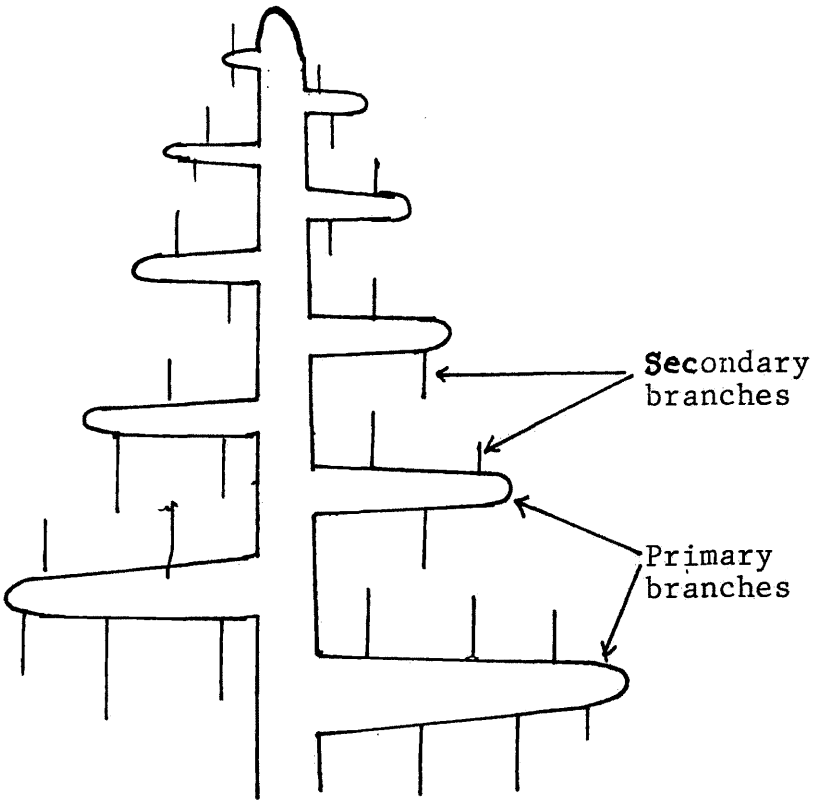

Fig. 2.19 Dendritic growth.

dendritic growth as a transport problem, for if solutions the diffusion or in the melts the heat flow, is weak and inhomogeneous, some places (the corners) of the growing crystals are in a preferred position, and this leads to a dendritic growth. Other considerations suggest that dendritic crystallization may be explained by the presence of impurities. The most common factor is that the dendrites form during the early stage of crystallization. Growth occurs quite readily in thin liquid layers, probably because of the high rate of evaporative cooling. The formation of dendrites is favoured by the substances which have high latent heat of crystallization and low heat conductivities.

In the present work dendrites have been observed in CsI, CsBr and sometimes in CsCl (Fig. 2.7, 2.8 and 2.13).

When a drop of solution is placed on a grid with perforated carbon film and drained from beneath by a filter paper, it is broken into small droplets and these are captured by the holes in the carbon film. Most of these droplets have lens-like shapes rather than spherical, as explained in the KCl crystal formation. These lens shaped droplets behave like thin layers of solution where the evaporation is quick enough to produce supersaturation for rapid crystallization which then produce dendrites. In a separate experiment a relatively large drop of 10 % solution of CsI was put on to a carefully prepared greas-free glass slide and smeared with a clean thin glass rod. Rapid growth was observed in the rapidly evaporating solution film, resulting in dendritic crystals.

If the droplet, formed on the perforated carbon film, is within a hole the resulting dendritic crystals are shown in Fig. 2.7 (a), where main stem and all the branches are within the hole. If the droplet has some part on the carbon support film the dendritic growth starts somewhere on the support film and the main stem or the branches advance into the hole. This type of growth shown in Fig. 2.7 (b). The dendrites shown in Fig. 2.8 (a) and (b) are formed when the holes in the carbon support film are relatively small, the droplets of the solution are so near to each other that the edges of some of them are connected together and formed thin layers of solution on large parts of support film containing more than one hole.

The dendrites are formed by rapid crystallization on the surface of carbon film as well as in the holes. These kinds of dendritic crystals are thinner than the previous that formed only within the hole. The parts of the stem or branches over the holes in the carbon film are fairly transparent. Possible configurations of the droplets to form different kinds of dendritic crystals are shown in Fig. 2.20.

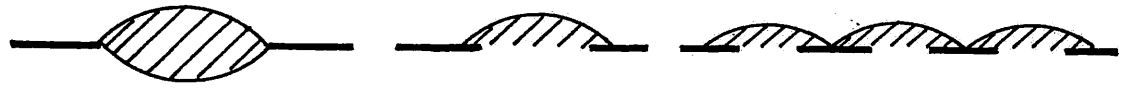

(a) (b) (c)

Fig. 2.20. Different profiles of droplets to form a variety of dendrites. Droplets similar to (a) produce crystals within the hole and from droplets similar to (b) the growth starts on the support film and advances into the hole. Droplets similar to (c) form dendrites all over the support film as well as in the holes.

2.8 Thickness Measurement.

There are several standard techniques of measuring film thickness which are commonly used to determine the thickness of very thin films up to an accuracy of 0.2 to 1 nm.

Pliskin and Zanin (1970) gave a comprehensive review of some of the more common techniques together with their useful ranges and accuracies. But most of them can only be applied to the macroscopic thin films i.e., to the films with thicknesses 10 nm and above, like optical interferometery, color comparision, VAMFO, stylus, x-ray absorption and Beta backscattering. When the sizes of the films are microscopic, only a few reliable techniques are available which can be applied in special cases. For example ellipsometry and gravimetric can be used only for the films having average thickness on large area, in other words on a continuous thin film. When there is a wedge shaped crystal, the thickness can be found from thickness fringes. Also, when there is a defect ending on both faces of a crystal and lying in a known plane, again it is possible to find out the thickness. The well-known shadowing technique is not applicable to the crystals which are entirely inside the holes. Besides, when the thickness of crystal varies from place to place especially near the edge, the shadowing technique could give an inaccurate result.

A technique which makes use of bending fringes and has been suggested by Amelinckx (1964) is extended here to be applicable to the crystals in the holes of carbon support film. In a large flat crystal of thickness t, the variation of diffracted intensity in a direction normal to the crystal, parallel to the electron beam, in the electron microscope is given by,

$$I \propto \frac{\mathrm{Sin}^2 (\pi t \ s)}{(\pi s)^2}$$

where s is the distance between the Ewald sphere and the reciprocal lattice point in the direction parallel to the electron beam in reciprocal space. For s = 0 , the reciprocal lattice point coinside with the Ewald sphere, and the intensity is a maximum. The zero points of the intensity satisfy the following equation:

$$s\ t = n$$

where n is an integer (according to kinematic theory this is only correct for large s). The distance between successive zero point is constant:

$$\Delta s = \frac{1}{t}$$

The profile of intensity variation with s is shown in Fig. 2.21

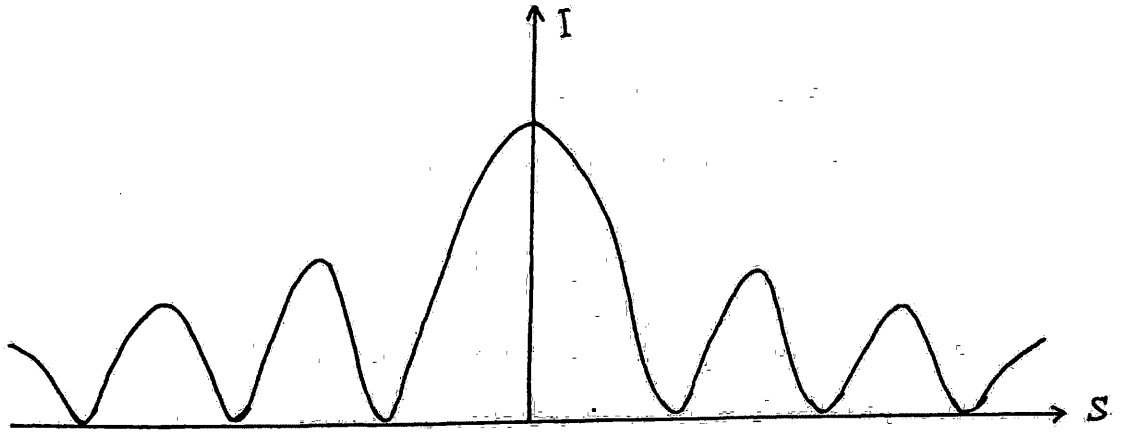

Fig. 2.21 Diffraction intensity verses the deviation from exact Bragg condition.

Now consider a crystal with a symmetric bend with respect to the electron beam in such a way that two parts of the crystal, P_1 and P_2 in Fig. 2.22 (a) are exactly in the Bragg condition i.e. their reciprocal lattice vectors end on the Ewald sphere. The position of the planes between P_1 and P_2 gradually varies from the exact Bragg condition. In other words, going away from P_1 and P_2, s increases giving rise to a series of fringes. In bright field image two strong (and wide) dark fringes are observed (Fig. 2.8 and 2.9) which correspond to P_1 and P_2 and few more faint fringes at both sides of them, these are shown schematically in Fig. 2.22 (b).

At 100 KV (accelerating voltage in the electron microscope) the λ = 0.0037 nm, the radius of the Ewald sphere is very large, so it can be written

$$\Delta s = P_1'\theta = PP_1'\delta\theta$$

and

$$t = \frac{1}{\Delta s} = \frac{1}{PP_1'\delta\theta}$$

where PP' is the reciprocal lattice vector corresponding to the planes responsible for the reflection. Hence

$$PP_1' = \frac{1}{d_{hkl}}$$

From Fig. 2.22 (b) the number of fringes between two strong dark fringes, m, can be obtained from the relation

$$m = \frac{L}{\Delta L}$$

where L and ΔL are the distances between two dark fringes and between a dark fringe and faint fringe respectively.

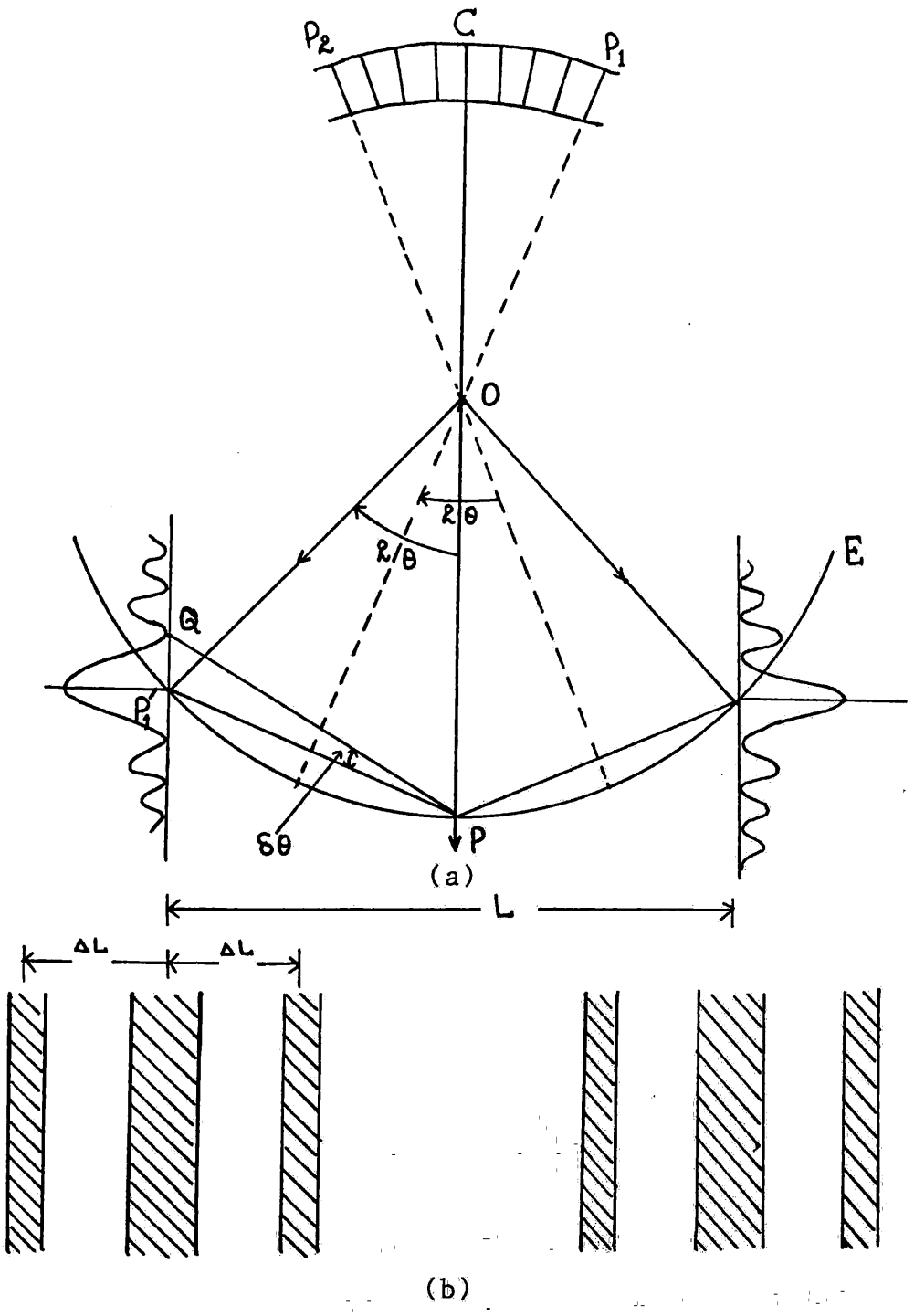

Fig. 2.22. (a) C is a crystal with symmetric bending with respect to the electron beam, OP. Planes P_1 and P_2 are in exact Bragg condition; E is the Ewald sphere, PP_1' is the reciprocal lattice vector corresponding to P_1; $\delta\theta$ is the angle between two successive zero points. (b) Schematic form of the fringes in bright field image.

In Fig. 2.22 (a) it is seen that the angle between planes P_1 and P_2 is 2θ. Dividing this angle by $\delta\theta$, the number of fringes, m, can be get again. Thus

$$m = \frac{L}{\Delta L} = \frac{2\theta}{\delta\theta}$$

or

$$\delta\theta = \frac{\Delta L}{L} 2\theta$$

so

$$t = \frac{L}{\Delta L} \cdot \frac{1}{PP'_1 2\theta}$$

As the angles involves are very small so

$$2\theta = \frac{\lambda}{d_{hkl}}$$

and

$$PP'_1 = \frac{1}{d_{hkl}}$$

so

$$t = \frac{L}{\Delta L} \cdot \frac{d^2_{hkl}}{\lambda}$$

where λ is the wave length of the electrons, L and Δ L can be measured from the bright field micrograph and if the responsible reflection is known, d_{hkl} can be calculated from its lattice parameter.

This technique is restricted in practice because it is not easy to find adequate bending contours. In particular the crystals in the holes are usually flat, because they are not on the support film which might give

them some curvature. Some large crystals in the holes produce fringes which can be used for thickness determination. The dendritic crystals, in CsI case, which have branches on the support film produced bending contours. When the crystals in the holes are covered with very thin, ~ 2 to 4 nm, deposits of a different alkali halide other than the substrate, the bending arises because of the stress between the overgrowth and substrate.

Most of the contours in the alkali halide crystals are parallel to <100> and <110> directions, therefore, the required interplanar distances, are d_{200} and d_{220} (d_{200} and d_{110} in case of CsI). The thickness of some crystals, inside the holes, have been measured by this technique. The results of these measurements show that the thickness of transparent crystals of KCl varies from 100 nm to 200 nm. The crystals of CsI are between 200 nm and 500 nm thick, while the dendritic crystals are 50 nm to 100 nm thick. The same size crystals have considerably different thicknesses or in other words there is no simple relation between the lateral size of crystal and its thickness.

2.9 Radiation Damage to the Crystals.

The act of observing a specimen in the electron microscope, causes it to be irradiated with high energy electrons which may produce a variety of defects especially in crystalline specimens. The effects produced by irradiation in the electron microscope and possible

causal mechanisms have been discussed by Cosslett (1969), Stenn and Bahr (1970), Thach and Thach (1970) and (1971) and Glaeser (1971). In transmission electron microscopy of alkali halidee crystals, the investigation of grown-in defects is complicated because of the relatively strong interaction between the imaging electron beam and the object. Equally the high senstivity of these crystals to electron beams offers a method for creation of crystal defects or damage structures in the electron microscope itself. Before discussing the results of the present investigation, the mechanisms of formation of these defects due to electron bombardment are cosidered.

When electrons are passed through a solid, they lose some of their energies by elastic (or inelastic) scattering. The possible effects of the dissipated energy in the solid are heating, chemical changes through rearrangement of bonds and displaced atoms and crystallographic defects. The first of these is reversible and depends on heat capacity, thermal conductivity and radiation to the surroundings. The other two are irreversible since the specimen does not return to its original state when the incident beam is removed. The concern with temperature rise, other than thermal scattering, is the effect it may have on the object which includes phase changes in the solid, local melting, annealing and recrystallization, and under intense bombardment, sublimation of the material. In addition to the heating of the object by energy dissipation there is a

quite different category of interaction under the heading of radiation damage. Temp rature rise is the result of an increase of the thermal vibration amplitude of the atoms which are still centred on their equilibrium position. It can happen that an individual atom rec ve sufficient energy from colliding particles to displace far enough from its equilibrium position that it does not return, at least not immediately. The displaced atom may be knocked into an interstitial position, thus leaving a vacant site that result in a 'point defect'. If the displaced atom is sufficiently energetic, it can become a primary source of collision energy with the ability to produce still more defects and so initiate a chain reaction. An energetic primary that produces further displacement is often called a "knock-on".

The formation of these so called "point defects" can not alter the condition of electrical neutrality of the crystal. In a metal the removal of an ion to form a vacancy also require the removal of an electron to fulfil this condition, while in pure ionic crystals (such as alkali halides) as many negatively charged defects as positive ones must be formed to maintain neutrality. Long- and short-rang forces exist between like and unlike defects which lead to the very important phenomenon of defect clustring in solids bombarded at high temperature, where one or both of the simpler types of defect are mobile. In ionic solids long-range electrostatic forces exist between defects with opposite sign.

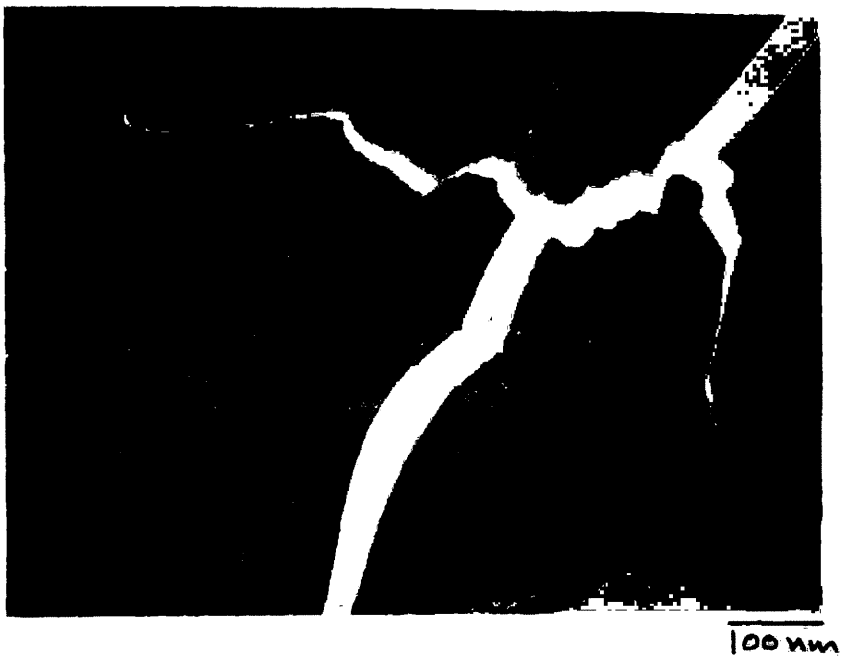

Fig. 2.14 (a)

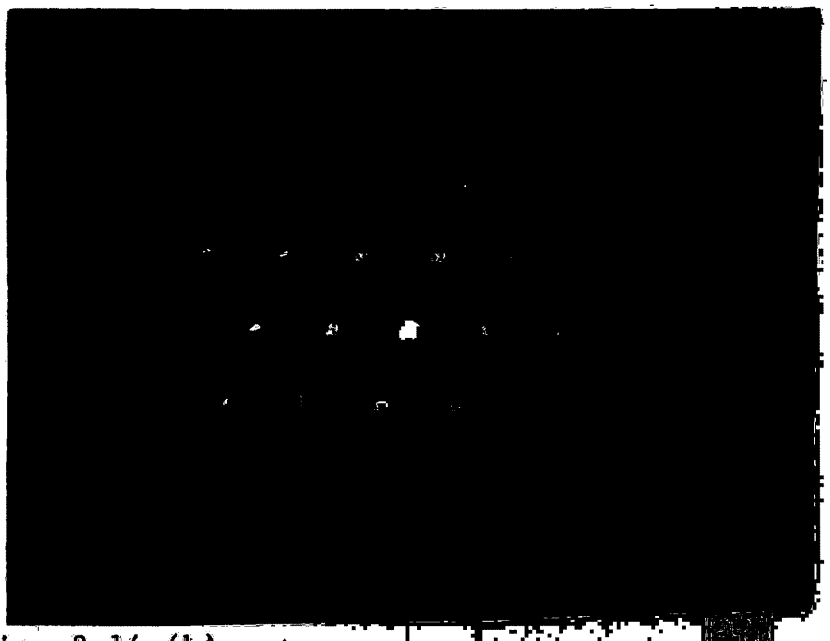

Fig. 2.14 (b)

Fig. 2.14. CsF crystals [illegible] formed inside the electron microscope and the diffraction pattern.

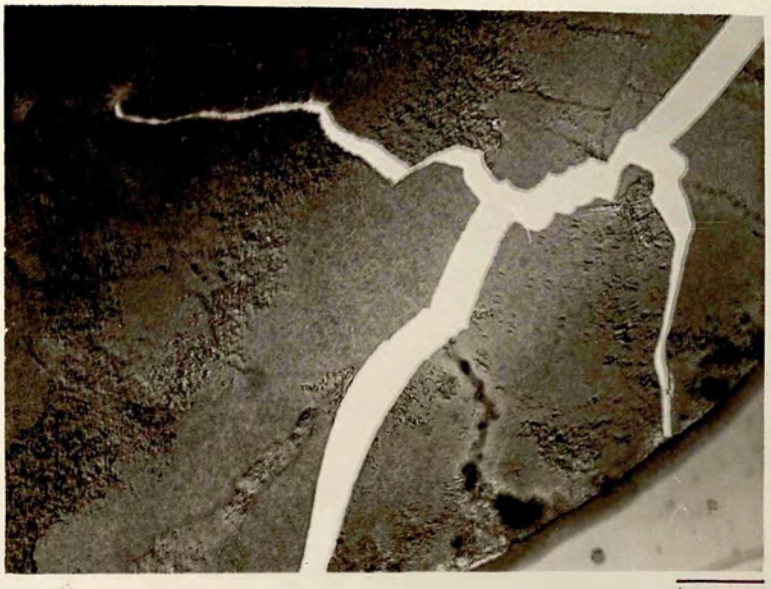

100 nm

Fig. 2.15 (a)

Fig. 2.15 (b)

Fig. 2.15 A damaged amorphous [illegible] film and its diffraction pattern.

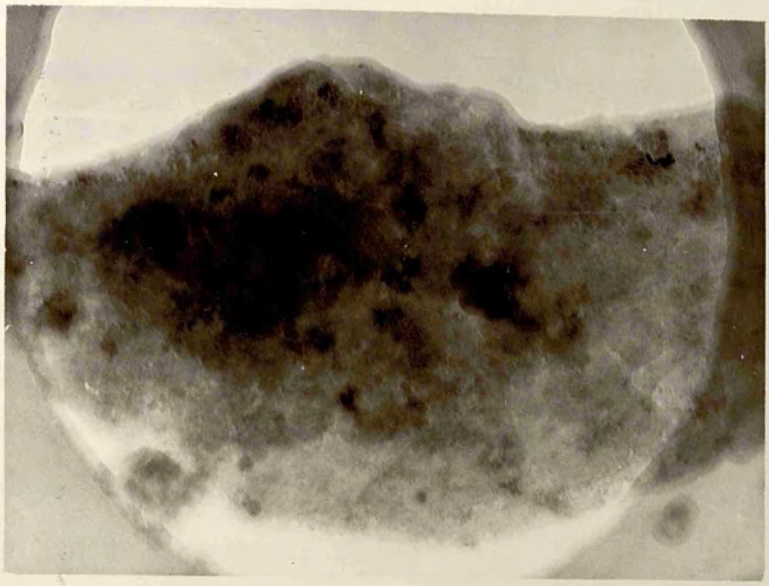

100nm

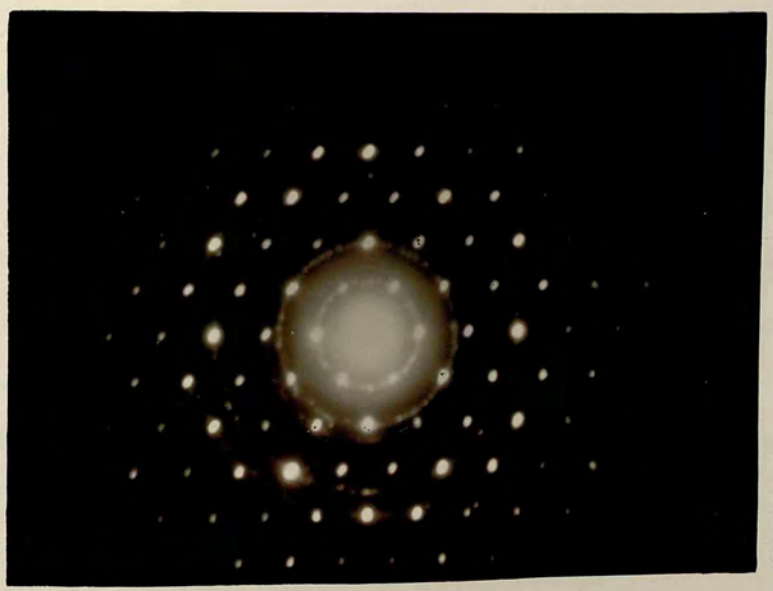

In any crystal lattice there are certain lattice planes which are more densely packed with atoms, and normal to which the lattice planes are more widely separated. In a situation in which interstitial atoms are able to aggregate, they will take up the minimum energy configuration which is in the form of platlets, one atom thick lying between the adjacent close-packed planes. For such a cluster containing more than about 100 atoms this may be considered as ring of edge dislocations with Burgers vector normal to the close-packed plane, the actual nature of the loop depending upon the crystal lattices. The case of vacancy condensation is a little different, for small numbers of vacancies; the form of an aggregate with least energy is the spherical void.

The kinetic energy loss by a colliding electron to a stationary particle of mass m_n as suggested by Heidenreich (1964) is

$$\Delta E = 4\ E\ \frac{m_e m_n}{(m_e + m_n)}\ \sin^2 \tfrac{1}{2}\theta$$

where θ is the angle of scattered electron with its normal path and E is the kinetic energy of the incident electron.

For $m_n >> m_e$ the loss in energy to the heavy particle is

$$\Delta E \cong 4\ E\ \frac{m_e}{m_n}\ \sin^2 \tfrac{1}{2}\theta$$

The maximum amount that the incident electron can lose to the nucleus is by a collision where electron reverses direction or

$$\theta = \pi$$

and

$$(\Delta E)_{max} = 4\frac{m_e}{m_n} E$$

In the more general case, a bombarding particle of mass m_1 with m_1 comparable to m_n gives a maximum energy transfer

$$(\Delta E)_{max} = \frac{4Em_1^\circ m_n}{(m_1^\circ + m_n\sqrt{1-r^2})^2}\sqrt{1-r^2}$$

where $\sqrt{1-r^2}$ is the mass correction and m_1° is the rest mass of the bombarding particle.

If $m_1^\circ \ll m_n$ this approximates to

$$(\Delta E)_{max} = \frac{4 E m_1^\circ}{m_n}\sqrt{1-r^2}$$

or

$$= \frac{4E(E+m_1^\circ c^2)}{m_n c^2}$$

There is a critical energy $(\Delta E)_c$, suggested by Dienes (1958), which must be imparted to the struck atom if it is to be dislodged from its normal site. The value of this critical energy, as given by Dienes, is approximately four times the sublimation energy. For tightly bound atoms such as in metals and their salts, $(\Delta E)_c$ is the order of 15 to 30 ev. Determinations of the threshold bombarding energy for several materials are not in good agreement, but values for electrons are in excess of $5X10^5$ volts. It would be expected that for inorganic objects, the incident electron energy must exceed about $3X10^5$ volts, if the atoms are to be displaced from their normal positions. [illegible] are dislodged.

Observations by Pashley (1959) and Pashley and Presland (1961) on small dot structures in gold foils, and suggestive of the small dislocation loops found in quenched aluminium by Hirsch et all., (1958) were therefore quite disturbing. Electrons of an energy 80 to 100 kv should not be able to transfer more than about 1 ev to a gold atom, which is far below the critical energy for displacement. Those dots or loops were produced during observations in the electron microscope and were finally accounted for by Pashley and Presland (1962) by a significant experiment which proved that the small loops were a result of radiation damage. The damage was produced by oxygen ions from the electron gun and not by the electron themselves. On the basis of above equation an oxygen ion with E = 10^5 volts could impart $(\Delta E)_{max} = 3X10^4$ electron-volts to a gold atom. The occurence of displaced gold atoms and primary knock-ons is easily possible.

The source of oxygen ions is the reaction of residual oxygen in the column with the tungsten filament of the gun to produce ions which are then accelerated by the gun.

Electron irradiation may cause loss of fine structure, change in shape and even change in the dimension of crystal unit cell. An associated change sometimes observed is the increase of granular structure in specimen after intense irradiation. Such granularity may mask fine structure which would otherwise be observed.

Since the alkali halide crystals are dielectrics,

they are very sensitive to electron irradiation. In other words the electron irradiation can cause various kinds of defects. The nature and the shape of these defects depends on the intensity of the electron beam, irradiation time, thickness and size of the crystals, and even the technique of producing the crystals. When an alkali halide crystal is observed in an electron microscope, moving extinction contours appear at the beginning, especially when the crystal is illuminated unevenly and by a rather intense electron beam. These extinction contours could be due to the creation of internal local stress centres. The abrupt electron irradiation can electrify the crystal through excitation or ionization of the bond electrons. There is a possibility of temperature gradient in the direction of the electron beam due to the increase in thermal vibration of the lattice atoms. When the crystal is illuminated evenly with a weak electron beam, the production of extinction contours slows down or even stops. Then small black spots, without any particular geometrical shape, appear. These are shown in Fig. 2.27 and 2.30 in KCl and KBr crystals respectively.

With further weak electron irradiation loop structures appeared as shown in Fig. 2.25 and 2.26. These loops are usually along <100> directions and are probably formed from the agglomeration of vacancies which appear due to the displacement of atoms by irradiation. The mechanism of formation of a dislocation loop due to aggregated vacancies is shown schematically in fig. 2.29.

Fig. 2.25

Fig. 2.26

Fig. 2.25 and 2.26. Dislocation loops formed in NaCl crystals by electron irradiation in the electron microscope.

200nm

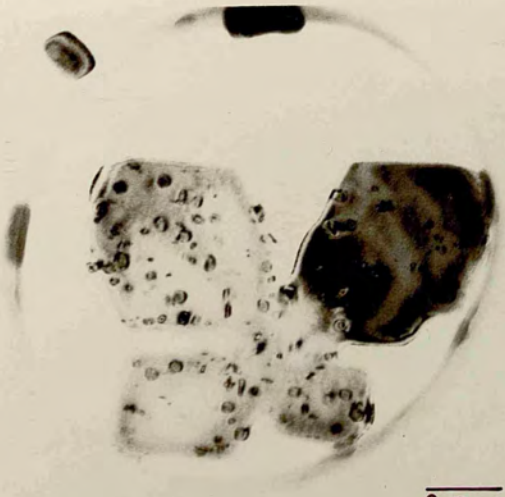

200nm

Fig. 2.27

Fig. 2.28

Fig. 2.27. Moving black spots appeared in a KBr crystal under weak electron irradiation.

Fig. 2.28. The appearance of large bright squares in KBr crystal under intense electron irradiation.

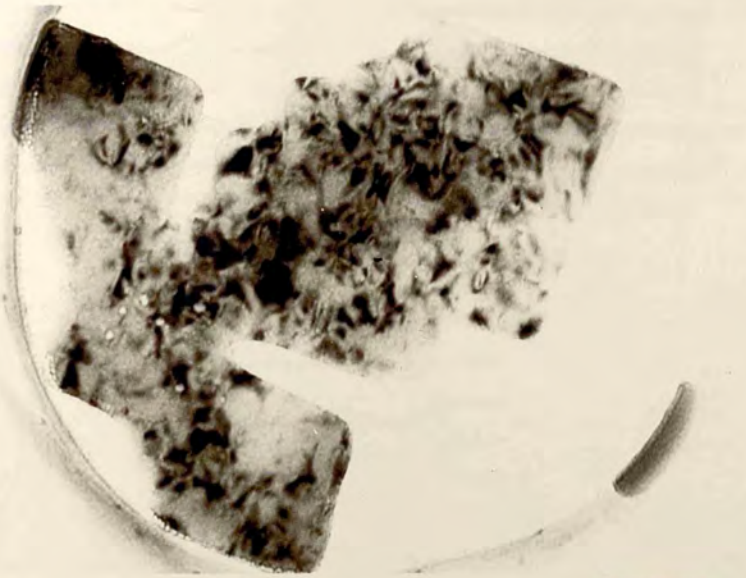
200nm


500nm

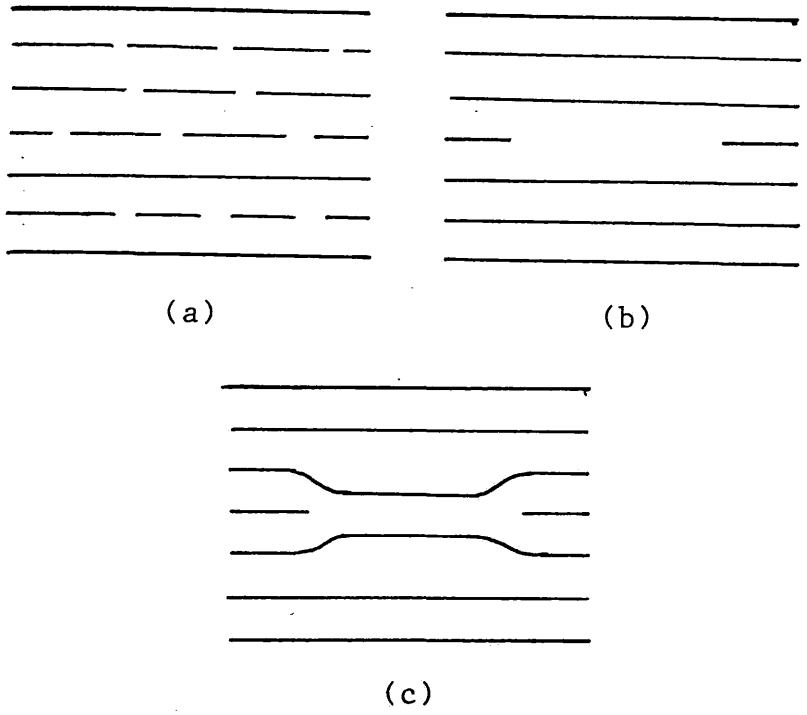

fig. 2.29 Collapsing of a ring-shaped cavity into a prismatic dislocation loop. (a) Vacancies are dispersed (b) Ring shaped cavity. (c) Vacancy loop.

While the loop structures are formed in the crystals due to weak electron irradiation, on the other hand, large bright squres appeared when the crystal was irradiated by an intense electron beam. Fig. 2.28 shows this change in a large KCl crystal under continuous intense electron irradiation. From the micrograph in this Fig., it has been observed that the squares are almost arranged in <100> directions. A possible explanation of these large bright squares is either sublimation of material due to heating caused by intense electron irradiation or the aggregation of small cube-like cavities. Under intense electron irradiation, small voids first appeared and become larger,

presumably by the aggregation of vacancies from various directions. Then the contraction of voids occured owing to the escape of vacancies in definite directions. The escaped vacancies then aggregated and very small square cavities, whose edges were arranged in <100> directions, were created here and there in the crystal. With further intese electron irradiation at this stage, these small cavities aggregated with one another and become large square-shaped cavities as shown schematically in Fig.2.31.

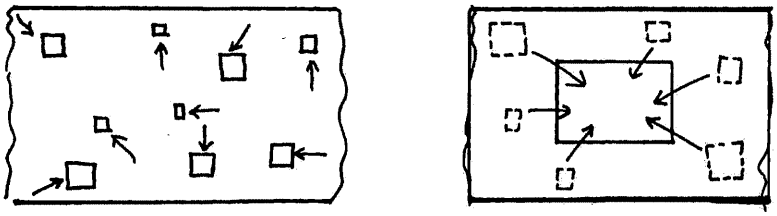

(a) (b)

Fig. 2.31 Schematic expression of the mechanism of vacancy coagulation in the crystal. (a) Small square cavaties. (b) Large square-shaped cavity.

The effect of intense electron irradiation on an NaCl crystal is shown in Fig. 2.32. It has been observed that there are a number of small square crystals appeared within the main crystal, their edges are lying with different directions but most of them have their edges along <100> directions and a few along <110> directions. Some of these square-shaped crystals are connected to each other by their corners parallel to <110> directions. The cause of production of these crystals is likely to be

either sublimation of the material around them leaving behind this type of shapes, or intense electron irradiation causing granularity on the surface which then rearranges to form small crystals. It is also possible that the intense electron irradiation divides the large single crystal into several small crystals at the surface. The granularity caused by electron irradiation has also been observed in a KBr crystal as shown in Fig. 2.33 (a). The whole crystal was covered by the small grains which were situated on the base crystal with different orientations. Most of them have fiber-like structure parallel to the electron beam as indicated by the diffraction pattern in Fig. 2.33 (b). From indexing of the pattern we know that the base crystal is normal to [233], (plane (233) of the crystal is normal to the electron beam). The observed orientations of the grains are [100], [111] and [211]. The [100] and [111] orientations have the fiber-like structure as all reflections due to these orientations appeared in arcs instead of spots.

When a crystal of CsI was observed in the electron microscope under weak electron irradiation, loop structure first appeared and then disappeared, showing many bright specks over the whole crystal. Whith the continued weak electron irradiation these bright specks diffused into each other, covering more area on the crystal. The sequence of this effect is shown in Fig. 2.34 (a), (b) and (c), and Fig. 2.34 (d) shows the diffraction pattern. The indexing of this pattern indicates that the

Fig. 2.30

Fig. 2.32

Fig. 2.30. Black spots produced in KBr crystal by weak electron irradiation.

Fig. 2.32. The effect of intense electron irradiation on a NaCl crystal. Many square-shaped crystals appeared on the surface of base crystal.

200nm

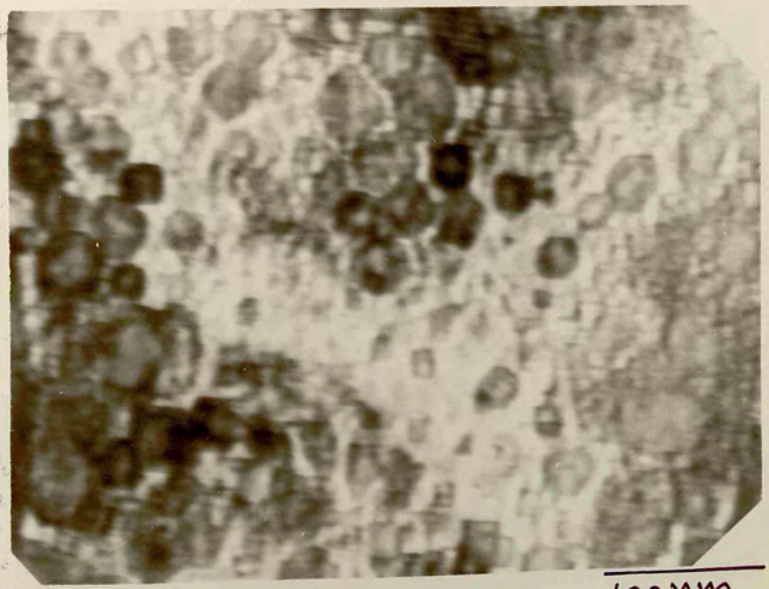

100nm

Fig. 2.33 (a)

Fig. 2.33 (b)

Fig. 2.33. Granularity caused by electron irradiation in a KBr crystal, some of the grains have fiber structure with [001] and [111] orientations (the thin crystal is normal to [100]).

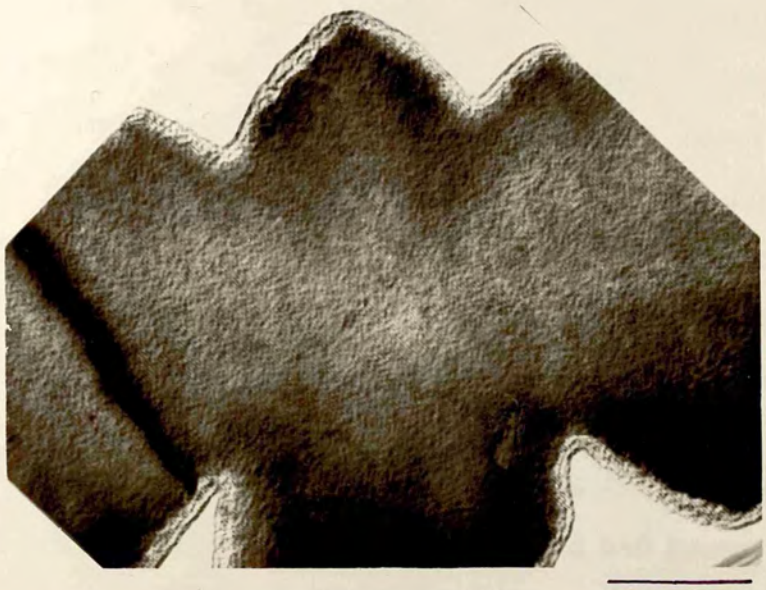
500 nm

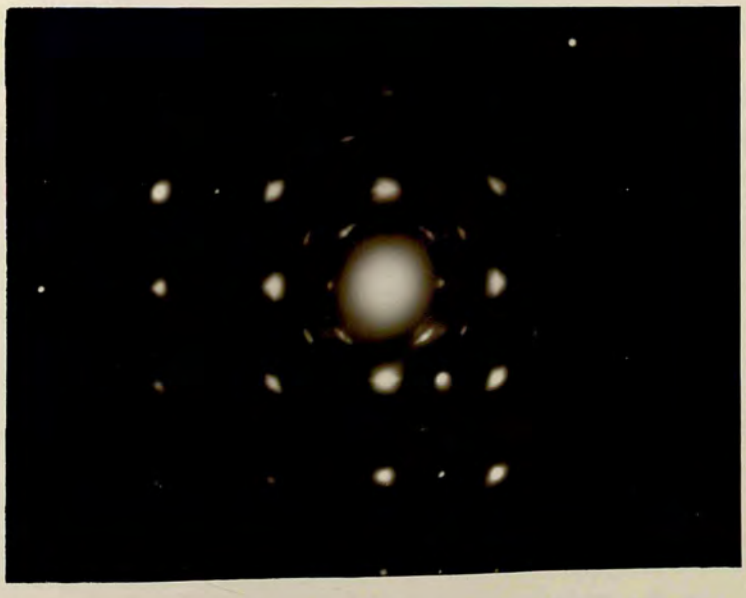

the more intense spots are caused by a crystal which is normal to [135]. The less intense spots which are streaked and abnormally spaced between the more intense spots, indicate disorder in the crystal. Defects such as vacancies or dislocations due to electron irradiation create extra planes in the crystal with abnormally spacings. An other possibility is lattice bending due to electron irradiation, which can also produce extra spots with streaks.

Fig. 2.35 shows a micrograph of a CsI crystal observed in the electron microscope after gold had been sputtered on it. The combined effect of ions bombardment in the sputtering unit and electron irradiation in electron microscope, appears to have produced grain boundaries in the crystal. The micrograph in Fig. 2.36 is from another CsI crystal with non-uniform thickness as indicated by the dark and bright areas separated by thickness fringes. It has been seen from this micrograph that the vacancy loops appeared only in the thinner area of the crystal . These loops are usually along <100> direction and a few loops are perpendicular to them. In the thick region of the crystal there are several bright specks and small cube-like cavities have been observed . The large bright squares, observed in this micrograph, are formed by the aggregation of small cavities into a large cube cavity as discussed earlier in the case of KCl. These bright squares have their edges lying along <100> and <110> directions.

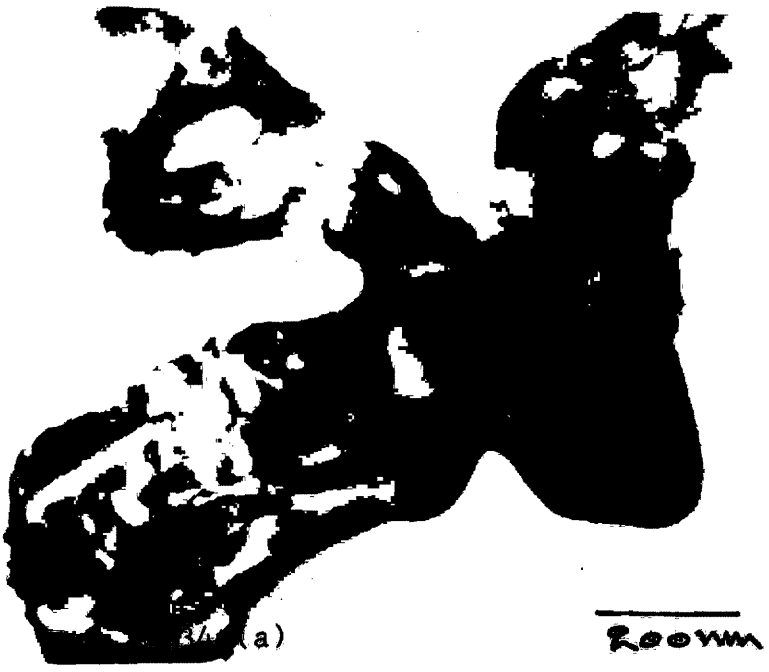

Fig.
under weak
1 minute


200nm


200nm

Fig. 2.34 (c)

Fig.

Fig. 2.3

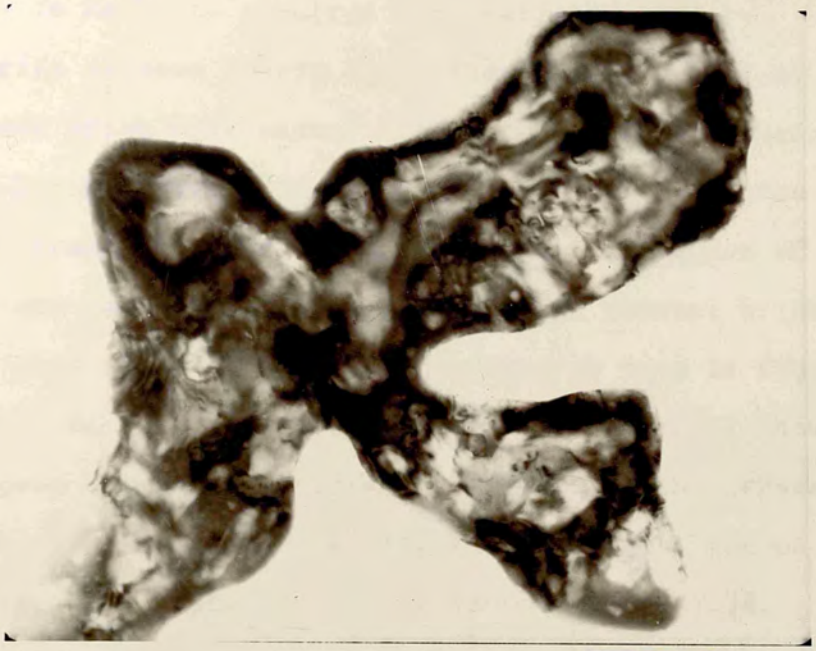
200nm

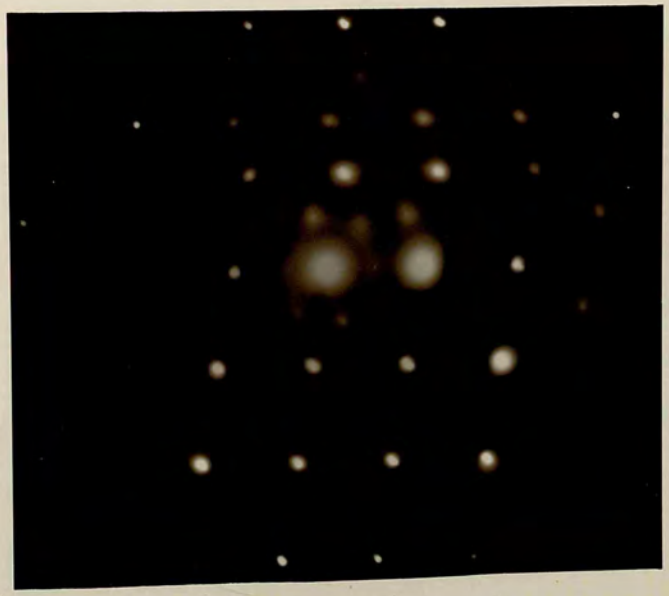

In CsCl the electron irradiation causes granularity as seen in Fig 2.37. There are a number of dark spots which move across the whole dendritic crystal leaving behind bright specks. With further irradiation large dislocation loops appeared in the thin region of the crystal and the relatively thick area has several bright specks, some of which are squared-shaped as seen in Fig. 2.39 (a). The diffraction pattern in Fig. 2.39 (b) shows extra spots due to misoriented fragments in the crystal caused by dislocations. The effect of intense electron irradiation on a CsBr crystal is shown in Fig. 2.38.

Fig. 2.40 (a) shows a micrograph of a CsF crystal after intense electron irradiation for a longer time (about 5 minutes). The whole crystal divided into several small cube-shaped crystals oriented randomly as indicated by its diffraction pattern in Fig. 2.40 (b).

2.10. Application of the Crystals as a Substrate.

The importance of electron transparent substrates in the study of nucleation and growth by transmission electron microscopy was explained in section 2.3. But there are a number of other advantages in using the crystals, in the holes of carbon support film, as a substrate. Some of them are discussed here:

1. Since these crystals are not located on an amorphous film, they are more transparent than similar

Fig. 2.35

Fig. 2.36

Fig. 2.35. The grain boundaries formed in a GaI crystal after sputtering of gold and then examined in the electron microscope (the combined effect of heavy and light particles bombardment).

Fig. 2.36. The formation of dislocation loops and bright square-shaped cavities in a GaI crystal by intense electron irradiation.

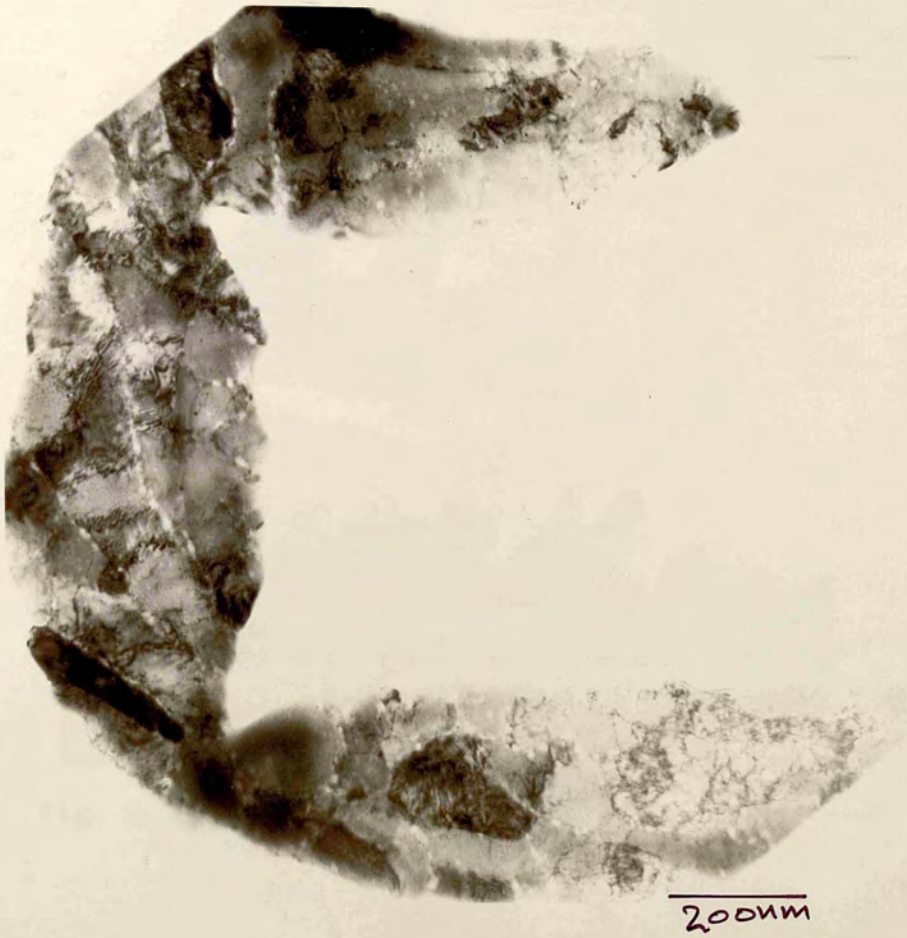
200nm

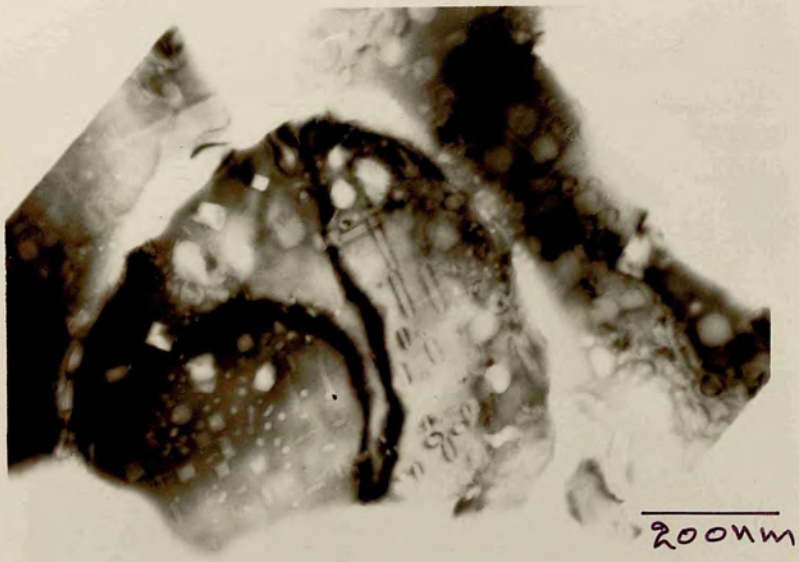
200nm

Fig. 2.37

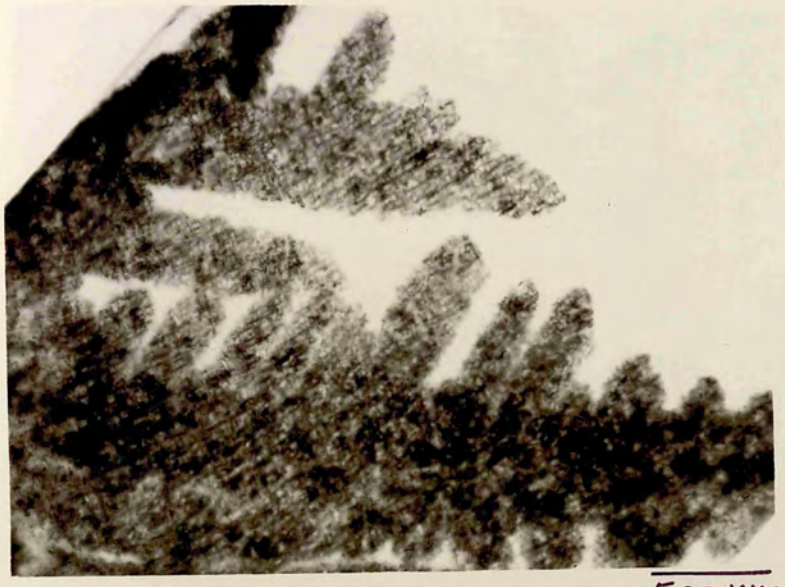
500 nm


500 nm

Fig. 2.39 (a)

Fig. 2.39 (b)

Fig. 2.39. Dislocation loops in CsCl crystal caused by electron irradiation. (a) Micrograph. (b) Diffraction pattern.

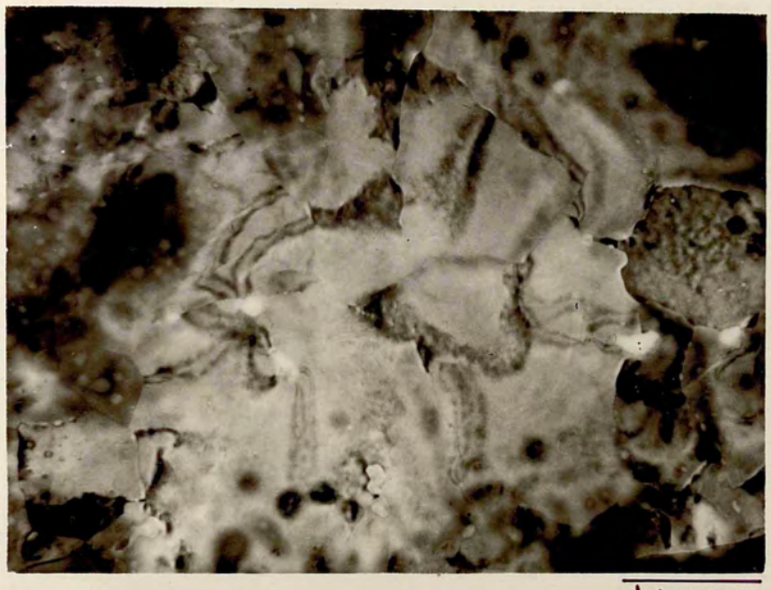

100nm

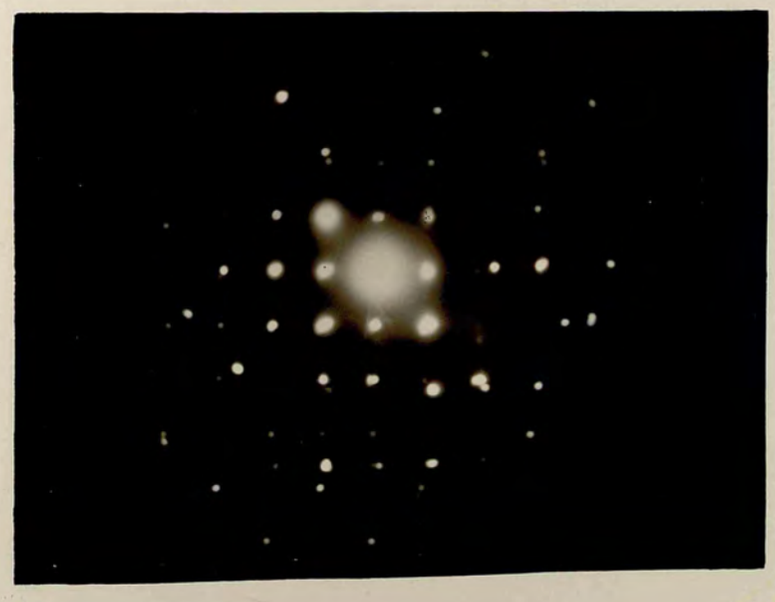

Fig. 2.40 (a)

Fig. 2.40 (b)

Fig. 2.40. The effects of [illegible] electron irradiation on [illegible] crystal. (a) Electron micrograph, the crystal [illegible] a large number of [illegible] small square-[illegible] crystals. (b) [illegible] particles.

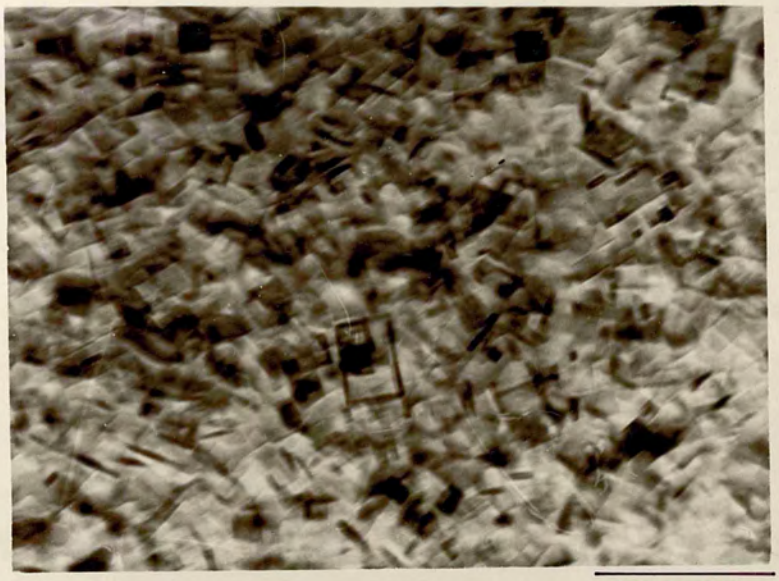
100nm

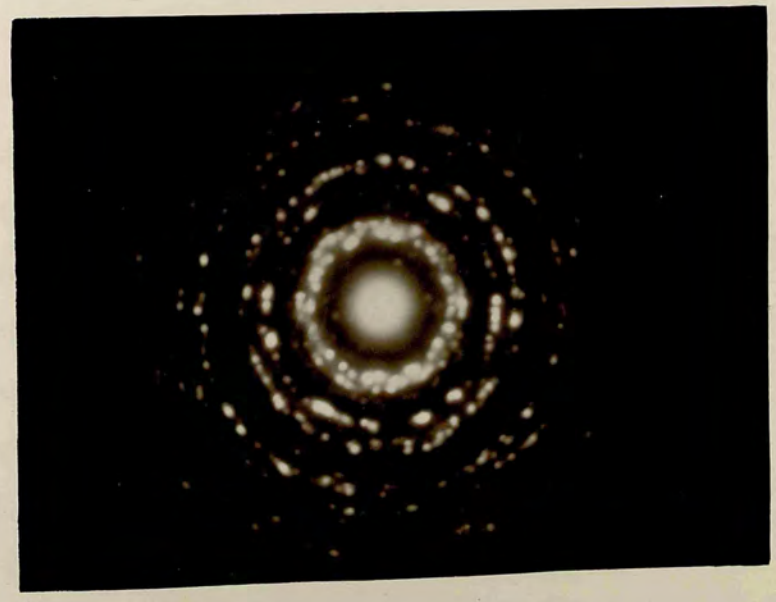

crystalline substrate which are on the support film. Although 15 to 20 nm carbon support film does not affect the transparency of the crystals on it, the lack of ordered structure in amorphous material gives rise to a considerable background scattering of electrons in the electron microscope which reduces the contrast of the observable features in the specimen. Very weak reflections in diffraction patterns can not be detected in the presence of a carbon support film.

2. The crystal growth occurs in free space, so these crystals have nearly the same structural properties as bulk crystals, especially their surfaces which have a vital role in the nucleation and growth studies. For crystals which are formed on the support film , the preparation of the support film, especially its surface state can affect the crystals and their surfaces.
3. Having two free faces these substrates provide a unique possibility for growing films on both sides of the crystals simultaneously or one at a time, so as to observe if there is any relation between the nuclei on the each side of the crystal.
4. The new technique of growing crystals in the holes of perforated carbon support film is practically much easier than the techniques discussed in section 2.5, and its reproducibility is remarkably good.

Nowadays freshly cleaved or vacuum cleaved substrates are used frequently, and it might be thought that this is an advantage over the crystals produced by the new technique, but as will be shown in chapter 5, alkali halides grow epitaxially on alkali halide substrates. Therefore a fresh surface of alkali halide can be obtained by depositing a layer of alkali halide as a substrate before depositing the overgrowth.

The crystals in the holes have quite flat surfaces. To study the surface flatness, different thicknesses of gold were deposited on the crystals and observed in the electron microscope . Fig. 2.41 (a) shows a micrograph of relatively thick gold on a single crystal of CsI. Small crystallites of gold grow randomly on the surface of the crystal as its diffraction pattern (Fig. 2.41, b) indicates. A similar result was obtained when a very thin deposit of gold was observed on dendritic crystals of CsI and on large single crystals of CsI (Fig. 2.42, 2.43 and 2.44, a). Crystals with spirally decorated lines of gold, which are seen on bulk NaCl crystals, are not observed here. No step structure has been observed, the crystallites of gold are evenly distributed on the surface of the substrate crystals, indicating the flatness of the surface. However on the surface of CsCl (Fig. 2.45, a), some irregular patterns are observed, but as indicated from diffraction pattern (Fig. 2.45, b) there is no regular orientation between the gold and CsCl. From these experiments it can be said that CsI has the flattest surface among the halides of Cs when grown in this way.

Fig. 2.41 (a)

Fig. 2.41 (b)

Fig. 2.41. A [illegible] of gold on [illegible] at room temperature [illegible] and corresponding diffraction [illegible]

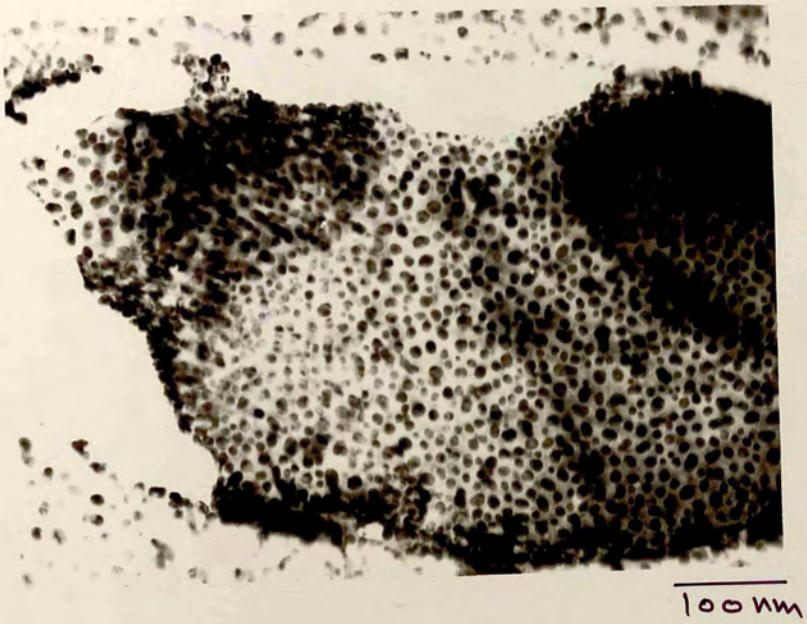
100nm

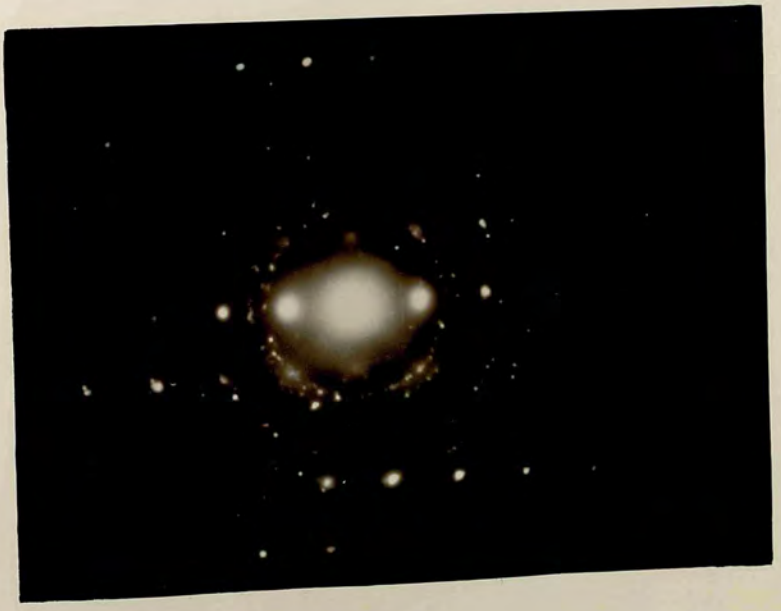

Fig. 2.42

Fig. 2.43

Fig. 2.42. A thin [illegible] dendrites.

Fig. 2.43. Thin [illegible] large crystal of CsI at room temperature. Thickness is less than 10 [illegible] evenly distributed [illegible] crystal.


500nm


100nm

Fig. 2.44 (a)

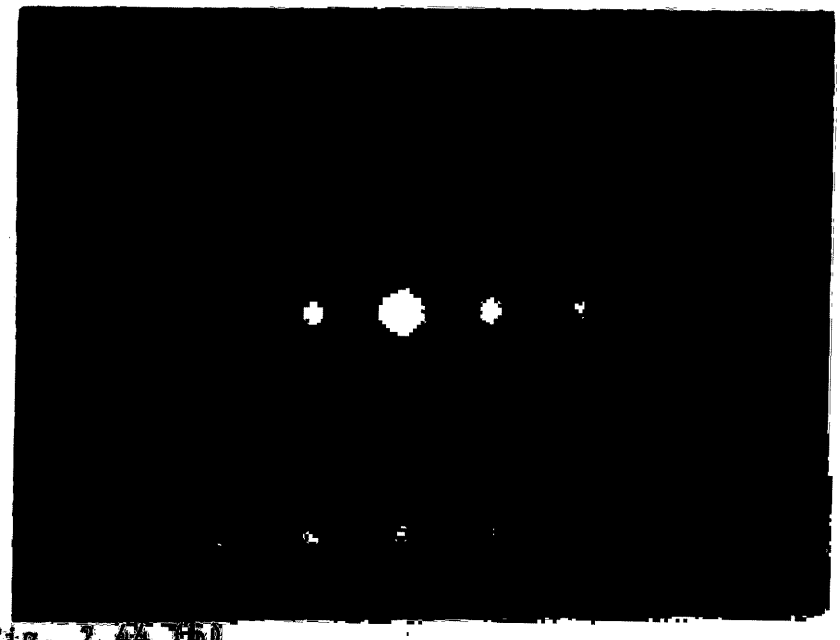

Fig. 2.44 (b)

Fig. 2.44. Gold deposit on a large crystal of CsI and corresponding diffraction pattern.


200nm

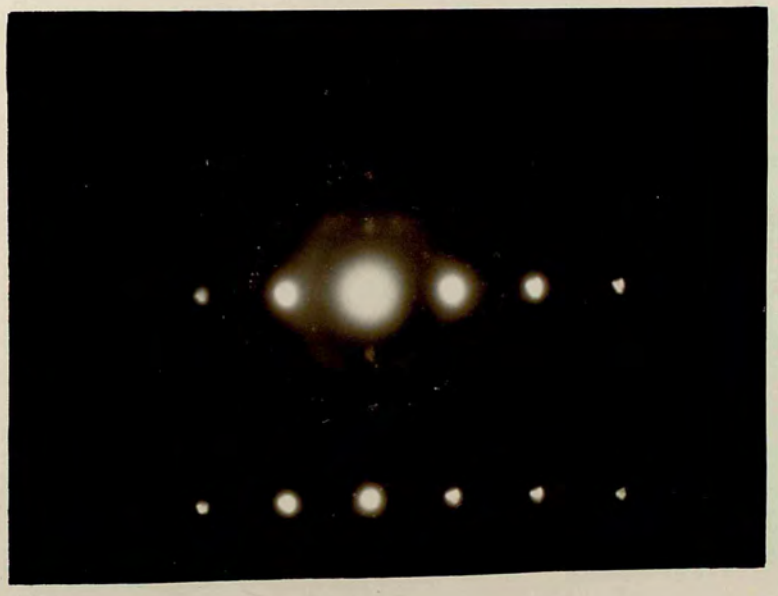

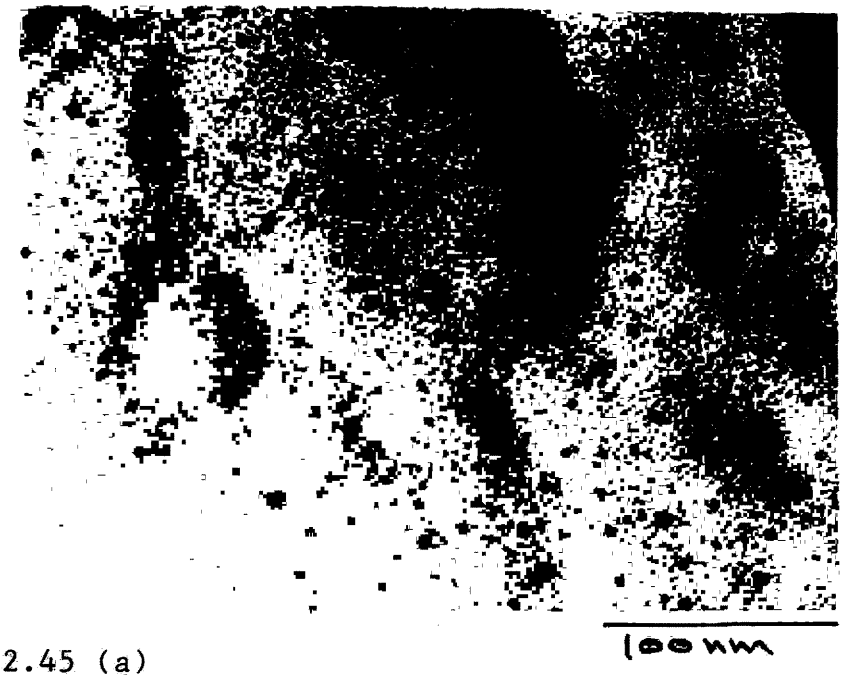

Fig. 2.45 (a)

Fig. 2.45 (b)

Fig. 2.45 (a). Electron micrograph of a gold deposit on CsCl crystal at room temperature. Deposit thickness = 20 nm and the deposition pressure

100 nm

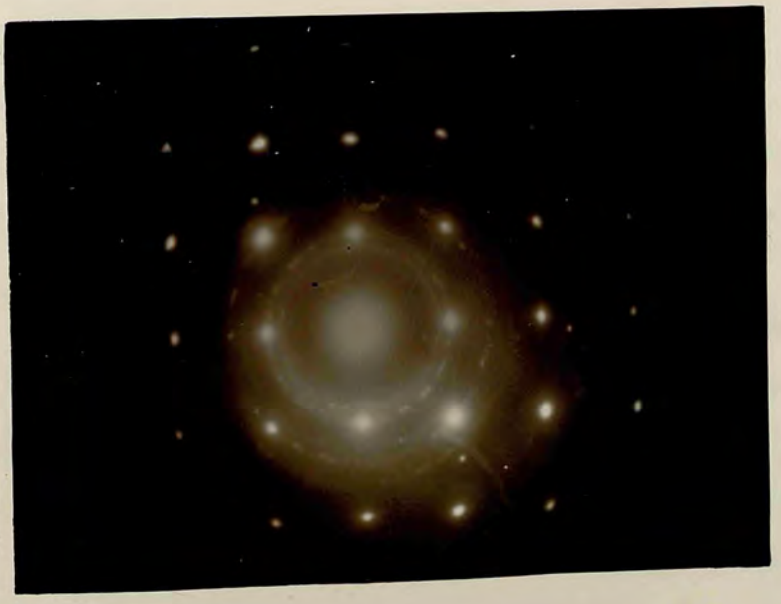

References

AMELINCKX,S. (1964). In "Solid State Physics," Supplement 6, 'The Direct Observation of Dislocations' page 123, Academic Press London.

BACHMANN,L. and HILBRAND,H. (1966). In "Basic Problems in Thin Film Physics," page 77, Vandenhoeck and Ruprecht, Goettingen.

BAUER,E. (1958). Z. Kristallogr. 110, 372.

BECKER,R. and DÖERING,W. (1935). Ann. Physik, 24, 719.

BECKER,R. (1938). Ann. Phys. 32, 128.

BENNEMA,P. and GILMER,G.H. (1973). In "Crystal Growth: an Introduction," (Hartman eds.). page 263. North-Holland Amsterdam.

BENNEMA,P. (1974). J. Crystal Growth, 24/25, 76.

BENNEMA,P. (1976). In "Industrial Crystallization," (Mullin ed.). page 91, Plenum Press New York.

BRICE,J.C. (1973). The Growth of Crystals from Liquids. North-Holland, Amsterdam.

BRICE,J.C. (1976). In "Crystal Growth and Materials," Review papers ECCG-1 (First European Conference on Crystal Growth), Zurich (Kalidis and Scheel eds.). page 571. North-Holland Publishing Co. Amsterdam.

BRICE,J.C. (1976). In "The Growth of Crystals from Liquids" Vol. XLI, 'Selected Topics in Solid State Physics', (Wohlfarth ed.). North Holland Publishing Co.

BROCKWAY,L.O. and MARGUS,R.B. (1963). J. Appl. Phys. 34, 921.

BUCKLEY,H.E. (1951). Crystal Growth. Chapman & Hall London.

COSSLETT,V.E. (1969). Q. Rev. Biophys. 2, 95.

DEINES,G.J. (1958). In "The Effect of Radiation on Materials" (Harwood, ed.). page 1, Reinhold Publishing Co. New York.

DEMNY,J. (1965). Z. Naturforch, 20 (a), 1047.

ELWELL,D. and SCHEEL,H.J. (1975). Crystal Growth from High-Temperature Solutions. Academic Press New York.

GIBBS,J.W. (1928). Collected Works, Vol. 1, Longmans Green London.

GLAESER,R.M., COSSLETT,V.E. and VALDRE,U. (1971). J. Microscopie. 12,133.

GREEN,A.K., BAUER,E. and DANCY,J. (1969). In "Molecular Processes on Solid Surfaces," page 479. McGraw-Hill, New York.

GREEN,A.K., DANCY,J. and BAUER,E. (1969). J. Vac. Sci. Technol. 7, 159.

GREEN,A.K., BAUER,E., PEEK,R.L. and DANCY,J. (1970). Krist. Tech. 5, 345.

GREEN,A.K., DANCY,J. and BAUER,E. (1970). J. Vac. Sci. Technol. 7, 159.

HARRIS,W.J. (1962). Nature 196, 499.

HEIDENREICH,R.D. (1964). In "Fundamentals of Transmission Electron Microscopy" page 61, Interscience Publishers, John Wiley & Sons, New York.

HEYDENREICH,J. (1969). Rev. Roum. Phys. 10, 1255.

HIBI,T. and YADA,K. (1960). J. Electron Micr. 9, 101.

HIRSCH,P.B., SILCOX,J., SMALLMAN,R.E. and WESTMACOTT,K.H. (1958). Phil. Mag. 3, 897.

INO,S., WATANABE,D. and OGAWA,S. (1964). J. Phys. Soc. Japan, 19, 881.

IZUMI,K. (1969). J. Phys. Soc. Japan 26, 6.

JAEGER,H., MERCER,P.D. and SHERWOOD,R.G. (1969). Surface Sci. 13, 349.

KAY,D. (1967). In "Techniques for Electron Microscopy" (Second Edition). page 71, Blackwell Scientific Publications Oxford.

MATTHEWS,J.W. and GRUNBAUM,E. (1965). Phil. Mag. 11, 1233.

MEEK,G.A. (1970). In "Practical Electron Microscopy for Biologists". page 324, Interscience Publishers, John Wiley & Sons, New York.

MIERS,H.A. (1904). Phil. Trans. A 202, 459.

MIERS,H.A. and ISAAC,F. (1906). J. Chem. Soc. 89, 413.

MIERS,H.A. and ISAAC,F. (1907). Proc. Roy. Soc. A 79, 322.

MIERS,H.A. (1927). J. Inst. Metals 37, 331.

MILLER,R.F. and HOFFMAN,R.W (1968). Vacuum Sci. and Tech. 6, 1.

MOLL,J. (1963). le Vide, no. 105, page 248.

MOLLENSTEDT,G., GRAFF,K. and SPEIDEL,R. (1962). Z. Phys. 167, 367.

MULLIN,J.W. (1972). Crystallization, 2nd ed., Butterworth London.

MULLIN,J.W. (1976). Industrial Crystallization. Plenum Press New York.

NYVLT,J. (1971). Industrial Crystallization from Solutions. Butterworth London.

PASHLEY,D.W. (1959). Phil. Mag. 4, 316.

PASHLEY,D.W. (1959). Phil. Mag. 4, 324.

PASHLEY,D.W. and PRESLAND,A.E.B. (1961). J. Inst. Metals 87, 419.

PASHLEY,D.W. and PRESLAND,A.E.B. (1962). Phil. Mag. 6, 1003.

PLISKIN,W.A. and ZANIN,S.J. (1970). In "Handbook of Thin Film Technology" (Maissel and Glang eds.), page 11-1 MeGraw-Hill Book Co. New York.

ROBERTS,R.W. (1963). Brit. J. Appl. Phys. 14, 537.

SELLA,C. and TRILLAT,J.J. (1964). IN "Single Crystal Films" (Francombe and Sato eds.), page 201, Pergamon Press, New York.

STENN,K. and BAHR,G.F. (1970). J. Ultrastruct. Res. 31, 526.

STRICKLAND-CONSTABLE,R.F. (1968). In "Kinetics and Mechanisms of Crystallization," Academic Press London.

TAVASSOLI,M.T. (1978). Ph.D. Thesis, page 24, University of London.

THACH,R.E. and THACH,S.S. (1970). Proc. 7th Int. Cong. Electron Microscopy, Grenoble. 1, 465.

THACH,R.E. and THACH,S.S. (1971). Biophys. J. 11, 204.

VOLMER,M. (1929). Z. Phys. Chem. 25, 555.

WALTON,D., RHODIN,T.N. and ROLLINS,R.W. (1963). J. Chem. Phys. 38, 2698.

WILHELM, and OSTWALD, (1897). Z. Phys. Chem. 22, 289.

YAGI,K. and HONJO,J. (1964). J. Phys. Soc. Japan 19, 10.

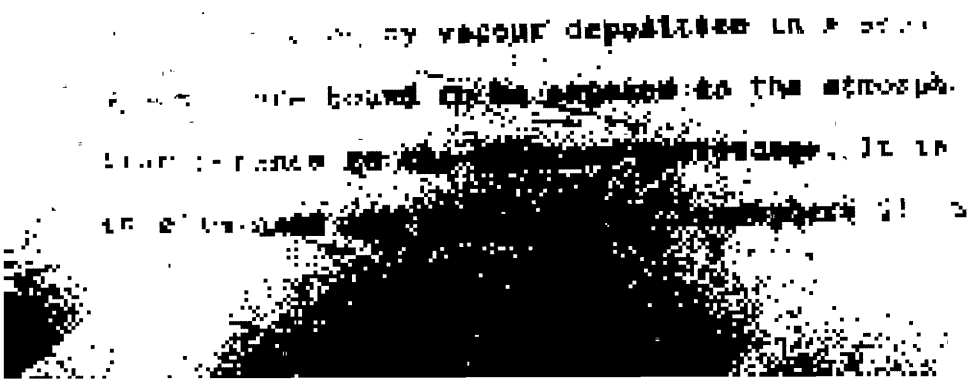

CHAPTER THREE

INSTRUMENTATION

This chapter describes some of the devices which have been designed and used for this work. They are:

1. A transport chamber to transfer the specimen from a vacuum deposition system to the electron microscope without exposing it to the atmosphere.
2. An intermediate chamber which is used to attach the transport chamber to the vacuum deposition system.
3. A heater for the substrates transferred to the electron microscope by means of transport chamber.
4. A device to heat the substrates on the electron microscope grids, which can also be used in α sputtering system.
5. A special specimen holder which used to determine the variation in camera constant with objective lens current in JEM-6 electron microscope.

3.1 Introduction.

Thin films prepared either by stripping from a bulk sample or by vapour deposition in a separate vacuum system, are bound to be exposed to the atmosphere during transference to the electron microscope. It is necessary to eliminate the effect of the atmosphere if the

nucleation and growth of atmospherically reactive or hygroscopic materials are to be studied by transmission electron microscopy.

One simple method is to carry out deposition on a substrate inside the electron microscope. This technique allows the nucleation and growth process to be observed continuously. Ennos (1953), Pashley and Stowell (1962) and Pashley (1965) have used this meathod to study the structural changes in deposits during growth. Although this technique has advantages, there are several major problems that make in situ growth experiments difficult. For example the extreme space limitation in the region of the specimen inside the electron microscope restricts the choice of type, angle and distance of the evaporating system with respect to the substrate. The relatively poor vacuum in the electron microscope column is a further drawback. Carbonaceous contamination also forms on the specimen during illumination by the electron beam. In the long term there is also a possibility of contaminating the electron microscope by sample materials, which can effect its performance and lead to serious reduction in image quality.

Another method of overcoming the problem of atmosphere reactivity is to cover the film with an inert, preferably amorphous, film before exposing to the atmosphere. The main disadvantage in this technique is that the protective film increases the thickness of the specimen thereby reducing the image visibility, contrast

and resolution, all of which are vital in the observation of the early stages of the nucleation and growth.

3.2 Transport Chamber.

Nearly all alkali halides are reactive with the atmosphere and most of them are hygroscopic. Therefore, a device was designed and constructed to transfer a specimen of such a material from a vacuum deposition system into the JEM-6 electron microscope without exposure to the atmosphere. We refer to this device as a "transport chamber".

Fig. 3.1 is a photograph and Fig. 3.2 (a) and (b) show its schematic drawings, side view and top view respectively. The main body of the chamber is machined from solid duralumin. It is cylindrical, about 22 cm long and 12 cm in outer diameter. The size and shape of the outer surface is such that it can be easily inserted horizontally into the column of JEM-6 electron microscope in place of specimen chamber. The photograph in Fig. 3.3 shows the transport chamber in the electron microscope column. Two vertical o'rings on either side of the main body (13 in Fig. 3.2) provide the vaccum seal. There is a vertical hole about 4 cm in diameter (3 in Fig. 3.2) for the electron beam. There is a horizontal tube (2 in Fig. 3.2) about 6.5 cm long which has an L shape base on one end by which it is fitted inside the main body from one end. This tube is sealed by an o'ring and made tight by

six screws with the main body. The other face has a groove for an o'ring (12 in Fig. 3.2). The depth of the groove is nearly twice the thickness of the o'ring used here , so that the o'ring can be placed deep in the groove. This tube is closed by a sealing cap (3 in Fig. 3.2) which comes forward by turning the lead screw controlled by an external knob. The open side of sealing cap has a sharp edge which comes into the groove in the tube and compresses the o'ring in the groove , providing good vacuum seal for the interior of the small chamber formed by the tube and cap.

Both ends of the main body are closed by lids (6 and 7 in Fig. 3.2). Lid (7) has a central hole for the lead screw in which there is placed a small o'ring providing a vacuum seal on this end of the main body. A small circular plate is fitted to this lid which works as a bearing for the screw. The lid on the other end (6) also has a hole, an extension tube (11 in Fig. 3.2) is fitted by means of a plate to this hole. This extension tube together with a valve permits other systems (vacuum pumps and gauges for evacuation of the transport chamber alone, and gases and water vapour stream to treat the specimen inside the transport chamber) to be connected with the transport chamber. Integral with the sealing cap, are two push rods (22 in Fig. 3.2) which operate the specimen lifting mechanism. The specimen lifting device is fixed on a bracket support attached to the lid inside the tube (14 in Fig. 3.2). This mechanism consists of a lever and a

Fig. 3.1. [illegible]

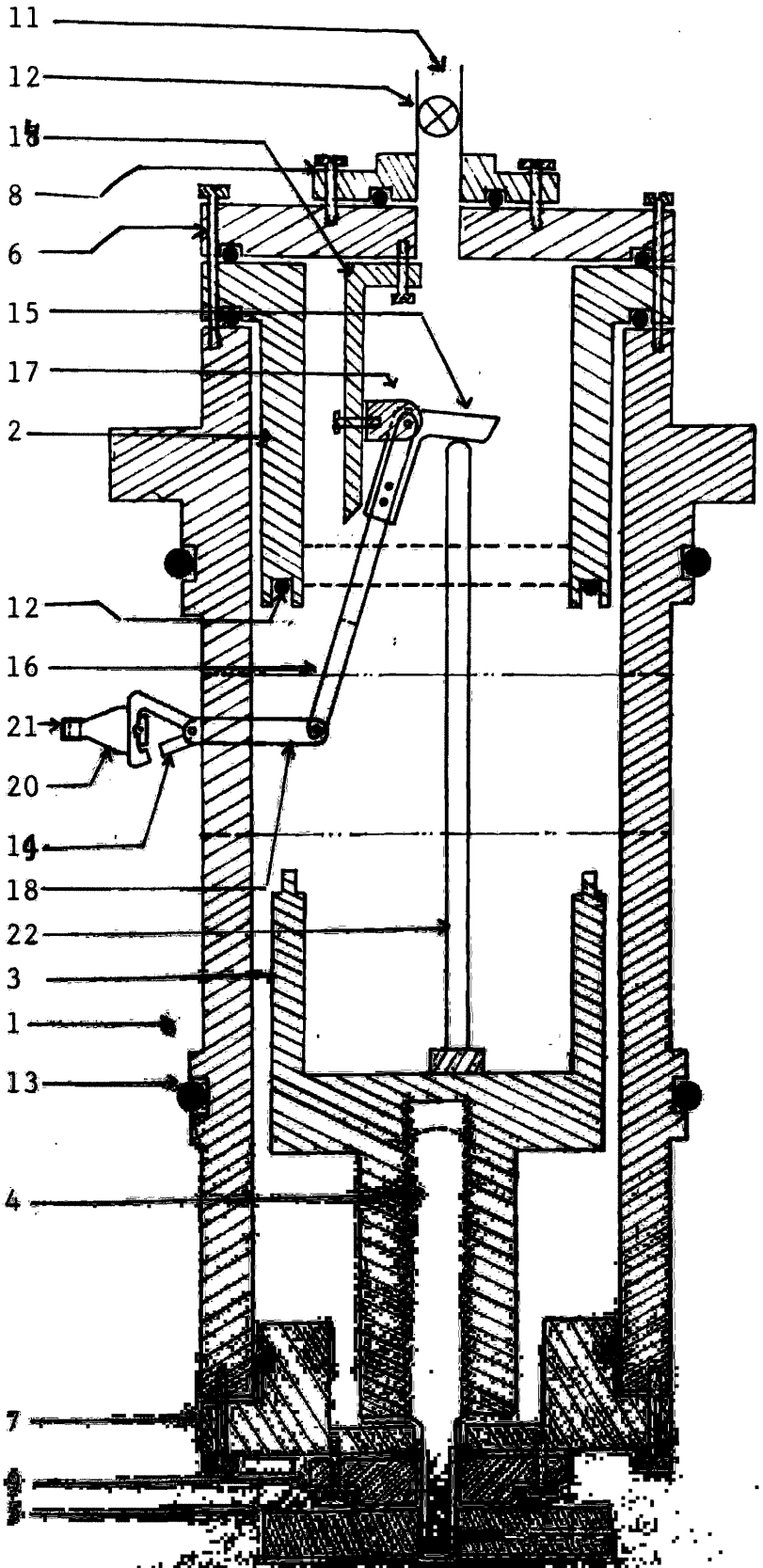
11
12
8
6
15
17
2
12
16
21
20
18
22
3
1
13
4
7

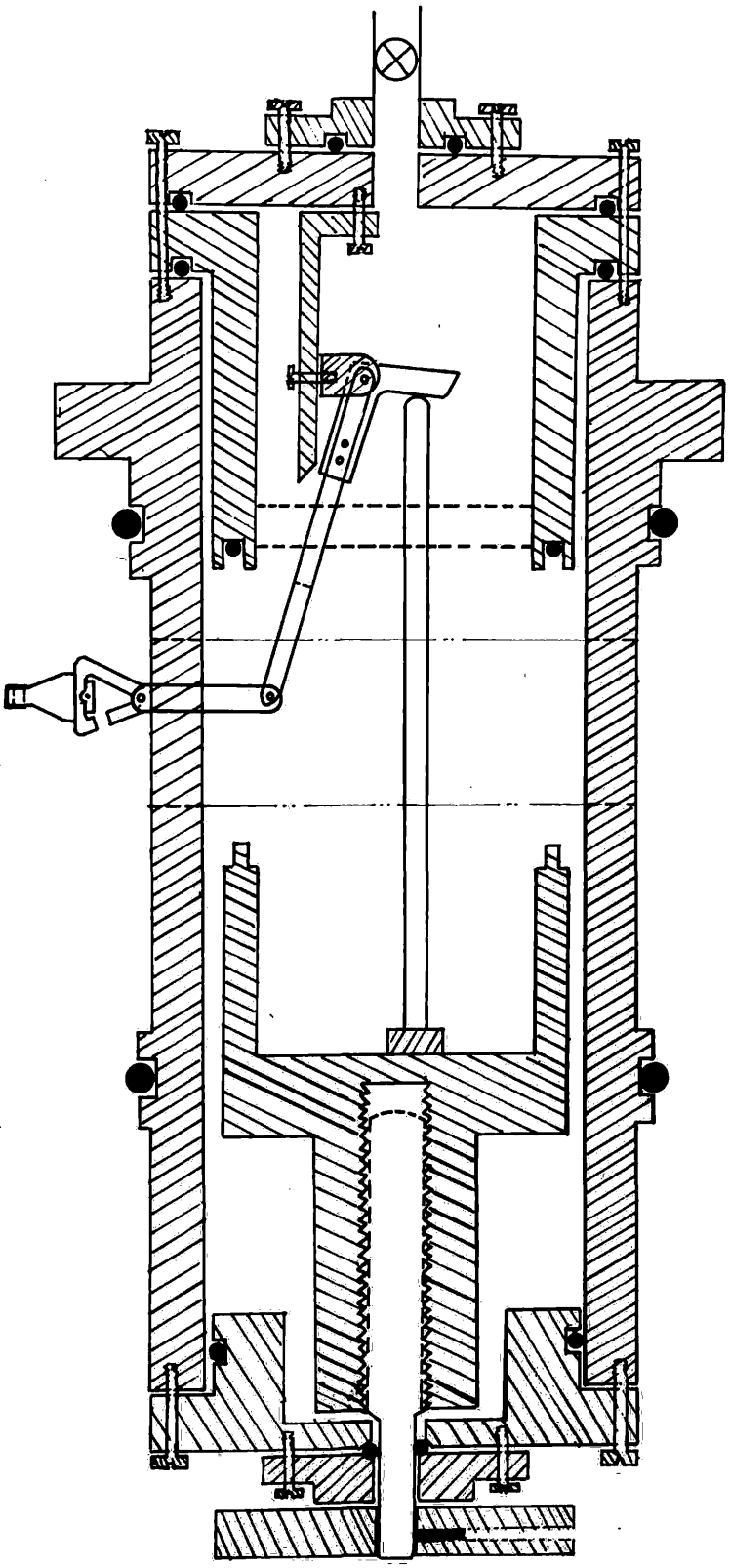

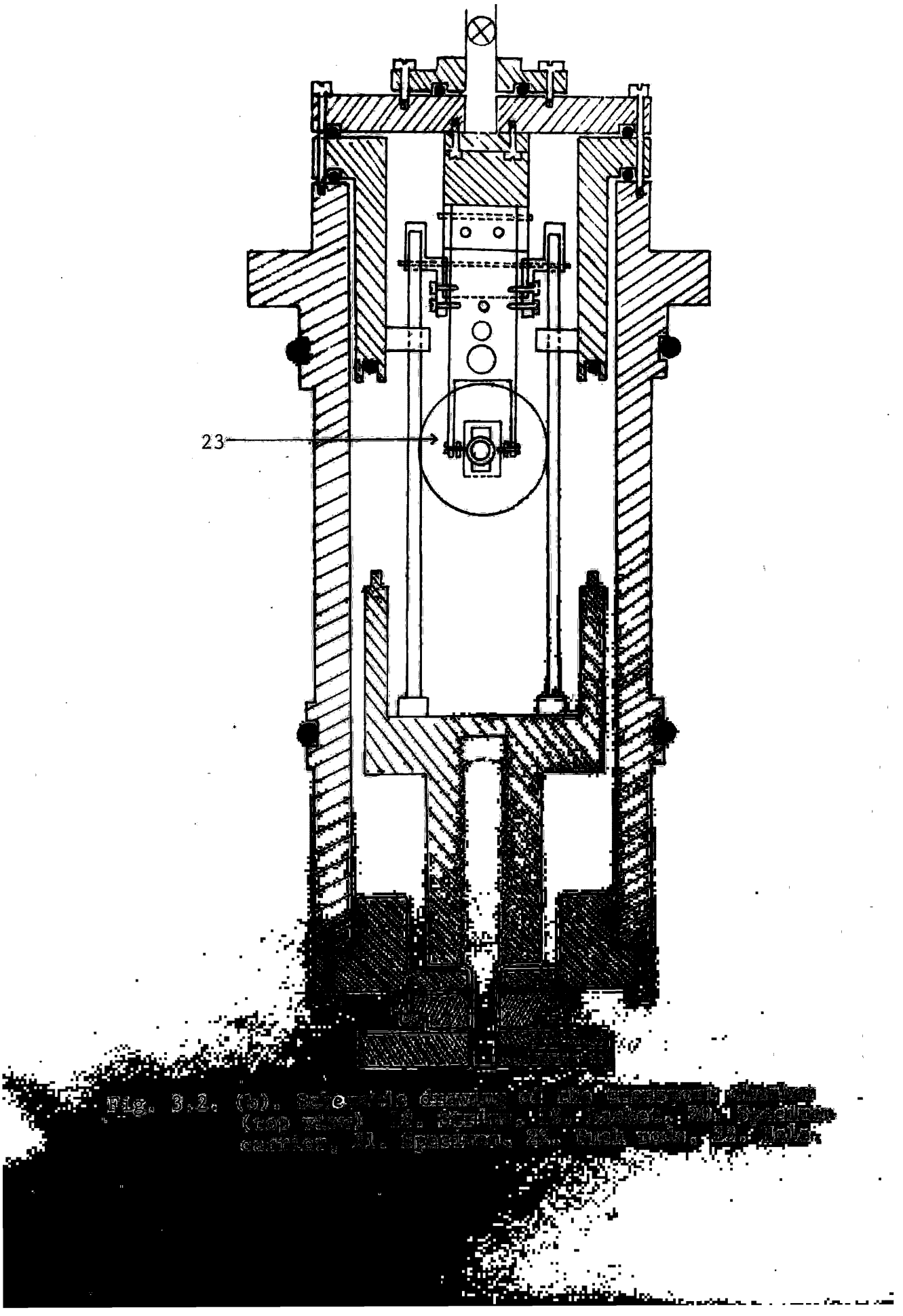

Fig. 3.2. (b). Schematic drawing of the specimen chamber (cap removed). 23. Specimen, 24. Specimen carrier, 25. Spacers, 26. Rack rods, 27. Hole

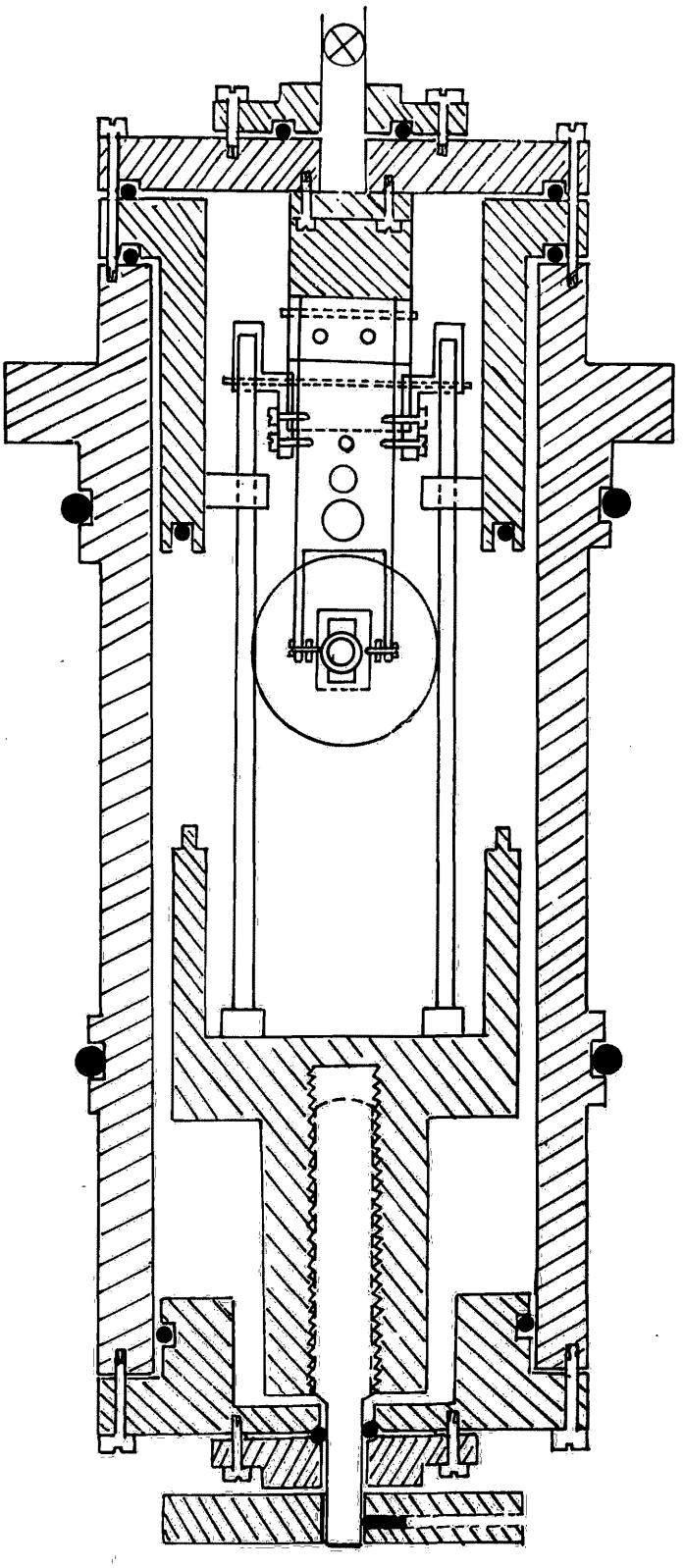

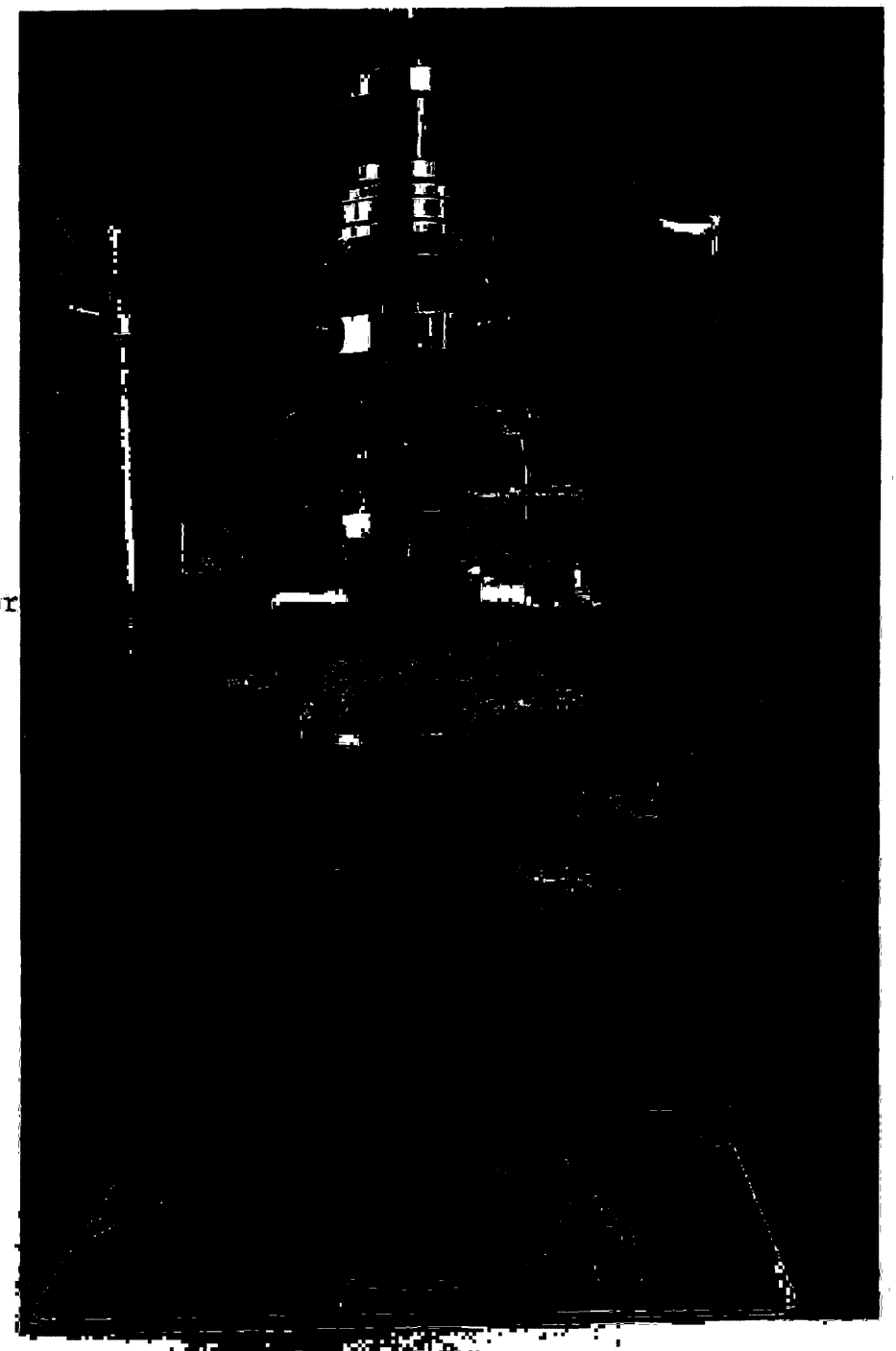

Fig. 3.3a. Preparation chamber in the JEM-6 Electron microscope column.

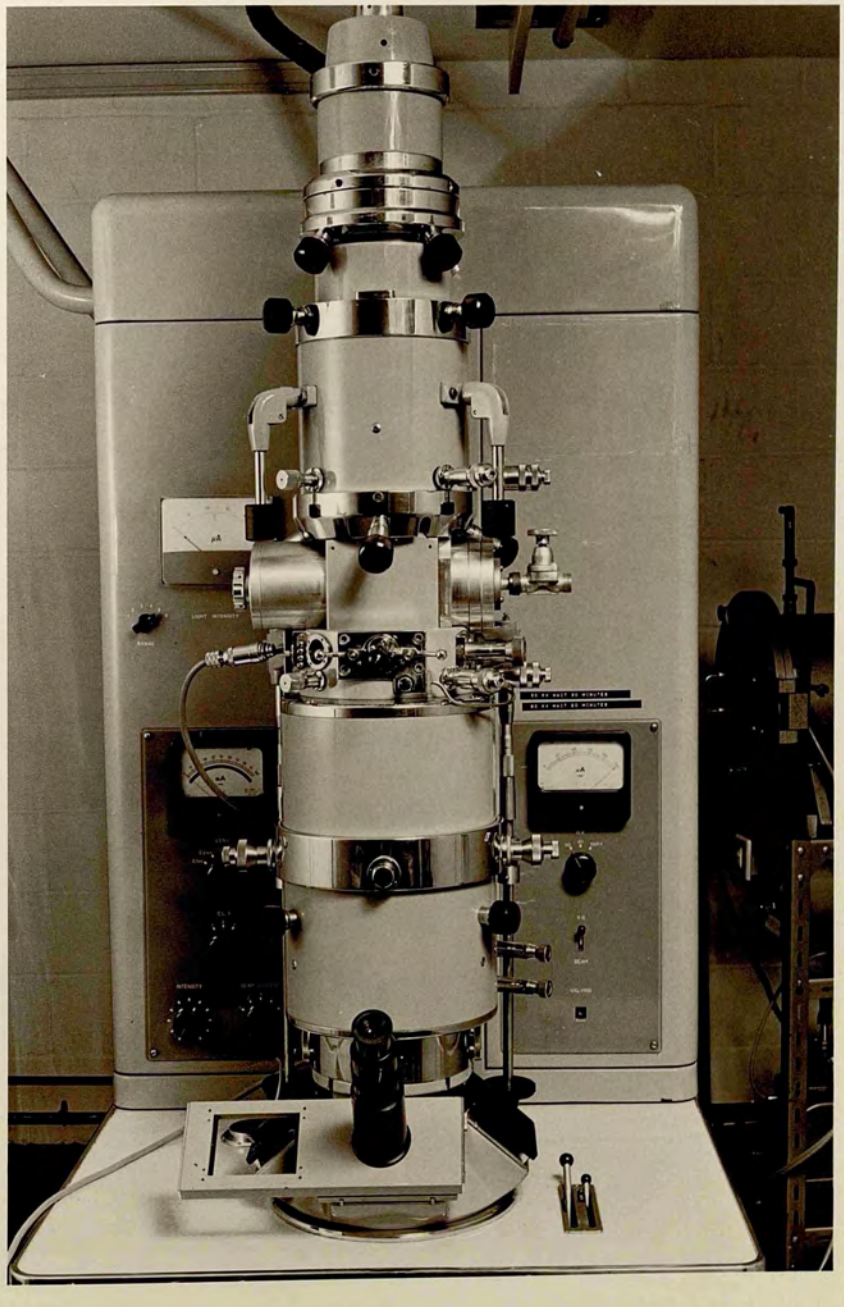

long fork arm pivoted with a loose pin on a fulcrum (15, 16 and 17 in Fig. 3.2). A basket is hung vertically on the other end of the fork arm with the help of two metal strips. The specimen carrier is nearly the same as the original one for the JEM-6 electron microscope but has longer pins on either side, so that it can be easily hung into or removed from the basket.

To close the system the knob (5 in Fig. 3.2) is turned anticlockwise, this causes the sealing cap to move forward and simultaneously causes the specimen carrier to lift by the action of push rods on lever. The transport chamber is inserted into the electron microscope instead of the specimen chamber as shown by the photograph in Fig. 3.3. To open the system, the knob is turned clockwise, the sealing cap is retracted and so the push rods, allowing the specimen carrier to lower into position in the specimen stage. When it is fully lowered the carrier disengages from the basket and any area of the specimen can be exposed to the electron beam.

3.3 Intermediate Chamber.

To grow a film on a substrate which is in the transport chamber from vapour phase, it is necessary to fix it on a deposition unit. For this purpose an other device was designed and constructed. This "intermediate chamber" is shown in Fig. 3.5 and its schematic drawings are shown in Fig. 3.6 (a) and (b), side view and top view

respectively. It is a metal cube about 18 X 13 X 13 cm and is a copy of the section of the JEM-6 electron microscope column between condenser lens and objective lens assemblies. Like the column it has a horizontal hole where the transport chamber can be inserted, and a 4 cm diameter aperture (5 in Fig. 3.6) in the bottom side, aligned with the hole in the main body of the transport chamber. A glass window is fitted on the top side for viewing.

A circular base plate (3 in Fig. 3.6), about 1.5 cm thick and 22 cm in diameter with a 4 cm wide hole in the centre, is attached to the intermediate chamber in such a way that the bottom hole in the cube aligned with the hole in the plate. They are clamped together by 4 small screws and sealed by an o'ring (2 in Fig. 3.6). The intermediate chamber together with base plate is fixed on a stainless steel jar, by means of six 4BA screws. This jar is used on a deposition unit; the jar and the evaporation unit is adjusted in such a way that the hole in the base plate faces the evaporant. The intermediate chamber with the transport chamber on the stainless steel jar is shown in Fig. 3.4.

3.4 Procedure.

An electron microscope grid with a suitable substrate is carefully put in the specimen carrier and inserted in the basket of the transport chamber. By turning the knob anticlockwise, the sealing cap comes

Fig. 3.4.

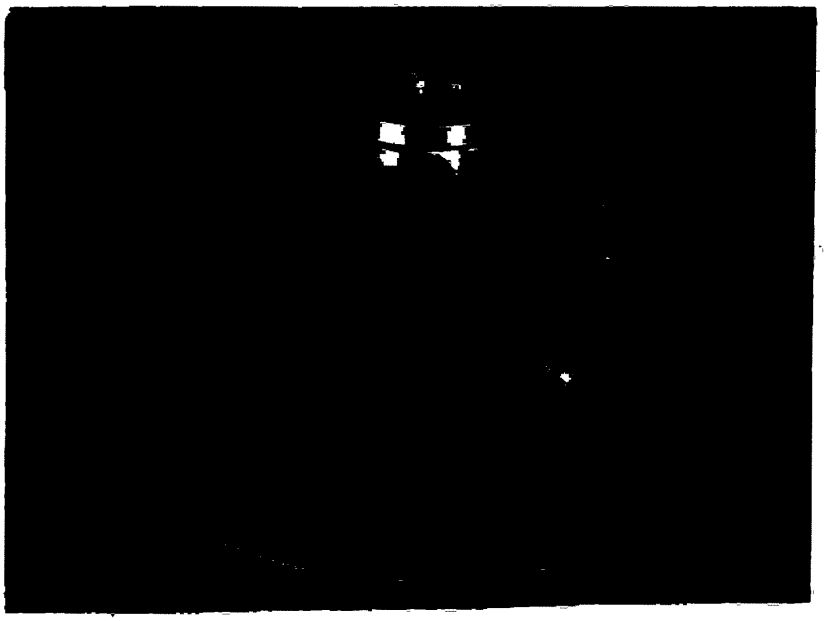

Fig. 3.5.

Fig. 3.4. Intermediate chamber with transport chamber on the stainless steel jar.

Fig. 3.5. Intermediate chamber.

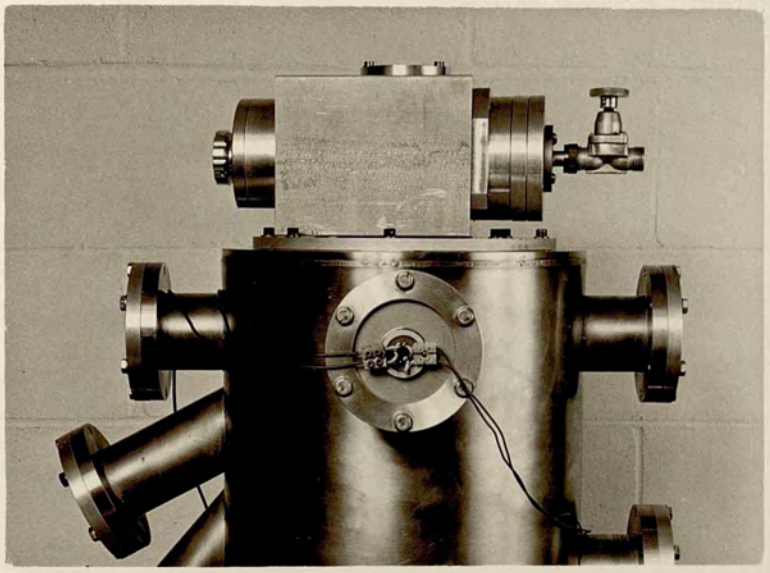

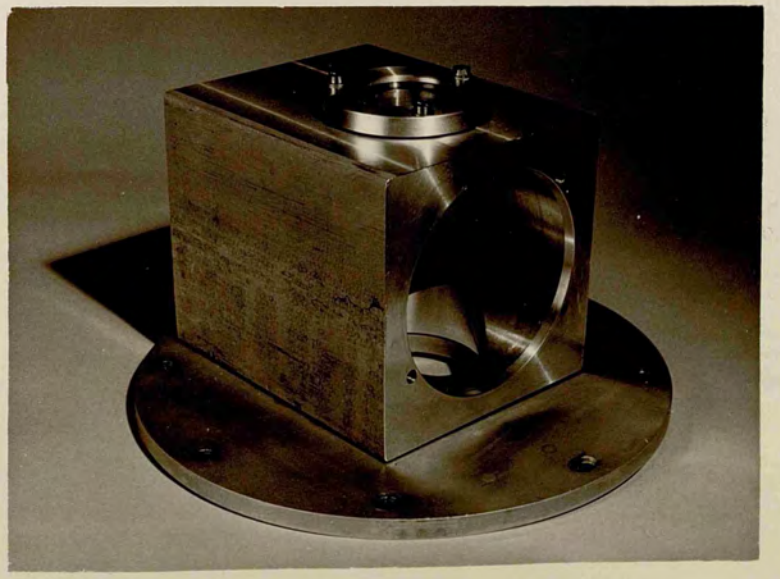

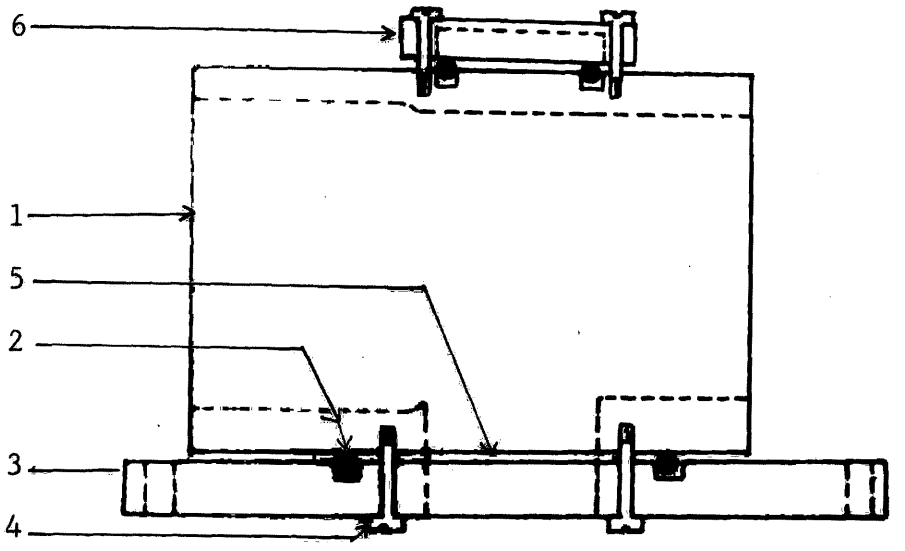

(a)

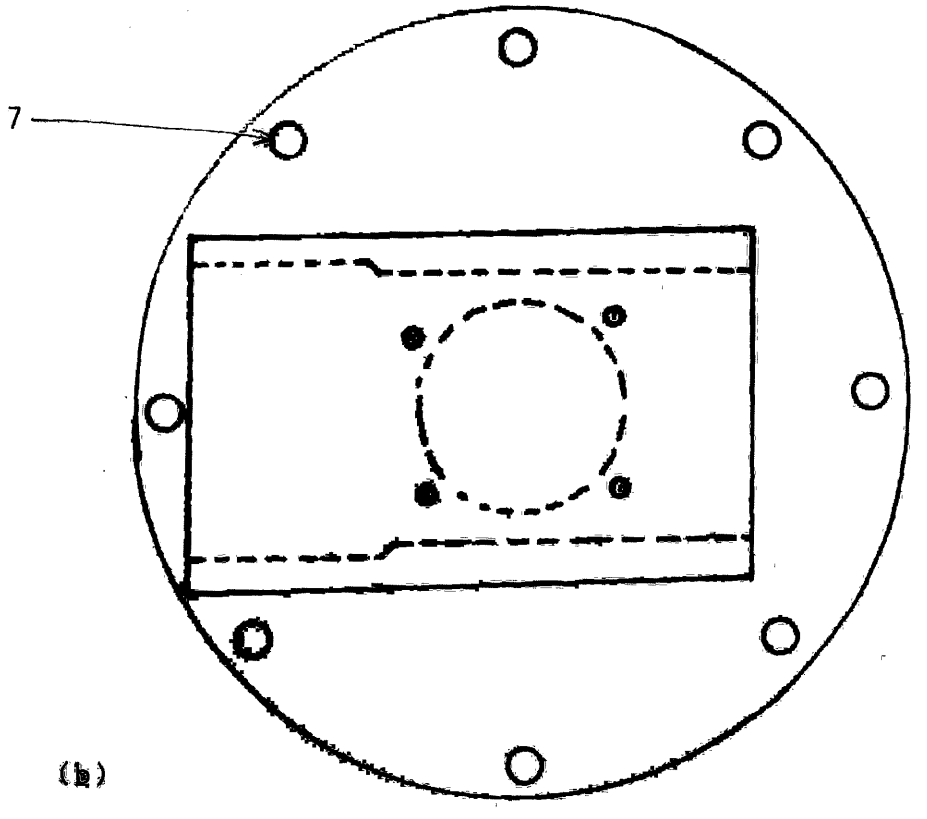

(b)

Fig. 3.6. Schematic drawing of intermediate chamber (a). Side view. (b). Top view.
1. Chamber body. 2. O'ring. 3. Base plate. 4. Support. 5. Side. 6.Glass window. 7. Small glass window.

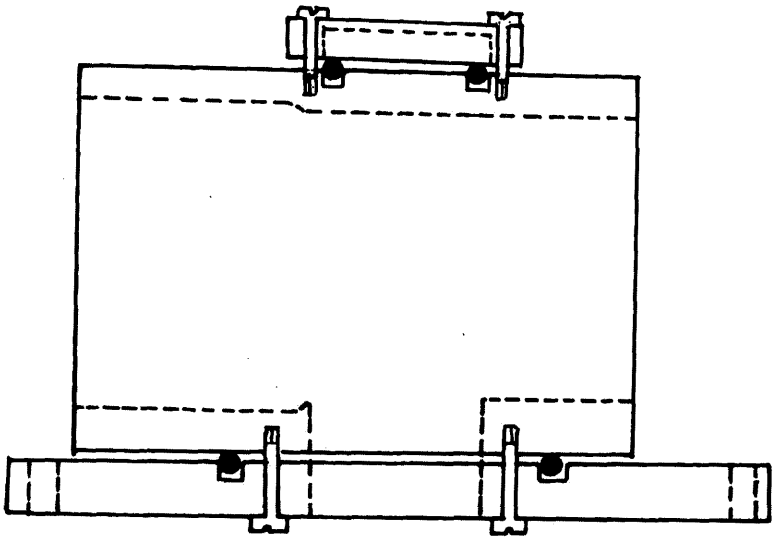

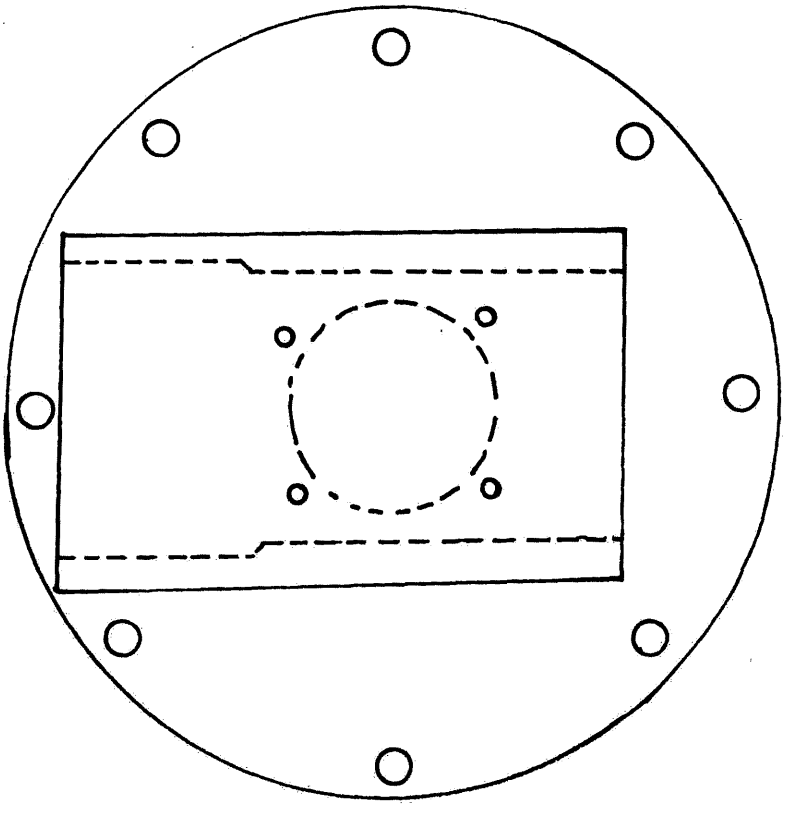

towards the tube mean while lifting the specimen carrier. When the carrier is fully inside the transport chamber, it is inserted into the intermediate chamber. The intermediate chamber is fixed on the stainless steel jar which is placed on a deposition system. By turning the knob clockwise, the specimen carrier comes down through the hole in the main body of the transport chamber, then through the aperture in the intermediate chamber and finally through the base plate. The substrate on the grid inside the specimen carrier is thus exposed to the deposition system. After closing the valve of the transport chamber the whole system is evacuated. The schematic diagram of the whole system is shown in Fig. 3.7.(a).

After completion of the evaporation the sealing cap is closed by turning the knob and specimen enclosed in the small chamber formed by the sealing cap and horizontal tube. The air inlet valve of the deposition system is opened, allowing air into stainless steel jar but the specimen is isolated and still in vacuo so that the material cannot react with the atmosphere. The transport chamber is withdrawn from the intermediate chamber and carefully replaced by the specimen chamber assembly in the electron microscope column. The electron microscope is then evacuated and the sealing cap is opened. The specimen carrier comes down into the specimen stage of the objective lens assembly. The specimen is now ready for electron microscopic observation.

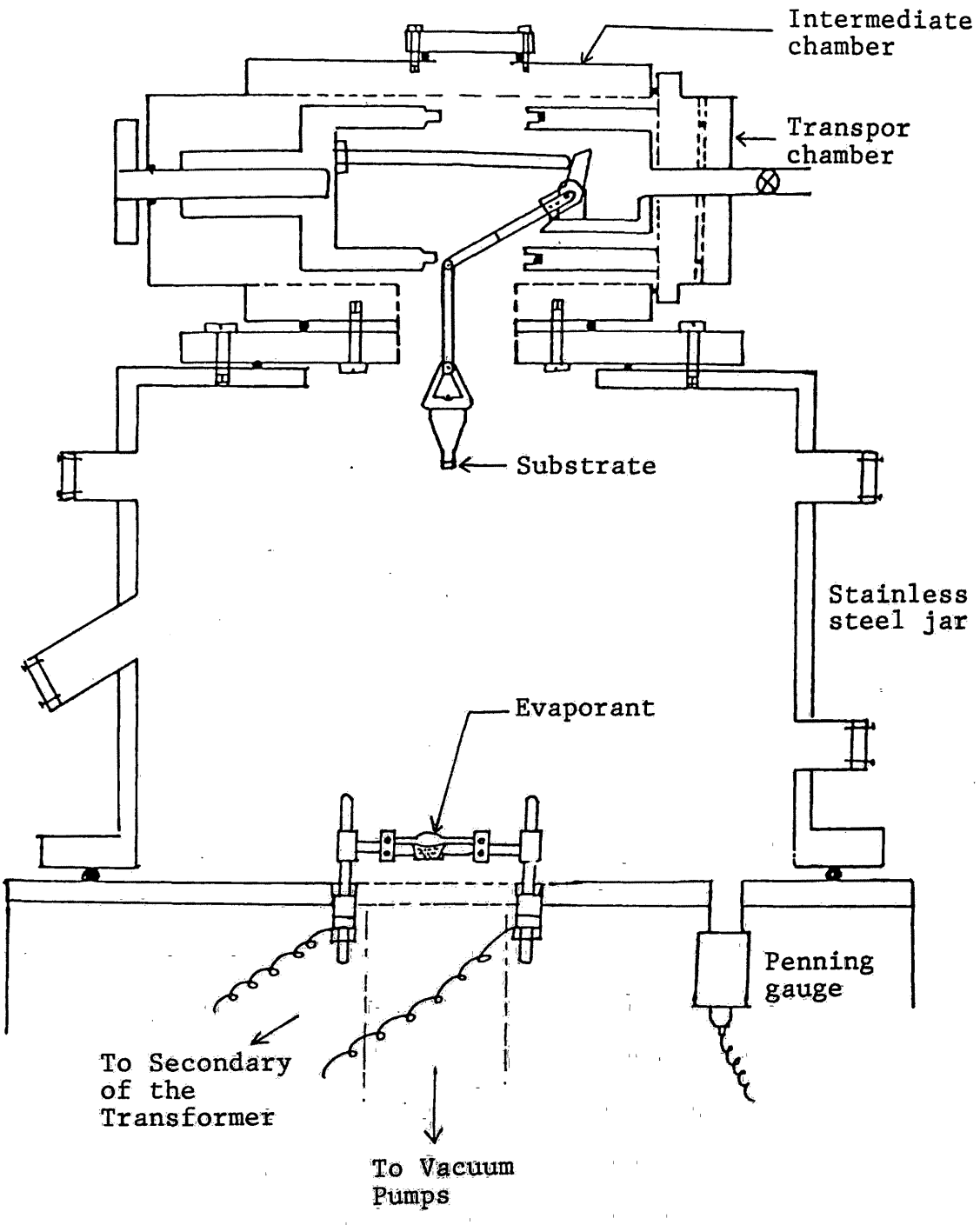

Fig. 3.7 (a). Schematic diagrame of transport chamber in the intermediate chamber, fixed on a stainless steel jar and vacuum deposition system.

If the specimen needs to be exposed to the atmosphere at any stage, there is no need to break the vacuum in the column, the sealing cap is closed and the specimen in the small chamber isolated from the microscope column. When the valve of the transport chamber is opened, air enters into the small chamber. The specimen can be exposed to any other gas by connecting a suitable source to the open end of the valve. To put the specimen again in the electron microscope, the small chamber is evacuated by means of an auxiliary pump. After 10 to 15 minutes the valve is closed and sealing cap is opened, the specimen is again ready to examine.

To determine the pressure inside the transport chamber by the time it is transferred from the vacuum deposition system to the electron microscope, the following experiment was carried out: First the transport chamber was installed in the intermediate chamber which was placed on the stainless steel jar of the vacuum system. A Penning gauge was attached to the side valve of the transport chamber, this valve was opened and also the small chamber inside the transport chamber was opened as in the film deposition procedure. Then the whole system was evacuated to 10^{-9} bar i.e. normal working pressure. The small chamber was closed and air let into the stainless steel jar. The pressure in the transport chamber was then recorded as a function of time. The resulting graph is shown in Fig. 3.7 (b). This shows that after about 8 minutes the pressure in the transport chamber is still

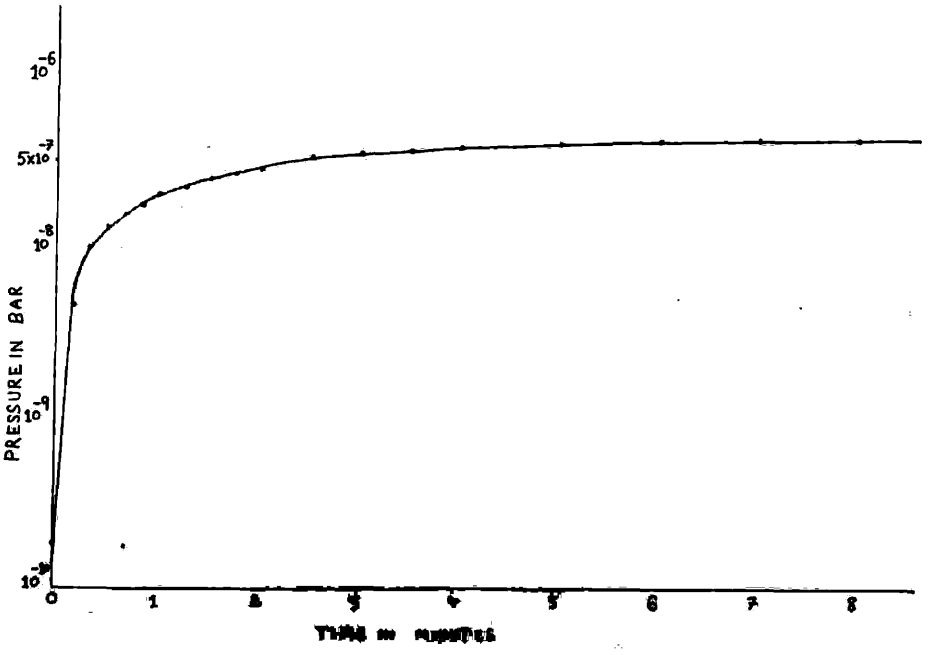

Fig. 3.7(b) The graph of pressure inside the transport chamber as a function of time.

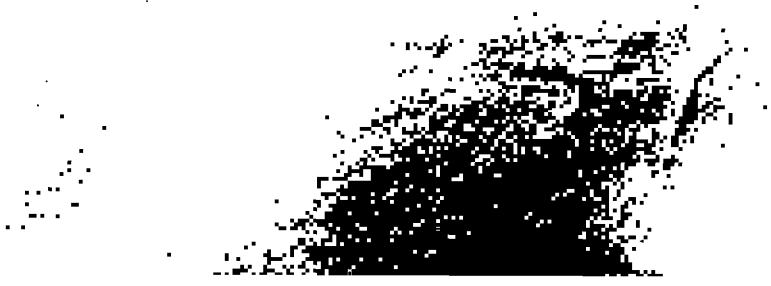

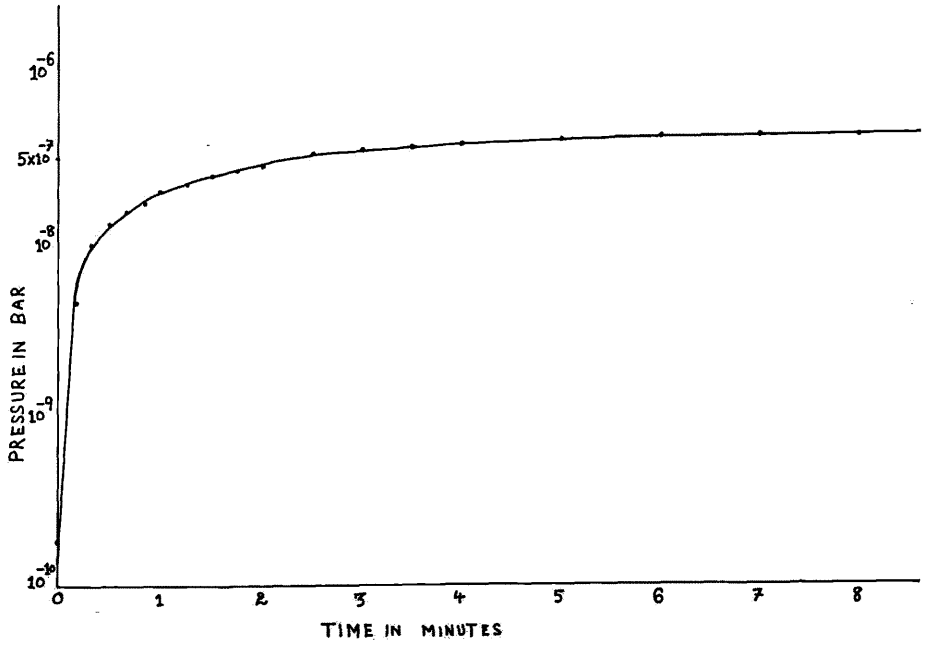
10^{-6}
5×10^{-7}
10^{-8}
10^{-9}
10^{-10}
PRESSURE IN BAR
0
1
2
3
4
5
6
7
8
TIME IN MINUTES

less than 10^{-6} bar. The time taken from closing the transport chamber in the vacuum system to opening it in the electron microscope is about 6 minutes. Thus the pressure inside the transport chamber when it is opened in the electron microscope is much less than 10^{-6} bar, which means that the effect of the atmosphere is reduced by a factor of more than 10^{6} times.

The curve in Fig. 3.7 (b) shows the pressure rise as the function of time when the pressure around the transport chamber is at atmosphere. The transport chamber is transferred into the electron microscope in 2 to 3 minutes and then the electron microscope vacuum system is started, the leakage is therefore, smaller than indicated by the curve and the effect of the atmosphere is further reduced.

3.5 Substrate Heater.

A heater was designed and constructed to heat the substrate that is transferred by the transport chamber. Fig. 3.8 (a) shows its photograph and its schematic diagram is shown in Fig. 3.9. It consists of a circular sheet of mica about 4.5 cm diameter with a hole in the centre of about 0.5 cm diameter. It has also a number of small holes, through which a suitable size nichrome wire is wound to make heater coil (Fig. 3.9 c). This heater plate is sandwiched between two other mica sheets of the same size for insulation. This heater is placed between

two metal plates as shown in Fig. 3.9 (a). The lower plate has a 0.4 cm centre hole and a deep hole from one side close to the centre, parallel to the plane of the plate, for a thermocouple. A taper hole in the centre of upper plate (4 in Fig. 3.9) is designed to engage the specimen carrier of the transport chamber. A metal rod is attached to the side edge of this plate for support. The whole assembly is held together by two screws.

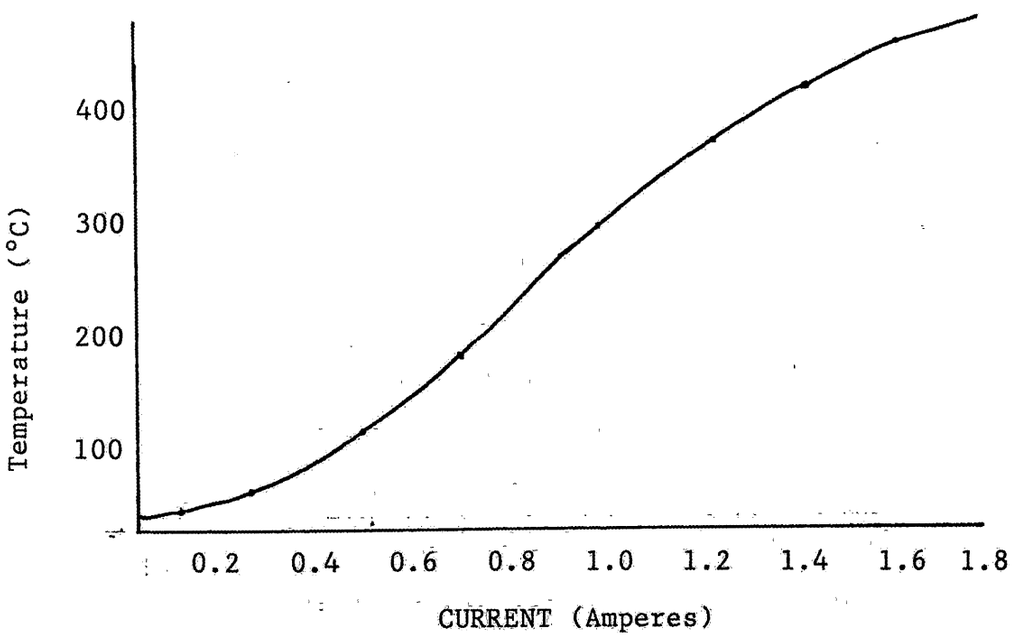

Fig. 3.10. The temperature measured by thermocouple versus heater current.

This heater is attached to the base plate of the intermediate chamber via a three way adjusting mechanism. When the transport chamber is inserted into the intermediate chamber and the specimen carrier is lowered,

it is engaged in the taper hole of the upper plate of this heater. The substrate, on the electron microscope grid in the specimen carrier, is close to the thermocouple so that the temperature of the substrate can be measured. Fig. 3.10 shows the curve between current through the heater coil and the temperature of the substrate measured by a T_1-T_2 thermocouple.

3.6 Grids Heater.

An other heater was designed to heat the substrates on the grids. By this heater a number of grids can be heated at the same time. These grids are used in the ordinary electron microscope specimen carrier for electron microscopical studies of those materials which are not reactive with atmosphere. Fig. 3.8 (b) is a photograph and a schematic diagram is shown in Fig. 3.11. This heater is same as the substrate heater described previously, except that it has two upper plates. In the top upper plate there are six clearance holes 2.5 mm in diameter as shown in Fig. 3.11 (b) and the second upper plate has taper holes opposite to those in the top upper plate . These holes are 3.5 mm in diameter at the surface and 2.5 mm deep to receive the grids. The grids are 3 mm in diameter so there is no risk that they will be bent by heating. These two plates are joined to gether by two small screws. The thermocouple is placed in the second upper plate close to the base of one hole. The whole

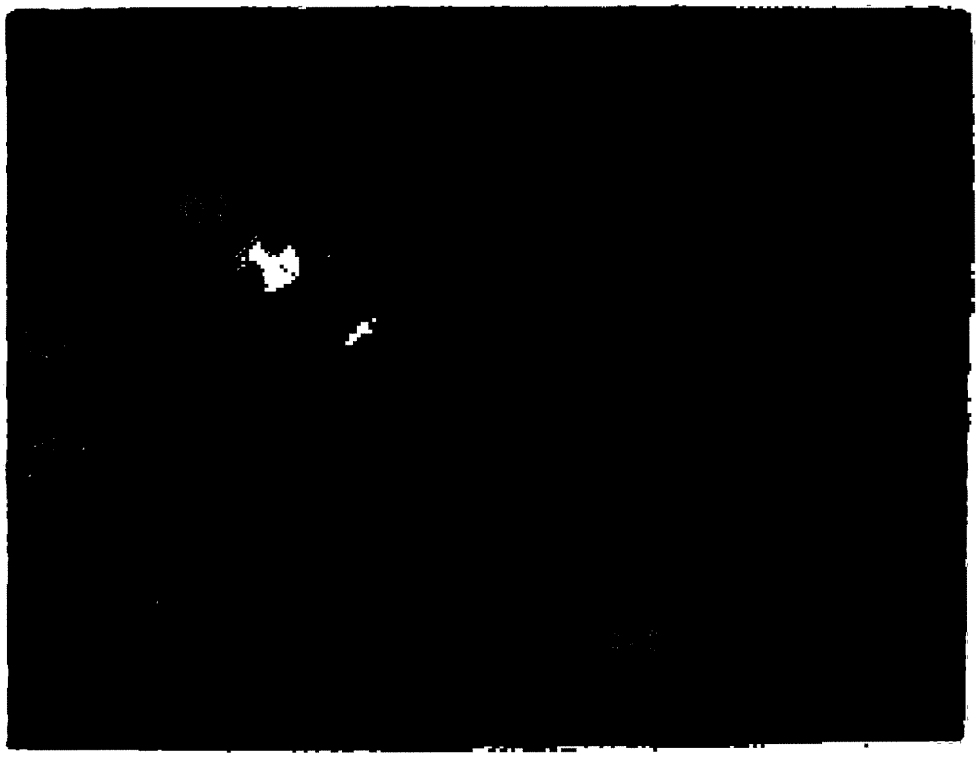

Fig. 3.8. [illegible]. (a). [illegible]. (b). Grids heated.

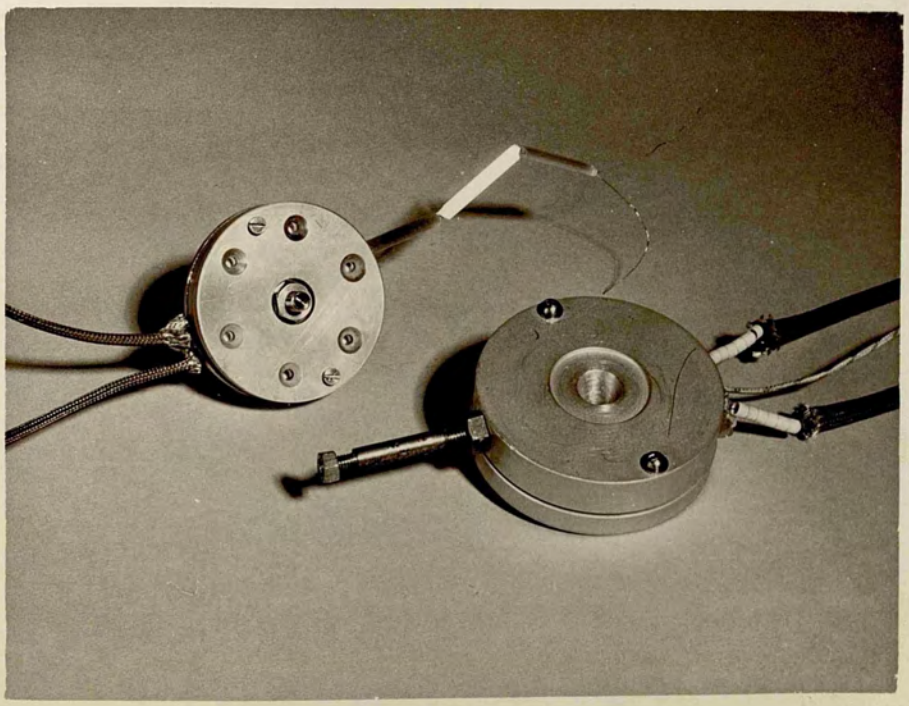

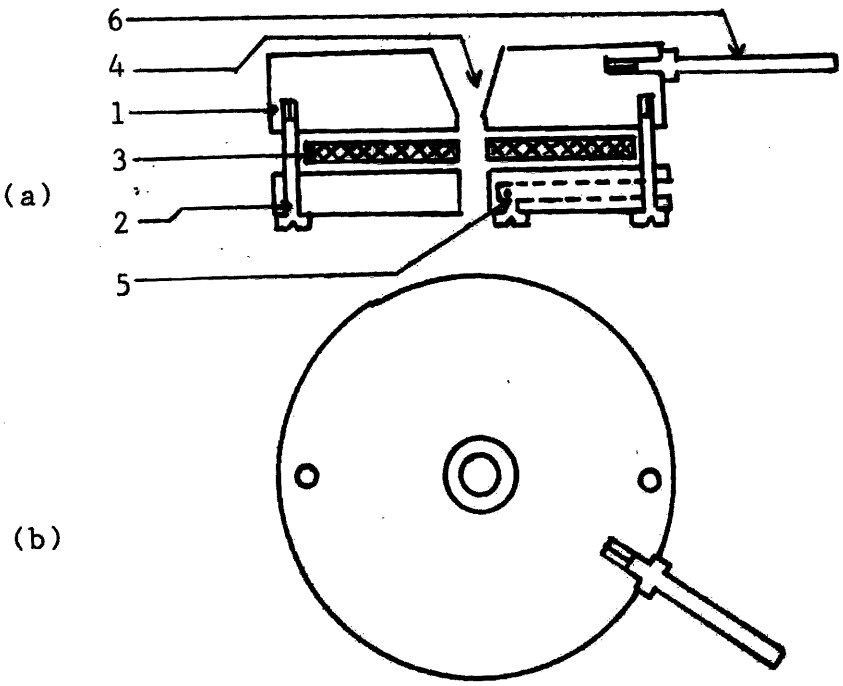

Fig. 3.9. [illegible] 1. Upper plate, 2. [illegible] 4. Hole for operation [illegible] 5. Support. [illegible]

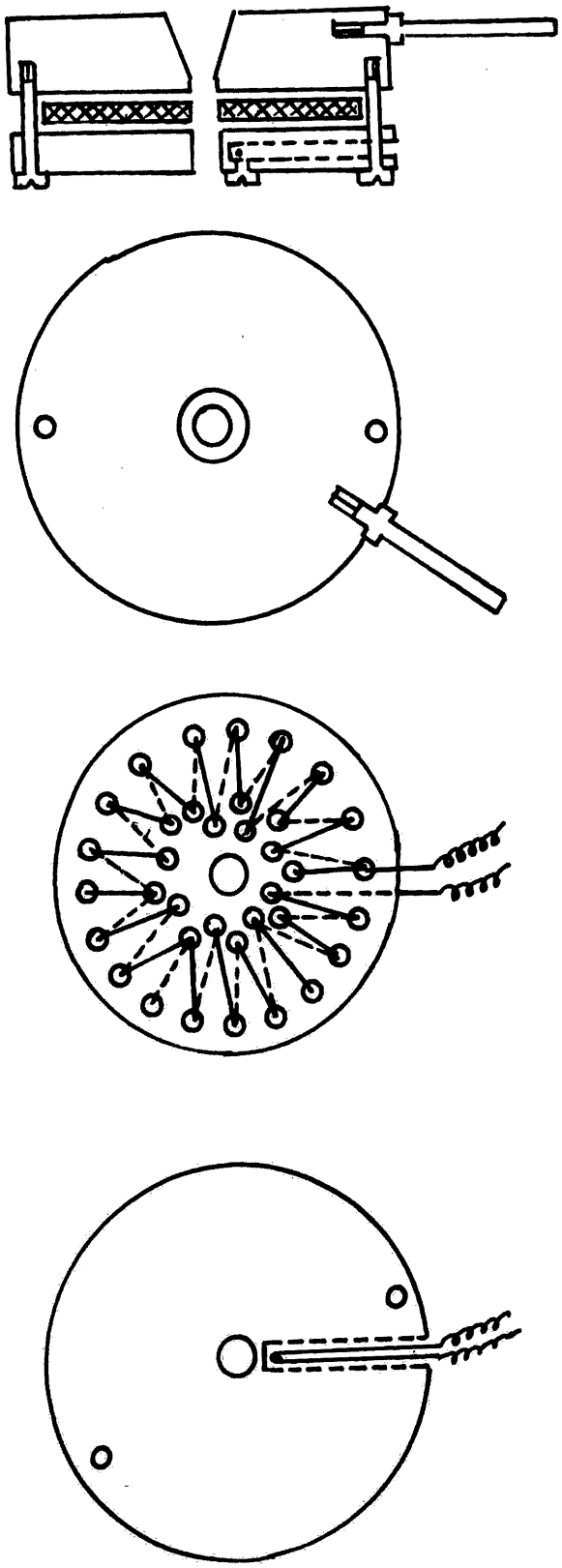

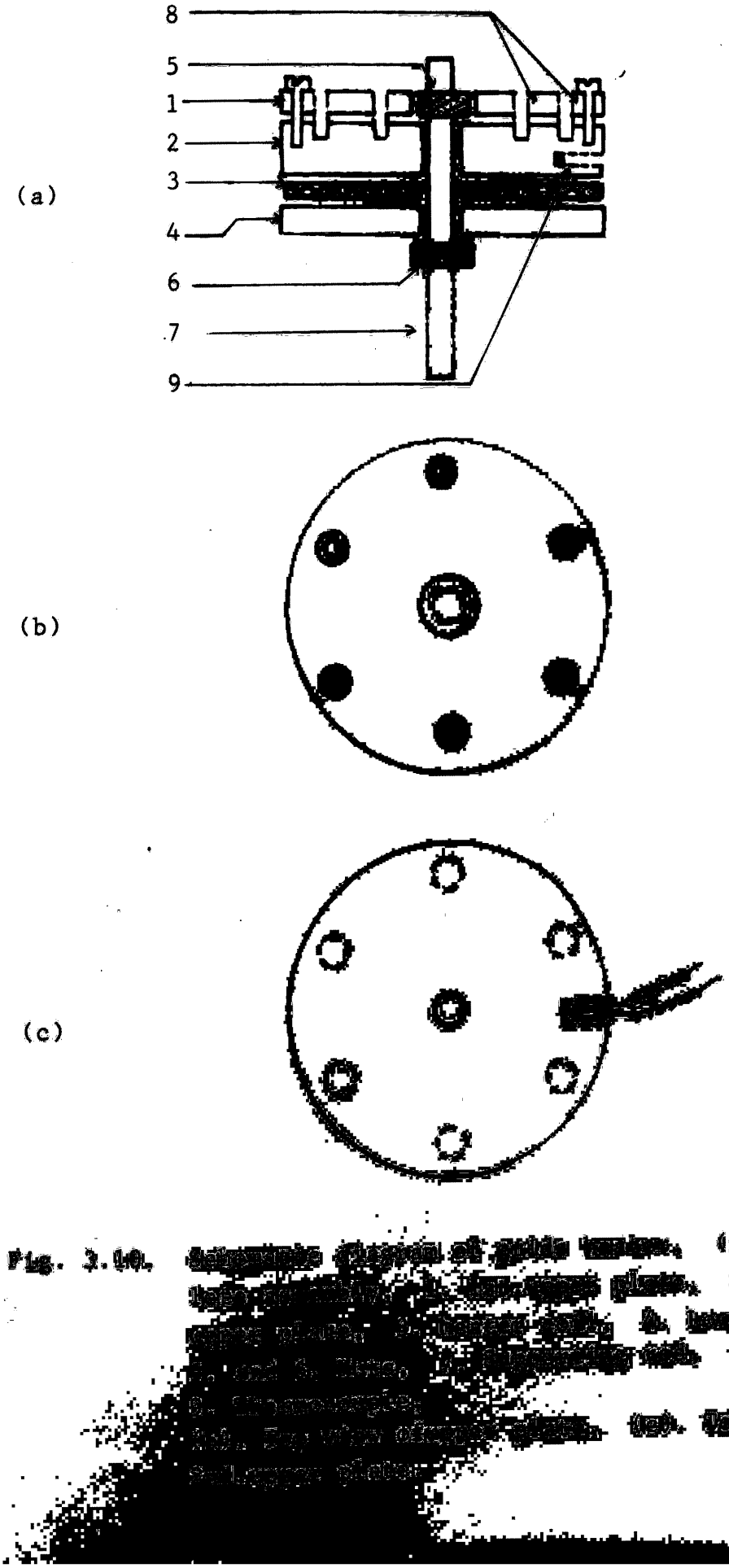

Fig. 3.10. [illegible] (a). Comp- [illegible] 2. 3rd. [illegible] 5. lower plate [illegible] 8. Spring [illegible] (b). Top view of [illegible]

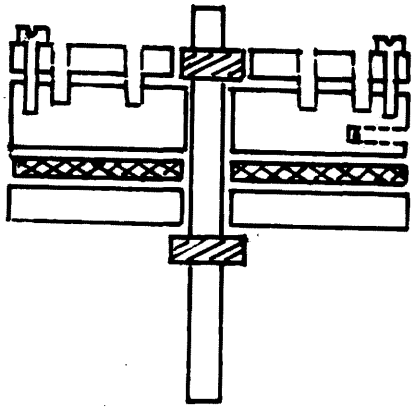

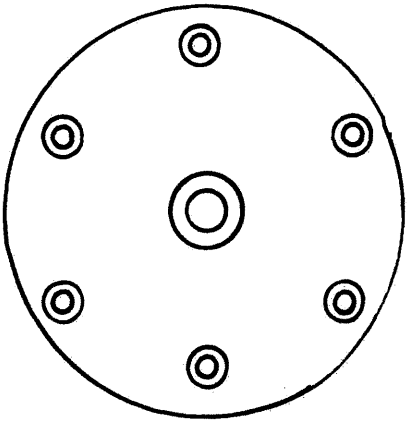

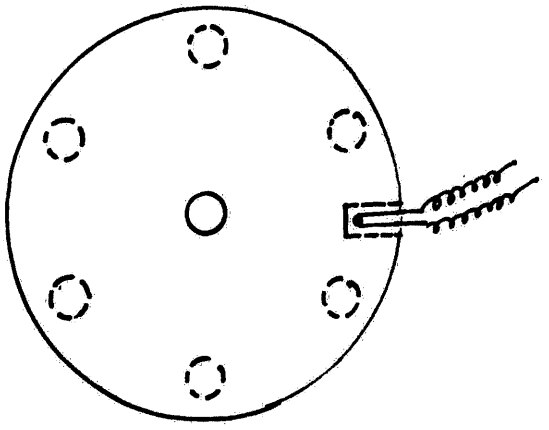

assembly is compressed by a long screw in the centre which also acts as support rod (7 in Fig.3.11). The top plate can be detached without separating the whole assembly. The grids are placed in the holes of the second upper plate, with the substrates on the top side. The top plate is then replaced so that the substrates on the grids are exposed through the holes in this plate. The heater is fixed upside-down in the deposition system if the charge is in the boat so that the vapour can go straight on to the substrate. This heater can also be used in a sputtering unit.

3.7 Camera Constant.

The diffraction effects, which arise when a monochromatic beam of electrons of wave length λ impinges on the surface of a crystal or passes through the crystal, can be ascribed to the regular path differences between the wavelets elastically scattered by every atom. Bragg (1913) showed that the effect could be explained by considering a plane electron wave partially reflected at successive lattice planes. The Bragg equation

$$n \lambda = 2 d \sin \theta \qquad 1$$

can also be written with n equal to unity

$$1/d = (2/\lambda) \sin \theta \qquad 2$$

This is a useful form for interpreting the diffraction pattern from a single crystal in the electron beam. A simple experimental arrangement for electron diffraction

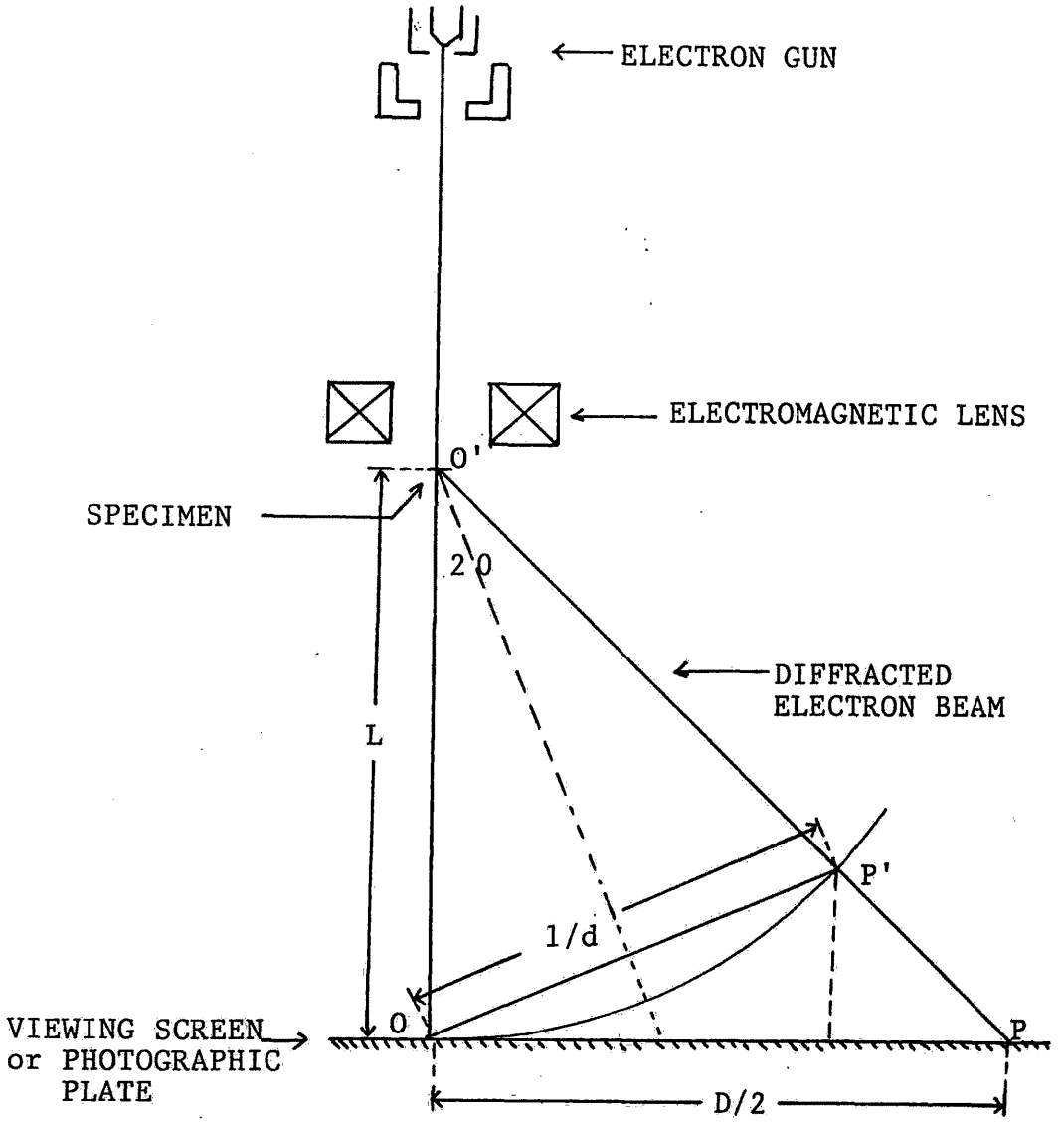

Fig. 3.12. Basic elements and geometry of the electron diffraction.

(Lebedev, 1931) is shown in Fig. 3.12. It consists of an electron gun, an electromagnetic lens for focusing the electron source on the fluorescent screen or photographic plate and the specimen. The pattern is recorded on a flat film or plate, which is usually normal to the incident

beam direction OO'. The diffracted ray proceeds along O'P' and makes a diffraction spot at P. Thus

$$\left.\begin{aligned} O\,P' &= 2\,L \sin\theta \\ \text{and} \\ O\,P &= L \tan\theta \end{aligned}\right\} \qquad 3$$

where L is the effective camera length: the distance between the specimen and film.

For high energy electron diffraction the wave length of the elctron is small (λ = 0.0037 nm at 100 kv), so θ is very small ($< 3^{\circ}$) Therefore, P' is very near to P and the distance OP' and OP approximate to 2 L θ, (the scale is deliberately enlarged in Fig. 3.12). If D/2 is the distance of any spot from the centre of the pattern then

$$D/2 = L \tan 2\theta \qquad 4$$

Eliminating θ from equation 4 by using Bragg relationship and assuming θ is very small, so that

$$\tan 2\theta = 2 \sin\theta = 2\theta$$

$$D = 2\,L\,2\theta$$

$$= 4\,L\,\lambda/2d$$

Therefore,

$$D\,d = 2\,\lambda\,L \qquad 5$$

D is the ring diameter or distance between the spots on either side of the centre and λ L is called the "camera constant". In practice 2 λ L is used as the camera constant for easy measurement of D and calculation made simple. This camera constant may be determined by

calibration with a sample of known lattice parameter that gives sharp rings or spot pattern. This procedure eliminates the difficulty of exact measurement of L.

In transmission electron microscope, the electron diffraction patterns are obtained from selected areas of the sample. Defocusing the intermediate lens to collect the diffracted image from the objective lens, enables a magnified image of the diffraction pattern to be obtained on fluorescent screen. An aperture may be inserted in the object plane of the intermediate lens to select a restricted region of the microscopic image. There is a diffraction pattern at the cross-over plane between the objective and intermediate lenses. If the intermediate lens is defocused the image of the pattern extends downwards until it coincides with the object plane of the projector lens. It is thus focused by the projector lens on the fluorescent screen.

Agar (1960) has outlined the correct procedure for obtaining a diffraction pattern from a selected area of the specimen and Phillips (1960) has suggested some modification in the procedure.

In equation 5 it has been assumed that $2 \lambda L$, the camera constant, is in fact a constant. However, small variations in its value will be obtained because of fluctuations in the accelerating voltage and in the voltage supply to the instrument, incorrect procedure in obtaining the diffraction patterns, changes in specimen height and errors of measurement. The fluctuation in

voltage supply is negligible in modern instruments due to stabilised power supplies. Variation by lenses is as given by Phillips (1960)

$$\frac{\Delta L}{L} = \frac{\Delta f_o}{f_o} + \frac{\Delta m}{m} + \frac{\Delta M}{M} \qquad 6$$

where $\Delta L/L$ is the proportional error in the camera length L, $\Delta f_o/f_o$ is in the focal length f_o of objective lens, $\Delta m/m$ is in the magnification of the intermediate lens and $\Delta M/M$ is the proportional error in the magnification of the projector lens. In modern instruments the strength of the projector lens for diffraction mode is fixed so $\Delta M/M = 0$. By using the correct procedure $\Delta m/m$ is very small. As indicated above, an error Δf_o in f_o can arise when focusing the image in the same plane as the selector aperture or from variations in specimen height.

Since the effective camera length defined as

$$L = f_o \times m \times M \qquad 7$$

where m is the magnification of the intermediate lens and M of the projector lens, the focal length of the objective lens, f_o, is the most sensitive factor which effects the reproducibility of L. In turn, f_o, depends on the plane of the object. The factors which effect this are specimen holders of different length, support grids with different thicknesses or are not flat, thick and buckled specimens and effects due to tilting the specimen. Armitage and MacConaill (1964) showed that a change of 0.8 mm in specimen height changes the $2\lambda L$ from 34 mmA° to 45 mmA°. This represents a 25 % variation.

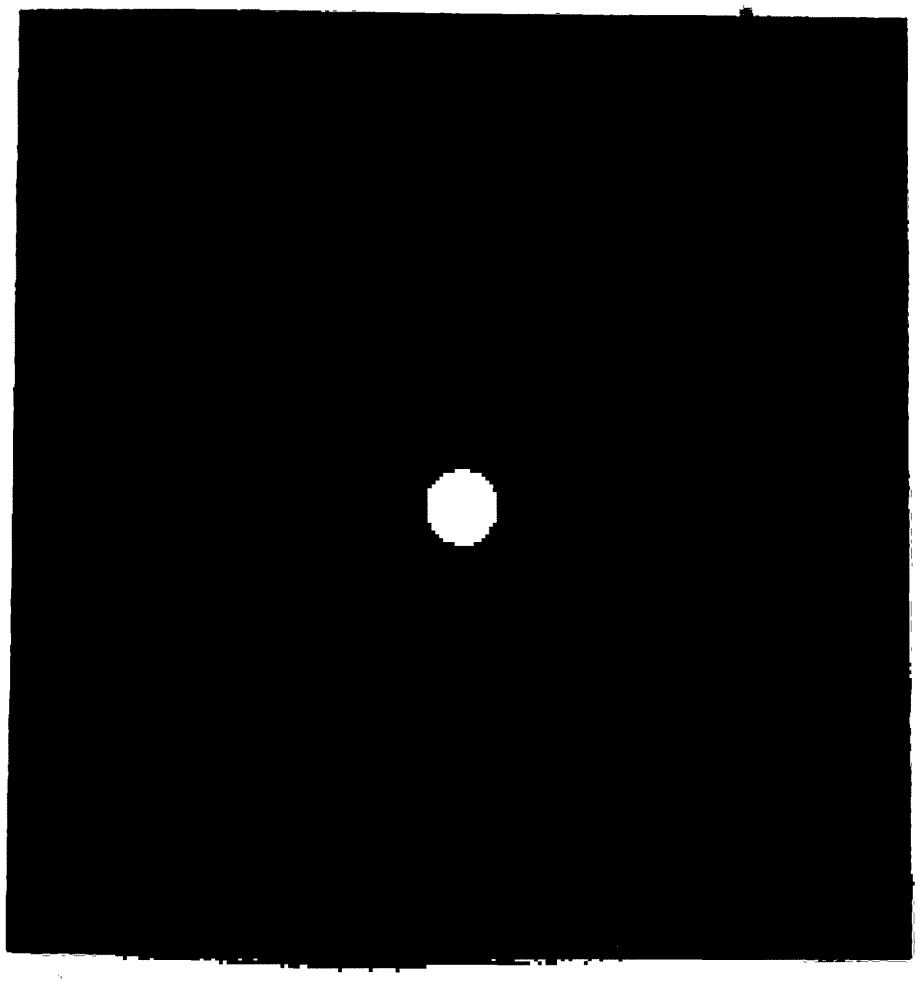

Fig. 3.14. Ring pattern from polycrystalline gold film (used for determination of camera constant)

Objective lens current =64.25 mA
Average camera constant $2Rd = 44.65$ mm²
(Plate magnification =42)

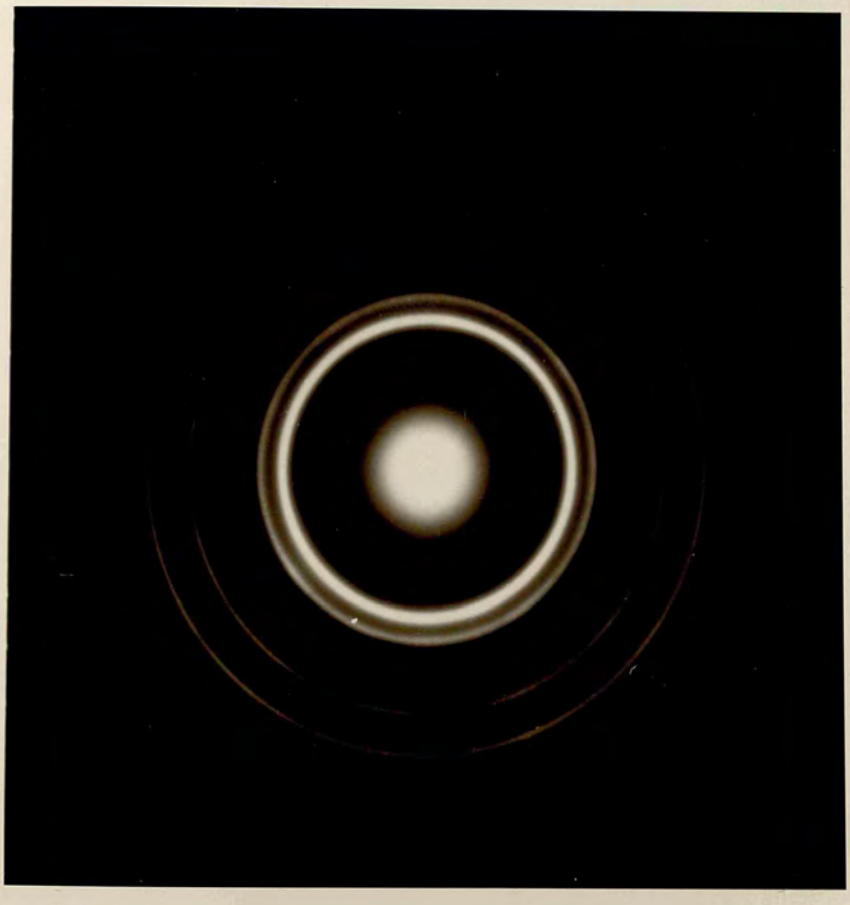

In the present work a JEM-6 electron microscope is used which has a well stabilized power supply (fluctuation ~ 5 parts per million), and can be changed from transmission to diffraction mode by turning a switch, which means that the magnifications of the projector and intermediate lens are fixed for every diffraction experiment. But as the ordinary specimen carrier and the one used with the transport chamber are different in length. The specimen grids stand at different height when used with the transport chamber's specimen carrier. A variety of substrates are used for epitaxial growth, the height of the specimen in the object plane of the objective lens, varied in different experiments. The strength of the objective lens, therefore, must be varied for exact focusing the microscopic image, which effects the camera constant.

An experiment has been done to observe the variations in camera constant due to changes in the height of specimen in the object plane of objective lens, which is as follow: A special specimen carrier was made (Fig. 3.13) to enable the height of specimen in the objective lens to be changed. It consists of a cone-shaped metal cylinder like the ordinary specimen carrier for JEM-6 electron microscope. The lower part has thread and the specimen holder cap also has thread which can be tight on various position by the help of a small ring. A thin polycrystalline film of gold on a suitable grid was placed in this specimen holder and the image of the film brought

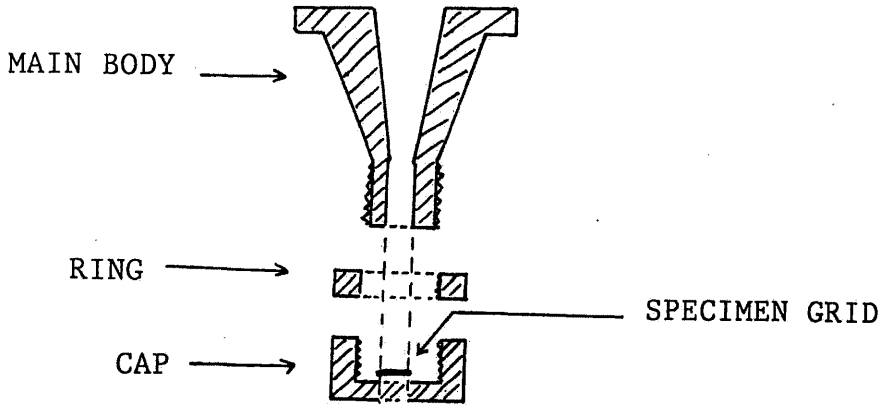

Fig. 3.13. Specimen carrier used to determine the variations in camera constant.

into focus at a certain height, the objective lens current and diffraction pattern were recorded. The height of the specimen grid was then changed and new in-focus objective lens current and diffraction pattern were recorded. A number of readings were made by changing the height of the grid.

Fig. 3.14 shows a ring pattern from polycrystalline gold film at a certain height of the specimen grid in the objective lens. By using the relation

$$D\,d = 2\lambda L$$

and measuring the ring diameter D by a travelling microscope and using the interplanar spacing d for that ring, obtained from x-ray data, the camera constant $2\lambda L$ was calculated for different objective lens currents. The camera constant $2\lambda L$ is plotted as a function of objective lens current in Fig. 3.15.

This curve was used to calculate the d-spacing (interplanar distance) and corresponding Miller indices from diffraction patterns of epitaxial layers by determining the camera constant for corresponding in-focus objective lens current and measuring the distance D on the diffraction patterns.

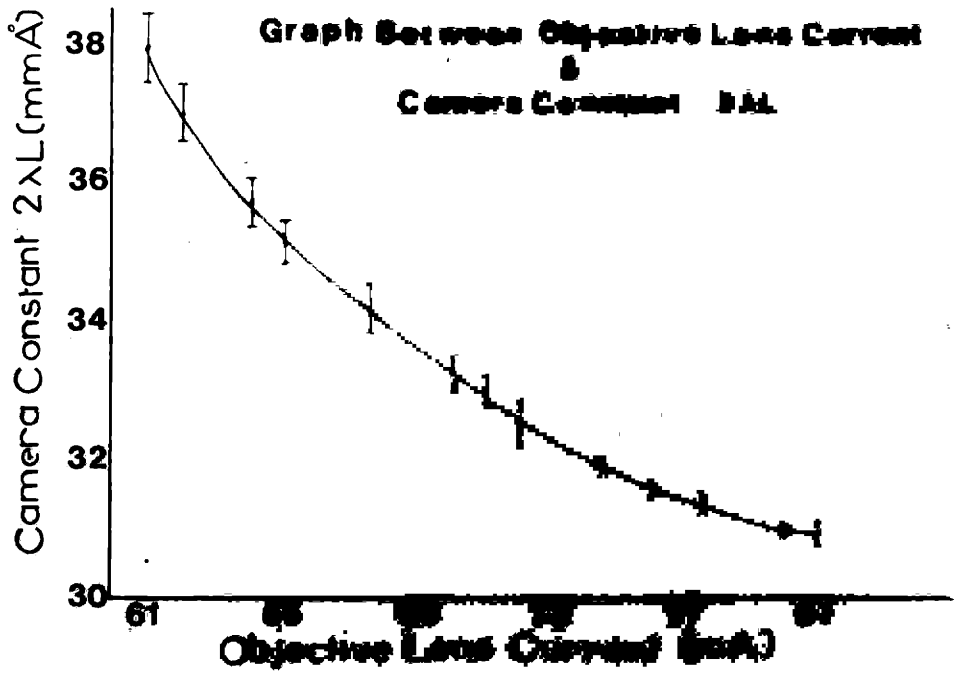

Fig. 3.15. Variation of camera constant with objective lens current.

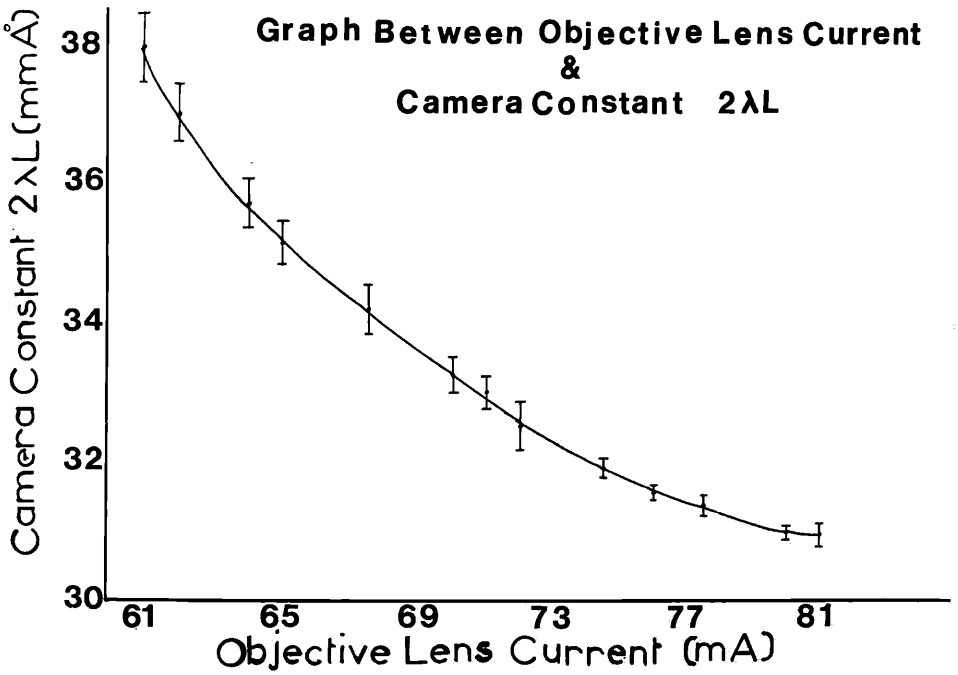
Graph Between Objective Lens Current
&
Camera Constant 2λL
Camera Constant 2λL (mmÅ)
38
36
34
32
30
61
65
69
73
77
81
Objective Lens Current (mA)

References

AGAR,A.W. (1960). Brit. J. Appl. Phys., II, 185.

ARMITAGE,W.K. and MacCONAILL,A. (1964). J. Sci. Instrum., 41, 401.

BRAGG,W.L. (1913). Proc. Camb. Phil . Soc., 17, 43.

ENNOS,A.E. (1953). Brit. J. Appl. Phys., 4, 101.

ENNOS,A.E. (1954). Brit. J. Appl. Phys., 5, 27.

LEBEDEV,A.A. (1931). Nature, 128, 491.

PASHLEY,D.W. and STOWELL,M.J. (1962). Proc. 5th, Int. Con. Electron Microsc., Philadelphia, 1962. (Breese ed.), paper GG-1. Academic Press, New York.

PASHLEY,D.W. (1965). Advan. Phys., 14, 327.

PHILLIPS,R. (1960). Brit. J. Appl. Phys., II, 504.

CAPTER FOUR

NUCLEATION AND GROWTH OF THIN LAYERS OF ALKALI HALIDES ON CARBON

4.1 Introduction.

Evaporation is the most frequently used method for the preparation of thin films. The source material is transformed into its gaseous state by raising its vapour pressure through an increase in temperature. The vapour expands into the evacuated space between the evaporation source and substrate and finally condenses on the substrate. A comprehensive review, the theory and practice of vacuum evaporation has been published by Glang (1970).

In this chapter the nucleation and growth of thin films and crystals of alkali halides from the vapour phase are discussed. Thin films of CsI, CsCl, CsBr, CsF and LiF were evaporated on to continuous carbon films and studied by transmission electron microscopy and electron diffraction. The early stages of nucleation have been studied by examining the evaporated films without exposure to the atmosphere, in the transport chamber described in chapter 3. Some of the films were exposed to the atmosphere or water vapour, after evaporation and then examined in the electron microscope.

4.2 Theories of Nucleation and Growth.

Thin films are formed on a substrate by a process of nucleation and growth. The initial stage is the formation of small clusters of the film material from individual atoms and molecules. As time progresses, more clusters are nucleated and these clusters grow, coalesce and finally a continuous film is formed, which then thickens. The growth of small clusters is called nucleation. A number of theories on the nucleation and growth of thin films are stated in the published work and some comprehensive reviews of these are given by Rhodin (1965), Holland (1970), Neugebauer (1970), and Venables and Price (1975).

The general formulation of nucleation theory, given by Hollomen and Turnbull (1953), is based on this criterion: statistical fluctuations occur in the density of small volumes of matter, clusters form in supersaturated vapour by the sequential addition of single molecules. They grow initially with an increase in free energy until a critical size is reached when growth is continuous with an overall decrease in free energy of the system. The nucleation rate is the product of the concentration of critical nuclei and the impingment frequency of the critical nucleus by single molecules.

Theoretical investigation by Cabrera (1959), Zwanzig (1960) and McCarroll and Ehrlich (1963) indicate that for the case of a 'hot' atom impinging on a

one-dimensional lattice, the accommodation coefficient is less than unity only if the incident kinetic energy is larger than twenty-five times the energy necessary for desorption after equilibration with the substrate. It was also predicted that the likelihood of complete thermal accommodation, i.e., $\alpha_T = 1$, increases if the ratio of the mass of the impinging atom to that of the substrate lattice atoms increases (α_T is thermal accommodation coefficient).

It was reported by McFee (1960) and Lennard-Jones (1937) that the time required for an incident atom to lose its excess kinetic energy and to accommodate thermaly with the substrate is of the orderof 2/v, where v is the frequency of the substrate lattice vibrations. Thus, the impinged atoms effectively lose all their excess energy within a few lattice oscillations. Condensation of a permanent deposit on the substrate does occur at sufficiently high impingement rates, because the interaction between adsorbed single atoms cannot be neglected. Adsorbed atoms can migrate over the surface, giving rise to collisions with other atoms, and aggregates of adsorbed atoms can now exist. Aggregates should be more stable toward re-evaporation than single adsorbed atoms, since they are bound to each other by the condensation energy.

Hirth and Pound (1963) have given an other theory of heterogeneous nucleation, based on the capillarity model and a review article has been published by Sigsbee

and Pound (1967) on this theory. The classical capillarity model for homogeneous nucleation from the vapour phase by Volmer and Weber (1925) and Becker and Doering (1935) has to be modified slightly to take into account the presence of the substrate. The capillarity model predicts that the free energy of formation of a condensed aggregate goes through a maximum: i.e., the aggregate has a stability minimum with respect to dissociation into the vapour phase as it grows through its "critical" size. This maximum in free energy arises from the very large surface-to-volume ratio of the small aggregates, tending to decrease their stability, and the condensation energy, tending to increase it, as they grow in size.

Walton (1962) and Rhodin and Walton (1964) have pointed out that the application of bulk surface energies to droplets of very small size is not, strictly speaking, correct. This difficulty would be avoided if the nucleation process could be treated by writing the partition functions and potential energies for the reacting species and products. An approximate treatment of this was given by Walton, Rhodin and Rollins (1963). The principal feature of this approach is to introduce a potential (internal) energy, which is the dissociation energy of a cluster containing atoms into adsorbed monomers.

Lewis (1967) has compared the small-cluster and capillarity models. He has shown that the fundamental concepts upon which both are based, are identicle.

The general picture of the sequence of nucleation and growth steps to form a thin continuous film, which emerges from nucleation theories and electron microscopic observations, is as follow:

1. Formation of adsorbed monomers.
2. Formation of subcritical embyos of various sizes.
3. Formation of critically-sized nuclei (nucleation stage).
4. Growth of these nuclei to supercritical dimensions with the resulting depletion of monomers in the capture zone around them.
5. Clusters touch and coalesce to form a new island occupying an area smaller than the sum of the original two, thus exposing fresh substrate surface.
6. Monomers adsorbed on these freshly exposed areas, and secondary nucleation occurs.
7. Large islands grow together, leaving channels or holes of exposed substrate.
8. The channels or holes fill via secondary nucleation to give a continuous film.

Pashley, Stowell, Jacobs and Law (1964) distinguish the four stages of the growth process: nucleation and island structure, coalescence of islands, channel formation and formation of the continuous films.

4.3 Substrate.

To observe how an alkali halide condenses on a solid surface in vacuum, a thin continuous carbon film, suitable for use in a transmission electron microscope, was used as a substrate. The growth of alkali halides on a crystalline substrate will be discussed in chapter 5 and 6. A thin carbon film has greater mechanical strength and stability under electron bombardment than some other amorphous thin films and for high resolution work a very thin film of the order of 2 nm in thickness can be made easily. The very fine background structure present is of low contrast and does not interfere significantly with the overgrowth structures.

The method for vacuum evaporation of carbon thin films developed by Bradley (1954) was used, modified as follows: A microscope glass slide is held vertically in the solution of 1 % w/v of formvar in equal parts of ethylene dichloride and dioxane and then transferred to a jar, which contains some etylene dichloride or chloroform. The slide is kept there for 10 minutes and then transferred to a dust-free place and kept there for 20 minutes or so to dry thoroughly. At this stage the formvar films on the lateral sides of the slide are stripped off with a sharp knife. Then the film on one side of the slide is floated on to the surface of distilled water in a bowl. After putting 10 to 20 electron microscope grids on to the film it is picked up with a dry glass slide in such a way

that the grids are sandwiched between the formvar film and the slide. The grids with formvor film on them are then placed in a carbon evaporating unit and coated with 2 to 5 nm carbon. The formvar substrate is washed away by placing them in the vapour of ethylene dichloride for 3 to 4 hours. The carbon films prepared in this way are quite uniform and adhere well to the grids.

4.4 Apparatus and Experimental Procedure.

A simple boat of folded tungsten sheet was used to evaporate the alkali halides in a vacuum unit. An electron microscope grid with a thin carbon film on it, was placed in the specimen holder so that the carbon film side of the grid faces the evaporant. The holder was attached to the manipulating system in the transport chamber (discussed in chapter 3). The transport chamber was inserted into the intermediate chamber and fixed on a stainless steel jar, which is placed on the vacuum unit. The whole assembly is shown by a schematic diagram in Fig. 4.1. The system was evacuated to 10^{-9} bar by a diffusion pump backed by a rotary pump. A liquid nitrogen trap was used between the diffusion pump and the system to prevent pump oil back streaming to contaminate the evaporated films.

The evaporation of alkali halides were performed under the following conditions:

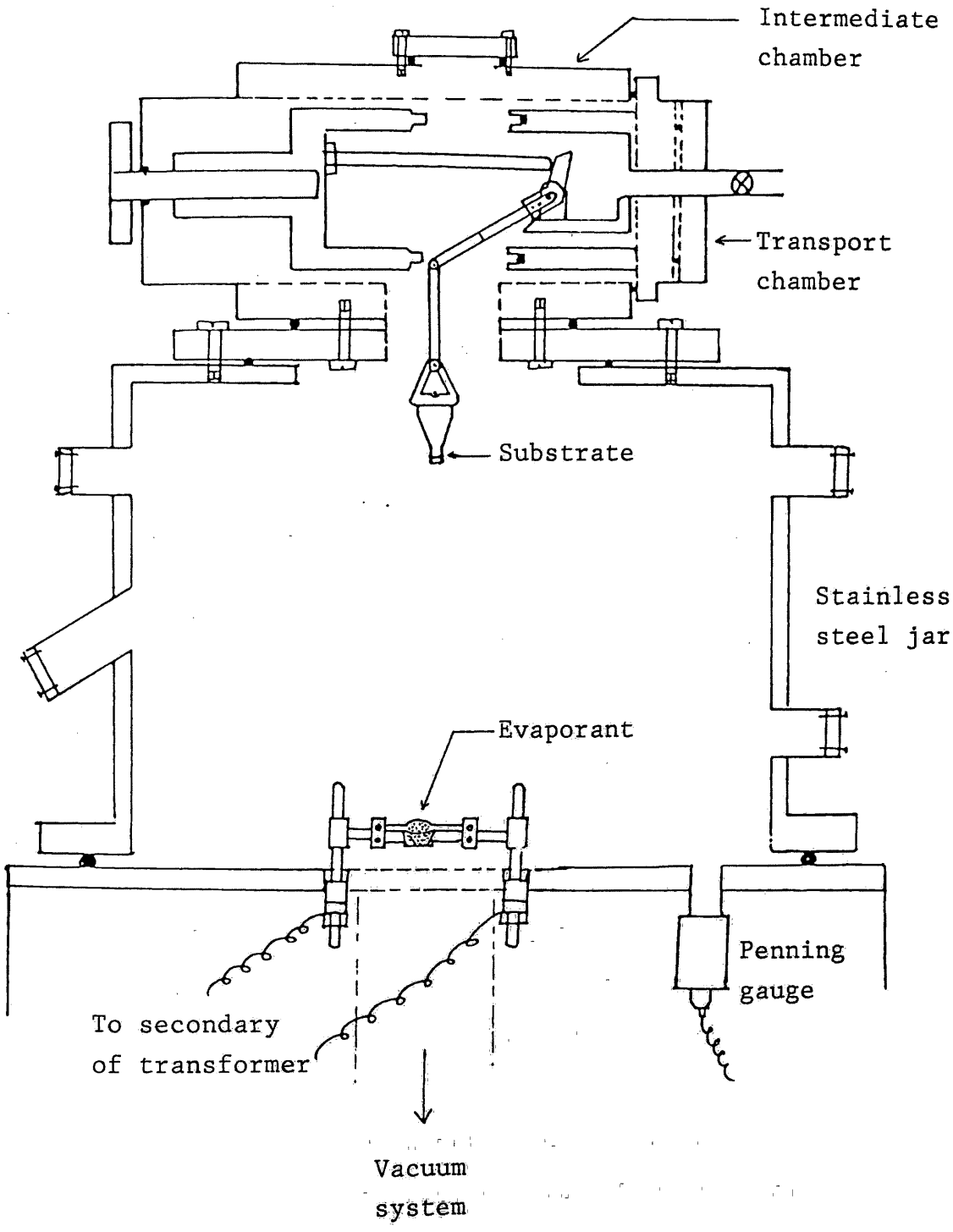

Fig. 4.1. Schematic diagram of vacuum evaporation assembly.

Temperature of the substrate = 20°C (room temperature)

Residual gas pressure = 10^{-9} bar

Rate of deposition = less than 1 nm sec^{-1}.

After evaporation the specimen was transferred to the electron microscope, via the transport chamber, for observations without exposure to the atmosphere. The transfer procedure has been discussed in detailed in chapter 3. Some of the specimens were exposed to the atmosphere or water vapor after evaporation and then examined in the electron microscope.

4.5 Observations and Discussion.

Examination in the electron microscope of the unexposed deposits of alkali halides with average thickness less than 15 nm revealed the presence of very small crystallites situated randomly on carbon film substrate in a nearly continuous film. The diffraction patterns of these deposits show that most of them are polycrystalline.

The micrograph of about 15 nm thick unexposed deposit of CsI is shown in Fig. 4.2 (a). The small black spots are stabilized clusters with average diameter between 5 and 10 nm. There are also some large clusters with diameter up to 50 nm, due to the coalescence of small nuclei and multilayer condensation on the previous clusters. The clusters are connected to each other by

bridges shown by grey areas in the micrograph and the whole deposit resembles to a network of islands separated by clear areas of uncoverd substrate. Fig. 4.2 (b) shows the diffraction pattern of the above which clearly indicates that the deposit consists of large numbers of crystallites situated randomly on the substrate. Although the substrate is an amorphous material but thin films of carbon prepared by the method described in section 4.3 have flat surfaces. The evaporated films of alkali halides are rather porous and composed of relatively independent crystals (Schulz, 1951). Some of the crystallites in CsI deposit have their planes parallel to the substrate surface, this is almost equivalent to decreasing the number of crystallites, since some 'randomness' has been lost and causes the discontinuity in some rings. The more intense spots along the rings represent a mixed and weak [001] and [011] orientations normal to the substrate surface. This means that some crystallites have their {001} and {011} planes parallel to the substrate surface.

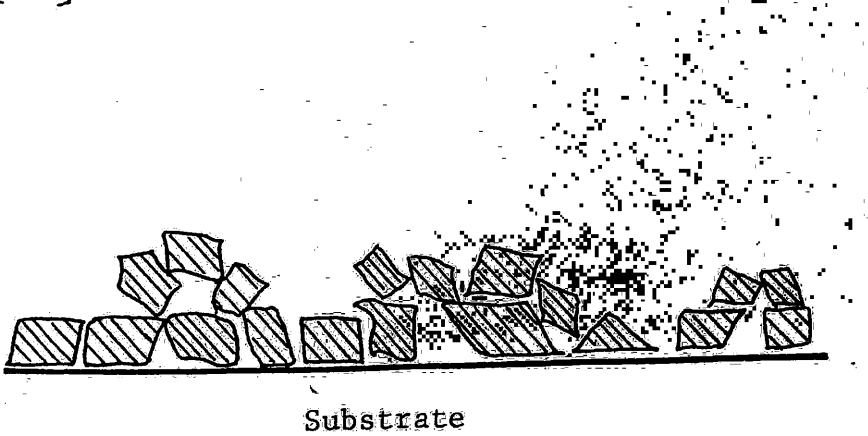

Fig. 4.3. Schematic structure of a thin film.

Fig. 4.2 (a)

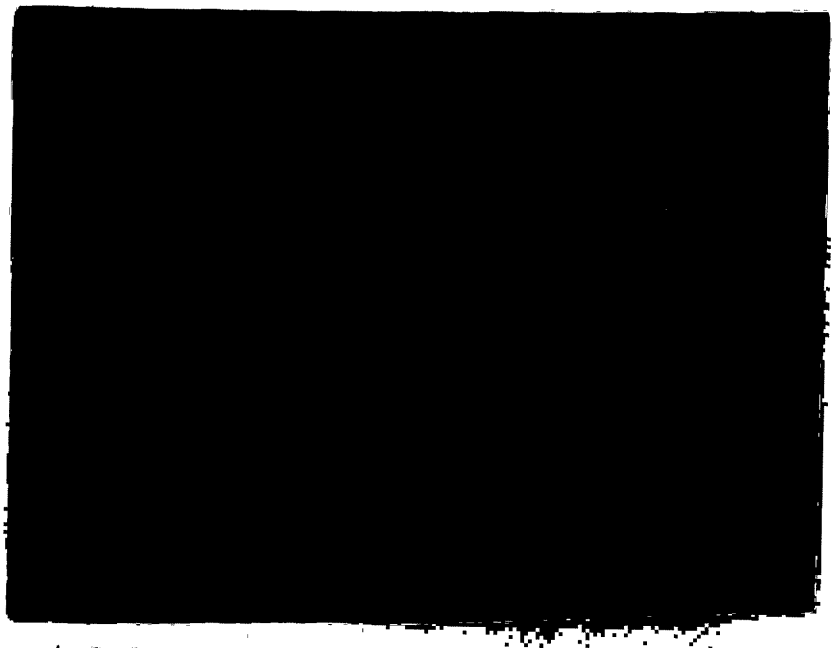

Fig. 4.2 (b)

Fig. 4.2. Unexposed [illegible] on-continuous carbon film. [illegible] (b) [illegible] diffraction pattern

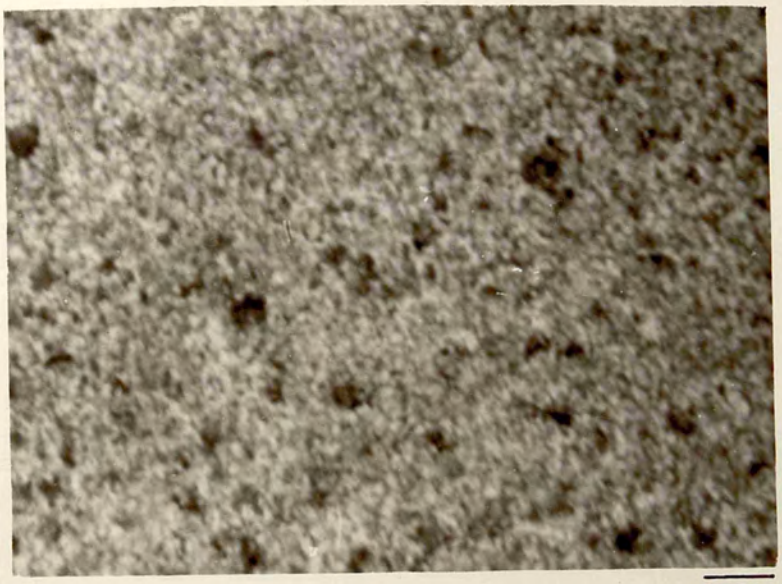

100 nm

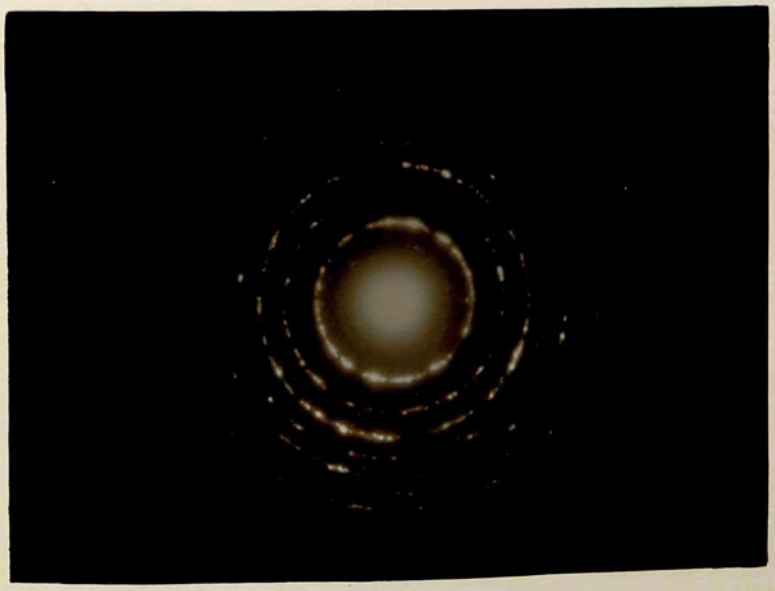

Fig. 4.4 (a)

Fig. 4.4 (b)

Fig. 4.4 Unexposed deposit of [illegible]
(a). micrograph, [illegible]

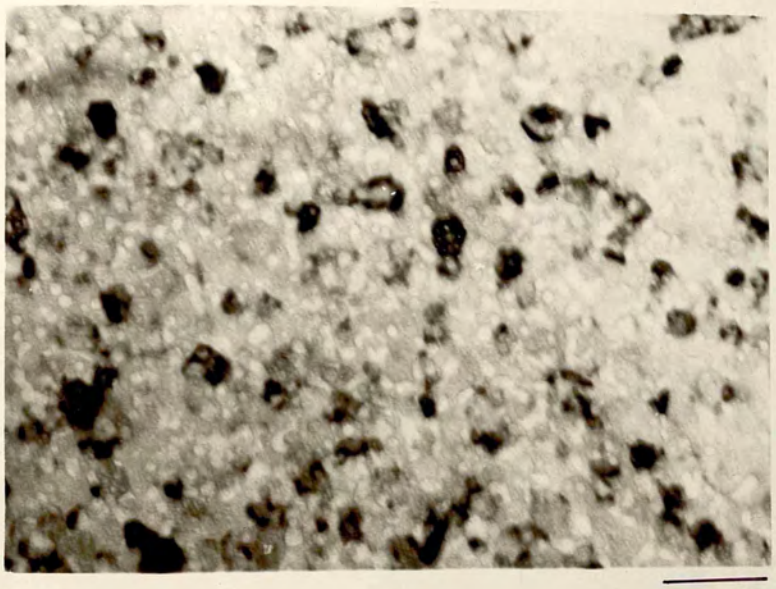

100nm

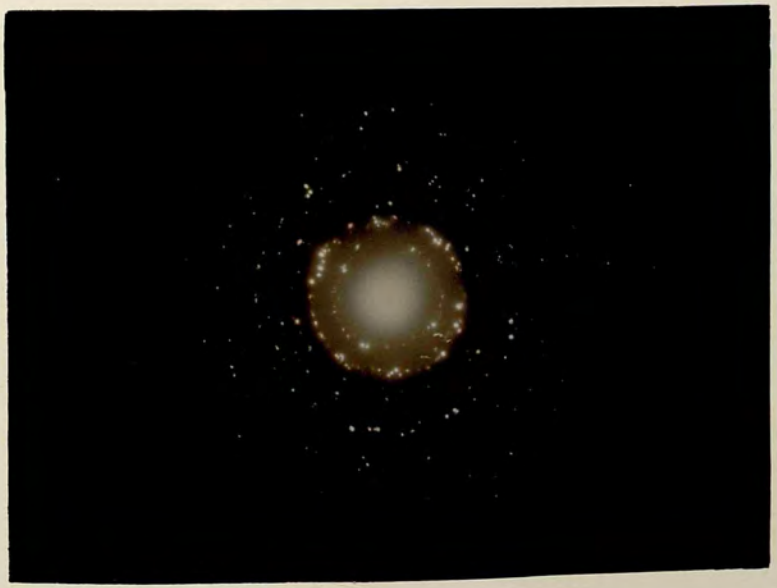

Thin film in an intermediate state, between island structure and the continuous film, has a structure with voids which makes these films less dense than the bulk material (Raether, 1976). The possible configuration of the crystallites in a thin evaporated film is shown in Fig. 4.3. The indexing of the diffraction pattern (Fig. 4.2 (b) shows only indices with h + k + l = even number occur i.e., the deposit has a bcc lattice structure.

The micrograph in Fig. 4.4 (a) from an unexposed deposit of CsCl and shows the presence of large clusters situated randomly on the substrate with diameter up to 35 nm. There are also some small nuclei of the order of 5 to 6 nm in diameter but most of them coalesce to form bigger clusters. This means there are insufficient small crystallites to make a complete ring in the diffraction pattern as shown in Fig. 4.4 (b). The intense spots on some rings represent a weak [001] orientation. In this diffraction pattern the rings corresponding to reflections from $\{100\}$, $\{110\}$, $\{111\}$, $\{200\}$, $\{210\}$ and $\{220\}$ planes, indicate that the lattice structure of CsCl is a simple cubic. (CsCl is sometimes referred to as bcc but logically is two interpenetrating simple cubic lattices separted by half the cube diagonal). The clear areas in the micrograph are due to the re-evaporation of the clusters by electron irradiation in the electron microscope.

Fig. 4.5 (a) is a micrograph of a thin deposit ($\cong$ 10 nm) of CsBr before exposure to the atmosphere. The clusters sizes are of the order of 5 to 20 nm and situated

randomly on the carbon substrate. The rings in its diffraction pattern, shown in Fig. 4.5 (b), consist of spots which indicate fewer larger crystallites without any particular orientation contributing to the pattern.

CsF is a highly hygroscopic halide and dissolves in conditions of high atmospheric humidity very rapidly, so great care is needed to observe unexposed deposits of this material. The micrograph in Fig. 4.6 (a) is from an unexposed deposit ($\simeq$ 15 nm) of CsF. The clusters sizes are from 7.5 nm to 15 nm in diameter and most of them are connected to each other to form islands, leaving channels or holes of uncoverd substrate. The large dark clusters are formed due to the multi nucleation on previous clusters. The crystallites are randomly situated on the substrate surface as indicated by diffraction pattern in Fig. 4.6 (b). The discontinuity in the rings and intense spots on the rings represent a weak [111] orientation normal to the substrate surface, i.e., some crystallites have their $\{111\}$ planes parallel to the substrate surface. The diffraction pattern contains indices only corresponding to fcc lattice structure, (h, k, l, either all even or all odd).

LiF is one of the alkali halides which is nearly insoluble in water and is therefore less reactive with the atmosphere. It can be evaporated and transferred to the electron microscope for observations without transport chamber. The thin film ($\simeq$ 10 nm) of LiF, shown in the micrograph in Fig. 4.7 (a), has very small nuclei detected

on low background structure substrate carbon. The average diameter of the smallest nuclei is between 2 and 4 nm, there are also a few large clusters about 12 nm in diameter. The islands, formed by the coalescence of small nuclei and further nucleation between the stable nuclei, appear grey in the micrograph. Its diffraction pattern is shown in Fig. 4.7 (b).

In the study of nucleation and growth of thin layers of alkali halides from the vapour phase, there has been observed three stages of the growth sequence: growth of small nuclei and clusters, coalescence of clusters to form islands and channel formation in nearly continuous film. The observations so for from electron micrographs and diffraction patterns are summarized in Tables 4.1 and 4.2.

Table 4.1

The sizes of nuclei and clusters and film thicknesses.

Halides	Lattice parameter a (nm)	The size of smallest nucleus (nm)	The size of largest cluster (nm)	Approximate film thickness (nm)
CsI	0.4568	5	50	15
CsCl	0.411	5	35	20
CsBr	0.429	5	20	10
CsF	0.6008	7.5	15	15
LiF	0.4017	2	12	10

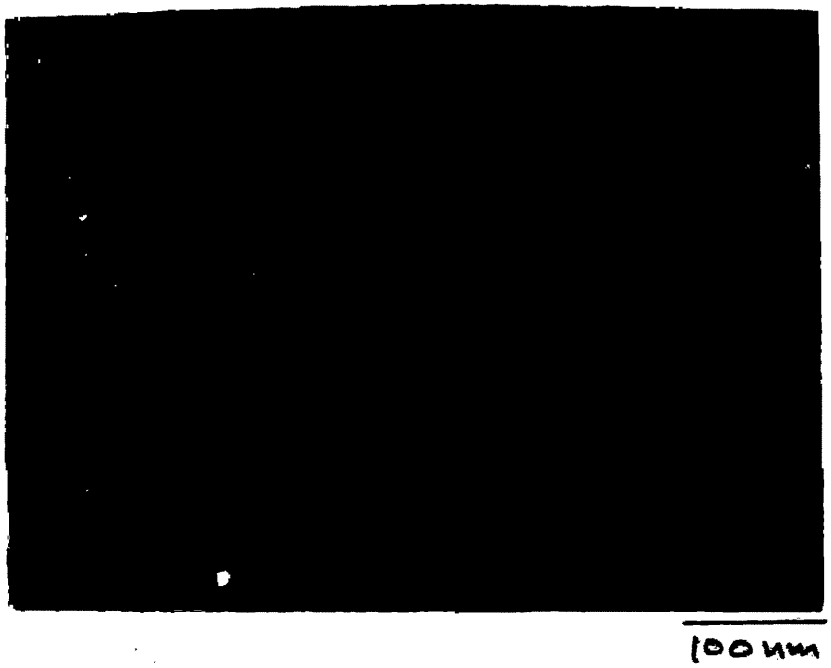

Fig. 4.5 (a)

Fig. 4.5 (b)

Fig. 4.5. Evaporated [illegible] on carbon before exposure to [illegible] atmosphere.
(a). [illegible] (b). [illegible]

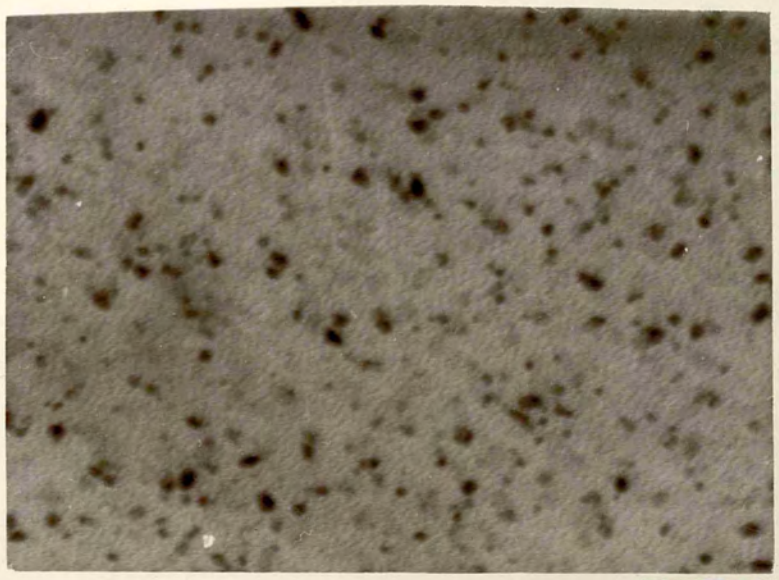

100 nm

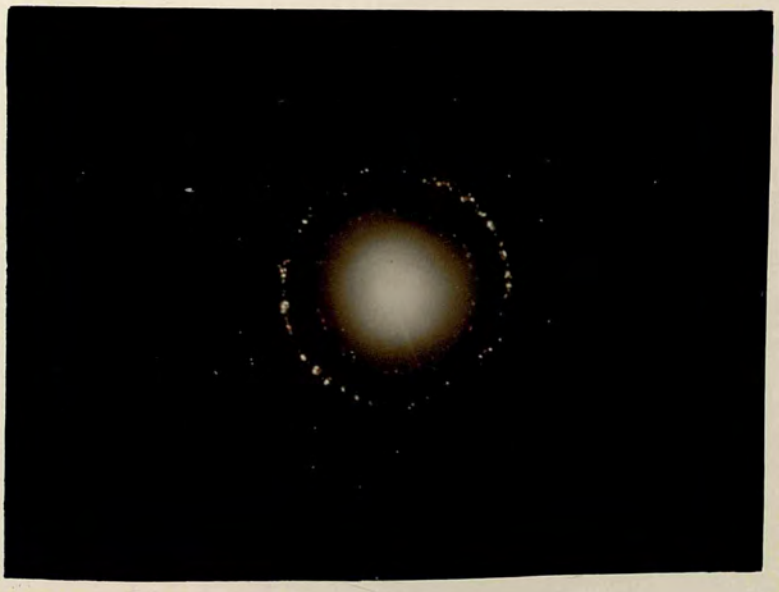

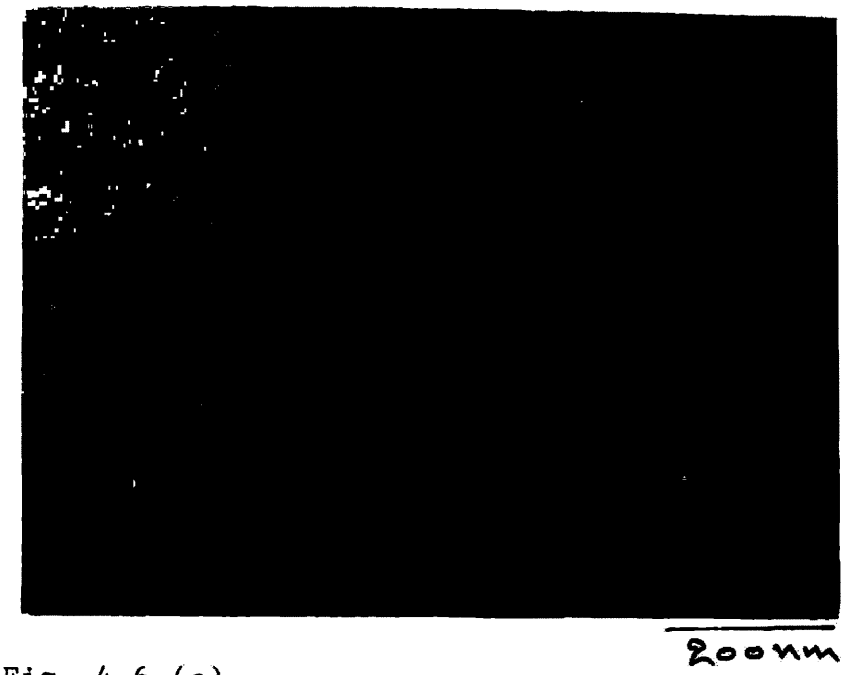

Fig. 4.6 (a)

Fig. 4.6 (b)

Fig. 4.6 Unexposed deposit of [illegible] film. (a). [illegible] pattern.

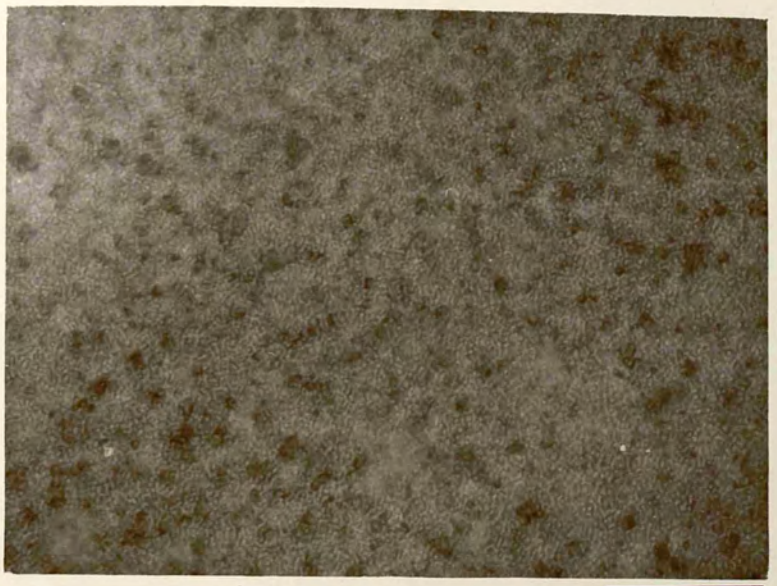

200nm

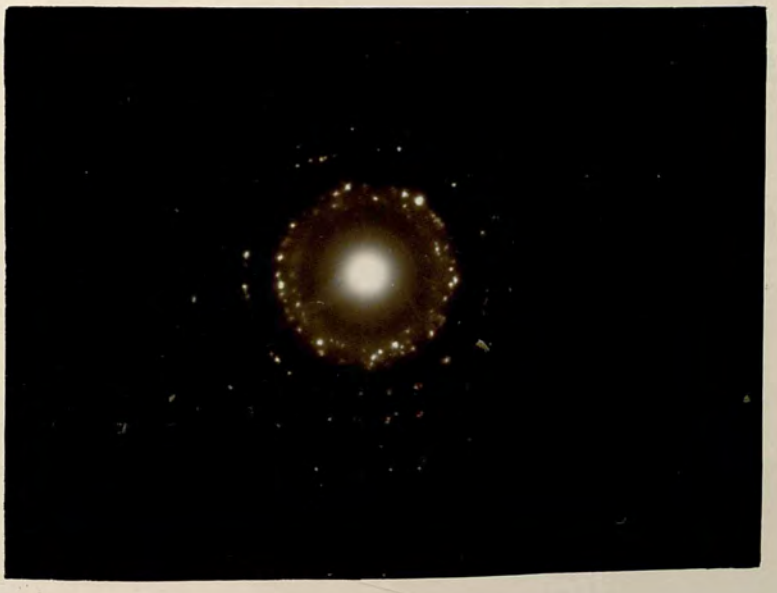

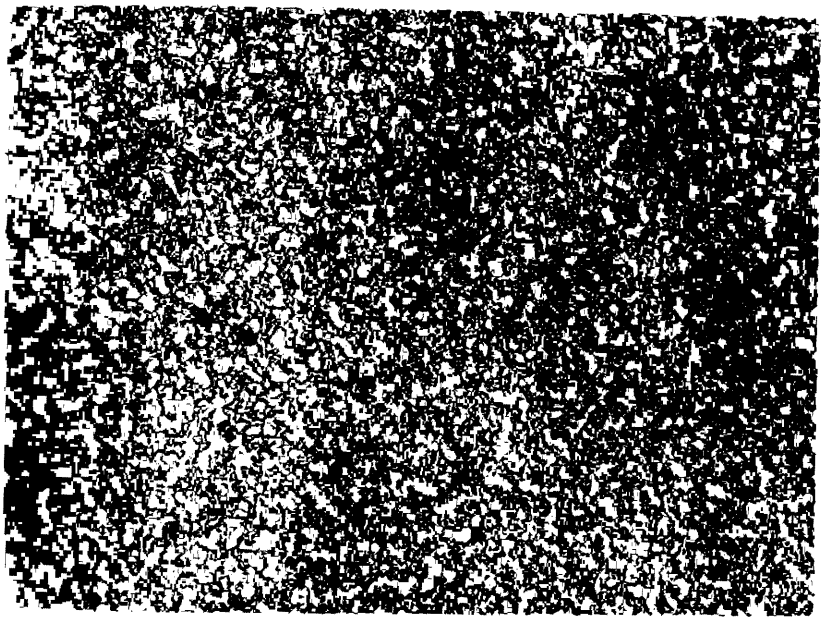

Fig. 4.7 (a)

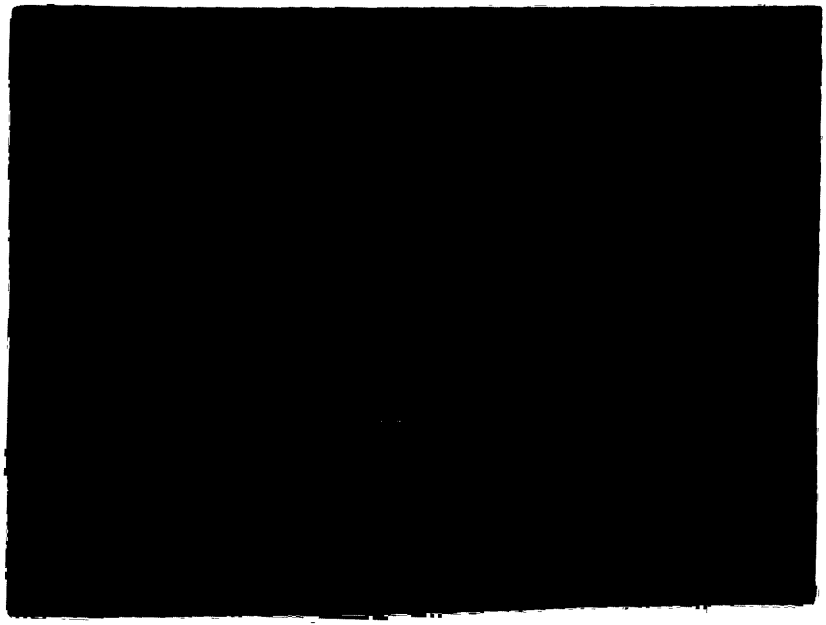

Fig. 4.7 (b)

Fig. 4.7 evaporated thin film of LiF on carbon
(a). micrograph, (b). diffraction pattern.


200nm

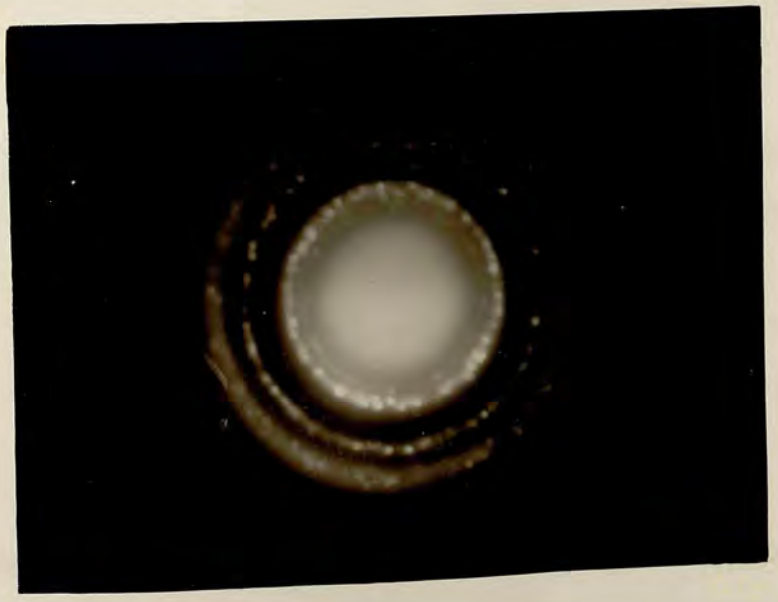

Table 4.2

The occurence of indices in diffraction patterns.

Halides	Indices occur in diffraction patterns
CsI	All indices of a bcc lattice structure.
CsCl	All indices of a simple cubic lattice structure.
CsBr	All indices of a bcc lattice structure and weak {100}.
CsF	All indices of an fcc lattice structure.
LiF	All indices of an fcc lattice structure.

4.6 Effect of Atmosphere on Thin Deposits.

Most of the alkali halides are more or less hygroscopic. When thin deposits of these materials are exposed to the atmosphere, they react with it and absorb water to make tiny droplets of their solution. In the electron microscope the water evaporates leaving behind a number of oriented small crystals or a quite large single crystal, depending on the thikness of the unexposed deposit and time of exposure. Although the substrate carbon film is amorphous, a crystal said to be oriented means one of the plane of crystal is parallel to the surface of the substrate. The perfection and the shape of the crystals depends on the rate of crystallisation.

The mechanism of formation of these crystals is the same as growth from solution, as discussed in chapter 2. Schulz (1951) used this technique to grow crystals of alkali halides from solution on to substrates of mica.

Fig. 4.8 (a) is an electron micrograph showing a 10 nm thick deposit of CsI after exposure to the atmosphere for 5 minutes. Clusters without any crystallographic shape are formed with dimensions between 25 nm and 50 nm. A film of nearly the same thickness exposed for 10 minutes to atmosphere, forms fewer bigger clusters, some of these are in contact and coalesce to form larger linked islands, as shown in Fig. 4.8 (b). The average diameter of these clusters is 150 nm.

After atmospheric exposure of 1 hour, the 50 nm thick deposit of CsI formed the large dendritic single crystal as shown in Fig. 4.9 (a). The deposit with this thickness formed a relatively thick continuous film on the substrate and having nearly the bulk density. (As stated in section 4.5, the thin deposits are less dense, according to Raether (1976) less than 10 nm thick film has only 10% of the bulk density and more than 50 nm thick film has nearly the same density). A thick deposit absorbs water from atmospheric humidity and forms few large drops of concentrated solution on the substrate. In the electron microscope the water evaporates very quickly and due to the high concentration of the material in the solution, rapid growth occurs and forms dendrites. The mechanism of the formation of dendrites from supersaturated solution is

discussed in chapter 2. The central part of the crystal is more thicker than the edges, the edges are fairly transparent to the electrons and show some bending contours. There are some small holes in the transparent areas which arise from the sublimation of the material by electron bombardment in the electron microscope. Its diffraction pattern is shown in Fig. 4.9 (b) which indicates that the crystal is normal to $[\bar{1}33]$, i.e., the $(\bar{1}33)$ plane of the crystal is parallel to the substrate surface.

Fig.4.10 (a) shows another large single crystal formed when a $\simeq$ 20 nm thick deposit of CsI was exposed for 1 hour and the growth rate decreased by covering the specimen to slow down the evaporation of water. The diffraction pattern (Fig. 4.10. b) shows the crystal has a $[\bar{1}11]$ orientation normal to the substrate surface and some extra spots in the pattern indicate the presence of some misoriented fragments.

CsBr behaves differently when exposed to the atmosphere after evaporation. Fig. 4.11 (a) shows a 10 nm thick deposit of CsBr after exposure to the atmosphere for 20 minutes. A number of clusters, with diameters between 40 and 50 nm, formed. Some of them are nearly square-shaped with average side length about 30 nm. These crystals are situated randomly on the carbon substrate as indicated by its diffraction pattern showing in Fig. 4.11 (b). As CsF is more hygroscopic than any other alkali halide, it reacts with the atmospheric moisture very rapidly.

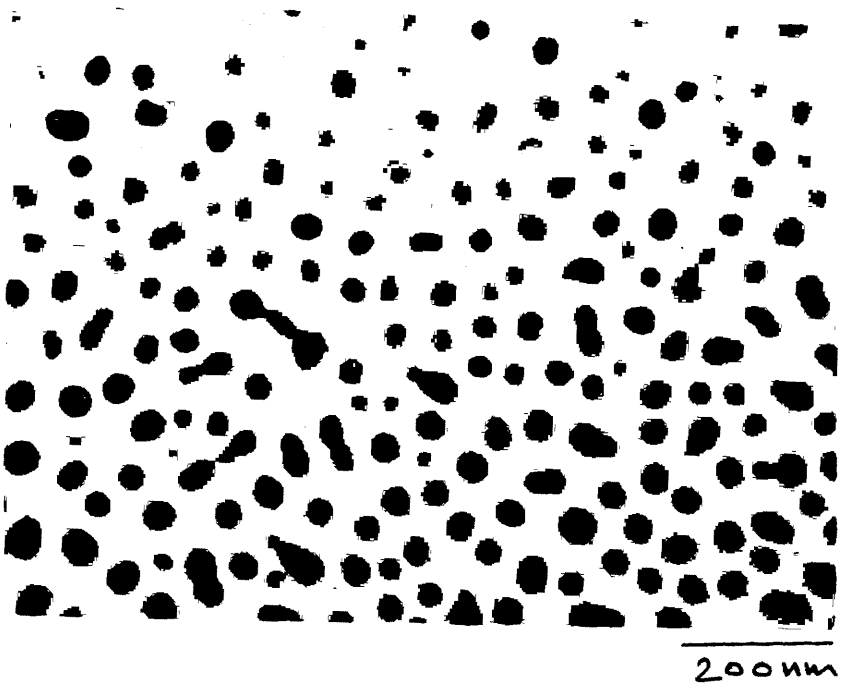

Fig. 4.8 (a)

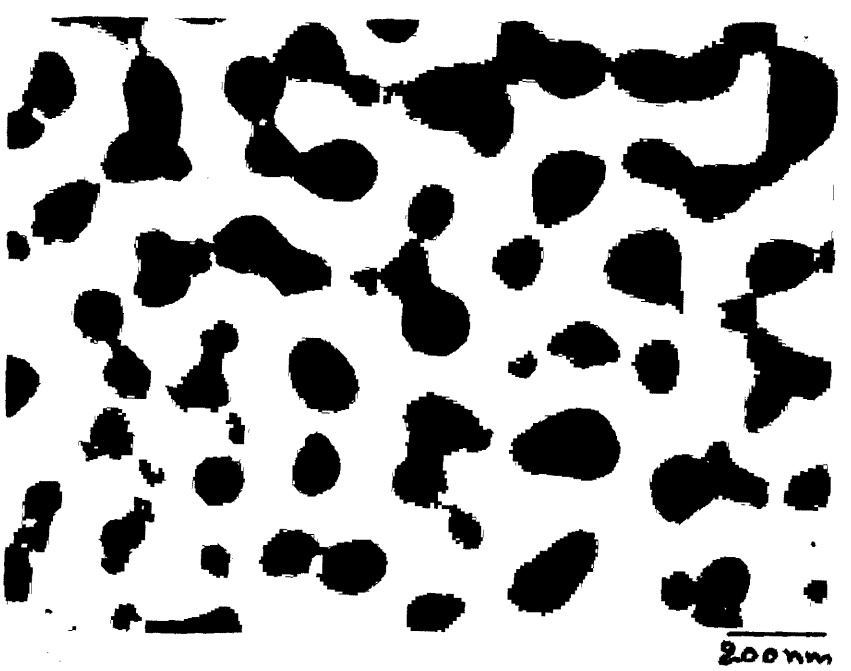

Fig. 4.8 (b)

Fig. 4.8 Thin deposit of CsI after exposure to the atmosphere, (a) for 5 minutes (b) for 10 minutes.

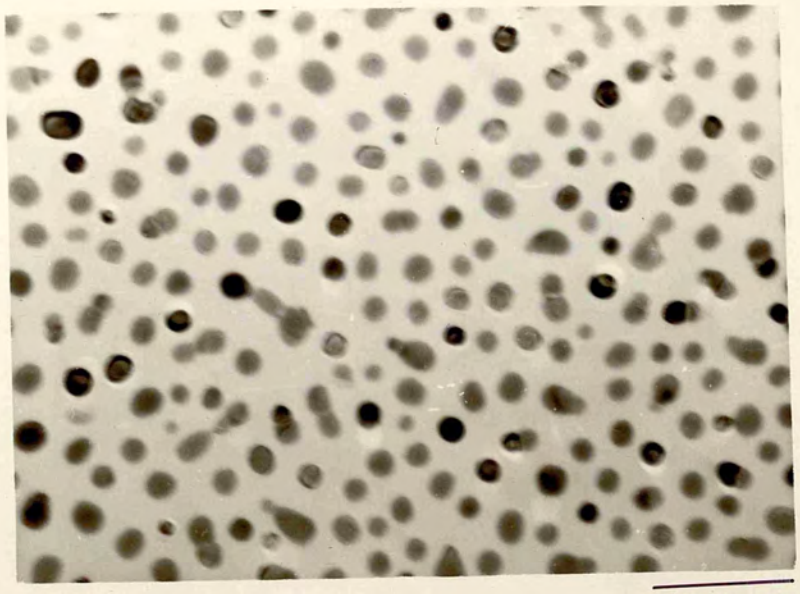
200nm

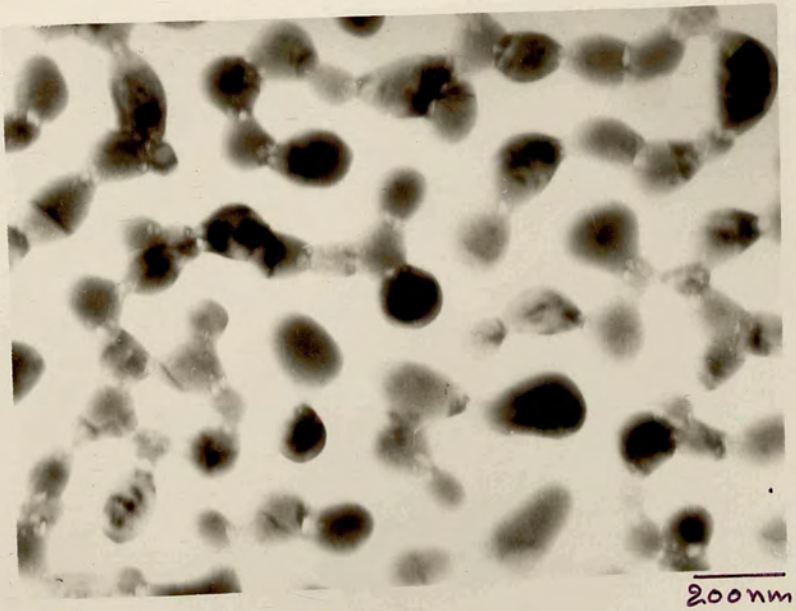
200nm

Fig. 4.9 (a)

Fig. 4.9 (b)

Fig. 4.9 A 50 nm thick deposit of CaI after exposure to the atmosphere for 1 hour.
(a) micrograph of dendritic crystal
(b) diffraction pattern.

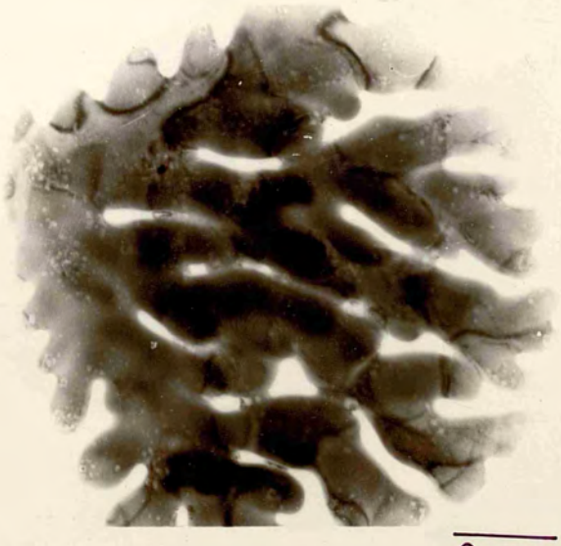

200nm

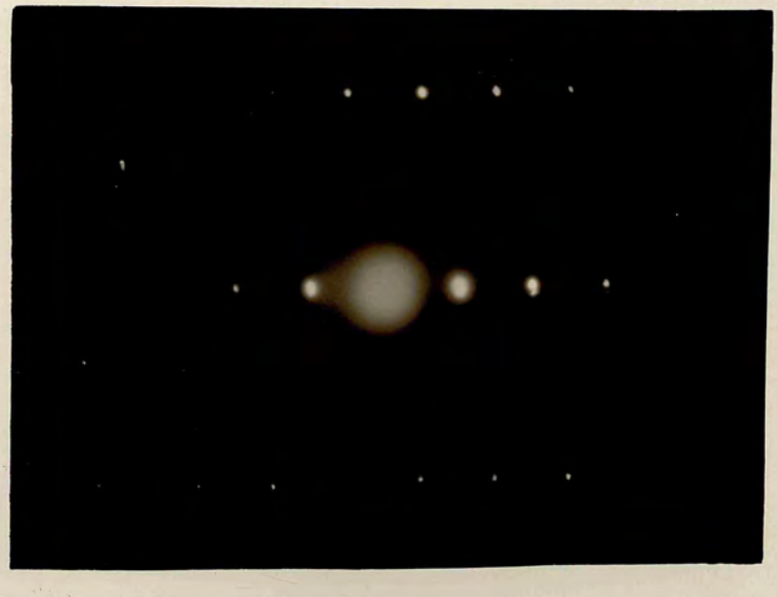

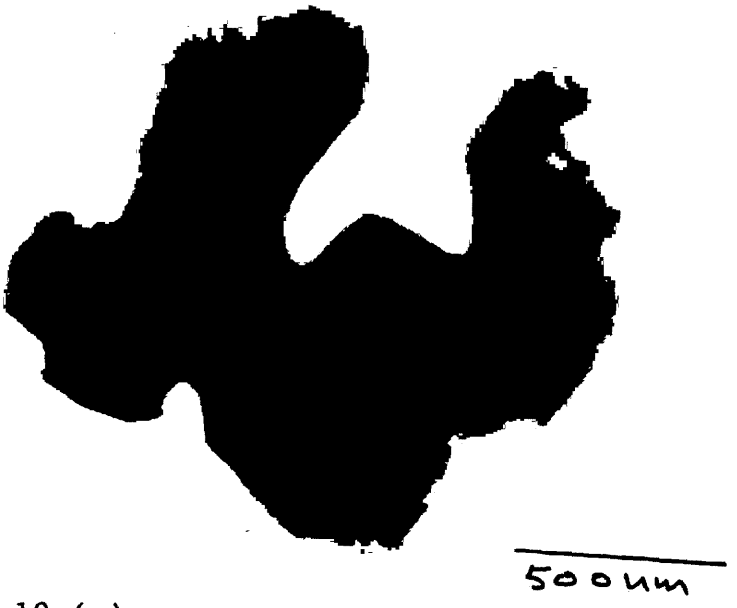

Fig. 4.10 (a)

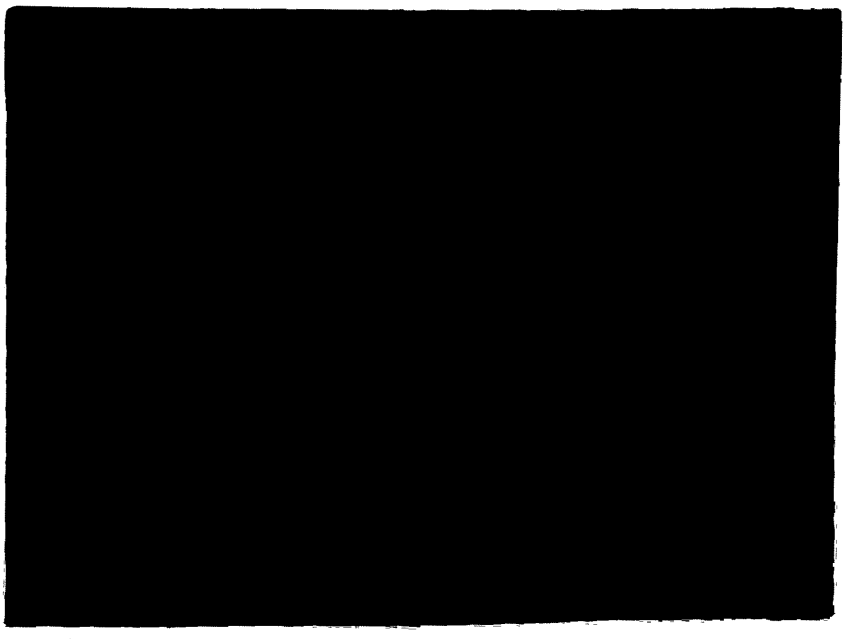

Fig. 4.10 (b)

Fig. 4.10 Evaporated CsI exposed to the atmosphere for 1 hour (with decreased rate of crystallization) (a) micrograph, (b) diffraction pattern.


500 nm

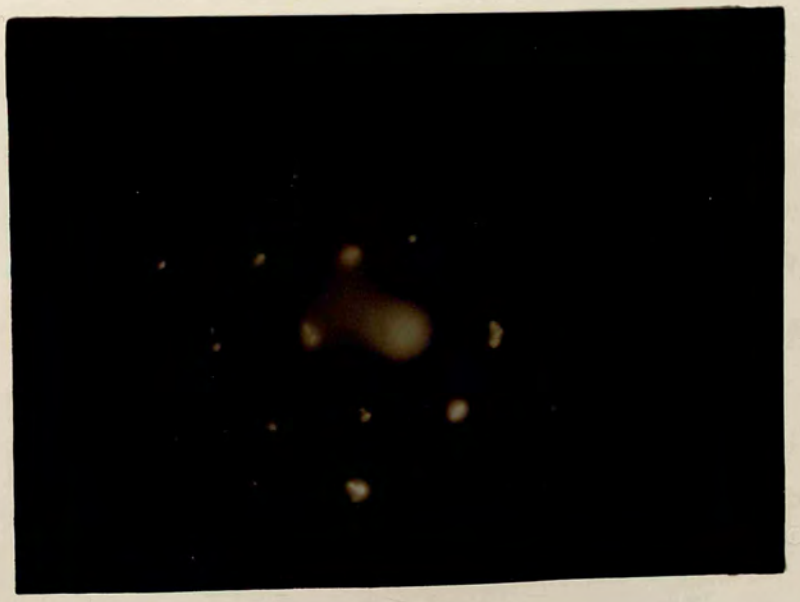

Fig. 4.12 (a) is a micrograph of a 20 nm thick deposit of CsF after exposure to the atmosphere for just 3 minutes, triangular-shaped single crystals were formed. The diffraction pattern of one of these crystals is shown in Fig. 4.12 (b), indicates that the crystal is oriented with $[\bar{1}12]$ normal to the substrate surface.

Finally LiF was investigated wich is nearly insoluble in water at room temperature and, therefore, much much less reactive with atmosphere. There has not been observed any significant change in an initially unexposed deposit after exposure to the normal atmosphere for severval hours. However, when a thin deposit of LiF was exposed to water vapour, the solution and recrystallization occurs. The experimental detail of this process of recrystallization is given as follows: An electron microscope grid, with a 10 nm thick deposit of LiF on continuous carbon film substrate, was held horizontally over a bowl containing very hot water, for 1 minute and then observed in the electron microscope. The resulted micrograph is shown in Fig. 4.13, which shows there are a number of small crystals with an average dimension of 15 nm were formed. Some of them coalesced into large clusters of several crystallites, thus clearing the surrounding substrate area. Although LiF is insoluble in water in bulk quantity as stated earlier thin evaporated films of alkali halides are porous and less dense as compared to the bulk. Since, LiF is not hygroscopic, it is unlikely that even a thin deposit of

this material dissolves in normal atmospheric humidity, which is only 40 % at room temperature. When thin deposit exposed to water vpour, where the humidity and temperature are much higher, the small crystallites in the unexposed deposit dissolve and make droplets of solution and in the electron microscope water evaporates leaving behind small crystals or clusters of small crystals.

The micrograph in Fig. 4.14, is from a 20 nm thick deposit of LiF after exposure to water vapour for 3 minutes, shows large number of cube shaped crystals were formed. Nearly all crystals are linked to one an other and most of them are electronically transparent. An other example of recrystallization of thin deposit of LiF is shown in Fig. 4.15 (a), where a 5 nm thick deposit was exposed to water vapour for 1/2 minute immediately after evaporation. Since, the deposit with such thickness does not form continuous film on carbon substrate, the isolated clusters in the unexposed deposit dissolve in water vapour and form droplets of solution, which produce quite separated crystals. The selected area diffraction pattern, of above is shown in Fig 4.15 (b) indicates an orientation [001] normal to the substrate surface and some extra spots represent some slightly misoriented superimposed crystals.

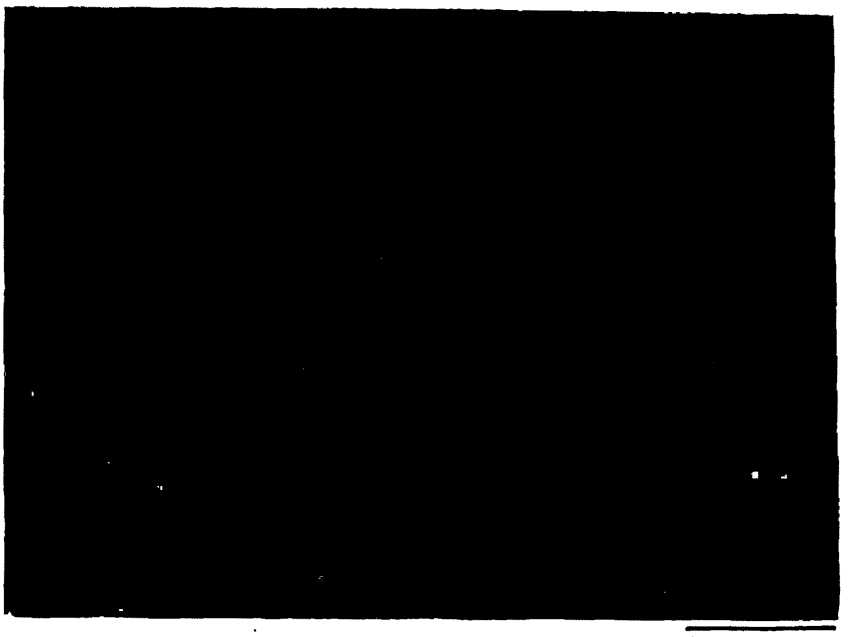

Fig. 4.11 (a)

Fig. 4.11 (b)

Fig. 4.11 (b) A 10 nm thick deposit of CsBr after exposure to the atmosphere for 20 minutes.
(a) micrograph, (b) diffraction pattern.

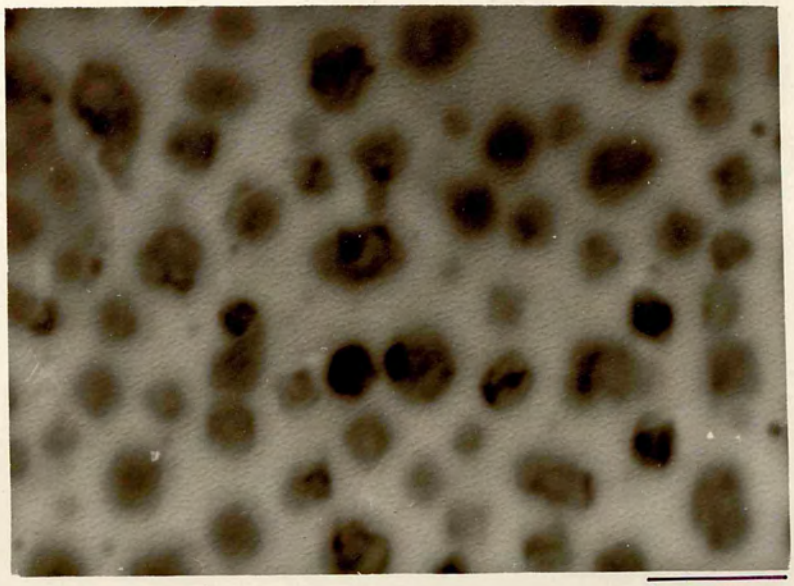
100nm

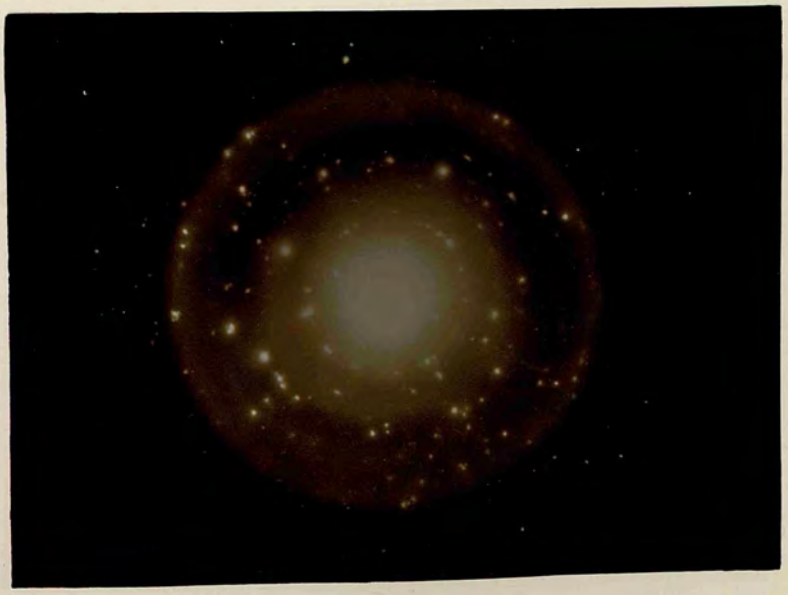

Fig. 4.12 (a)

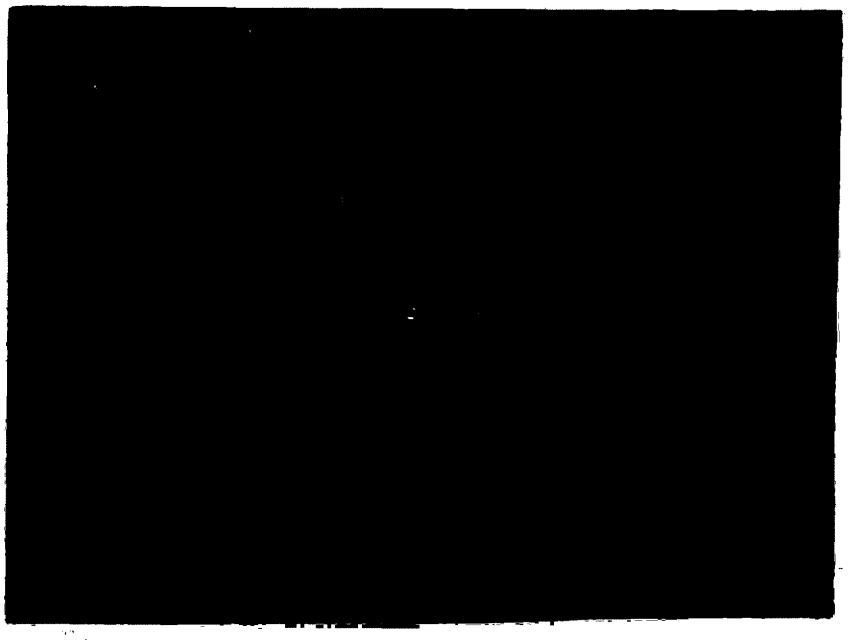

Fig. 4.12 (b)

Fig. 4.12 Evaporated Gnf after exposure to the atmosphere
(a) micrograph showing large single crystals
(b) diffraction pattern of one of the crystal.

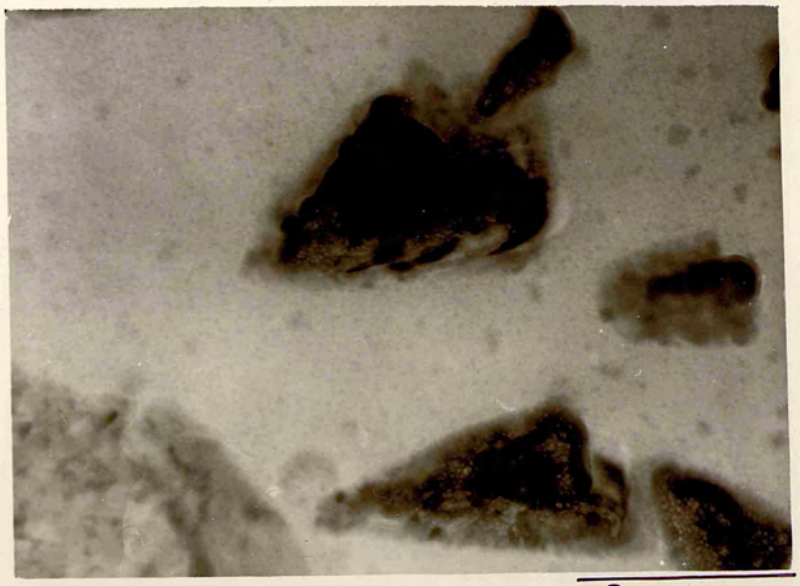

250 nm

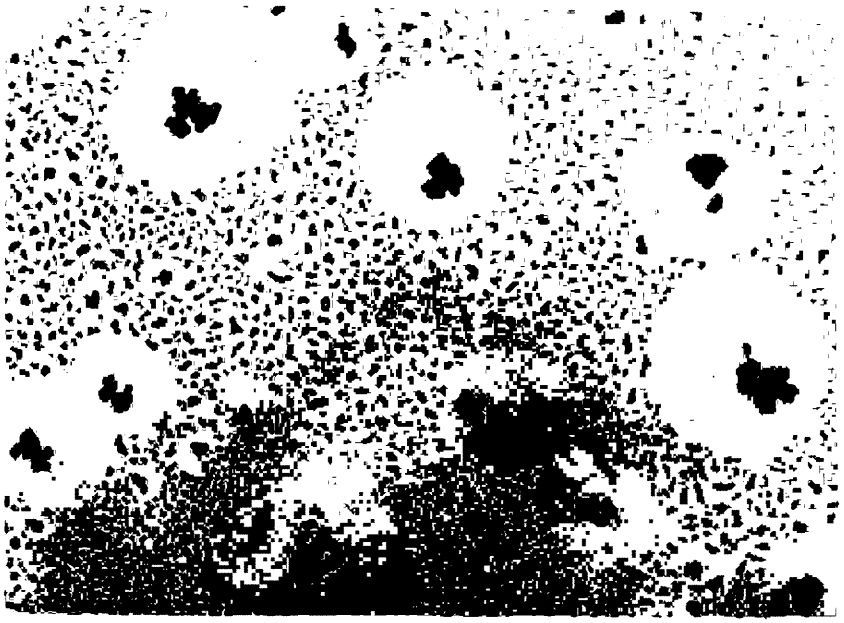

Fig. 4.13

Fig. 4.14

Fig. 4.13. Micrograph of a 10 nm thick deposit of LiF exposed to water vapour showing the formation of crystals and clustering of crystals. (exposure time 1 minute)

Fig. 4.14 A 20 nm thick deposit exposed to water vapour for 3 minutes, showing cube shaped crystals.

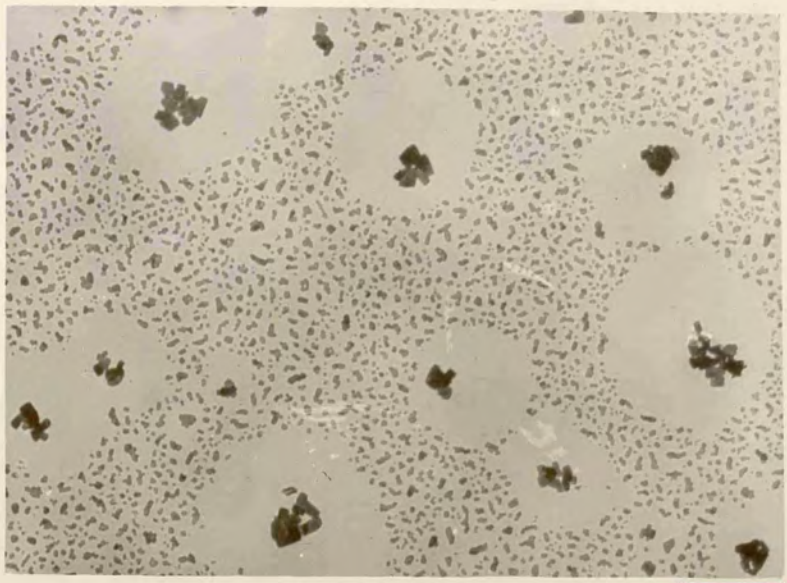

2000nm

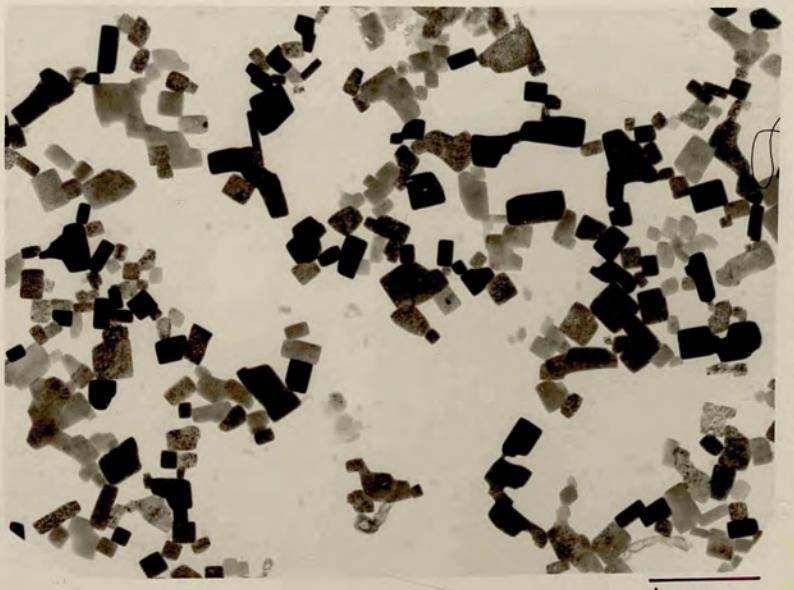

1000nm

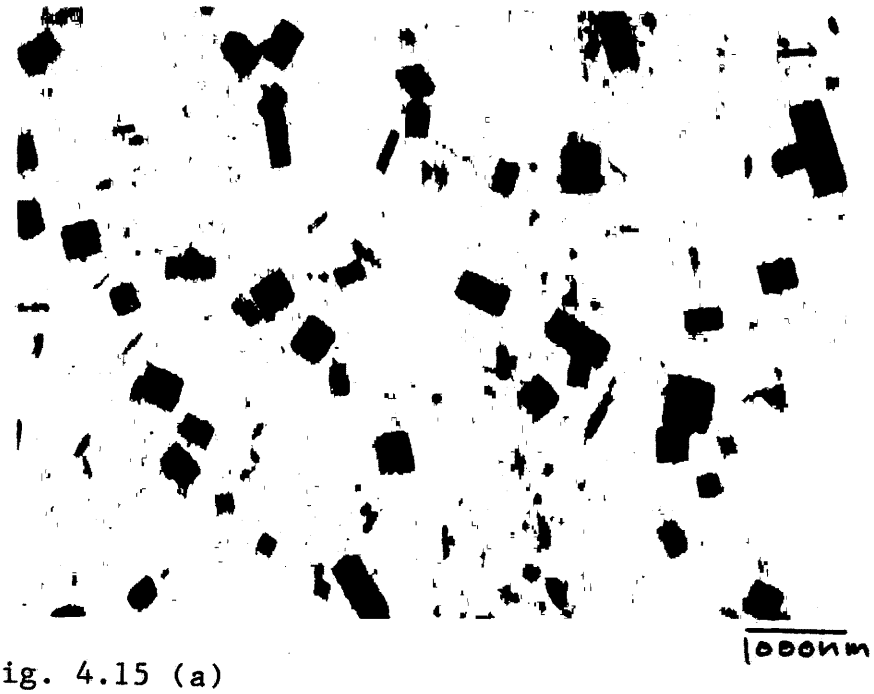

Fig. 4.15 (a)

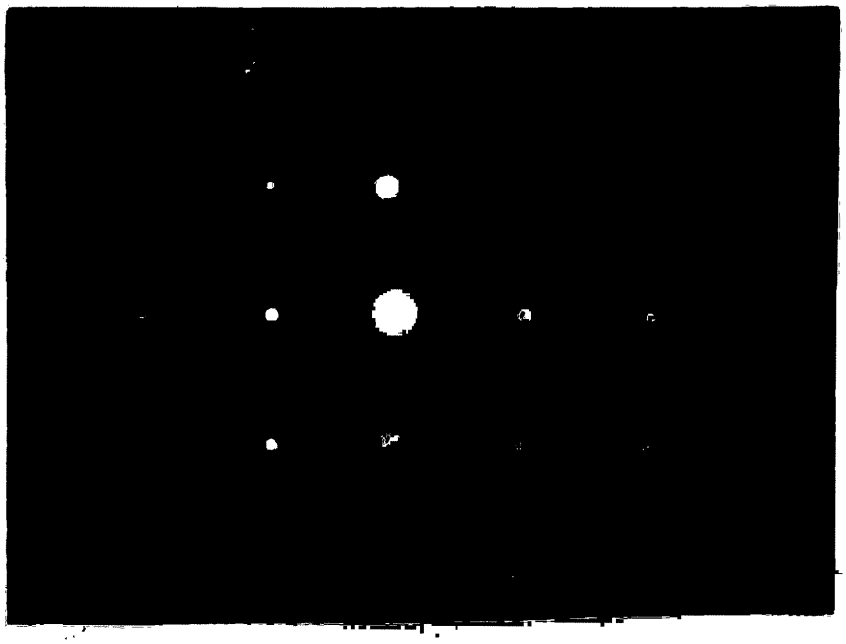

Fig. 4.15 (b)

Fig. 4.15(a)A 5 μm thick deposit of LiF after exposure to water vapour for 1 minute showing separated crystallites and twins.
(b) Selected area diffraction pattern.

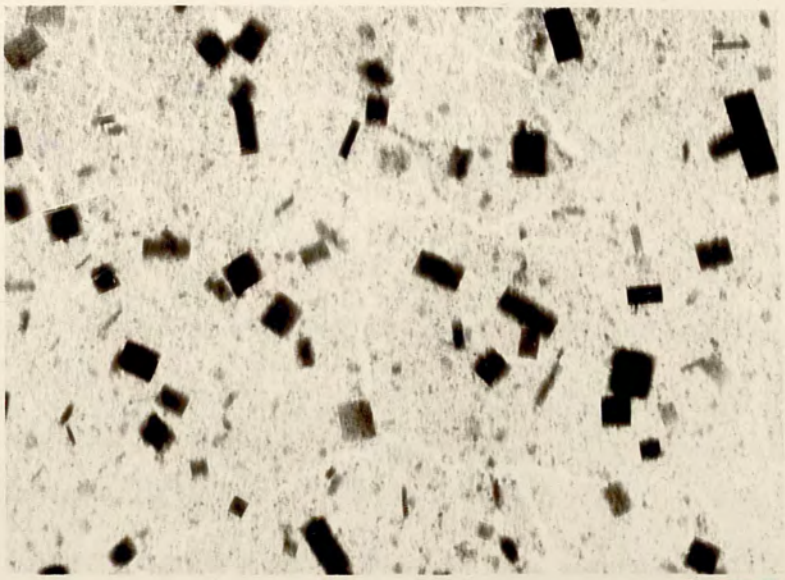
1000nm

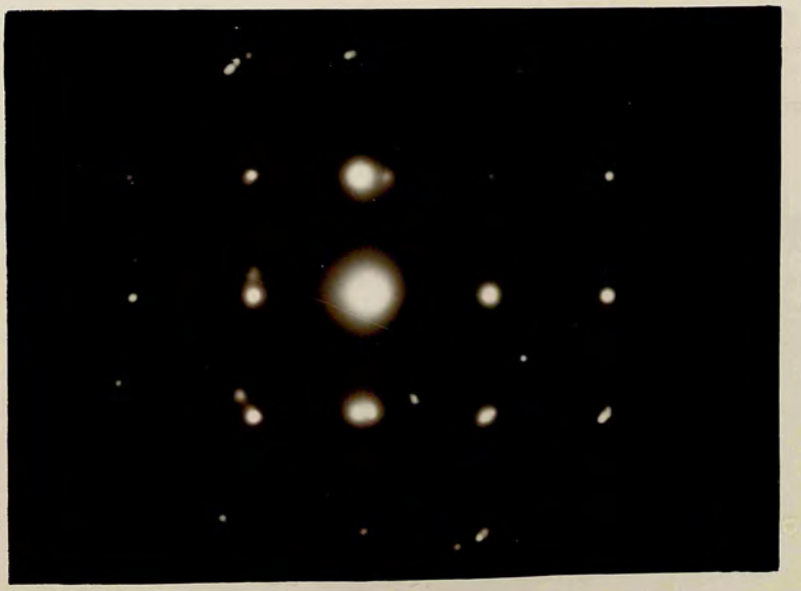

4.7 Conclusions

From the studies presented in this chapter the following conclusions are drawn:

1. The growth process in thin films of alkali halides is the same as that observed in growth of metallic thin films.
2. Alkali halides form very stable nuclei in the early stages of growth.
3. The smallest stable nuclei detected were 2 nm in size and the largest 50 nm in thin films with average thickness less than 20 nm.
4. The crystallites are randomly distributed on the carbon substrate.
5. A few crystallites in unexposed deposits have planes parallel to the surface of the substrate and show weak orientations.
6. These small crystallites form large sigle crystals when exposed to the atmosphere.
7. The thin deposits of LiF do not dissolve in normal atmospheric humidity, but form crystals when exposed to water vapour.

References

BECKER,R. and DOERING,W., (1935). Ann. Physik. 24, 719.

BRADLEY,D.E. (1954). Brit. J. Appl. Phys. 5, 65.

CABRERA,N. (1959). Discussions Faraday Soc., 28, 16.

GLANG,R. (1970) In "Handbook of Thin Film Technology" (Massel and Glang ed.) ch. 1. McGraw-Hill Book Company, New York.

HIRTH,J.P. and POUND,G.M. (1963). In "Condensation and Evaporation" Progress in Material Science. (B.Chalmer ed.) vol. 11, p. 41. MacMillan, New York.

HOLLAND,L. (1970). In "Vacuum Deposition of Thin Films" (Holland ed.) ch. 7, Chapman and Hall. London.

HOLLOMAN,J.H. and TURNBAL,D. (1953). In "Progress in Metal Physics" vol. 4, p. 333.

LENNARD-JONES,J.E. (1937). Pro. Roy. Soc. London. A, 163, 127.

LEWIS,B. (1967). Thin Solid Films, 1, 85.

McCARROLL,B. and EHRLICH,G. (1963). J. Chem. Phys. 38, 523.

McFEE,J.H. (1960). Ph.D. Thesis, Carnegie Institute of Technology.

NEUGEHAUER,C.A. (1970). In "Handbook of Thin Film Technology" (Maissel and Glang eds.) ch. 8, McGraw-Hill Book Company, New York.

PASHLEY,D.W., STOWELL,M.J., JACOBS,M.H. and LAWNT.J. (1964). Phil. Mag. 10, 127.

RAETHER,H. (1976). In "Physics of Nonmetallic Thin Films" (Dupuy and Cachard eds.) p. 123, Plenum Press. New york.

RHODIN,T. and WALTON,D. (1964). In "Single Crystal Films" p. 331, Pergamon Press, New York.

RHODIN,T. (1965). In "The Use of Thin Films in Physical Investigations" (Anderson ed.) part 3, Academic Press London.

SCHULZ,L.G. (1951). Acta Cryst. 4, 483.

SCHULZ,L.G. (1951). Acta Cryst. 4, 487.

SIGSBEE,R.A. and POUND,G.M. (1967). Advan. Coll. Interf. Sci., 1, 335.

VENABLES,J.A. and PRICE,G.L. (1975). In "Epitaxial Growth" (Matthews ed.) ch. 4, Acadamic Press New York

VOLMER,M. and WEBER,A. (1925). Z. Phys. Chem., 119, 277.

WALTON,D. (1962). J. Chem. Phys., 37, 218.

WALTON,D. (1962) Phil. Mag., 7, 1671.

WALTON,D., RHODIN,T. and ROLLINS,R.W. (1967). J. Chem. Phys., 38, 2698.

ZWANZIG,R.W. (1960). J. Chem. Phys., 32, 1173.

CHAPTER FIVE

NUCLEATION AND GROWTH OF ALKALI HALIDES ON CsI SUBSTRATES

5.1 Introduction

Alkali halides include a large number of materials which are extensively used in industry and scientific research. Studies of the nucleation and growth of these materials can provide information wich may be useful in the manufacturing of thin layers and crystals with desirable qualities.

Most of the published work on the nucleation and growth of alkali halides on other alkali halides deals with the common halides of sodium, potassium and lithium. The substrates used have usually been NaCl, KCl and LiF. Very little work has been reported on the growth of caesium halides: Royer (1928) (CsF on NaCl and KCl), Schulz (1950) (CsBr on LiF), Schulz (1951) (CsCL, CsBr and CsI on LiF, NaCl and KBr) and Ludemann (1957) (CsCl on LiF and CsBr on KCl).

CsI has not been used as a substrate before the present work. As explained in chapter two single crystal of CsI can be produced with reasonable flat surface. The experiments of gold decoration on alkali halides show that CsI has the flattest surface of all the halides of caesium and is, therefore, the best substrate for nucleation and growth of other alkali halides.

5.2 Lattice Structure of CsI.

X — ray crystallographic data shows the lattice structureof CsI to be body— centred cubic as shown in Fig. 5.1.

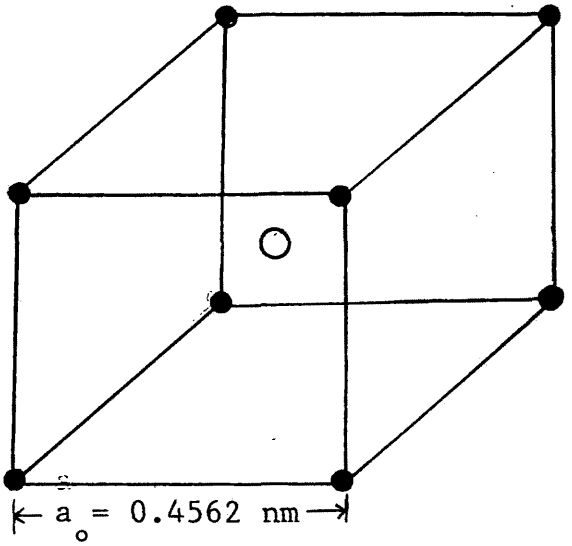

Fig. 5.1. Unit cell of CsI.
● — Cs, o — I .

The lattice complex for CsI is as follows:

(i) Cs^+ at (0,0,0)

I^- at $(\frac{1}{2},\frac{1}{2},\frac{1}{2})$

(ii) with alternate choice of origin,

I^- at (0,0,0)

Cs^+ at $(\frac{1}{2},\frac{1}{2},\frac{1}{2})$

The lattice parameter a_o= 0.4562 nm and the Cs——I contact distance lies along the body diagonal of the cube, giving an effective radius sum

$$r_{Cs} + r_I = \sqrt{3}\, a/2 = 0.395 \text{ nm}$$

The structure-factor equation for CsI can be written as:

$$F_{hkl} = f_{Cs} e^{2\pi i(0)} + f_{\bar{I}}\, e^{2\pi i(\frac{1}{2}h+\frac{1}{2}k+\frac{1}{2}l)}$$

$$= f_{Cs} + f_I\, e^{\pi i(h+k+l)}$$

which means, if

$$h + k + l = \text{even number}$$

then

$$F_{hkl} = f_{Cs} + f_I$$

and, if

$$h + k + l = \text{odd number}$$

then

$$F_{hkl} = f_{Cs} - f_I \ .$$

The atomic number of Cs is 55 and of I is 53,wich means Cs^+ has 54 electrons and I^- also has 54 electrons i.e. electronically, the ions are identical and their scattering factors are similar. In a diffraction pattern of CsI the reflection from a plane whose indices' sum is odd has zero intensity. The diffraction pattern of CsI derives only from planes whose index sums are even. It makes the diffraction of CsI relatively easy to index, and helps to locate the spots reflected from overgrowth.

Fig. 5.2 shows the diffraction pattren from a single crystal of CsI made by the technique explained in chapter two. It is shown from indexing that the crystal is normal to $[\bar{1}11]$,(the crystal is said to be normal to $[\bar{1}11]$ means $(\bar{1}11)$ plane of crystal is normal to electron beam), and all the spots have indices whose sum is even. The diffraction pattern in Fig. 5.3 is from a polycrystalline film of CsI grown on continuous carbon film. The indexing shows the rings correspond to $\{110\}$, $\{200\}$, $\{211\}$, $\{310\}$, $\{222\}$,------- and so on.

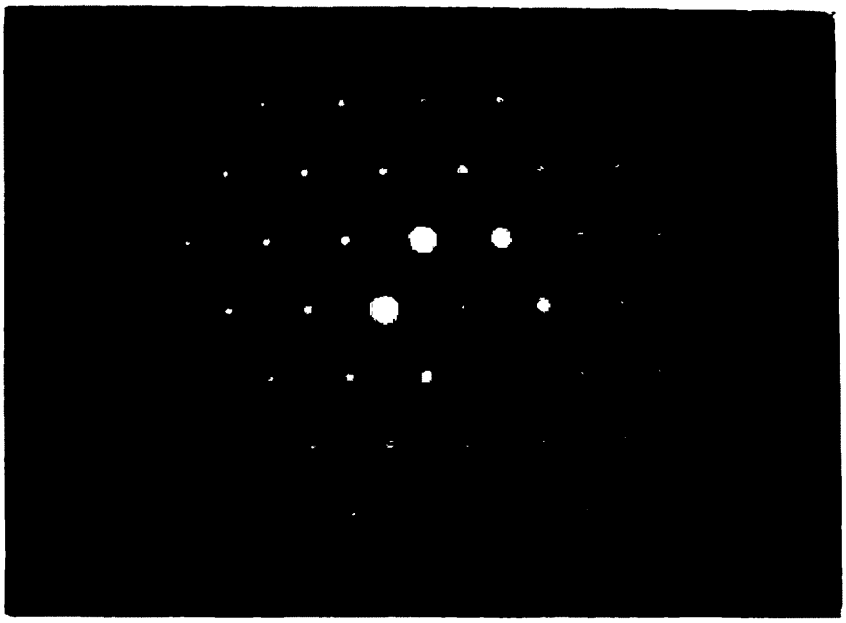

Fig. 5.2.

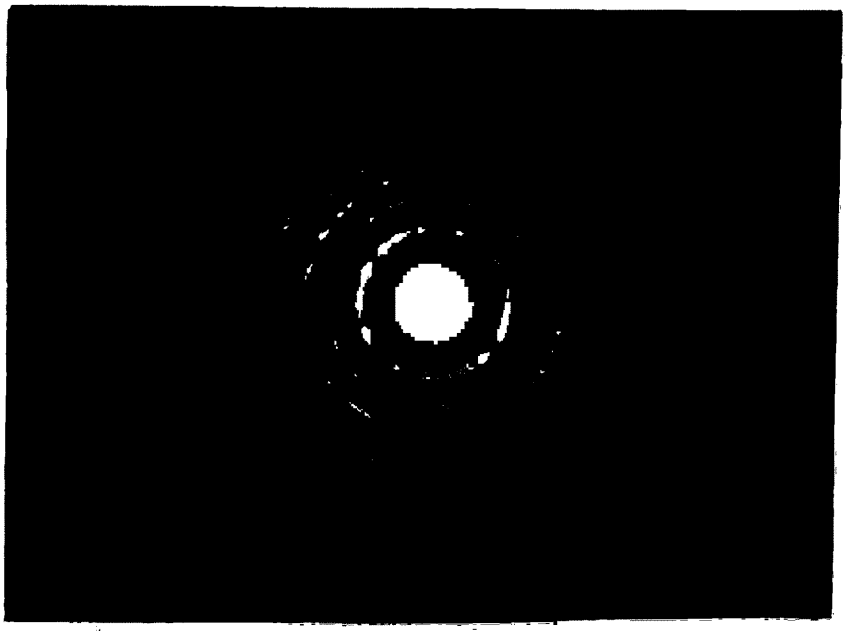

Fig. 5.3.

Fig. 5.2. Electron diffraction from a [$\bar{1}$11] single crystal of CsI.

Fig. 5.3. Ring pattren from a polycrystalline film of CsI (grown from vapour phase on continuous carbon film).

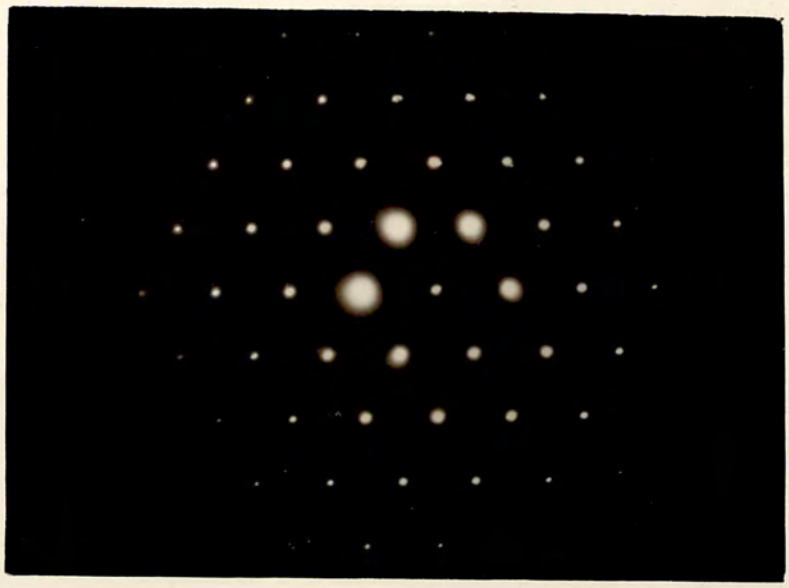

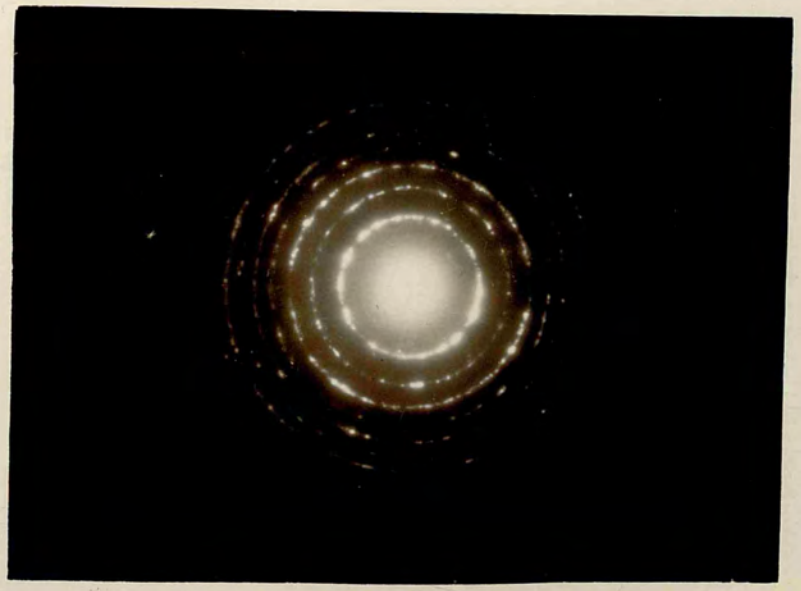

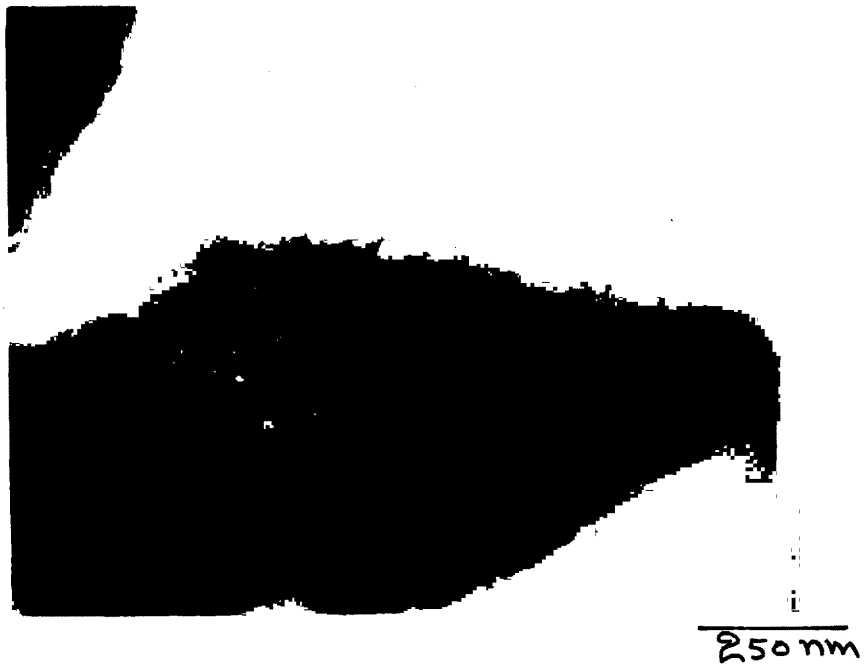

Fig. 5.4. (a)

Fig. 5.4 (b)

Figs. 5.4. (a) and (b). Unexposed deposit of CsI on [111] CsI.

250 nm

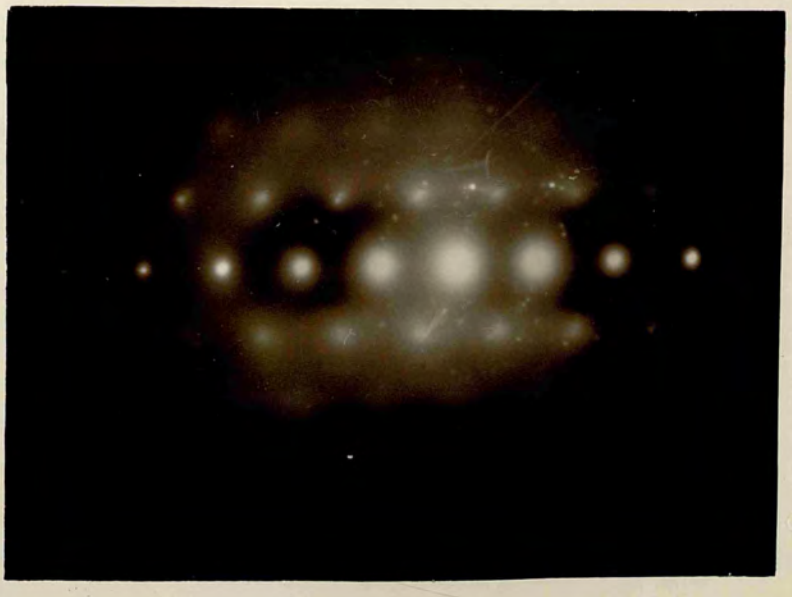

5.3 Experimental Procedure.

A tungsten boat was used for evaporation of CsI, CsCl, CsBr and CsF in a vacuum unit. The single crystals of CsI were produced in the holes of carbon films on electron microscope grids as described in chapter two and used as substrates. Two kinds of experiments have been carried out . In the first the film grown by evaporation was transferred into the electron microscope without exposing it to the atmosphere , by means of transport chamber. The schematic diagram of the complete evaporation unit with transport chamber is shown in Fig. 4.1 in chapter four and the transfer procedure is described in chapter three. This kind of deposits are referred as " unexposed ". In the second type of experiments the film was exposed to the atmosphere before being observed in the electron microscope (an " exposed " deposit).

The evaporation of alkali halides was performed under the following conditions:

Residual gas pressure	$= 10^{-9}$ bar
Temperature	$\cong 20\,^{\circ}C$ (room temp.)
Average deposition rate	$\cong 1$ nm sec^{-1}

5.4 Observations and Discussion.

(a) CsI on CsI

The unexposed deposits of CsI with average thickness 10 nm on a single crystal of CsI show either no orientation or very weak orientation, as seen in the diffraction patterns in Figs. 5.4 and 5.5

In Fig. 5.4 (a) the micrograph of an unexposed deposit of CsI on [$\bar{1}$11] CsI single crystal shows a number of small

crystallites situated randomly on the substrate. The sizes of these crystallites vary from 7.5 nm to 15 nm. As the overgrowth is on the lower surface of the substrate, the strong reflected beams from the substrate act as primary beams with respect to the overgrowth. As a result there are a number of secondary electron diffraction patterns as seen in Fig. 5.4 (b). The displacement of these patterns relative to one an other is the same as the separation of the corresponding reflections from the substrate. Schulz (1950) had observed the two secondary difraction patterns in examining the CsBr on LiF. Some more intense spots on the rings related to a very weak [111] orientation.

FIg. 5.5 shows another unexposed deposit of CsI on CsI. In the diffraction pattern of this deposit the more intense spots from the substrate and indicates that it is normal to $[\bar{1}12]$. The overgrowth gives two very weak rings correspond to $\{211\}$ and $\{321\}$ which indicate the randomness of the crystallites on the substrate. Two relatively weak orientations $[\bar{1}11]$ and $[\bar{1}13]$ are also been observed.

When a thin deposit of CsI on CsI is exposed to the atmosphere before examining in the electron microscope, recrystallization occurs and usually the overgrowth is well-oriented on the substrate surface, as seen from their diffraction patterns in Figs. 5.6, 5.7 and 5.8. Fig. 5.6 (a) is an electron micrograph showing a ~ 10 nm thick deposit of CsI after exposure to the atmosphere. There are a number of small crystallites, 5 to 10 nm in size and well-oriented on the $[\bar{1}11]$ CsI substrate as indicated by the diffractin pattern in Fig. 5.6 (b). There are two fairly large and a few small

Fig. 5.5 (a)

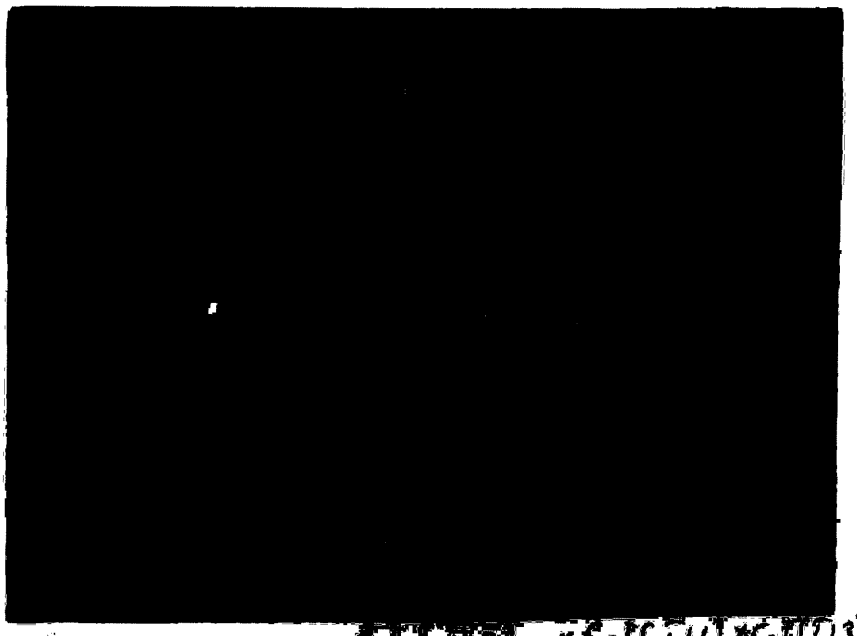

Fig. 5.5. (b)

Figs. 5.5 (a) and (b). Decorated deposit of CsI on [111] CsI.

500nm

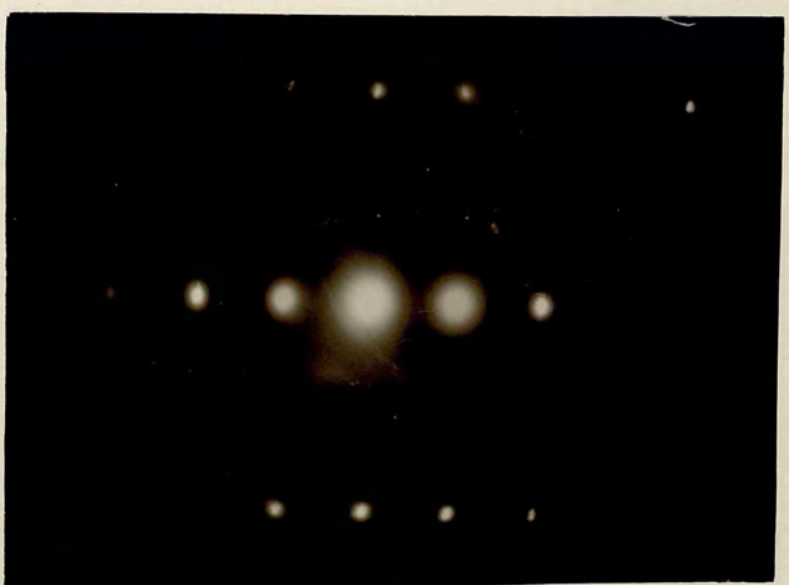

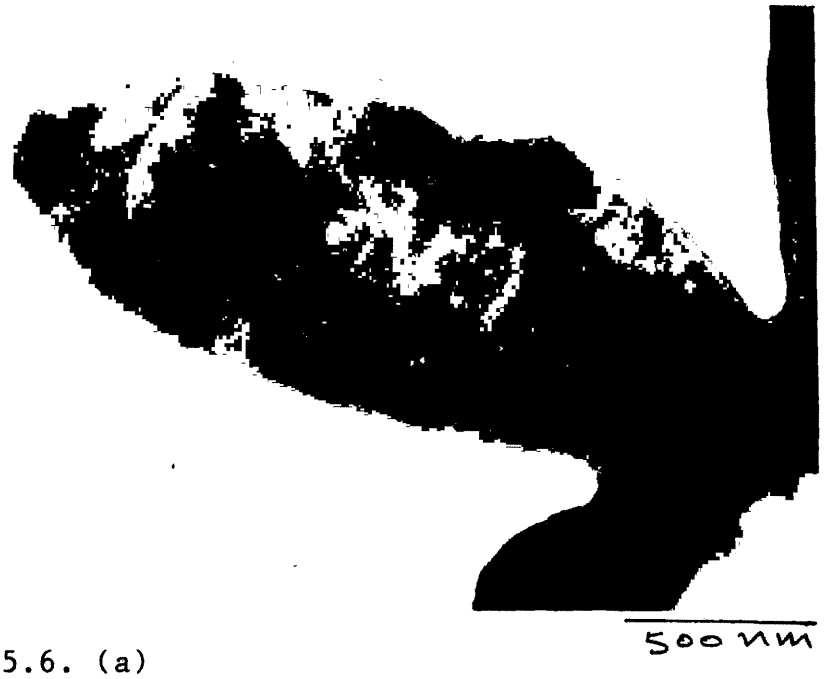

Fig. 5.6. (a)

Fig. 5.6. (b)

Figs. 5.6. (a) and (b). Exposed deposit of CsI on [$\bar{1}$11] CsI.

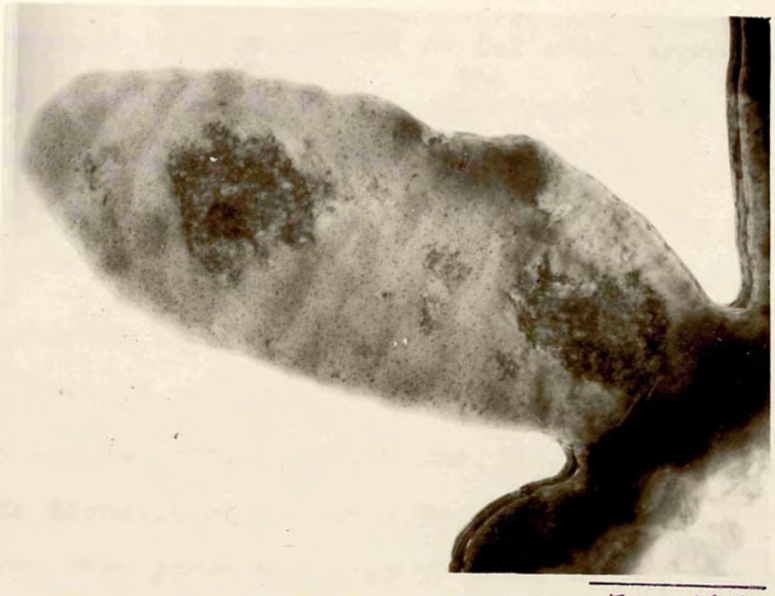
500 nm

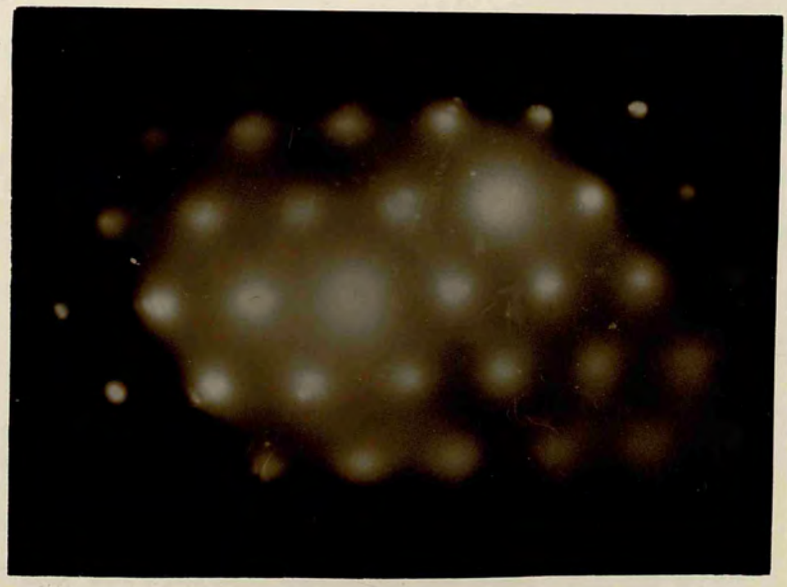

clusters formed by coalescence of the small crystallites during recrystallization. The diffraction pattern in Fig. 5.7 is from a thin deposit (< 5 nm) of CsI on CsI after exposure. The substrate is normal to the [011] and the overgrowth has a simple cubic lattice structure, oriented with its axes parallel to those of the substrate as seen from the indexing of the pattren.

CsI has normally a bcc lattice structure which is stable below the melting point. Some polymorphic transitions occur in CsI in certain conditions. Schulz (1951) has reported thin deposits of CsI were found to have the NaCl-type structure, when grown from vapour phase on appropriate single crystal substrates. Much work has been reported on ultra-highspeed polymorphic transitions in alkali halides, induced by preliminary heat treatment or heterogeneity of the pressure medium. The most important observations are by Sizova and Urusouskaya (1977) on the microplasticity of CsI crystals. Urusouskaya (1979) has explained the slip geometry of the {110} <100> slip system in CsI crystals. According to Schulz (1949) the evaporated films of alkali halides are rather porous and are composed of relatively independent crystals. CsI is a comparatively loosely packed lattice. Impurities, even in very low concentrations, usually occur between the atoms in CsI. All these properties of CsI crystals favour the observed polymorphic transitions.

The diffraction pattern in Fig. 5.8 is from a very thin (< 2.5 nm) exposed deposit of CsI on [011] CsI single crystal. There is few reflections from the overgrowth, two small spots correspond to {110} and four spots nearest to

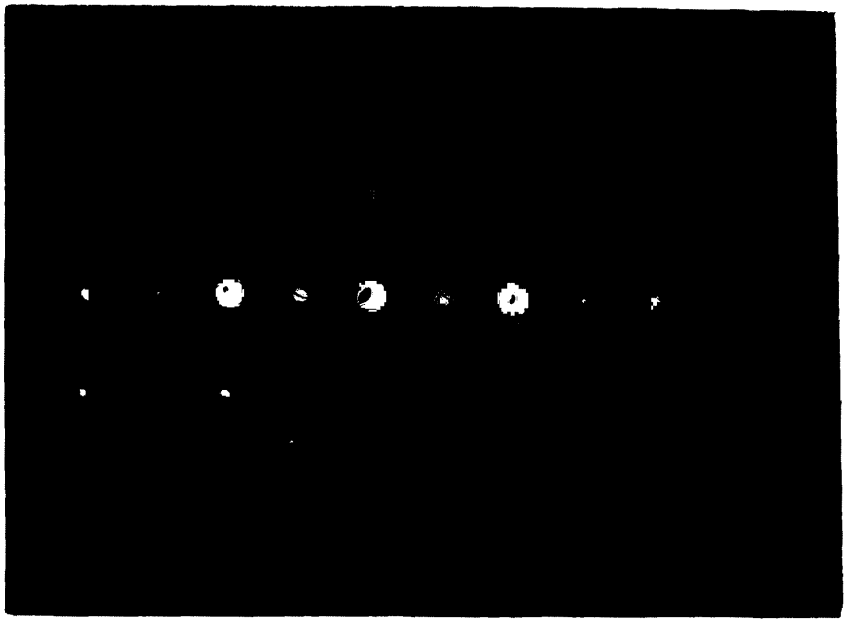

Fig. 5.7.

Fig. 5.8.

Fig. 5.7. Diffraction pattern from an exposed deposit of CaI on [111] CaA.

Fig. 5.8. Diffraction pattern from a very thin exposed deposit of CaI on [111] CaI.

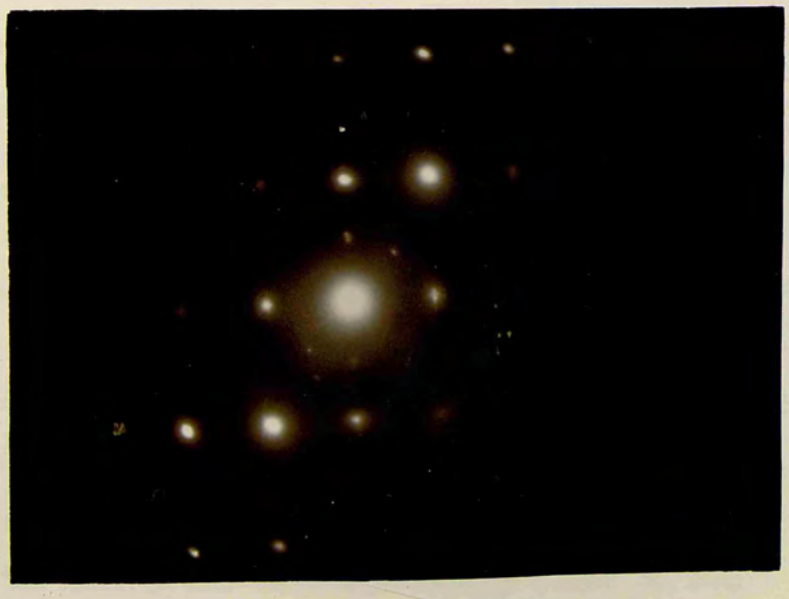

the centre have d-spacing 0.425 nm, since the lattice parameter of CsI is 0.4562 nm, so they do not correspond to any particular planes. The possible explanations of these extra reflections are either due to some kind of impurities or some extra planes formed due to various kinds of defects caused by electron irradiation in the electron microscope.

(b) CsCl on CsI.

The diffraction patterns of unexposed and exposed deposits of CsCl on CsI show good orientation in all cases (Figs. 5.9 to 5.12).

Fig. 5.9 (a) shows an unexposed deposit of a 10 nm thick CsCl on a [011] CsI single crystal substrate. The diffraction pattren in Fig. 5.9 (b) indicates that the overgrowth crystals are oriented with their axes parallel to those of the substrate. The white specks in the micrograph of Fig. 5.9 (a) are due to the point defects (vacancies) caused by the electron irradiation in the electron microscope. Fig. 5.10 (a) shows another unexposed deposit, ~ 5 nm thick, of CsCl on [012] CsI. The indexing of its diffraction pattern indicates that the lattice structure of overgrowth to be simple cubic. CsCl is said to occur in two polymorphic forms at atmospheric pressure: the CsCl type and the NaCl type. the former is stable below 445°C and the latter between 445°C and the melting point, 646°C (Wagner and Lippert (1936)). Schulz (1951) had observed the CsCl $\longrightarrow$ NaCl transition in very thin deposits of CsCl grown from the vapour phase on NaCl— type substrates. This transition occurs with an increase in lattice parameter.

The space lattice for CsCl is simple cubic, although

Fig. 5.9. (a)

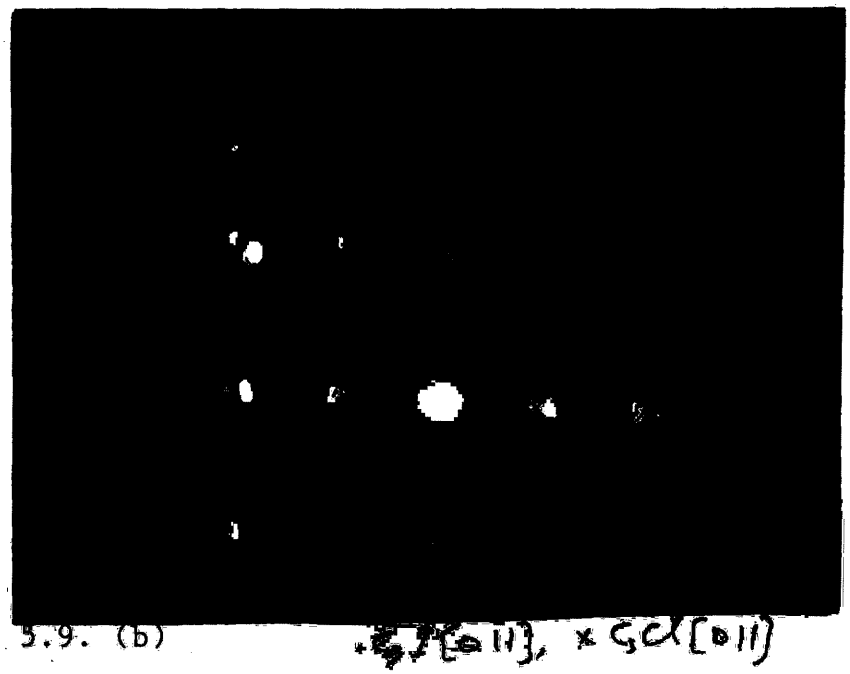

Fig. 5.9. (b)

Figs. 5.9. (a) and (b). Unexposed deposit of CsCl on [011] CsI.


350 nm

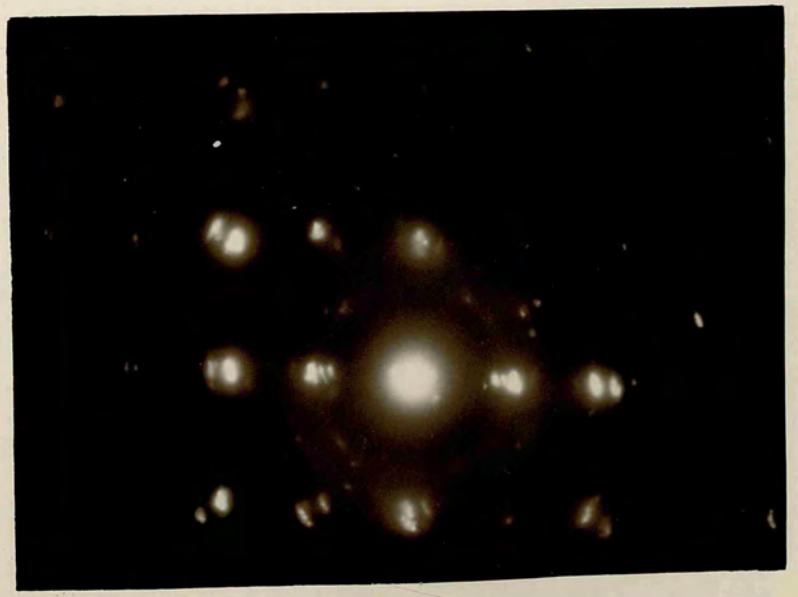

Fig. 5.10. (a).

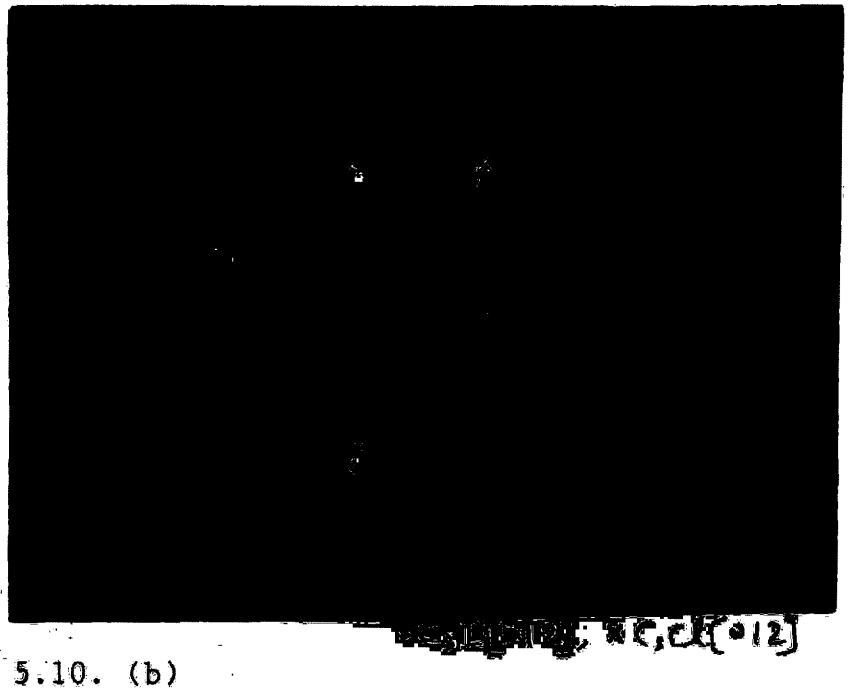

Fig. 5.10. (b)

Figs. 5.10. (a) and (b). [illegible] deposit of CsCl on [012] CsI.


500 nm

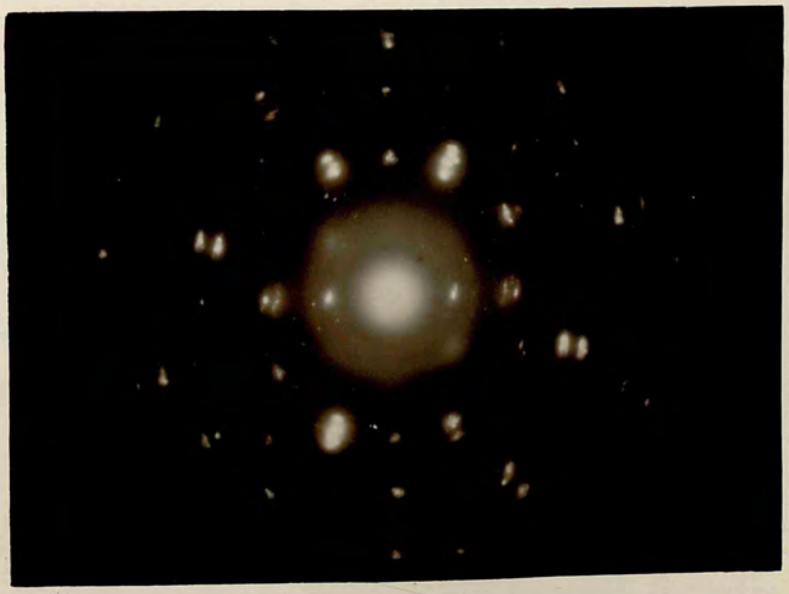

it is usually said to be bcc and sometimes behaves like bcc, as observed in the diffraction patterns in Figs. 5.9 and 5.11. In the crystal lattices each atom at the centre of a cube of the atoms of opposite kind, so that the coordination number is eight. In other words a simple cubic lattic is inserted into an other simple cubic lattice. Since Cs^+ and Cl^- ions have different number of orbital electrons, it is also possible CsCl has reflections from planes whose indices sums are odd number, therefore, it gives a diffraction pattern of simple cube without any change in its lattice parameter. Fig. 5.11 (a) shows a micrograph of a 20 nm thick deposit of CsCl on [$\bar{1}$11] CsI observed in the electron microscope before exposure to the atmosphere. The crystallites of the overgrowth are well—oriented on the substrate, as shown in the diffraction pattren of Fig. 5.11 (b).

When thin deposits of CsCl on CsI are exposed to the atmosphere, large crystals without any geometerical shape are formed during recrystallization. The micrograph in Fig. 5.12 (a) is from a 20 nm thick of CsCl on CsI after atmospheric exposure. Its diffraction pattern is shown in Fig. 5.12 (b) which indicates that the substrate is normal to [001] and the overgrowth crystals,with simple cubic lattice structure, are oriented with thier axes parallel to the corresponding axes of the substrate.

(c) CsBr on CsI

Neither the unexposed nor exposed deposits of CsBr on CsI show any orientation, as shown in the diffraction pattrens of Figs. 5.13 to 5.15.

Fig. 5.13 and 5.14 show the micro—graphs of the

Fig. 5.11. (a)

Fig. 5.11. (b)

Figs. 5.11. (a) and (b). Unexposed deposit of CsCl on $[\bar{1}11]$ CsI.

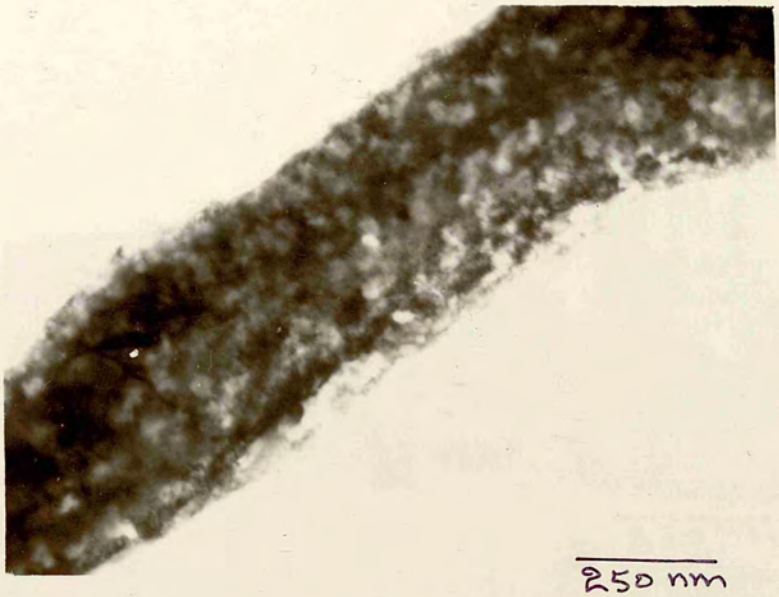
250 nm

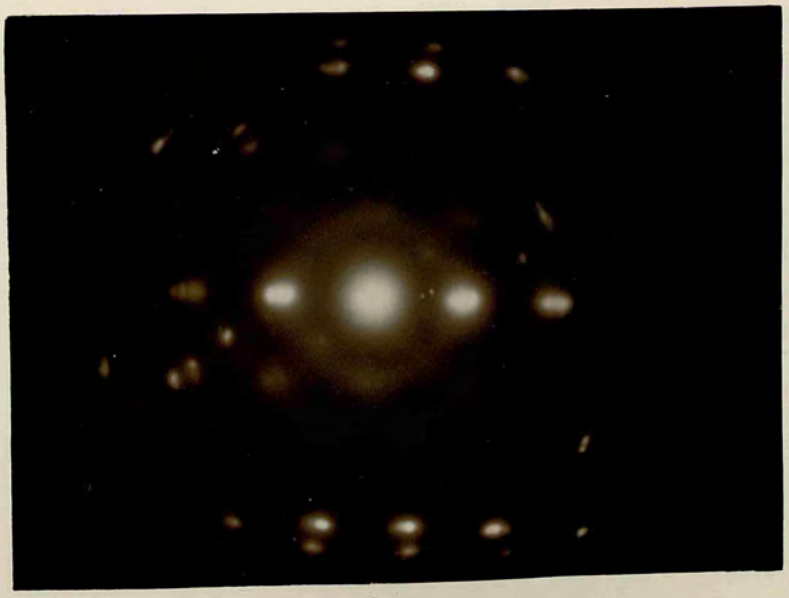

Fig. 5.12. (a)

Fig. 5.12. (b)

Figs. 5.12. (a) and (b). Epitaxial deposit of CsCl on [001] CsI.

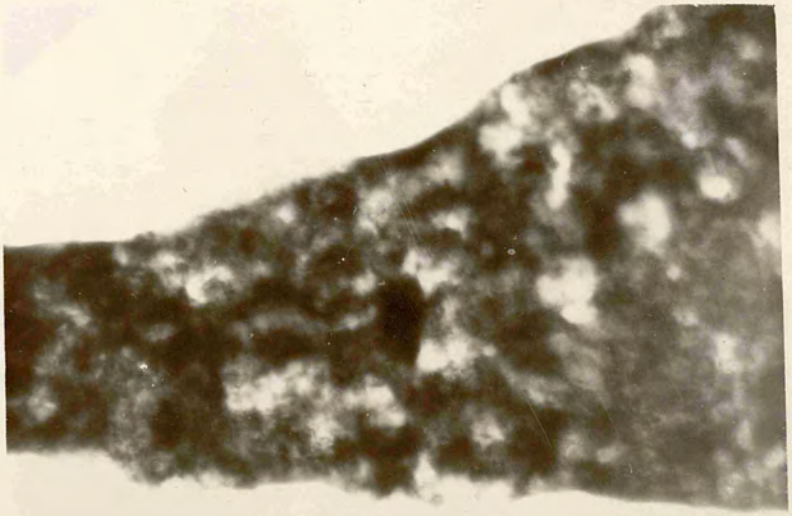
250 nm

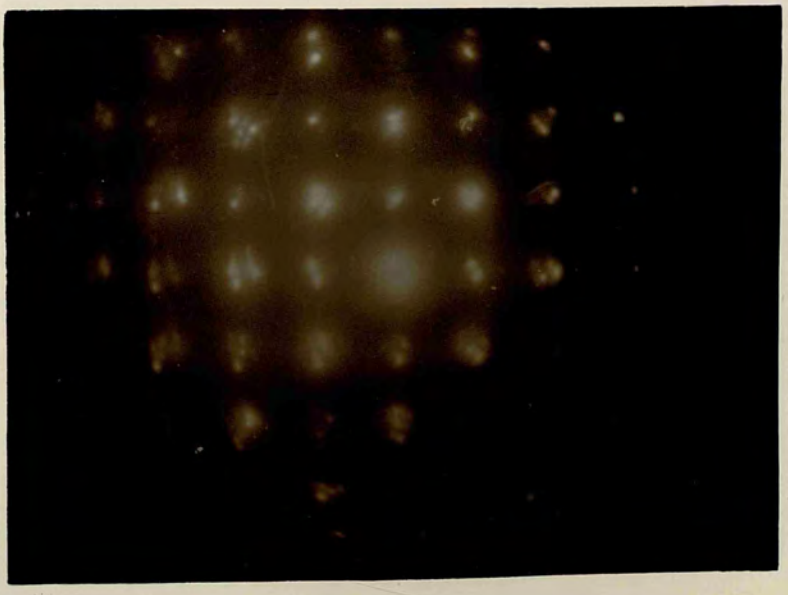

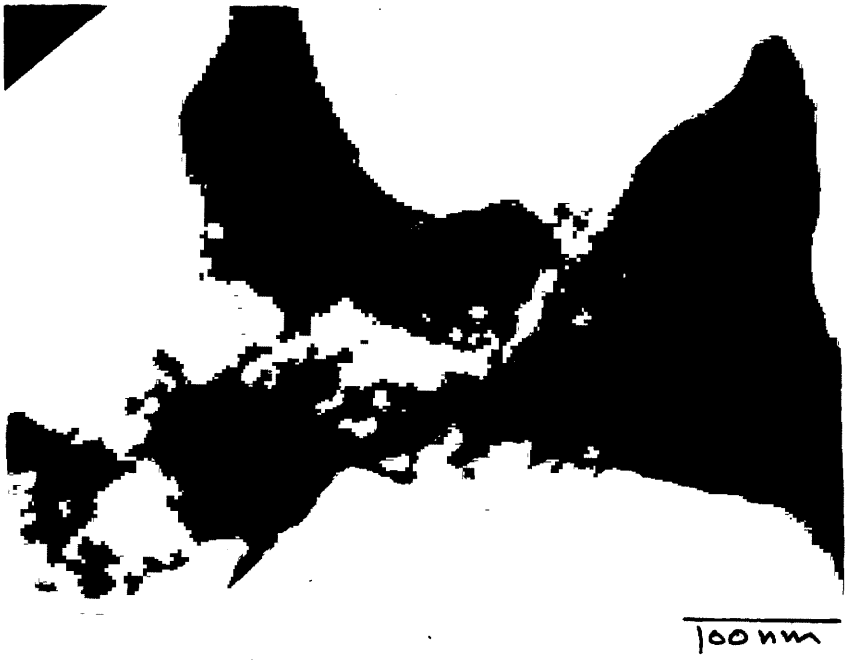

Fig. 5.13. (a)

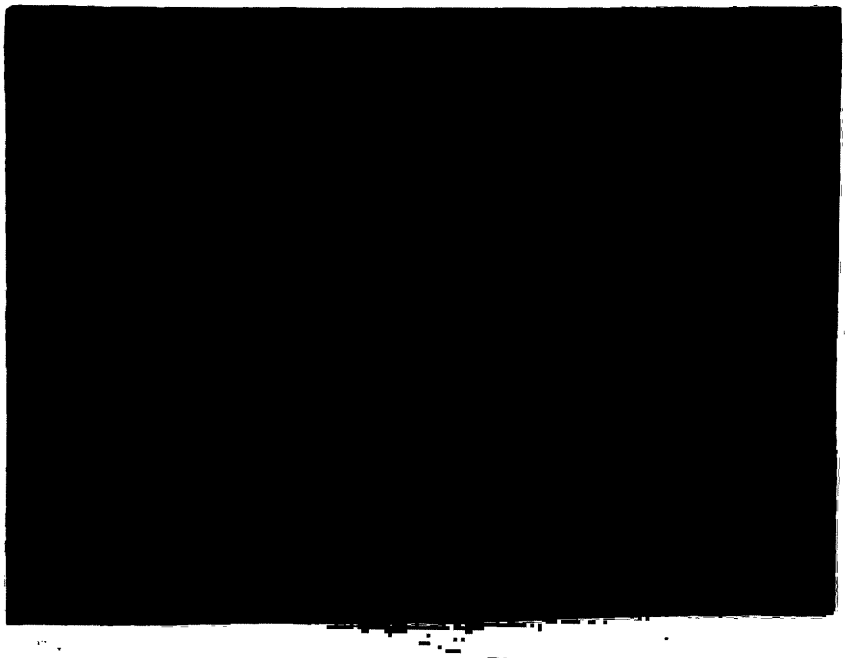

Fig. 5.13. (b)

Figs. 5.13. (a) and (b) Epitaxially deposited deposit of KBr on [111] CsI and its diffraction pattern.

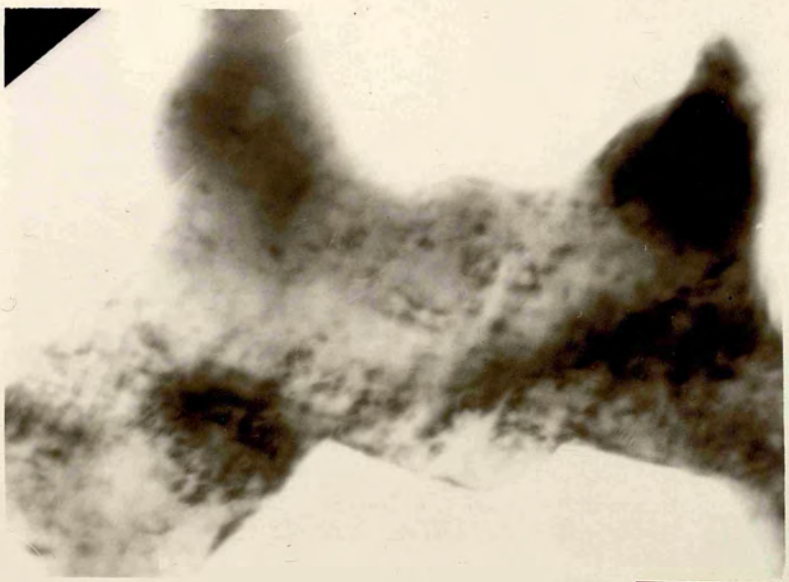
100 nm

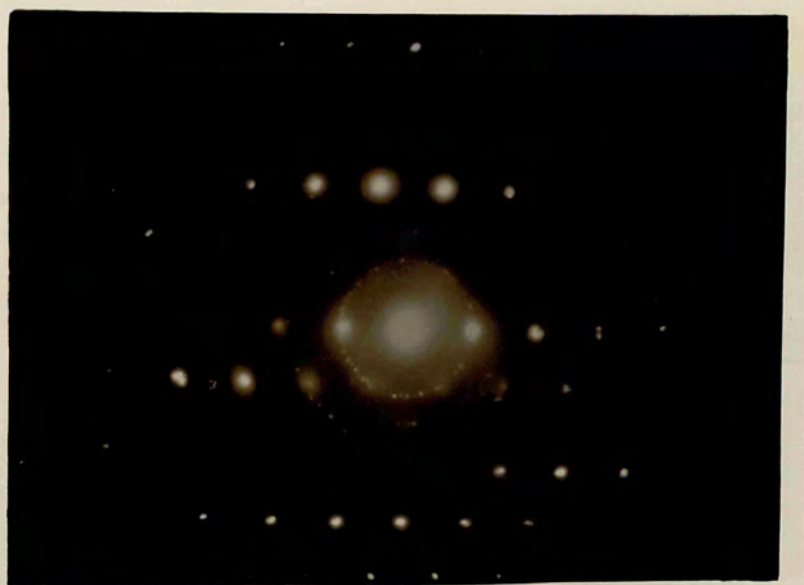

Fig. 5.14. (a)

Fig. 5.14. (b)

Figs. 5.14. (a) and (b) Epitaxial deposit of CsBr on [$\bar{1}11$] CsI.

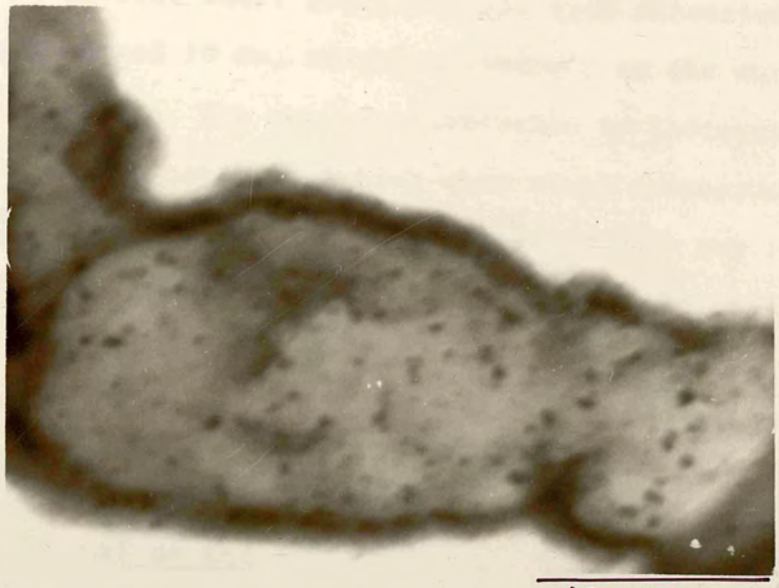
125 nm

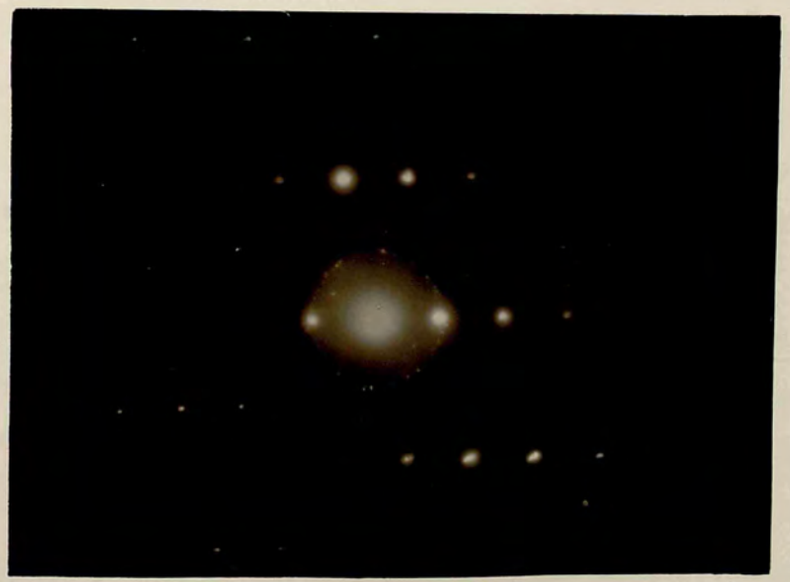

unexposed deposits of CsBr on [$\bar{1}$11] CsI single crystals. There are several small crystallites, with dimensions between 5 nm and 10 nm, situated randomly on the surface of the substrate. The random orientation is indicated by the diffraction patterns, which show rings corresponding to {110}, {200} and {211} in Fig. 5.13 and only one ring {110} in Fig. 5.14. The micrograph in Fig. 5.15 shows a deposit of CsBr on CsI after atmospheric exposure. Its diffraction pattern is complicated and does not show any recognisable orientation.

(d) CsF on CsI

In bulk and ordinary conditions CsF crystallizes with a coordination number of six (the NaCl structure) in contrast with the other caesium halides i.e. CsCl, CsBr and CsI, which adopt the CsCl structure with coordination number of eight. The lattice parameter of CsF is 0.6008 nm with the Cs—— F contact distance 0.300 nm.

Thin deposits, either unexposed or exposed, of CsF on single crystal substrates of CsI are well-oriented in all cases, as seen in their diffraction patterns. There are some structural changes in the deposits which are explained as follows. Fig. 5.16 (a) is a micrograph of a 2.5 nm thick deposit of CsF on a [001] CsI single crystal surface before exposure to the atmosphere. The overgrowth is shown by the diffraction pattren to be well-oriented. The indexing of the pattern shows (001) CsF // (001) CsI and <110> CsF // <100> CsI. The indexing of the overgrowth pattern belongs to a bcc lattice structure with the lattice parameter a_o = 0.649 nm ± 0.004 nm. This orientation is

shown schematically in Fig. 5.17.

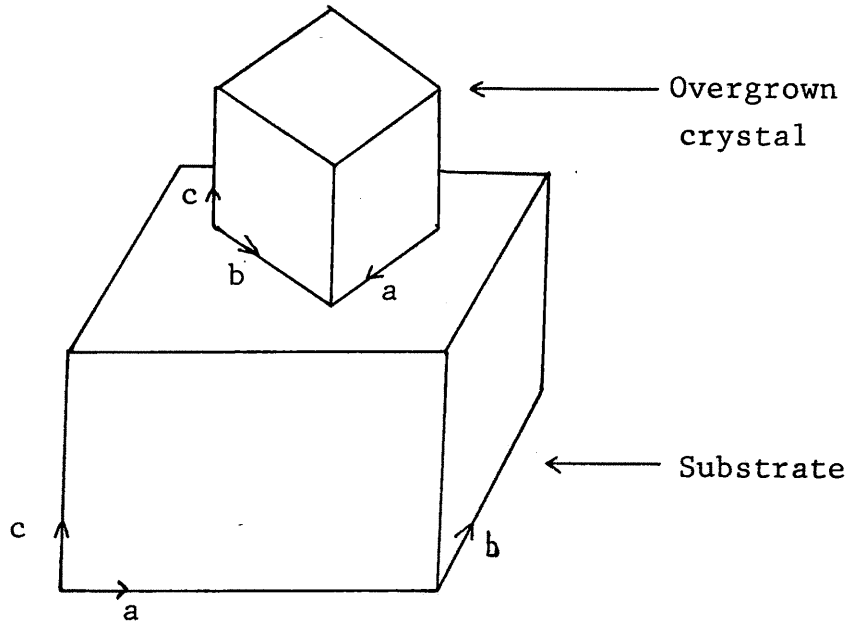

Fig. 5.17. Orientation observed between CsF and CsI,
(001) CsF // (001) CsI and
<110> CsF // <100> CsI

Similar observations were made when a 10 nm thick deposit of CsF was examined in electron microscope after atmospheric exposure. The micrograph and diffraction pattren are shown in Fig. 5.18. This orientation was first observed by Royer (1928) in examining CsF on NaCl and KCl. However, Schulz (1951) reported that this orientation is not observed. The polymorphic transition in CsF is not surprising, as under high pressures many of the alkali halides with the rock salt structure go over to the CsCl structure. This transition also occurs at lower pressures for the crystals with larger ions. Conversely alkali halides with CsCl structure change to rock salt structure at high

temperatures. A number of investigators such as Bassett, Takahashi and Campbell (1969) have studied experimentally and theoretically the phase transformation of B_1 (rock salt) —— B_2 (CsCl) in alkali halides. They use diamondanvil high-pressure cell methods to induce structural phase change. Rice (1958) and Fritz (1971) have used dynamic shock wave compression for similar experiments. The volume change at transition pressure and evaluation of the cohesive energy of the B_1 and B_2 phases are described in detail by Born and Huang (1954), Tosi and Fumi (1962) and Tosi (1964) and reviewed by Gordon and Kim (1974). Cohen and Gordon (1975) have given a detailed study of lattice energy, equilibrium structure, elastic constant and pressure-induced phase transitions in alkali halides. They showed how closely the electron-gass treatment describes the B_1 —— B_2 phase transformations in these crystals.

The polymorphic transition in CsF during the growth from vapour or solution on an appropriate substrate has not been studied before. Schulz (1951) studied polymorphism in CsCl-type crystals during growth from the vapour phase on NaCl substrates. Recently Burdett and Price (1982) have described a theoretical model for NaCl——CsCl phase transformation with a body-centred rhombohedral unit cell as an intermediate stage. The rock salt structure corresponds to a rhombohedral angle $\theta = 60^\circ$, and caesium chloride structure to $\theta = 90^\circ$. The transformation consists of increasing θ and adjusting the length of the side of the rhombohedron such that the shortest Na——Cl distance remained constant. The same model should apply to the transformation in CsF during the nucleation and growth from vapour and solution

on a bcc substrate (CsI). The model is shown in Fig. 5.19.

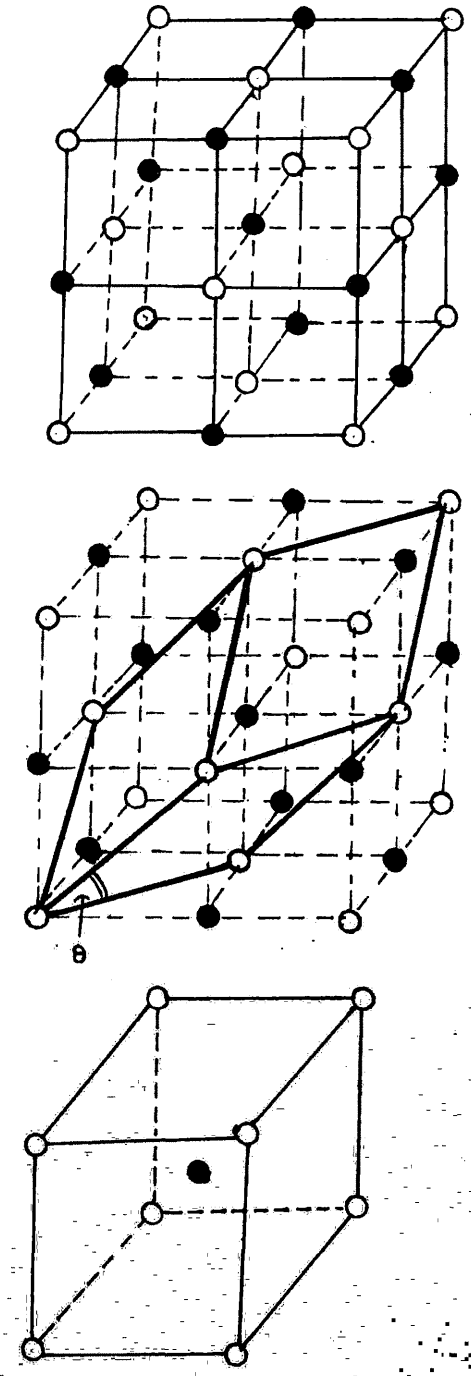

Fig. 5.19. Reaction coordinates for the rock salt to caesium chloride structural transformation.
(a) conventional unit cell for rock salt structure,
(b) rhombohedral unit cell for rock salt structure. On increasing the rhombohedral angle θ from 60° to 90°, this becomes the unit cell of the caesium chloride structure shown in (c).

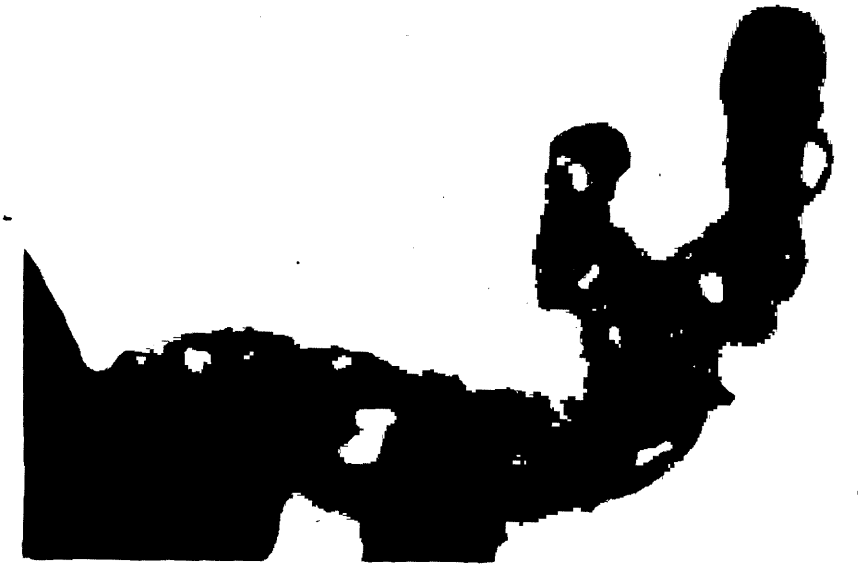

Fig. 5.15. (a)

Fig. 5.15. (b)

Fig. 5.15. (c) [illegible] deposit of CsBr on [illegible] CsI.

250nm

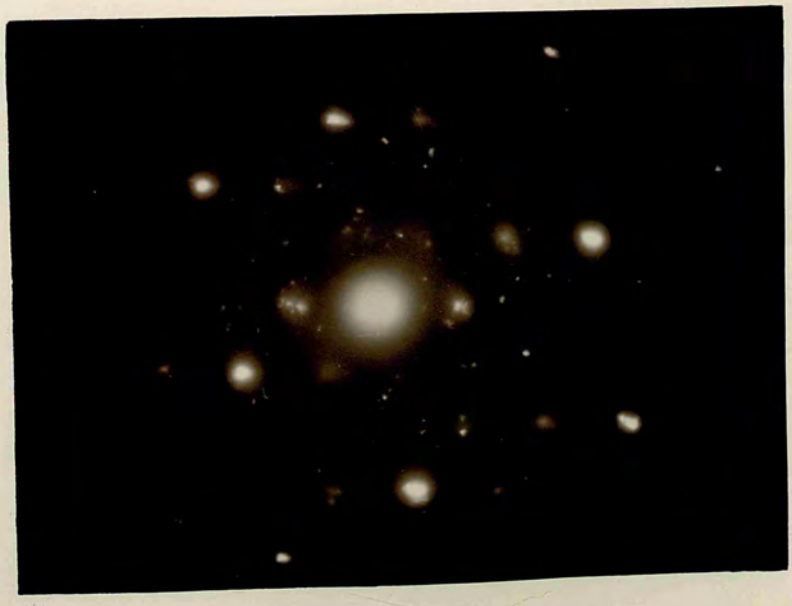

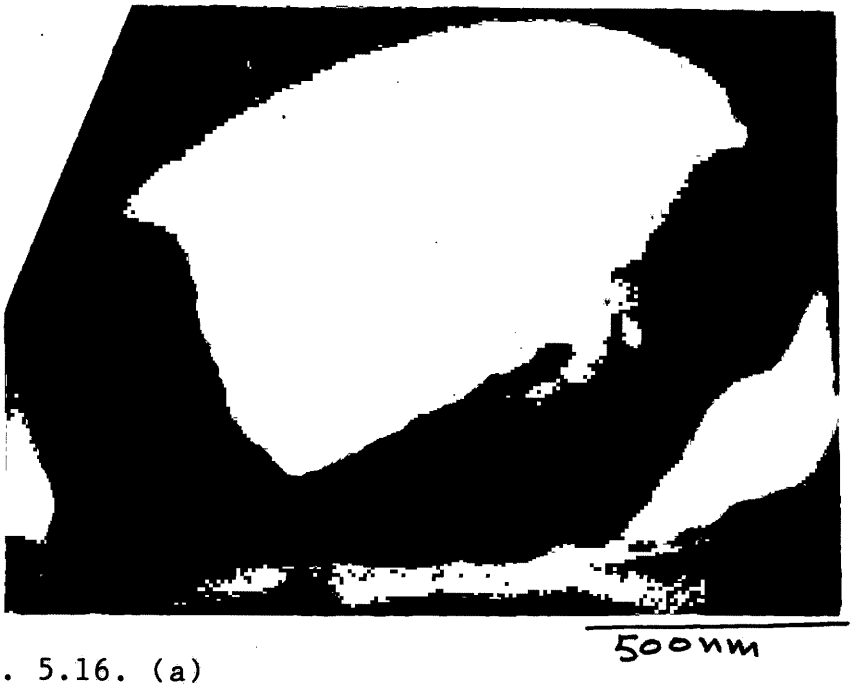

Fig. 5.16. (a)

Fig. 5.16. (b)

Figs. 5.16. (a) and (b). Unexposed deposit of CsF on [001] CsI and its electron diffraction pattren.


500nm

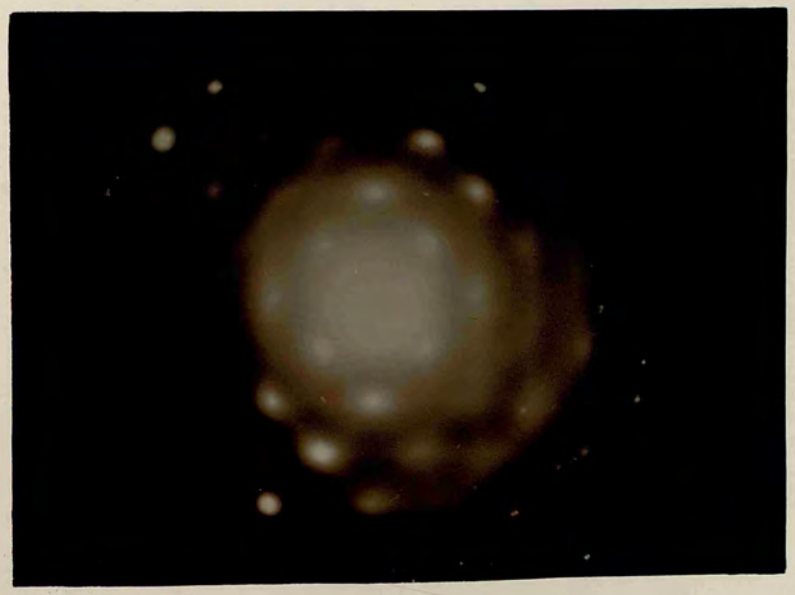

An other kind of orientation was observed in a ~ 10 nm deposit of CsF on CsI examined after exposure to the atmosphere. The micrograph and diffraction pattren are shown in Fig. 5.20. As seen from the indexing the substrate is normal to [012] and the overgrowth is with simple-cubic (or CsCl) lattice structure normal to $[3\bar{3}2]$, (the substrate and the overgrowth have planes (012) and $(3\bar{3}2)$ respectively normal to the electron beam). This means the $(1\bar{1}0)$ CsF // (001) CsI and $\langle 110\rangle$ CsF // $\langle 100\rangle$ CsI. The schematic drawing of this orientation is shown in Fig. 5.21.

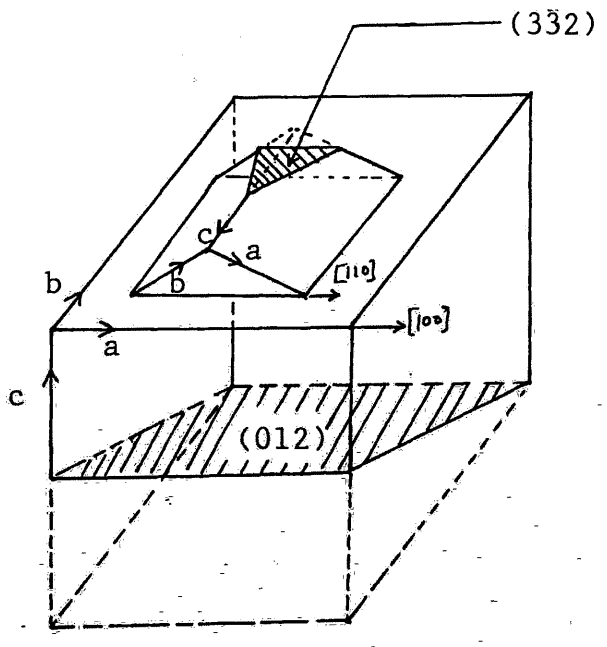

Fig. 5.21. Orientation between CsF and CsI, $(1\bar{1}0)$ CsF // (001) CsI and $\langle 110\rangle$ CsF // $\langle 100\rangle$ CsI.

Fig. 5.18 (a)

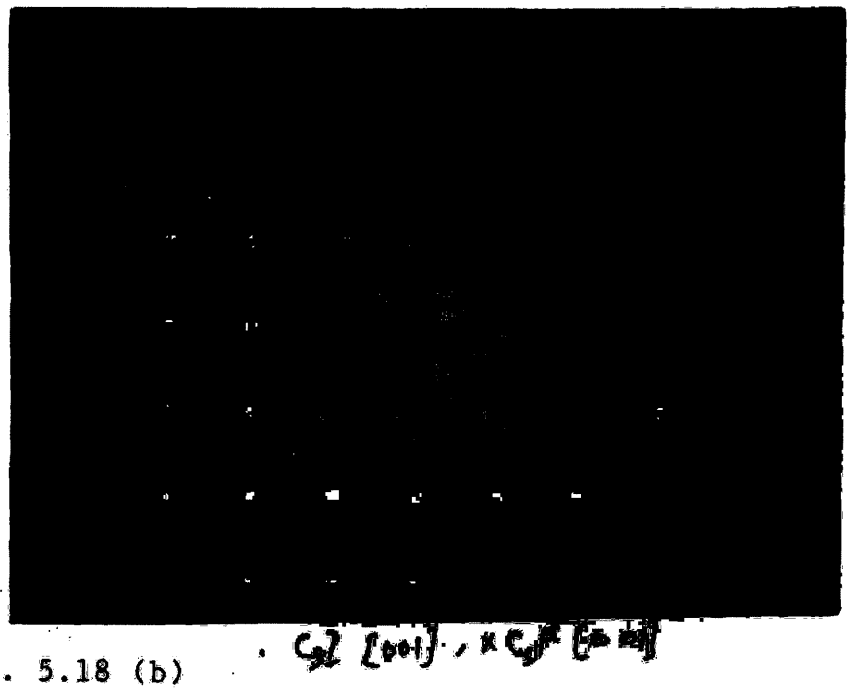

Fig. 5.18 (b)

Figs. 5.18. (a) and (b). Exposed deposit of CsF on [001] CsI and its electron diffraction pattrem.

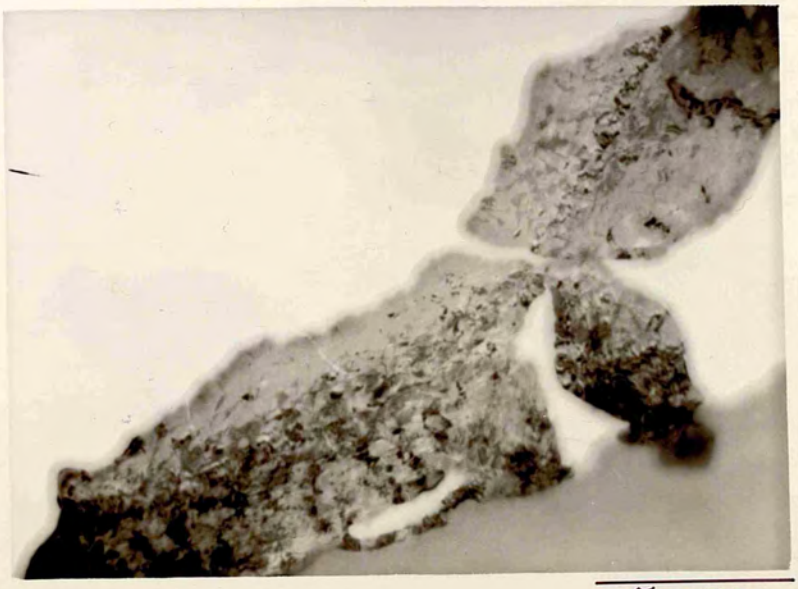

500nm

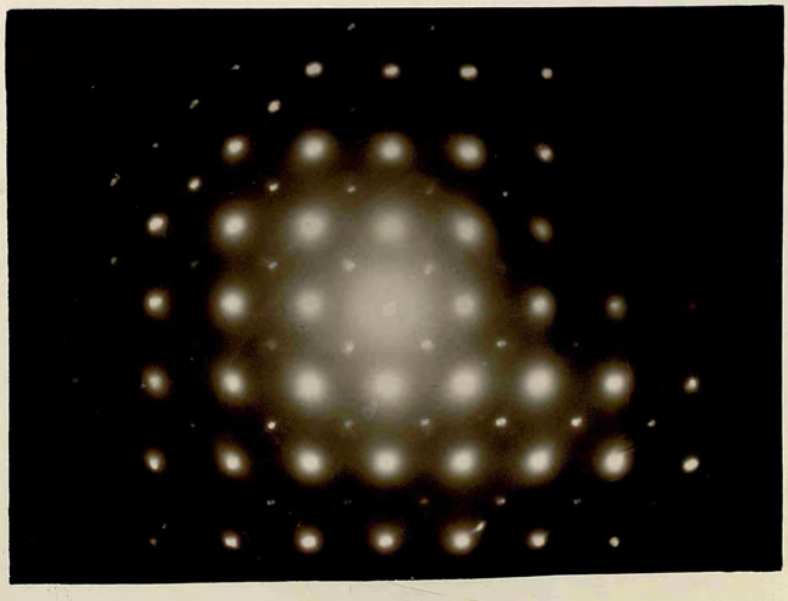

Fig. 5.20. (a).

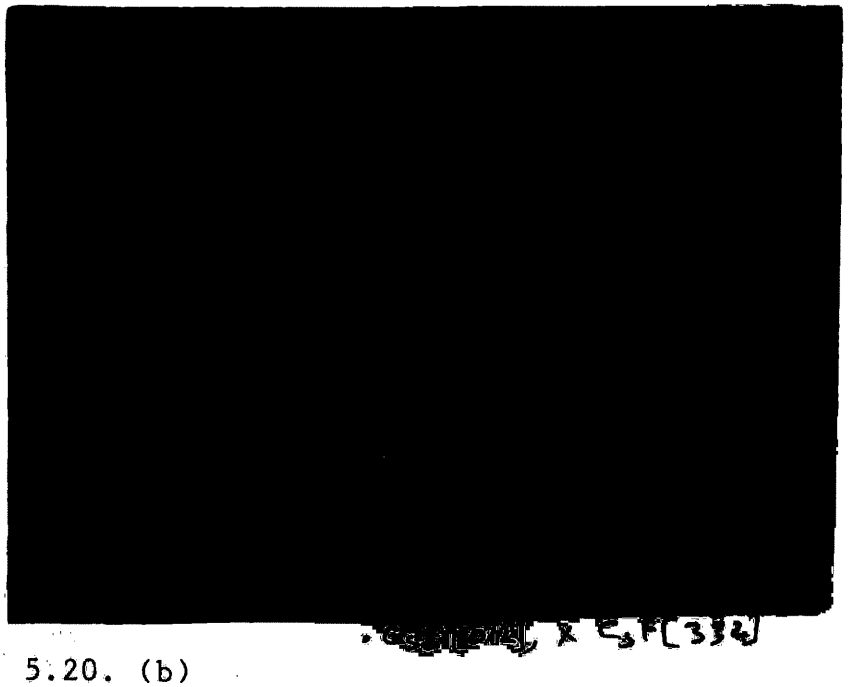

Fig. 5.20. (b)

Figs. 5.20. (a) and (b). Exposed deposit of CsF on [012] CsI and its electron diffraction pattren.

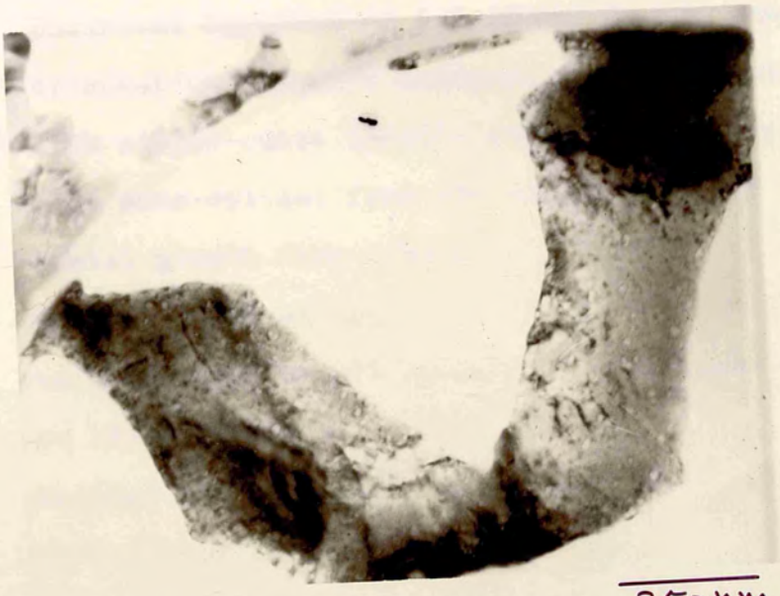

250nm

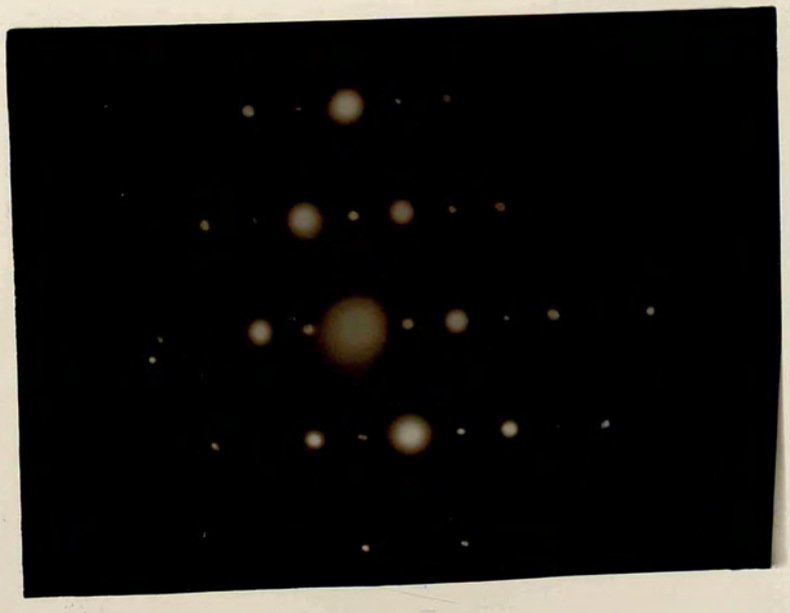

5.5 Conclusions

1. Unexposed deposits of CsI on CsI do not show any orientation. Exposed deposits are well-oriented with simple-cubic lattice structure, indicating poor homo-epitaxy from the vapour but good epitaxial growth from solution.
2. Unexposed and exposed deposits of CsCl on CsI are well-oriented in all cases with their axes parallel to those of the substrate.
3. Neither the unexposed nor exposed deposits of CsBr on CsI show any regular orientation.
4. Thin deposits of CsF either unexposed or exposed on CsI grow with two different orientations:
   i. (001) CsF // (001) CsI, with
      <110> CsF // <100> CsI.
   ii. $(1\bar{1}0)$ CsF // (001) CsI, with
      $\langle 11\bar{0} \rangle$ CsF // <100> CsI.
5. In (001) CsF// (001) CsI orientation, CsF transforms from NaCl structure to CsCl structure and in $(1\bar{1}0)$ CsF // (001) CsI, CsF transforms to simple-cubic structure. In either case the lattice parameter of CsF increases from 0.6008 nm to 0.649±0.004 nm.

References

BASSETT, W.A., TAKAHASHI, T., and CAMPBELL, J.K. (1969). Trans. Am. Crystallgr. Assoc. 5, 93.

BORN, M., and HUANG, K., (1954). Dynamic Theory of Crystal Lattices, Oxford U.P., London.

BURDETT, J. K., and PRICE , S. L., (1982). Phys. Rev. B, 25, 5778.

COHEN, A. J., and GORDON, R. G., (1975). Phys. Rev. B, 12, 3228.

FRITZ, J. N., MARSH,S.P., CARTER,W.J., and McQUEEN,R.G. (1971) Natl. Bur. Stand., Pub. No. 326.

GORDON,R.G., and KIM,Y.S., (1974). Phys. Rev.,B, 9, 3548.

LUDEMANN,H., (1957). Naturforsch., 12A,226.

RICE,M.H., McQUEEN,R.G., and WALSH,J.M., (1958). Solid State Phys., 6, 1.

ROYER,L., (1928). Bull. Soc. Franc. Mineral, 51, 7.

SCHULZ,L.G., (1950). J. Appl. Phys., 21, 942.

SCHULZ,L.G., (1951). Acta Cryst., C,4,487.

TOSI,M.P., and FUMI,F.G., (1962). J. Phys. Chem. Solids 23, 359.

TOSI,M.P., (1964). Solid State Phys., 16, 1.

URUSOVSKAYA,A.A., (1979). Sov. Phys. Crystallgr., 24, 711.

WAGNER,G., and LIPPERT,L., (1936). Z. physikal Chem. 33 B, 297.

CHAPTER SIX

NUCLEATION AND GROWTH OF ALKALI HALIDES FROM THE VAPOUR PHASE AND SOLUTION ON SUBSTRATES OF MICA

6.1 Introduction.

Many experiments have been carried out to produce oriented overgrowths on crystal surfaces and in the past, cleavage surfaces of mica have often been used as the substrate material (Van der Merwe, 1949). Royer (1928) gave a complete account of experiments in which the overgrowths were formed by crystallization from solution. The most extensive series, alkali halides, have been studied by several workers by a variety of growing techniques and observational methods. For example: West (1945) has studied growth from the melt by optical microscopy, Deicha (1945) and (1946), and Lisgarten (1954) have observed growth from solution by optical microscopy. Schulz (1951) has used reflection eletron diffraction to study the growth of eleven alkali halides from the vapour phase and from solution on to substrates of mica.

Transmission electron microscopical studies of the oriented growth of alkali halides from the vapour phase on mica were made by Zouckermann (1961), Green

(1971), Missiroli (1972) and Tavassoli (1978). Upreti and Walton (1966) have studied growth from solution by optical microscopy and replica electron microscopy. Rabbit et all., (1971) grew crystals in ultrahigh vacuum and studied them by reflection electron diffraction. Bauer (1956), Shimaoka and Herold (1967), and Koch and Vook (1971, 1972) have studied the growth of alkali halides from the vapour phase on mica by replica electron microscopy, reflection electron diffraction and transmission electron microscopy. All these workers used the (001) cleavage face of one kind of mica, muscovite, and most of them grew common halides of sodium, potassium and lithium. The halides of caesium have rarely been used: Schulz (1951) and Lisgraten (1954) have used CsBr and CsI as overgrowths on the substrates of mica.

In studies of a particular system (substrate-deposit combination), one sees that a number of features of the system are likely to be peculiar to that system or to a restricted class of systems. Thus the contribution to general understanding of the epitaxy, of such in-depth studies on a very restricted number of systems is limited. For a better understanding of the important parameters involved in oriented growth, it is necessry to study different types of materials. New substrate-deposit combination provide additional information about epitaxial growth. In the present work two different kinds of micas, muscovite and biotite, have been used as substrates to grow CsI, CsCl, CsBr and CsF.

6.2 Substrate: The structure of Mica.

Because their abundance in nature and excellence of crystalline perfection, the micas have been studied more than other layer silicate minerals. The mica minerals as a whole show considerable variation in chemical and physical properties, but all are characterized a platy morphology and perfect basal cleavage, which is a consequence of their layered atomic structure.

The first x-ray studies of the mica structure were made by Mauguin (1927, 1928), Pauling (1930) and are about the same time and in more detail, by Jackson and West (1930, 1933). Since these early studies, many detailed structural refinements of particular species have been published. The principal polymorphic variation were investigated by Hendricks and Jefferson (1939) and later by Heinrich, et al. (1953) and by Smith and Yoder (1956).

The basic chemical composition for mica is

$$X_2Y_{4-6}[(Si,Al)_8O_{20}](OH,F)_4$$

with

X is mainly K, Na or Ca

and Y is mainly Al, Mg or Fe.

The basic structural feature of a mica is a composite sheet in which a layer of octahedrally coordinated cations is sandwiched between two identical layers of linked $(Si,Al)O_4$ tetrahedra. Two of these tetrahedral sheets (of composition $(Si,Al)_2O_5$) are illustrated in Fig. 6.1. In

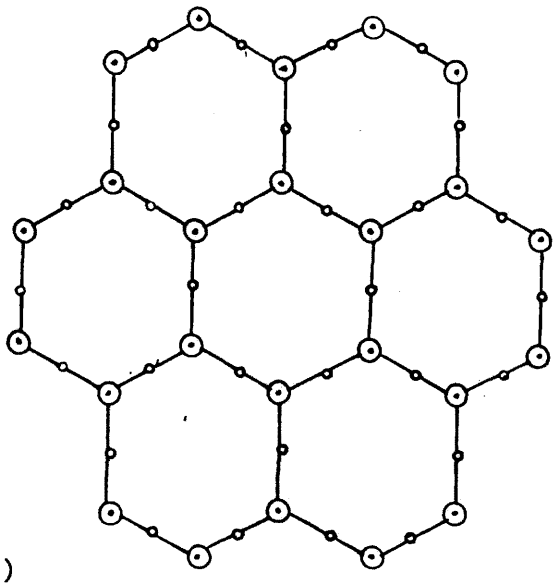

o Basal oxygens
⊙ Si with oxygen above it

Fig. 6.1 (a)

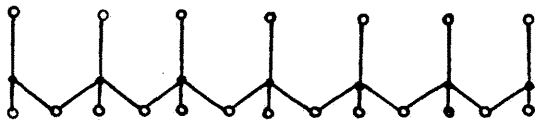

• Si
o Oxygen

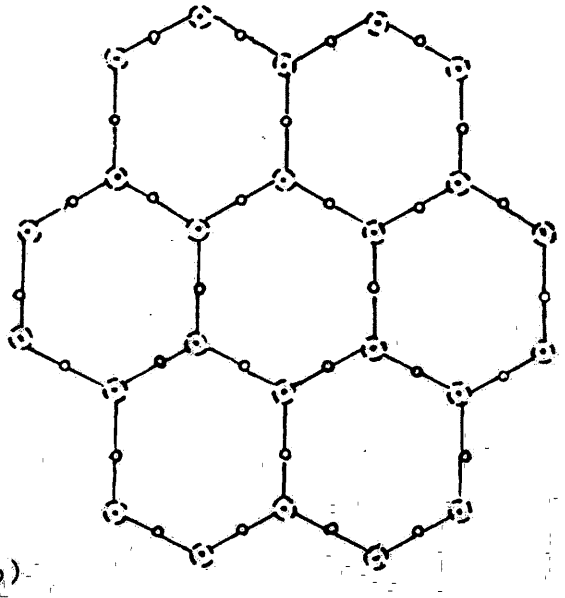

o Basal oxygen
⊙ Si with oxygen below it

Fig. 6.1 (b)

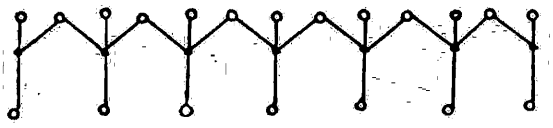

• Si
o Oxygen

Fig. 6.1. (a). Mica structure. Plan of tetrahedral layer (Si_4O_{10}) with tetrahedra pointing upwards, and end view of layer looking down y-axis.

Fig. 6.1 (b). Mica structure. Plan and elevation of tetrahedral layer with tetrahedra pointing downwards.

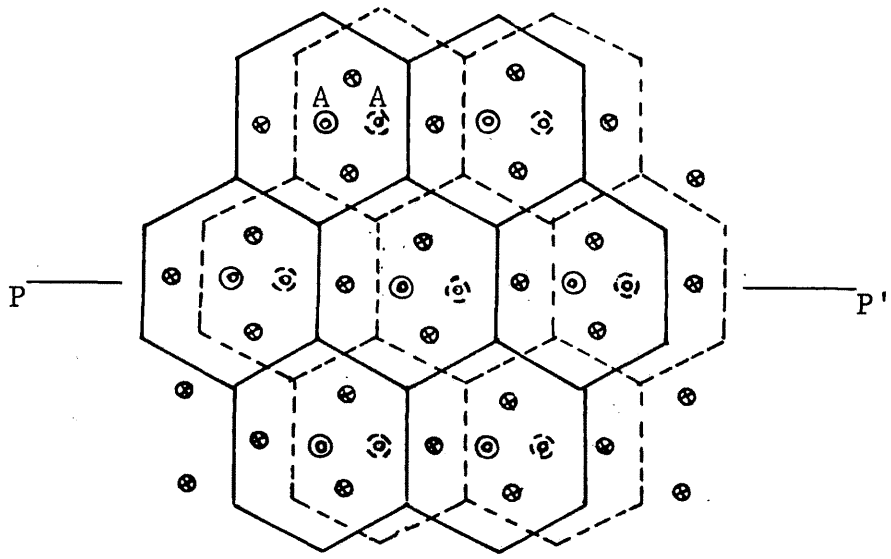

⊗ Octahedrally coordinated cations; mainly Mg,Al or Fe.
∘ Additional hydroxyl ions, ○ X ions below bottom layer (K,Na,Ca)
◌ X ions above upper layer (K,Na,Ca). Full lines:- bottom Si_2O_5 layer, Broken lines:- upper Si_2O_5 layer

Fig. 6.2. Mica structure. Plan of (a) and (b) of Fig. 6.1 superimposed and linked by layer of cations.

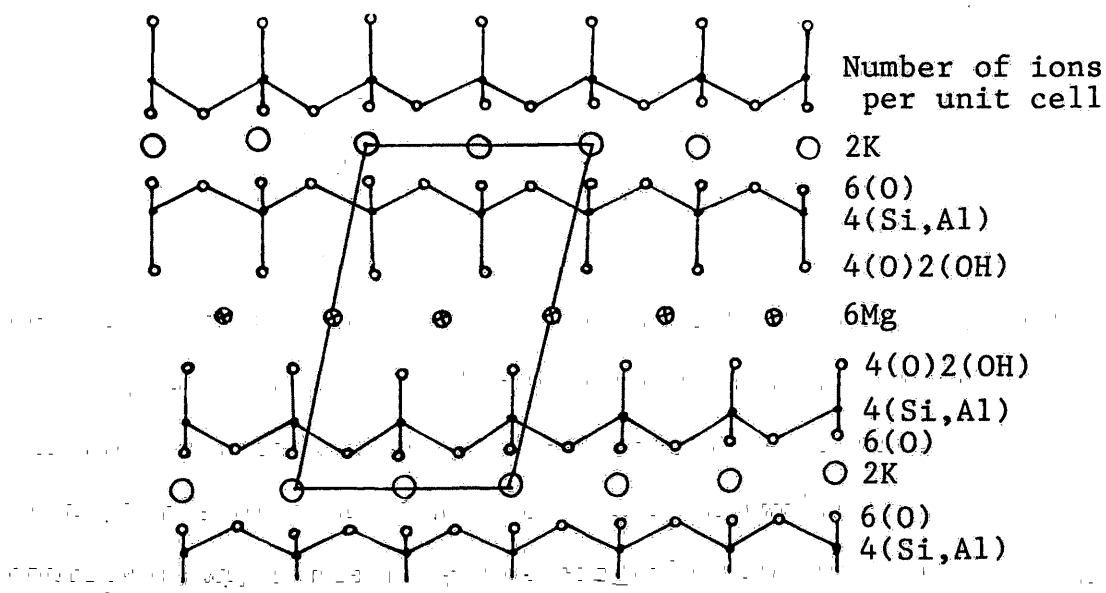

Fig. 6.3. Mica structure. Elevation of Fig. 6.1(a) and (b) superimposed and linked by a plane of octahedrally coordinated cations. Composite layers are shown linked by potassium ions, and the simplest unit cell is out lined. View along y-axis.

Fig. 6.1 (a) is a sheet in which all tetrahedra are pointed upwards as seen from the elevation drawing below it, and in Fig. 6.1 (b) is a sheet of tetrahedra which pointed downwards. The two sheets are superimposed and are linked by a plane of cations as shown in Fig. 6.2 and 6.3. Additional hydroxyl ions (marked A in Fig. 6.2), together with the apical oxygens of the inward-pointing tetrahedra, complete the octahedral coordination of the sandwiched cations. Alternatively the structure may be regarded as having a central gibbsite layer $Al_2(OH)_6$, in muscovite, or brucite layer $Mg_3(OH)_6$, in phlogopite, in which four out of six (OH) ions are replaced by apical oxygens of the tetrahedral layers (two on each side). The remaining (OH) ions are than situated at the centres of the hexagons formed by the tetrahedral vertices. The central Y-ions determine the positions of two tetrahedral sheets so that they are displaced relative to one another by a/3 in the [100] direction (Fig. 6.2 and 6.3). The composite layers have a centred plane group with a symmetry plane PP' and repeat on a rectangular network with dimension approxymately 0.53 X 0.92 nm. In micas these layers have a net negative charge which is balanced by planes of X ions (K, Na, Ca, etc.) lying between them, and the repeat distance perpendicular to the sheets is approximately 1 nm or multiple of 1 nm. The X ions are in twelve-fold coordination, since they lie centrally on the line joining the centres of hexagons formed by the basal oxygens of tetrahedral layers, and no lateral displacement is

introduced in going from the basal oxygens of one composite sheet to corresponding oxygens of its neighbour.

The hexagons may be superimposed, however, in six different ways. Thus one hexagon may be related to the next by rotation through 0° or by a multiple of 60°, and this, combined with the stagger of a/3 introduced by the Y layer, determines the location of corresponding atoms in successive cells.

Smith and Yoder (1956) have selected six simple stacking sequences which when repeated regularly, give rise to the unit cells described in Table 6.1.

Table 6.1

Some mica polymorphs (Smith and Yoder, 1956)

Polymorph	Symmetry	No.of layers	a_o (nm)	b_o (nm)	c_o (nm)	β°	Space group
1M	monoclinic	1	0.53	0.92	1.0	100°	C2/m or Cm
$2M_1$	monoclinic	2	0.53	0.92	2.0	95°	C2/c
$2M_2$	monoclinic	2	0.92	0.53	2.0	98°	C2/c
2O	orthorhombic	2	0.53	0.92	2.0	90°	Ccm2
3T	trigonal	3	0.53	--	3.0	--	$P3_112$ or $P3_212$
6H	hexagonal	6	0.53	--	6.0	--	$P6_122$ or $P6_522$

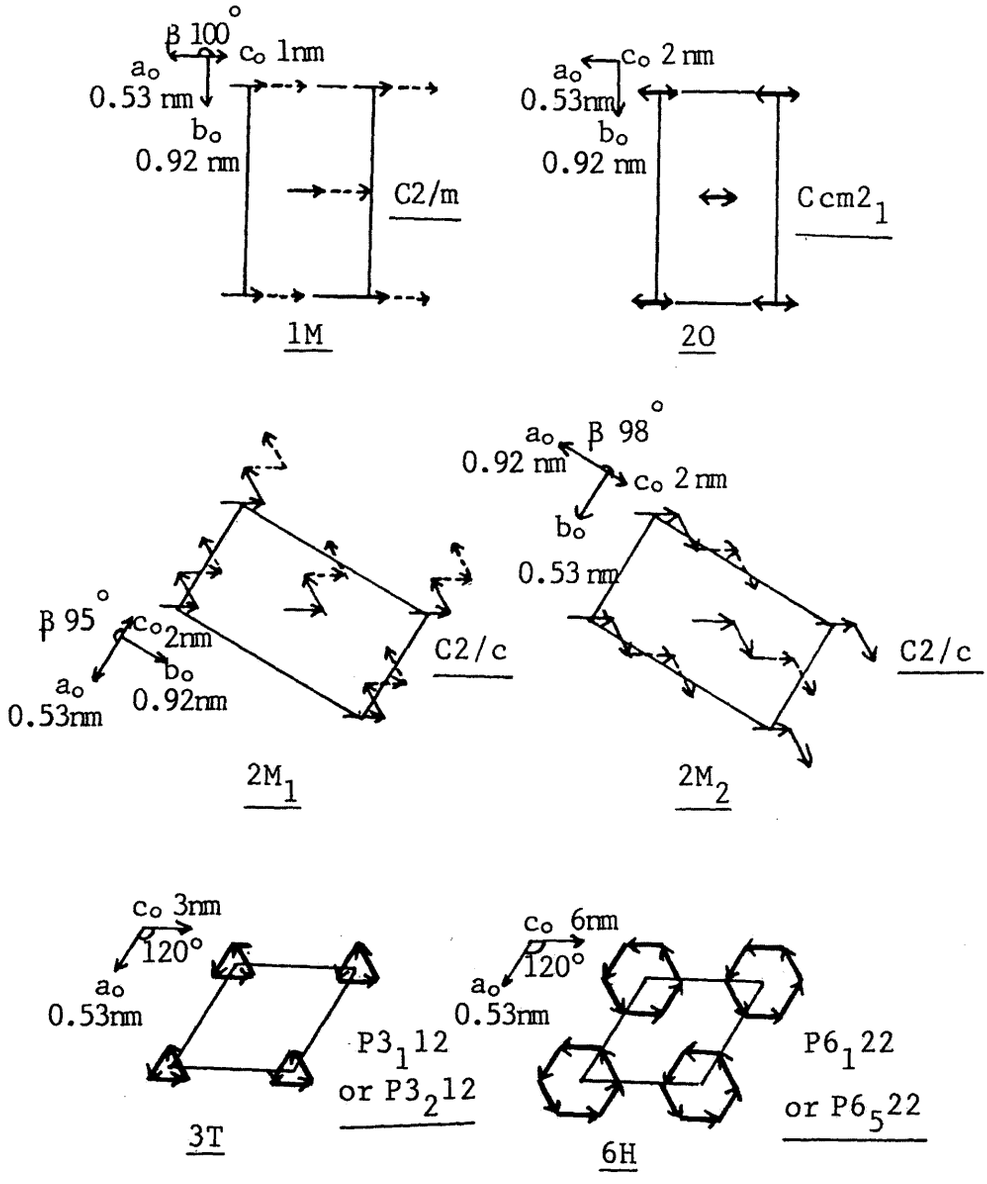

Fig. 4.6. The six simple ways of stacking mica layers in an ordered manner. Full line vectors show the layer stacking in one unit cell, whereas broken line vectors show the positions of layers in the next unit cell. The base of the unit cell is shown by thin lines, and the space group and lattice parameters are listed by the side of the diagram in each case (after Smith and Yoder, 1956).

A "stacking vector" may be defined which shows the displacement in the (001) plane between X ions in successive layers of the structure. Using these vectors Smith and Yoder illustrate the six polymorphs as shown in Fig. 6.4. Many more complex cells are possible and the existence of some of them has been reported, (Ross and Wones, 1965 and 1966; Takeda and Donnay, 1965; Takeda, 1966; Baronnet, 1975), but of the six polymorphs listed, 1M, $2M_1$, 3T (and $2M_2$) occur commonly in nature, and in some cases 12M, 18M and 8Tc (triclinic) polymorphs have been observed. The principal polymorphs exhibited by the different micas are as follows:

Muscovite and paragonite:	mainly $2M_1$.
Glauconite:	1M, $2M_1$, 3T.
Lepidolite:	mainly 1M and $2M_2$;3T also occurs.
Phlogopite, biotite and zinnwaldite:	mainly 1M; also $2M_1$ and 3T.

Zvyagin (1962) described the diffraction properties of polymorphous varieties of micas, determined on the basis of their diagnostic properties in photographs of single crystals, structure, and polycrystalline aggregates.

As stated earlier the general formula which describes the chemical composition of micas is:

$$X_2\ Y_{4-6}\ Z_8\ O_{20}\ (OH,\ F)_4$$

where X is mainly K, Na or Ca but also Ba, Rb, Cs etc.,

Y is mainly Al, Mg or Fe but also Mn, Cr, Ti, Li, etc.

and Z is mainly Si and Al but perhaps also Fe and Ti.

The micas can be subdivided into di-octahedral and tri-octahedral classes in which the number of Y ions is 4 and 6 respectively. In the common micas X is largely K or Na but in so called "brittle micas" X is largely Ca; these are not concerned here. Further subdivisions of the common micas are made according to the principal constituents in the categories X, Y and Z, and these are depicted with approximate formulae in Table 6.2.

As the structure of the mica minerals are complex and varied, although based on a relatively simple stacking arrangement. There is a six-fold multiplicity for the stacking of adjacent layers, resulting in a large number of possible stacking sequences and thus polytypes. X-ray diffraction techniques have been a powerful means of determining average stacking sequences and have solved the problems of mica polytypes, but they are not suitable for studying heavily disordered stacking sequences and their variations within a given crystal.

High resolution transmission electron microscopy has been recognized as a powerful means for studying structural irregularities in crystals, particularly linear and planar defects, occurring within one or a few unit cells. Iijima (1978) has observed disorder in stacking sequences in 1M muscovite and biotite using high resolution

Table 6.2

Approximate Chemical Formulae of Common Micas

Di-octahedral

	X	Y	Z
Muscovite	K_2	Al_4	Si_6Al_2
Paragonite	Na_2	Al_4	Si_6Al_2
Glauconite	$(K,Na)_{1.2-2}$	$(Fe,Mg,Al)_4$	$Si_{7-7.6}Al_{1-0.4}$

Tri-octahedral

	X	Y	Z
Phlogopite	K_2	$(Mg,Fe^{+2})_6$	Si_6Al_2
Biotite	K_2	$(Mg,Fe,Al)_6$	$Si_{6-5}Al_{2-3}$
Zinnwaldite	K_2	$(Fe,Li,Al)_6$	$Si_{6-7}Al_{2-1}$
Lepidolite	K_2	$(Li,Al)_{5-6}$	$Si_{6-5}Al_{2-3}$

electron microscopy. Recently Banos,Amouric, Fouquet and Baronnet (1983) studied the interlayering and interlayer slip in biotite by high resolution transmission electron microscopy.

In the present work four micas were observed by transmission electron microscopy and electron diffraction: they are muscovite, phlogopite, biotite and lepidolite.

The samples for observations were prepared in the following way:

A foil of several square centimeters of mica was cleaved to get a fresh surface and was cut at a small angle by means of a sharp knife. Holding the foil by a pair of tweezers on a folding electron microscope grid, the edge side was stripped by the knife, small flakes from the freshly cleaved cleaved surface were collected on the folding grid. The grid was then folded carefuly and put inside the electron microscope specimen holder and transferred to the electron microscope for observation. The cleavage in micas occurs along (001) plane where a monolayer of potassium ions separates the sheets (refer to Fig. 6.3). It is believed that upon cleavage these ions are distributed equally between the newly-created surfaces, so that a cleavage face would contain half a monolayer of potassium ions (Higginbotham, Williams and McEvoy, 1975). Because no extra spots are observed in the low energy electron diffraction patterns from cleaved mica surfaces, Muller and Chang (1968) have concluded that the potassium must be distributed randomly.

Muscovite is one of the most common of the micas and occurs in a wide variety of geological environments. Its well-known property of electrical insulation has made it a mineral of industrial importance. According to Jackson and West (1930) muscovite crystallizes in the monoclinic system with the following chemical composition:

$$K_2Al_4[Si_6Al_2O_{20}] (OH, F)_4$$

with z = 2.

Here z is the number of times the formula unit is contained in the unit cell. Its structure (Deer, Howie and Zussman, 1962) can be discribed as made up of SiO_4 tetrahedra arranged in infinite two dimensional sheets (of hexagonal rings, (refer to Fig. 6.1, 6.2 and 6.3) with one fourth of Si atoms are replaced by the Al ions. Two of such sheets joined together with the free oxygen anions of SiO_4 groups in contact forming, with the OH,F anions, a close-packed anionic layer. Al cations occupy the octahedral sites in the layer and bond the sheets together. The muscovite structure is a succession of such units held together rather weakly by means of K ions, located at the centres of oxygen hexagons. It should be realized that in Fig. 6.1 and 6.2, the lines outlining the hexagons are not bonds but lines linking up the vertices of the tetrahedra of the upper and lower sheets. The hydroxyl ions (OH,F) lie at the centre of each hexagon but since they are not opposite one another owing to the clos-packed true hexad axes cannot be common to a pair of sheets. The staggering lowers the symmetry to monoclinic.

As polymorphism in mica arises because an a/3 stagger in the octahedral region of each 1 nm layer. Smith and Yoder (1956) predicted, both theoretically and experimentally, that in mica six simple polymorphs should be observed. Although the polymorphism in muscovite has

been studied extensively, only 1M, $2M_1$, (and less commonly) 3T have been observed. Some more complicated polymorphs also have been reported but they are very rare. The most common polymorph $2M_1$ has the following crystallographic characteristics:

$$a_o = 0.519 \text{ nm}$$
$$b_o = 0.904 \text{ nm}$$
$$c_o = 2.008 \text{ nm}$$
$$\beta = 95^\circ\ 30'$$

Space group: C2/c.

Fig. 6.5 (a) shows the electron diffraction pattern from a single crystal of muscovite which was taken under the following experimental conditions:

Accelerating voltage = 100×10^3 volts

Objective lens current = 72.4 mA

The camera constant, $2 \lambda L$, is 3.245 mm nm (determined from the curve in Fig. 3.15 in chapter 3). The print magnification is X 3.5, so the total camera constant is 11.36 mm nm. The length of reciprocal vectors for three pair of spots (diametrically opposite across the centre of the pattern), were measured and converted into interplanar spacings using the above value of camera constant. These observed d-values were compared with the calculated values of interplanar spacings of (h k 1) planes using the monoclinic formula and above lattice

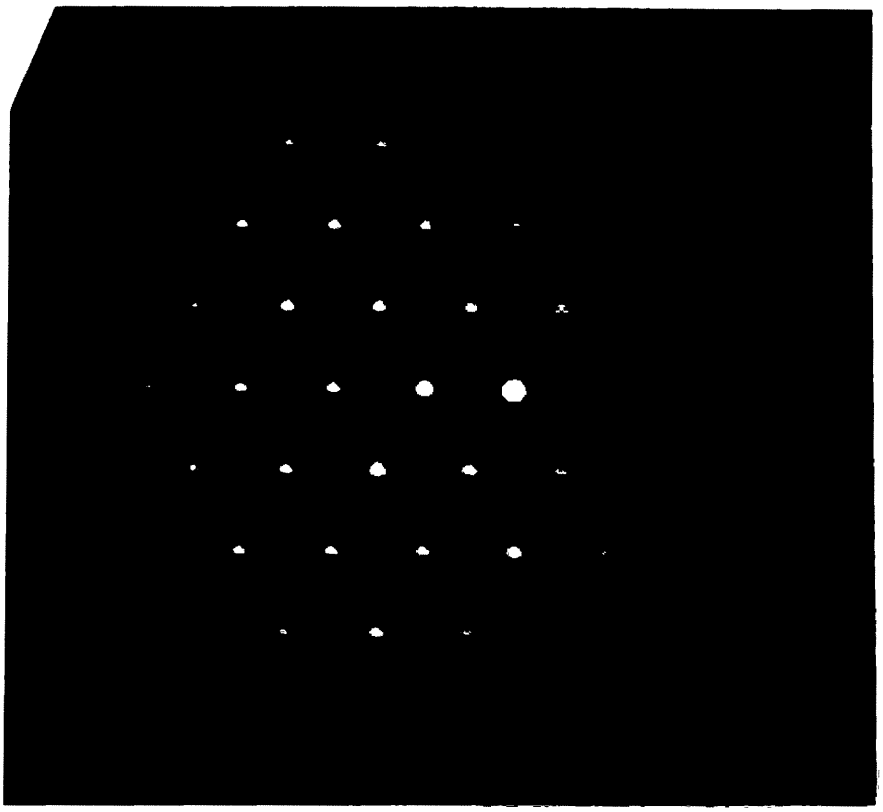

Fig. 6.5 (a)

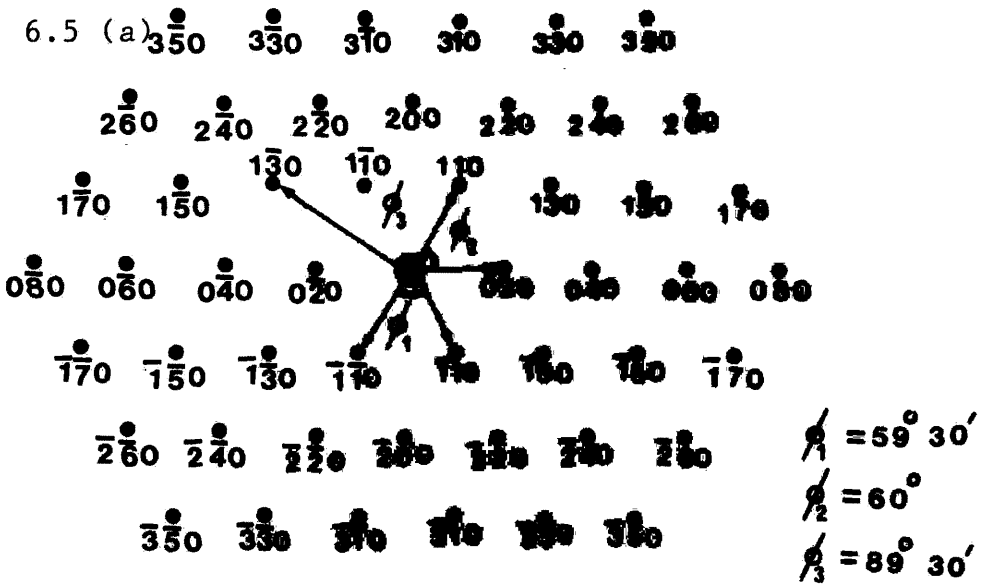

Fig. 6.5 (b)

Fig. 6.5. (a) Diffraction pattern of single crystal of muscovite. (b) Its solution.

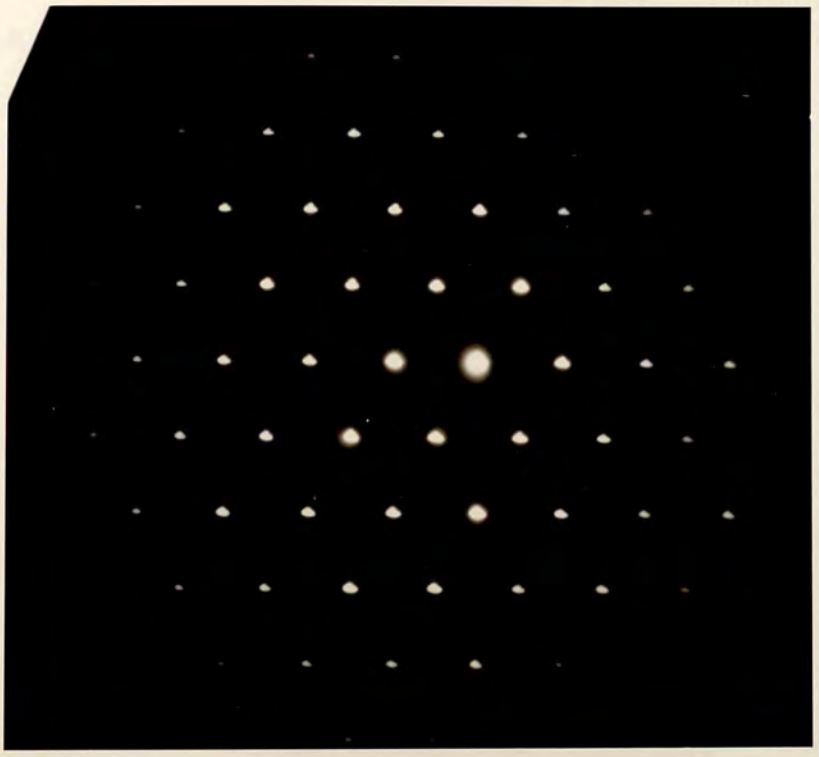

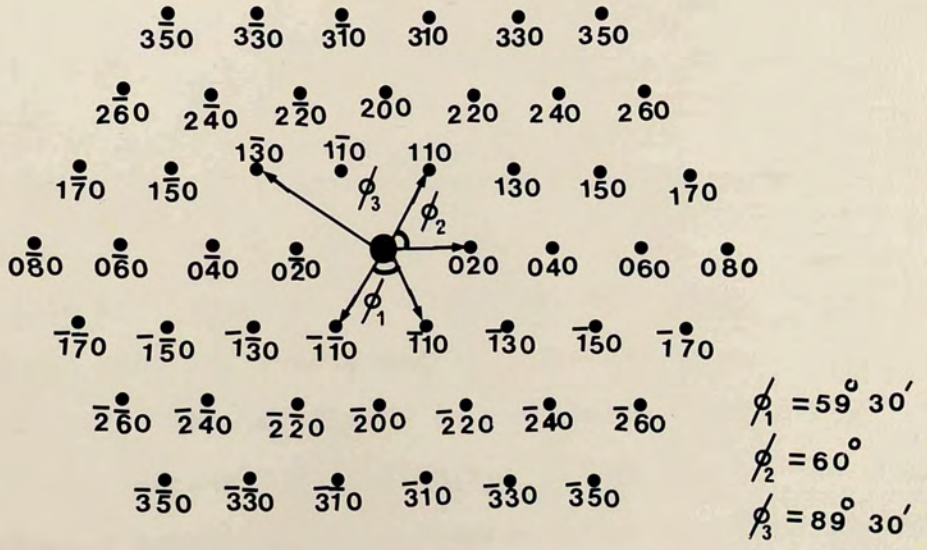

$\phi_1 = 59^\circ 30'$

$\phi_2 = 60^\circ$

$\phi_3 = 89^\circ 30'$

parameters. The indices h k l were determined for each spot, viz:

d-spacing		
observed	calculated	h k l
0.453 nm	0.452 nm	0 2 0
0.449 nm	0.448 nm	1 1 0
0.261 nm	0.260 nm	1 3 0

This indexing was checked by measuring the angles ϕ_1 , ϕ_2 and ϕ_3 subtended at the centre spot by pairs of reflections. These wre compared with the calculated ϕ - values for monoclinic system.

	h_1	k_1	l_1	h_2	k_2	l_2	observed	calculated
ϕ_1	1	1	0	1	$\bar{1}$	0	59° 30'	59° 29'
ϕ_2	1	1	0	0	2	0	60°	60° 15'
ϕ_3	1	1	0	1	$\bar{3}$	0	89° 30'	89° 29'31"

The solution of the diffraction pattern based on above measurements is given in Fig. 6.5 (b).

This most abundant form of mica, muscovite, possesses one other extremely useful characteristic, namely its mechanical behaviour. In particular mention may be made of its extremely high flexibility and almost perfect elastic behaviour until fracture. The origin of the unique elastic properties of muscovite is not yet known, however, some conclusion can be inferred if the mechanisms of slip and mobility of dislocations in it are known.

The literature reveals that the number of investigations reported on the dislocations in mica is very few and mainly depend on examination by X-rays. Transmission electron microscopic studies have rarely been carried out on this important subject.

Tolansky and Morris (1947) and Amelinckx (1952) used multiple beam interferometric technique. They showed that the number of dislocations emerging out of the basal planes are indeed very few, and that most of the dislocations in muscovite lie and operate mainly in the basal planes. The surface study of the {001} growth form of natural biotite (Amelinckx, (1952), first revealed the presence of growth spirals. Further studies (Sunagawa, 1964) confirmed the existence of such spirals on natural phlogopite. Afterwards various kinds of growth spiral developing on {001} form, at the outcrop of screw dislocations, have been observed on hydrothermally grown crystals of phlogopite (Baronnet, 1972), and of muscovite (Baronnet, Amouric and Chabot, 1972). Amelinckx and Delavignette (1961), and Silk and Barnes (1961) almost simultaneously published transmission electron microscopic studies on muscovite. The first one described straight lines lying in the basal plane whereas the other two reported hexagonal dislocation networks ending on cleavage steps as well as regions of parallel lines emanating from these steps (thought to be caused by cleavage preparation). Silk and Barnes (1961) also reported moire patterns revealing edge dislocation lines emerging on the {001} form.

Also by electron microscopy, Demny (1963) determined Burgers vectors of lines lying in the basal plane. 1/2[110], 1/2[1$\bar{1}$0] and [100] are the lattice vectors observed, the latter occurring less frequently than the former two. Williame and Authier (1966), using Lang's X-ray transmission topographic technique, observed that the dislocations lying in the basal plane of the muscovite frequently changed their directions, forming zig-zag lines.

A theoretical investigation of defects in layerd structures by Amelinckx and Delavignette (1961) has shown six different possibilities for Burgers vectors lying into the (001) plane. They were further explained by Caslavsky and Vedams (1970) on the basis that layers in mica held together rather weakly by means of K ions, located at the centres of the oxygen hexagons. Cleavage takes place on this plane; it is natural to expect that a slip plane will also be located there, since this is the 'weak' plane in the structure. The Burgers vector operates from a K ion to the nearest one, as shown in Fig. 6.6.

Amelinckx (1961) did not accept the possibility of the presence of partial dislocations because of a too high stacking fault energy. Caslavsky and Vedams (1970) have concluded, from the studies of a number of muscovite specimens by Lang topograph, that there exist dislocations with the six different Burgers vectors. Those having the [100], [110] and [1$\bar{1}$0] directions of the Burgers vector are the total dislocations and those with the [010], [310] and [3$\bar{1}$0] directions of Burgers vector are partial dislocations.

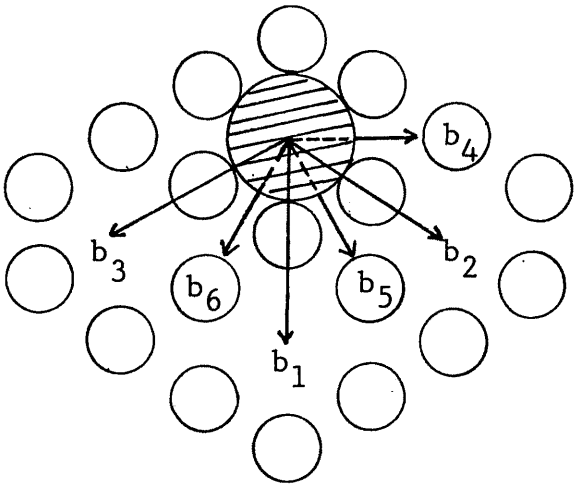

$b_1 = [100]$ $\quad\quad$ $b_4 = 1/3[010]$

$b_2 = 1/2[110]$ $\quad\quad$ $b_5 = 1/6[310]$

$b_3 = 1/2[1\bar{1}0]$ $\quad\quad$ $b_6 = 1/6[3\bar{1}0]$

Fig. 6.6. Possible Burgers vectors in (001) plane of mica (muscovite), ◯ = basal oxygen ions of tetrahedral sheet and ◓ = potassium ion, three other potassium ions have been removed from b_1, b_2 and b_3 positions.

The relation between the total and partial dislocations can be described by three dislocation reactions:

$$1/3[010] + 1/6[310] = 1/2[110]$$
$$1/3[010] + 1/6[3\bar{1}0] = 1/2[1\bar{1}0]$$
$$1/6[310] + 1/6[3\bar{1}0] = [100]$$

They gave the explanation for the presence of partial dislocations that these dislocations were formed in the

early history of crystal formation, probably during the growth period, because all the partial dislocations, they observed were decorated with impurities. Corny, Baronnet and Jourdan (1976) concluded from similar investigations that the bundle of dislocation lines appear to be associated with stresses induced by quartz inclusions entrapped during growth and by misorientations between the numerous grains of the crystal core. Earlier described defects in micas seem to be due to a slip mechanism between adjacent (001) levels, these defects being originated by post-growth external stresses of tectonic origin and or by specimen preparation damage. If the partial dislocations do exist in micas, then it is obvious that they will influence the various mechanical properties of mica considerably.

The conclusion from the studies so for on defects in mica is that these defects have two origins: first, defects are frozen from the growth period due to the inclusion of impurities and secondly, defects appearing in thin sheets are formed during the cleavage process.

In the electron microscope the mica crystals are generally bent and show extinction contours, as seen from the micrographs in Fig. 6.7, 6.8, 6.9 and 6.10. The formation of these contours can be explained by schematic construction in Fig. 6.11. If an ideal crystal slab of thickness D is bent on a radius R and if it is assumed that no local distortion occur, then a first approximation to the image is obtained by assuming a continuously

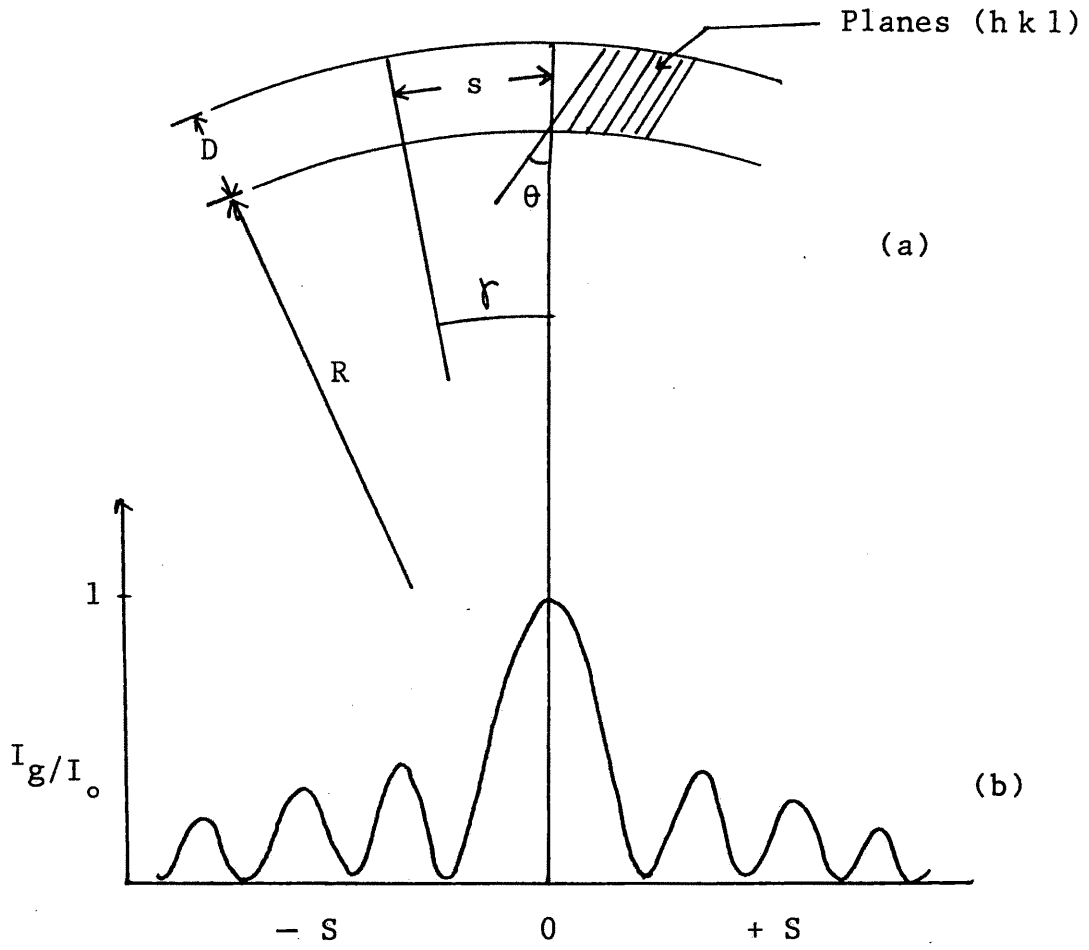

Fig. 6.11. (a) Geometrical construction for an ideally bent crystal. (b) Primary and secondary diffraction maxima predicted for the bent crystal.

varying orientation. The geometric construction is shown in Fig.6.11 (a). A plot of intensity as a function of distance from the primary line is sketched in Fig. 6.11 (b). On this basis, the electron image for cylindrically and spherically bent crystals would exhibit parallel fringes and concentric, circular fringes respectively (Heidenreich, 1949; Amelinckx, 1964). The contours which formed due to the bent in crystal, are also called

inclination contours, are very sensitive to changes in orientation; on tilting the specimen they move rapidly over the surface. In reciprocal lattice language one can say that along the main extinction contour $s \simeq 0$ for the considered reflection. On passing the contour s changes sign, i.e., the deviation from exact Bragg condition changes sense. This is the reason why the contrast for a given dislocation changes on crossing over a contour (Amelinckx, 1964).

Along the line where the crystal is (r + 1/2) D thick (r = integer) The diffracted intensity is maximum and a black line will be observed. The result from the periodic nature of the transmitted intensity as given by the formula

$$I_s = \frac{\sin^2 \pi D s}{(\pi s)^2}$$

The contours of this type are not very mobile when the specimen tilt is being changed. However, their appearance and their periodicity is sensitive to which reflection is operating. The latter effect can only be explained on the basis of dynamical theory. The difference in foil thickness between points where two successive fringes occur is equal to an extinction distance . The method of measuring foil thickness by extinction contours has been given in chapter 2.

Fig. 6.7 shows the extinction contours all over the micrograph, as the bending in the crystal is not ideal the fringes are not straight. In the electron microscope it was estimated that the electron beam could have produced a local heating of 100 °C to 200 °C (Cartz and Tooper, 1965). As the mica is an insulating material, the local expansion due to this thermal effect caused buckling in thin sheet of muscovite which produced parallel extinction contours as seen in the left half portion of the micrograph in Fig. 6.7. The extinction contours are disturbed by dislocation lines which appear from the right bottom of the micrograph and pass through the extinction contours where the contrast changes to produce a zig-zag effect.

A micrograph from the edge of a thin sheet of muscovite is shown in Fig. 6.8. As mica usually exhibits step structure at the edges and shows the thickness contours horizontally. Some dislocation lines also have been observed on the right side of the micrograph. The micrograph in Fig. 6.9 shows horizontal extinction contours which are disturbed by two dislocation lines, one at right angle and other on a different angle. The micrograph in Fig. 6.10 is also from a thin sheet of muscovite which shows extinction contours which are curved due to variation in thickness caused by the inclusion of impurities. The black spots on the micrograph suggest clusters of impurities in different regions of the muscovite.

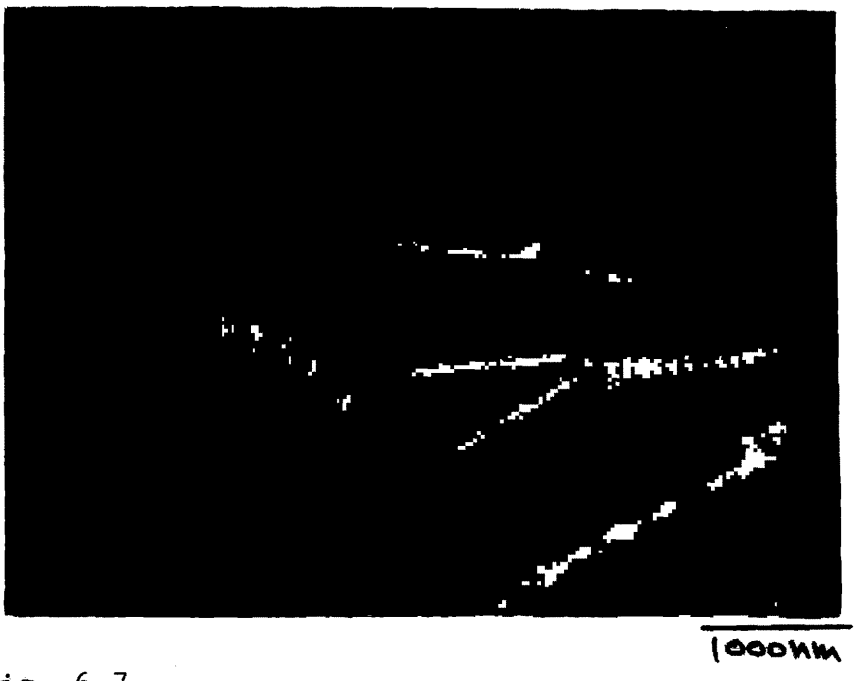

Fig. 6.7

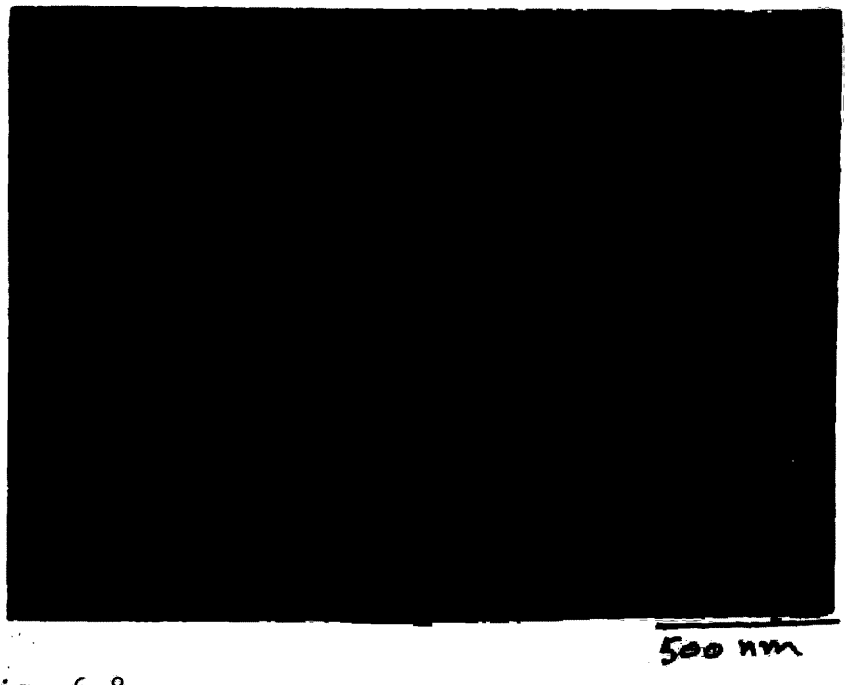

Fig. 6.8

Fig. 6.7 and 6.8. Micrographs of thin sheets of muscovite showing extinction contours disturbed by dislocation lines.

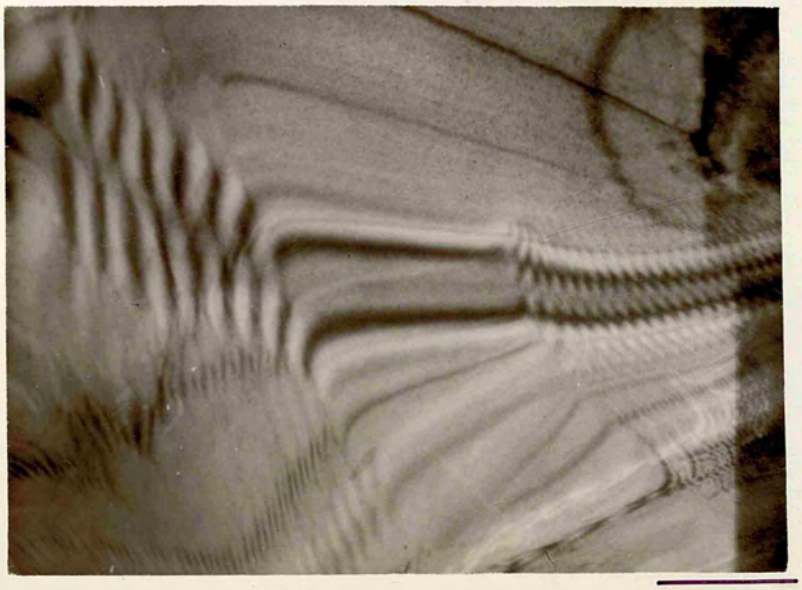

1000nm

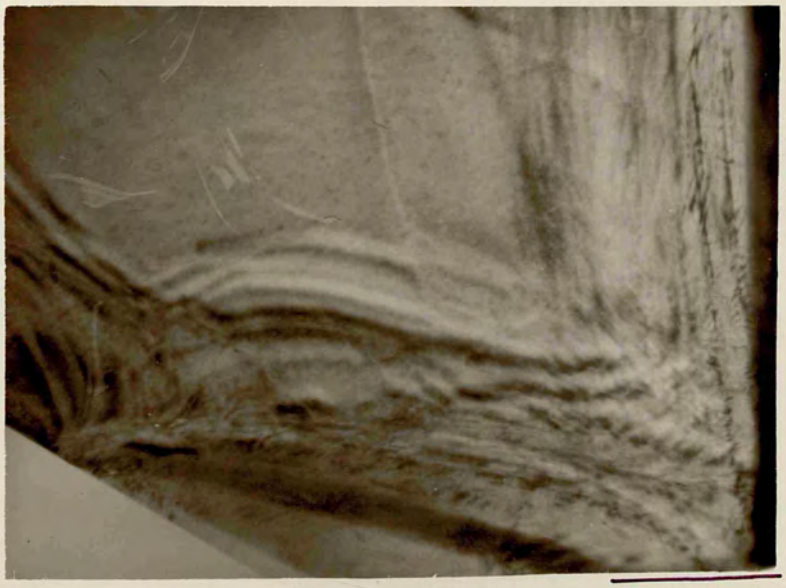

500 nm

Fig. 6.9

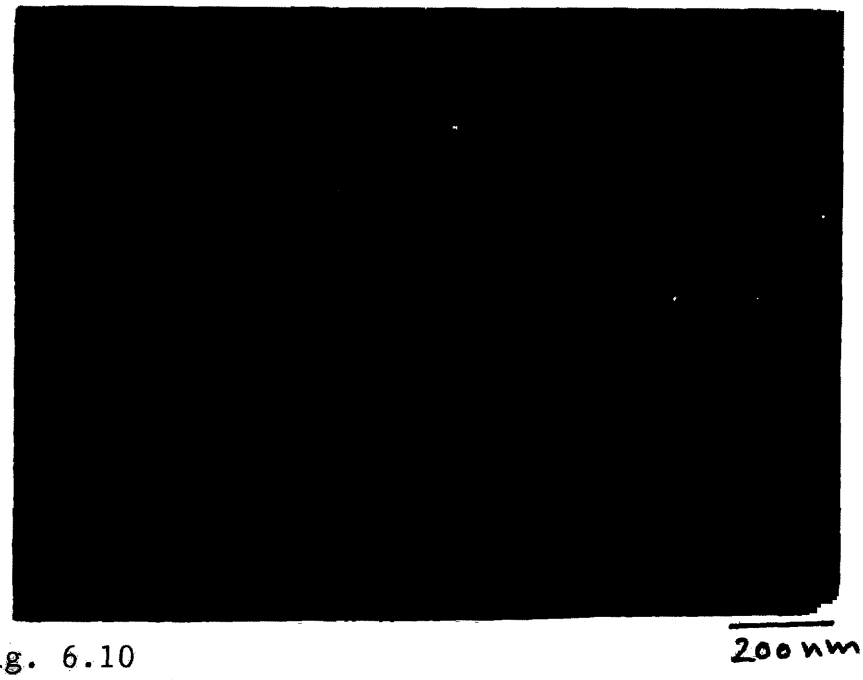

Fig. 6.10

Fig. 6.9. Micrograph of musovite thin sheet showing dislocation lines crossing the extinction contours.

Fig. 6.10. Clusters of impurities in mica (muscovite).


200 nm

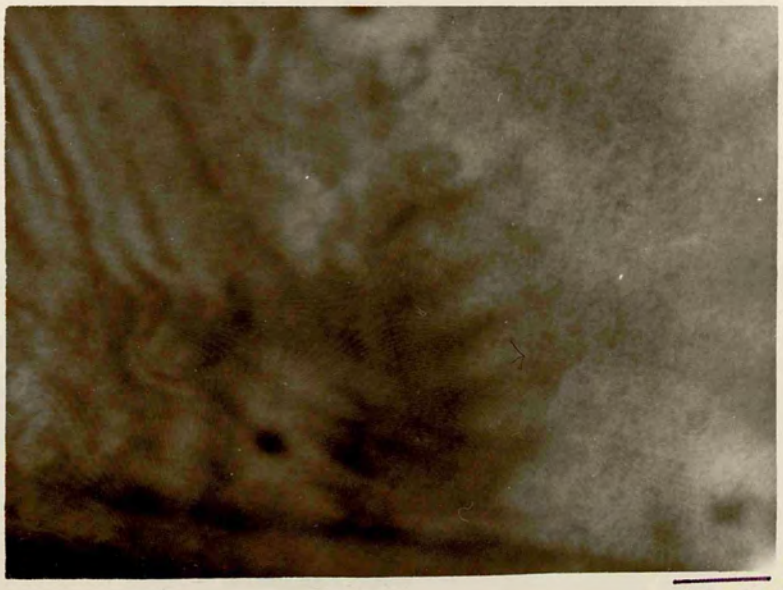
200 nm

Phlogopite is an important member of the mica group and belongs to the tri-octahedral class of minerals with layerd structure. The name is derived from the greek phlogopos, fire-like, which refer to the reddish tinge, which specimen often display. According to Deer, Howie and Zussman (1962), its chemical composition is as follows:

$$K_2 \ (Mg \ Fe^{+2})_6 \ [Si_6 \ Al_2 \ O_{20}] \ (OH, \ F)_4$$

with z = 1

Heinrich et all. (1953) suggested that the ratio of magnesium to iron atoms in phlogopite is greater than two to one. If the Mg:Fe ratio falls belw 2:1, the mineral is called biotite. Biotites, however, often have some further substitution of Al in the octahedral and tetrahedral sites. Phlogopites with very little iron, manganese, etc., are almost colourless, (generally the more iron-rich members of the micas are darker), and like muscovite are important ecnomically for their properties of electrical insulation.

In phlogopite the octahedral sites of the mica structure are completely filled. The most common polymorph is 1M but 2M and 3T polymorphs sometimes occur. The cell dimensions of the most common polymorph 1M are as follows:

a_o = 0.53 nm $\qquad$ b_o = 0.92 nm

c_o = 1.03 nm $\qquad$ β = 100°

Space group: Cm

Phologopite is also prepared synthetically, usually have all the (OH) replaced by F, and called fluorophlogotite.

Zvyagin and Mishchenko (1962), Joswig (1972) and Rayner (1974) have studied the natural phlogopite and gave various structural details. The synthetic fluorophlogopite has been studied by McCauley, Newnham and Gibbs (1973), and Takeda and Morosin (1975).

Fig. 6.12 shows the electron micrograph of a thin sheet of phlogopite which shows a number of dark clusters probably due to inclusion of impurities. As suggested by Cartz and Tooper (1965) that phlogopite micas contain water up to 4 % by weight and can contain very large amounts of occluded gas. The electron beam which can produce a local heating of 100°C to 200°C, causing loosely held liquids and gases at crystal interfaces and packing faults to be relesed rapidly. Water may be present within the crystal structure, at rather unstable structural sites between the silicate layers (Metsik ,1958), and concentrated on defects such as dislocation lines. The black spots in this micrograph may be abundant precipitates preceded by a mechanism in which brucite-like layers replaced T-O-T mica layers or the formation of iron oxide within the crystal. The white spots in the micrograph are probably the intergrowth of talc lamellae. The micrograph in Fig. 6.13 is also from a very thin sheet of phlogopite and shows dislocation lines. Bundles of dislocation lines, some crossing each other, are visible in the micrograph in Fig. 6.14 (a). The diffraction pattern in Fig. 6.14 (b) is from the above and indicates misorientations in the crystals.

Fig. 6.12

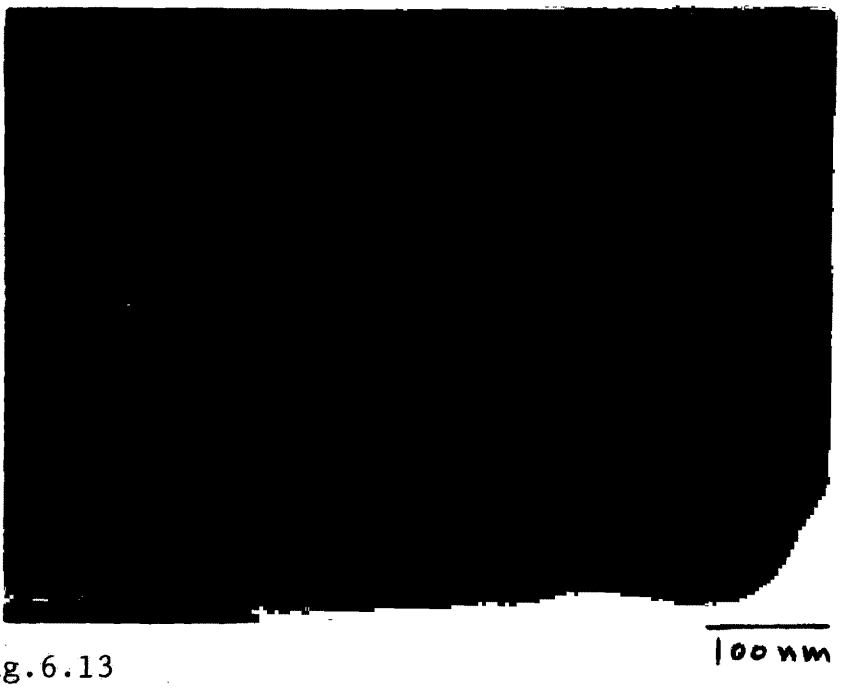

Fig.6.13

Fig. 6.12. Micrograph of phlogopite showing clusters of impurities.

Fig. 6.13. Dislocation lines in phlogopite.

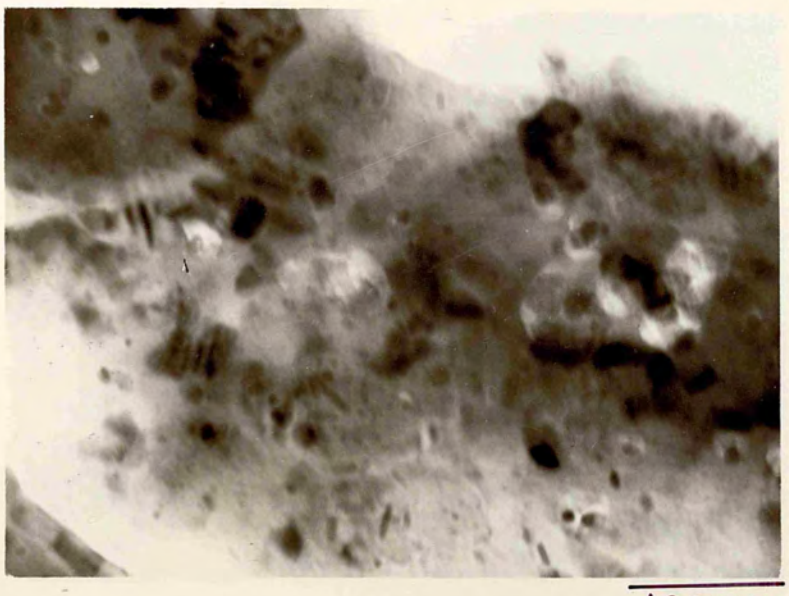
100nm

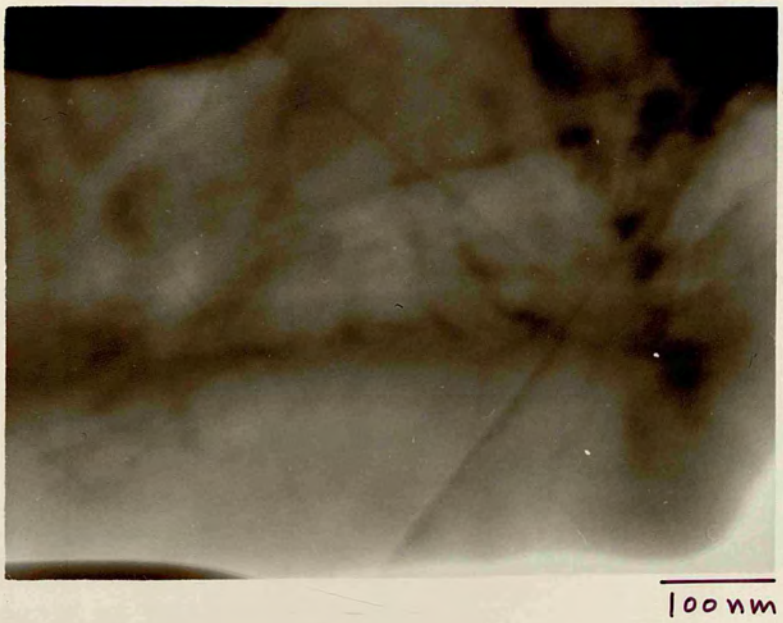
100nm

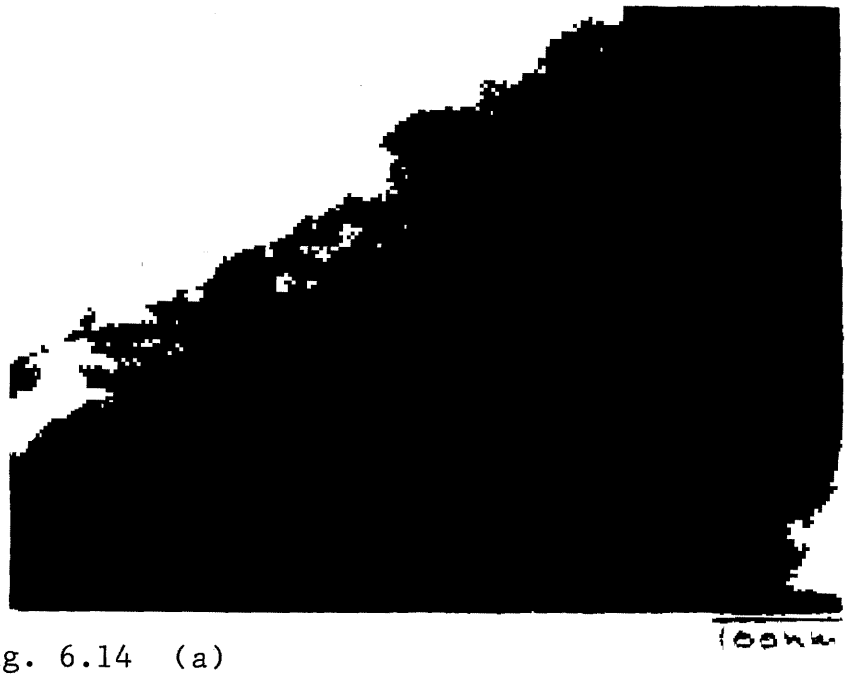

Fig. 6.14 (a)

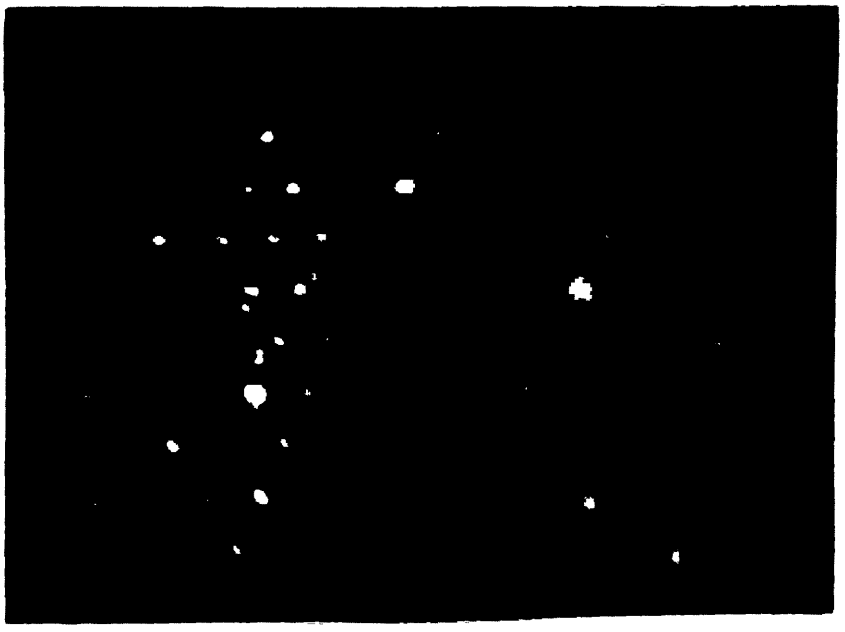

Fig. 6.14 (b)

Fig. 6.14 (a). Micrograph of phlogopite showing bundles of disLocation lines. (b) Diffraction pattern representing the misorientation in the crystals.

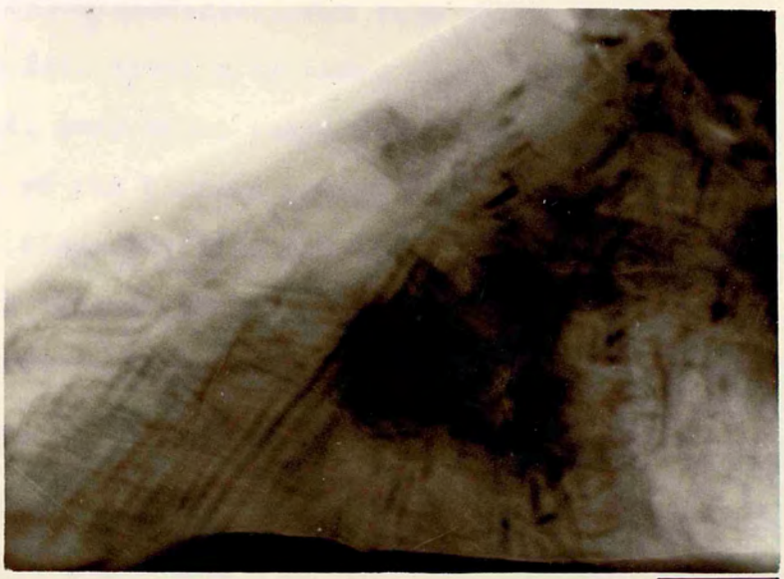
100nm

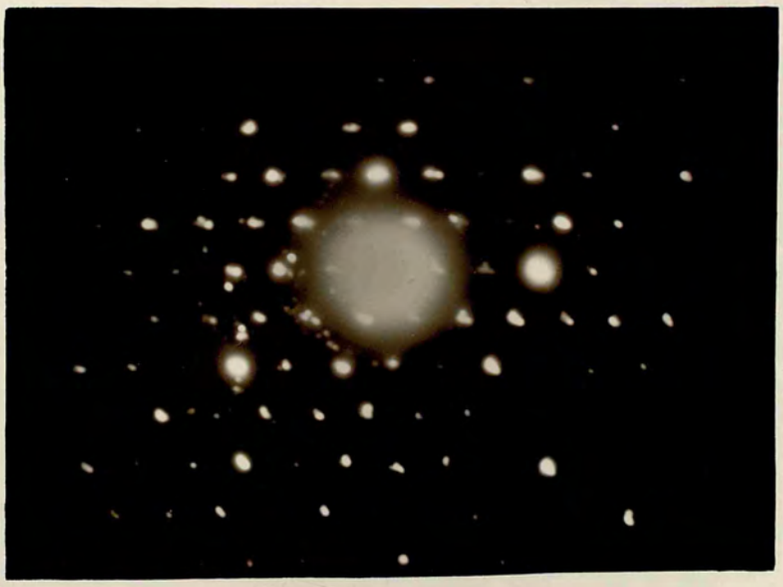

Biotite is an iron-rich tri-octahedral mica which is arbitrarily differentiated from phlogopite in having Mg:Fe < 2:1. Biotite is named after the mineralogist J.B.Biot; many other names have been used to describe the members of the biotite group, the more useful of which are annite, siderophyllite and lepidomelane. The detailed chemical composition of biotite as given by Deer, Howie and Zussman (1962), is

$$K_2\ (Mg,Fe^{+2})_{6-4}(Fe^{+3},Al,Ti)_{0-2}[Si_{6-5}Al_{2-3}O_{20}]\ O_{0-2}(OH,F)_{4-6}$$

From the analyses of more than 200 tri-octahedral micas, Foster (1960 a) found that for small amounts of substitution of Fe^{+3} for octahedral Mg (less than 0.3-0.4 atoms per 3.0 octahedral sites), charge compensation is achieved by an equivalent amount of substitution of Fe^{+3} (or Al) for Si in the tetrahedral positions. For large amounts of octahedral substitution, however, octahedral vacancies become increasingly important as an additional method of charge compensation. For most biotites, therefore, tetrahedral Fe^{+3} is greater than the 1.0 total needed to balance the interlayer cation and the octahedral cation total is less than 3.00. The maximum amount of substitution of Fe for octahedral Mg appears limited to one atom per three octahedral sites. Foster (1960 a) defined biotite as having Mg between 20 % to 40 %, and siderophyllite and lepidomelane less than 10 % Mg.

Foster (1964) found that a large percentage of tri-octahedral micas have low (OH, F) values. In some

cases this can be explained by internal oxidation of Fe and a compensating dehydroxylation of OH to O. Brindley and Brown (1980) have given a comprehensive review on the structure and substitution in tri-octahedral micas.

X-ray examination of large numbers of single crystals of natural tri-octahedral micas has shown that the majority crystallize as the 1M structure form, and only a few as the 3T or $2M_1$ structures (Levinson and Heinrich, 1954). A disordered stacking sequence 1Md also is of common occurrence. Several more complex stacking sequences have been identified in biotites (Ross, Takeda and Wones, 1966). Hendricks and Jefferson (1939) gave the following cell parameters for most common 1M polymorph of biotite:

$a_o = 0.53$ nm $\qquad b_o = 0.92$ nm

$c_o = 1.02$ nm $\qquad \beta = 100^\circ$

Space group: Cm

A large number of structural refinements have been conducted on tri-octahedral 1M micas of varying tetrahedral and octahedral compositions.

Fig. 6.15 (a) shows a diffraction pattern of a single crystal of biotite which was taken at 100 X 10^3 V accelerating voltage with objective lens current 80 mA. The camera constant $2\lambda L$ is 3.09 mm nm (determined from the curve in Fig. 3.15 in chapter 3). The print magnification is X 3.6, so the total camera constant is 11.124 mm nm. The indices h k l were determined with the

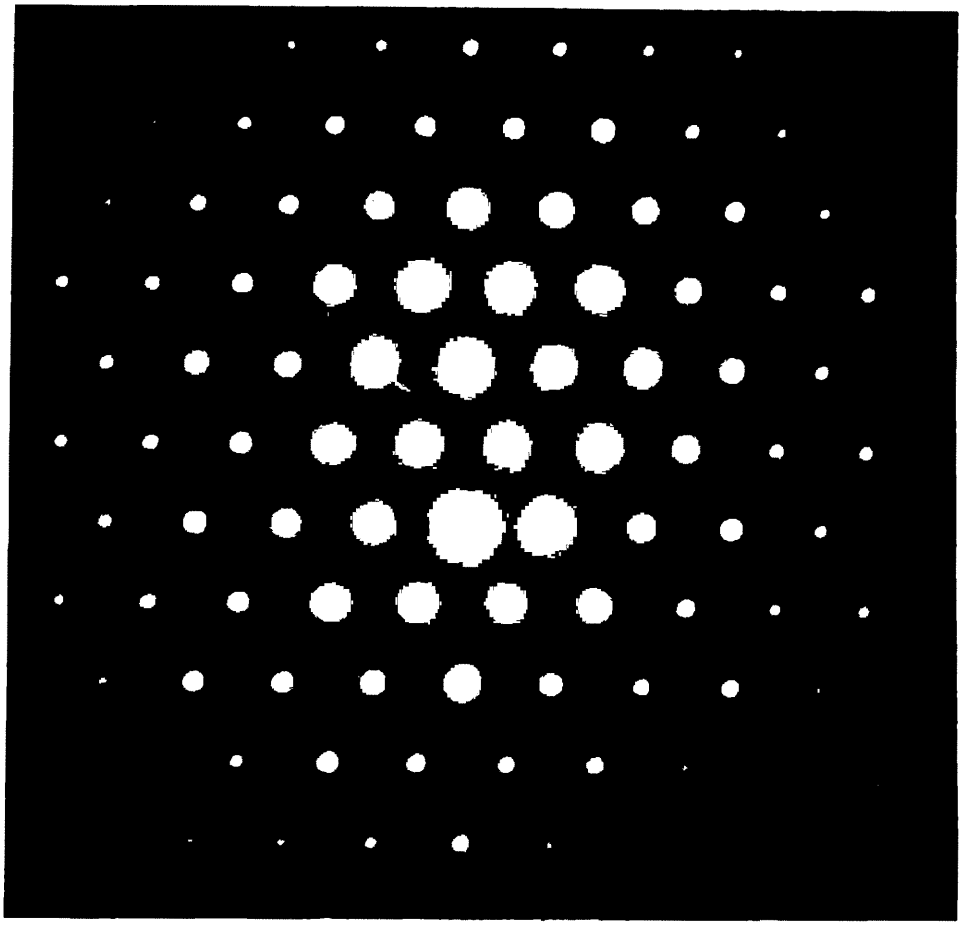

Fig. 6.15 (a)

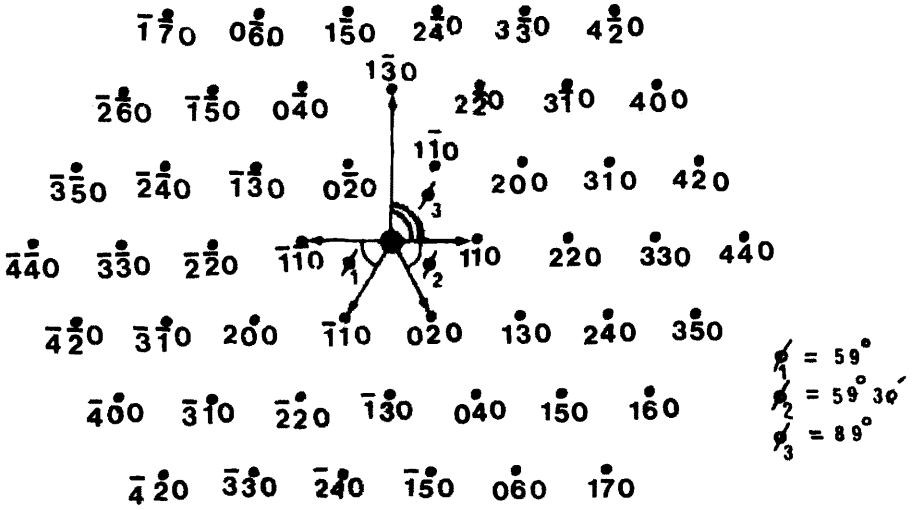

Fig. 6.15 (b)

Fig. 6.15. (a) Diffraction pattern of a single crystal of biotite. (b). Its solution.

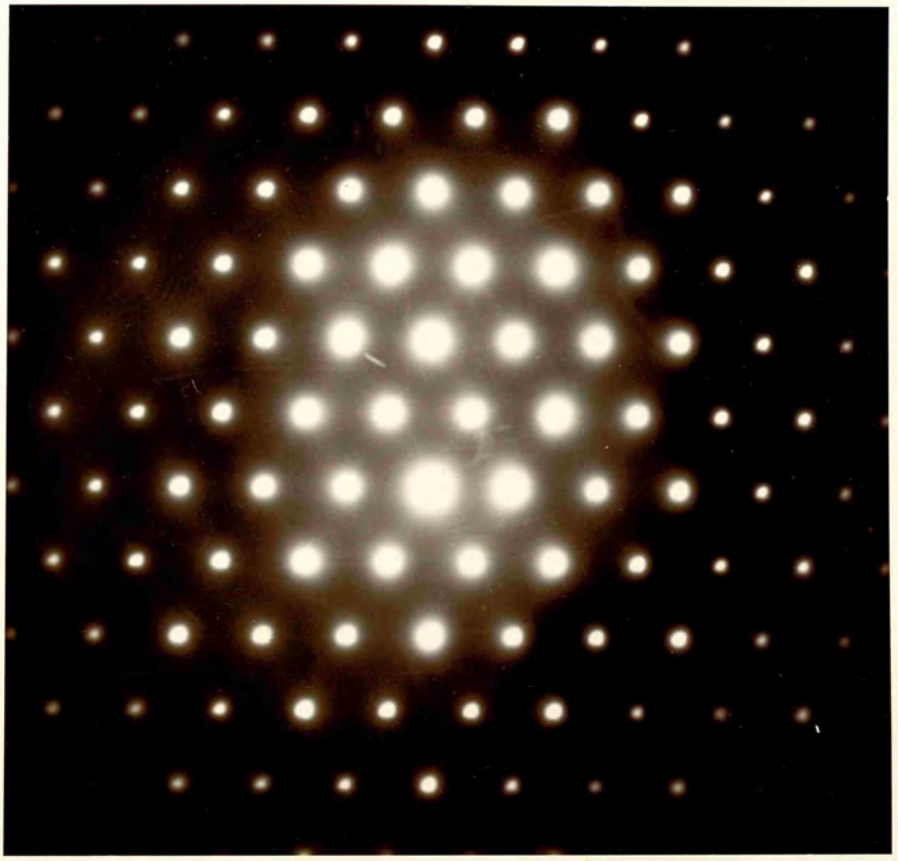

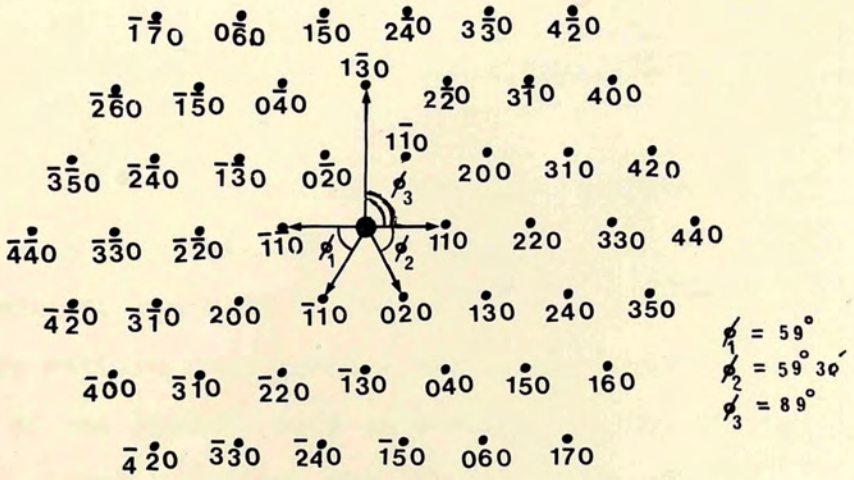
$\bar{1}\bar{7}0$ $0\bar{6}0$ $1\bar{5}0$ $2\bar{4}0$ $3\bar{3}0$ $4\bar{2}0$
$1\bar{3}0$
$\bar{2}\bar{6}0$ $\bar{1}\bar{5}0$ $0\bar{4}0$ $2\bar{2}0$ $3\bar{1}0$ $4\bar{0}0$
$1\bar{1}0$
$\bar{3}\bar{5}0$ $\bar{2}\bar{4}0$ $\bar{1}\bar{3}0$ $0\bar{2}0$ ϕ_3 $2\bar{0}0$ $3\bar{1}0$ $4\bar{2}0$
$\bar{4}\bar{4}0$ $\bar{3}\bar{3}0$ $\bar{2}\bar{2}0$ $\bar{1}\bar{1}0$ ϕ_1 ϕ_2 110 220 330 440
$\bar{4}\bar{2}0$ $\bar{3}\bar{1}0$ $2\bar{0}0$ $\bar{1}10$ 020 130 240 350
$\bar{4}0\bar{0}$ $\bar{3}1\bar{0}$ $\bar{2}2\bar{0}$ $\bar{1}3\bar{0}$ 040 150 160
$\bar{4}2\bar{0}$ $\bar{3}3\bar{0}$ $\bar{2}4\bar{0}$ $\bar{1}5\bar{0}$ 060 170
$\phi_1 = 59°$
$\phi_2 = 59° 30'$
$\phi_3 = 89°$

same method used for muscovite. The comparison of observed and calculated d-spacing is as follows:

d-spacing		
observed	calculated	h k l
0.459 nm	0.46 nm	0 2 0
0.451 nm	0.453 nm	1 1 0
0.265 nm	0.264 nm	1 3 0

and the comparison of angles is as follows:

	$h_1k_1l_1$	$h_2k_2l_2$	observed	calculated
ϕ_1	1 1 0	1 $\bar{1}$ 0	59°	59° 7'
ϕ_2	1 1 0	0 2 0	60° 30'	60° 26'
ϕ_3	1 1 0	1 $\bar{3}$ 0	89°	89° 8'.

The solution of the diffraction pattern based on above measurment is given in Fig. 6.15 (b).

Fig. 6.16 shows the transmission electron micrograph of a very thin sheet of biotite, the extinction contours indicate the bent in the sheet. The complexity of the contours pattern represents a rather peculiar distortion of the crystal such as a dimple in the form of clover leaf, local buckling, etc. The sharp changes in direction and discontinuties in the contours are hardly explained on the basis of simple bending or thickness change. Highly localized distortions or orientation changes are apparently required in order to explain the

fine details of these contours. In Fig. 6.17 an other micrograph of biotite shows bending in the foil and inclusion of impurities. The white marked areas are probably the intergrowth of talc layers in the biotite, surrounded by brucite layers (which appear as dark lines), as described by Veblen (1983).

The 'Newtons ring-like' fringes appeared all over the micrograph in Fig. 6.18. (a) which resulted when a thin foil of biotite was exposed to strong electron irradiation. As describe by Demny (1963) and Cartz and Tooper (1965), mica contains a small quantity of gas, Which collects in bubble-hallows on warming by the electron beam. The presence of similar bubbles in mica was first observed by Rang (1953 a,b). An illustration of these bubbles in mica is given in Fig. 6.19.

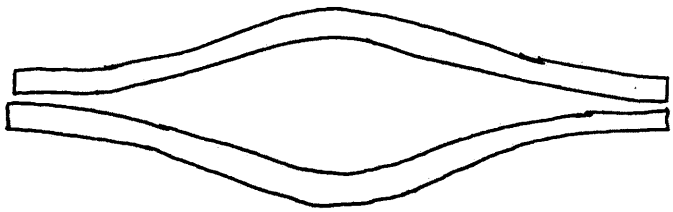

Fig. 6.19. The type of bubble (edge view) in thin sheet of mica (Rang, 1953 a b).

Iijima and Buseck (1978) have described them as "empty tunnels" Which occur in regions with lower electrostatic potentials in successive interlayers.

Recently Banos, et all. (1983), investigated interlayering and interlayer slip in biotite by high resolution transmission electron microscopy. They obtained structural information on micas having their basal plane parallel to the electron beam and reported that limited micro cleavage in mica is produced by basal slip in the layer level. They observed lens-shaped white spots between successive talc and brucite layers and interpreted them as corresponding to the "channels" (low electron density) situated between consecutive close-packed rows of interlayer cations (Iijima and Buseck, 1978). They made two different suggestions: that these spots are due to the micro cleavage of unsymmetric shape which has been produced by basal slip, or the interstratified brucite sheet has been destroyed by ion- electron beam irradiation.

The presence of the electron beam has a critical role in the nucleation of the lenticular flaws in micas. At room temperature or at higher temperature, the area of the specimen under view in the electron beam exhibited enhanced bubble nucleation and growth. Cartz and Tooper (1965) have given two explanations of this effect on the basis that micas contain a limited quantity of water and gas. One possibility is that the electron beam promotes the nucleation of these features by a charge effect, Perhaps ejecting the polar water molecule from low-stability sites in the micas. The other possible explanation is local hot-spot heating due to the intense electron irradiation. At these bubble-shaped hollows or

lenticular flaws, parallel moire' fringes were observed which together with the transverse Moire' fringes form "Newtons-rings"(Demmy, 1963).

Fig. 6.18 (b) shows the diffraction pattern of Fig. 6.18 (a), which indicates some extra spots, possibly due to misorientation caused by interlayer slip. Similar observations were found in an other sample of biotite and are shown in the micrograph of Fig. 6.20. The micrographs in Fig. 6.21 (a) and (b) are the inlargements of the selected parts of the micrograph in Fig. 6.20.

Lepidolite is a general name referring to lithium-rich aluminous micas of widly varying composition. They are a common constituent of many lithium-bearing granitic pegmatites. The chemical composition as given by Deer, Howie and Zussman (1962) is as follows:

$$K_2\ (Li,Al)_{5-6}[Si_{6-7}Al_{2-1}O_{20}]\ (OH,F)_4$$

In addition to the above substitutions for lepidolite, considerable amounts of sodium, rubidium and caesium may substitute for potassium, and iron, manganese and magnesium may enter octahedral sites. Other ions often present in small quantities are: Ca, Ba, Sr, Ga, Nb, Th and Ti. Heinrich et al., (1953) have given average content of some oxides and fluorine in 26 analysed lepidolites as follows: MnO 1.16, Li_2O 3.77, Rb_2O 0.54, Na_2O 0.41 and F 5.41 percent. The detailed chemical composition in lepidolite has been given by Winchell (1927 ,1942), Stevens (1938) and Foster (1960).

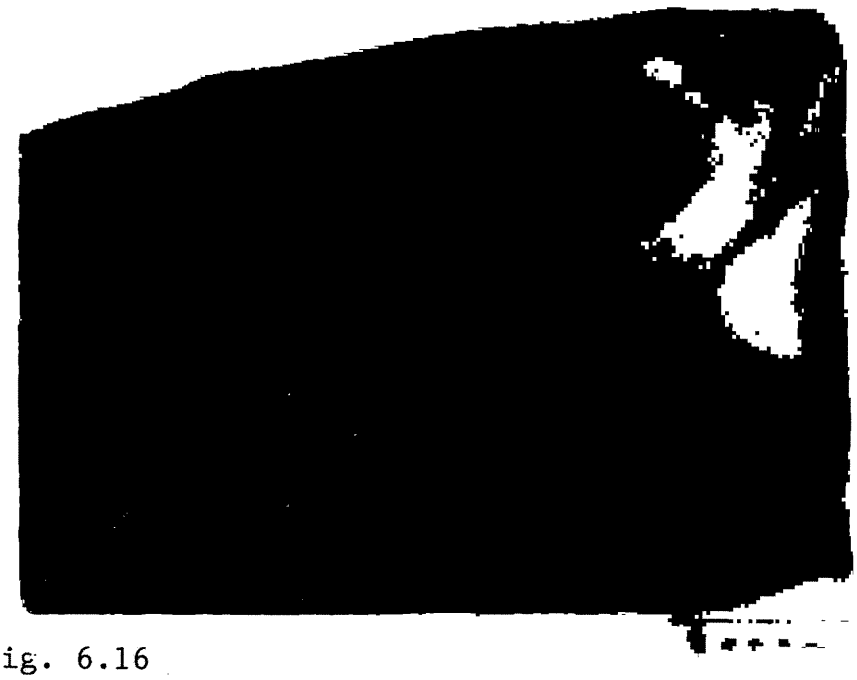

Fig. 6.16

Fig. 6.17

Fig. 6.17. Extinction contours in a thin sheet of biotite.

Fig. 6.18. Intergrowth of talc and other impurities in biotite.

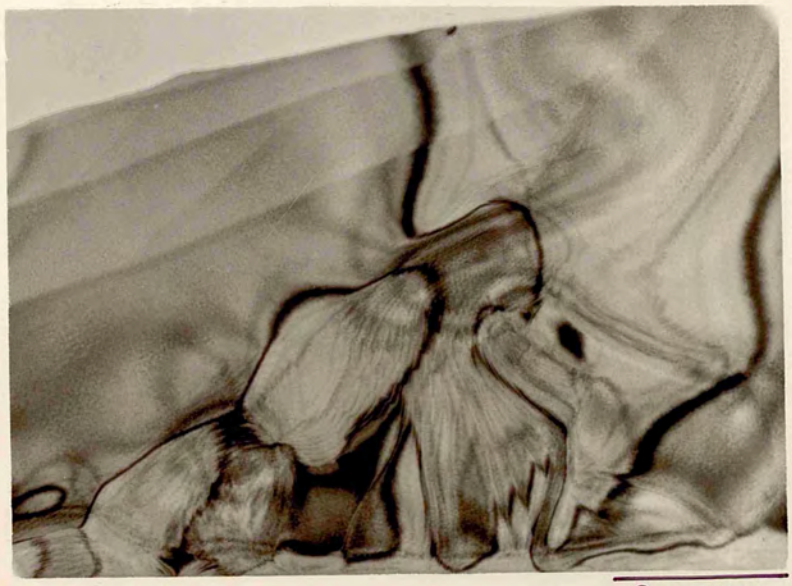
200nm

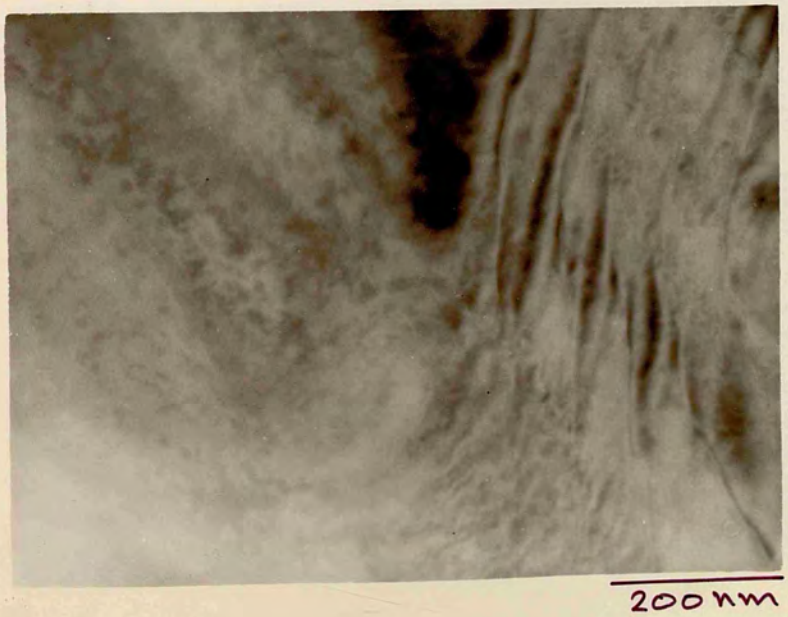
200nm

Fig. 6.18 (a)

Fig. 6.18 (b)

Fig. 6.18. Micrograph of thin sheet of a biotite showing Newtons' rings due to lenticular flaws or bubbles in the crystal. (b) Its diffraction pattern.

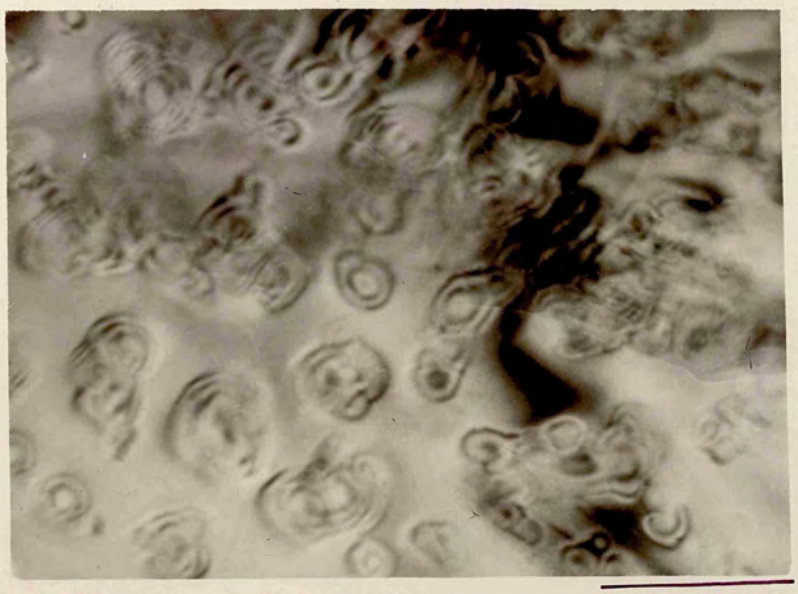

200 nm

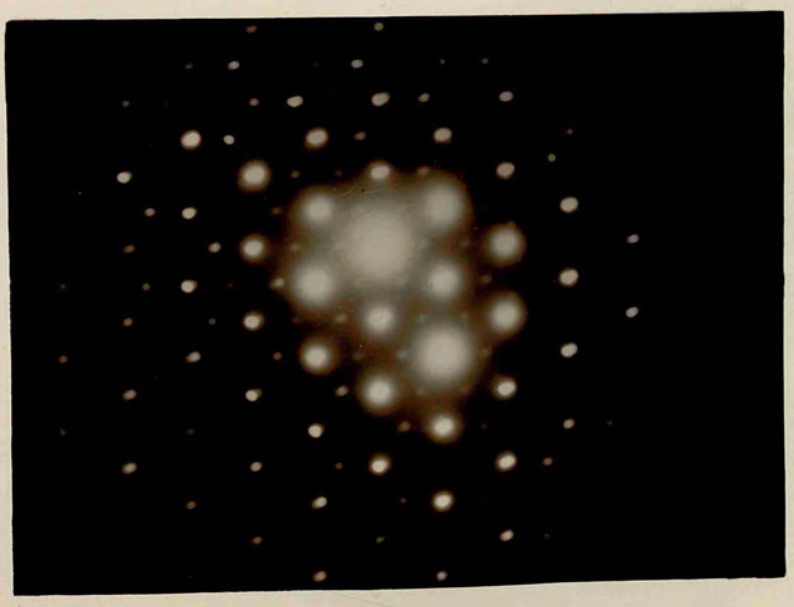

Fig. 6.20

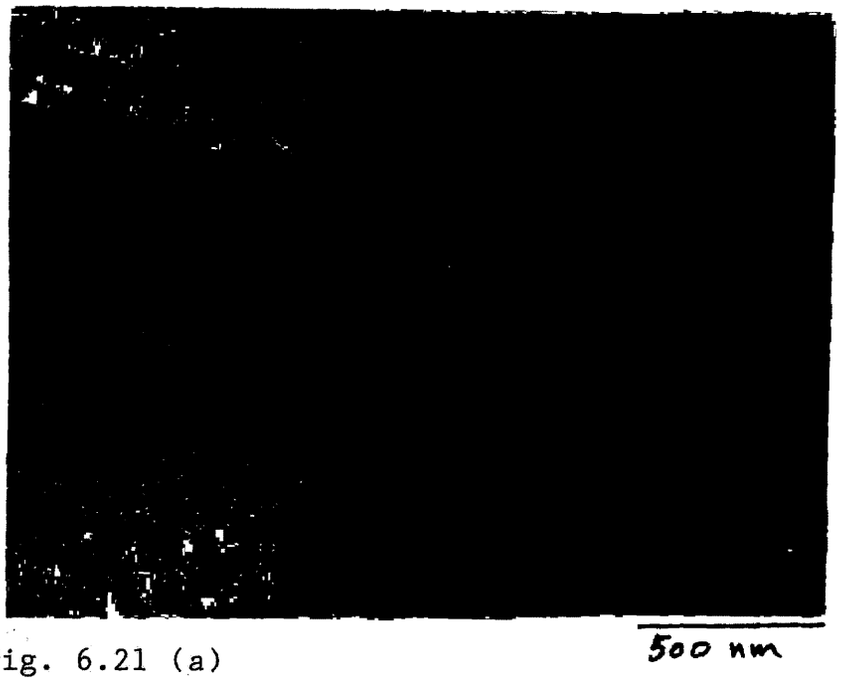

Fig. 6.21 (a)

Fig. 6.20. 'Newtons Ring'-shaped interference fringes dueto bubble-like hollows in biotite.

Fig. 6.21 (a). Enlargement of the micrograph in Fig. 6.20.

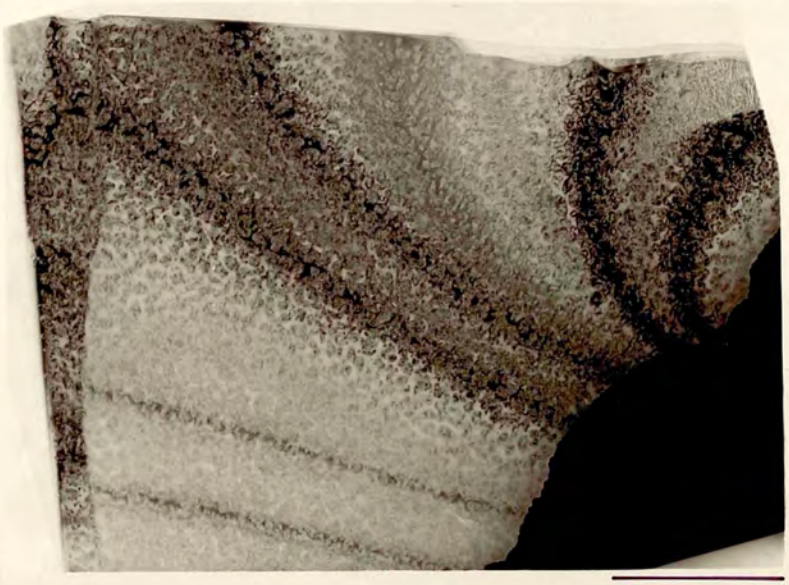

2000 nm

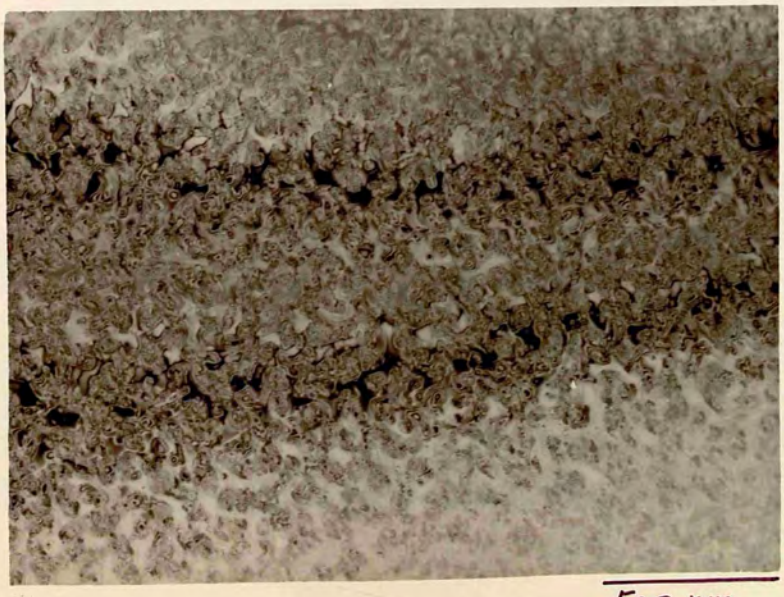

500 nm

Fig. 6.21 (b). The enlarged view of the micrograph in Fig. 6.20.

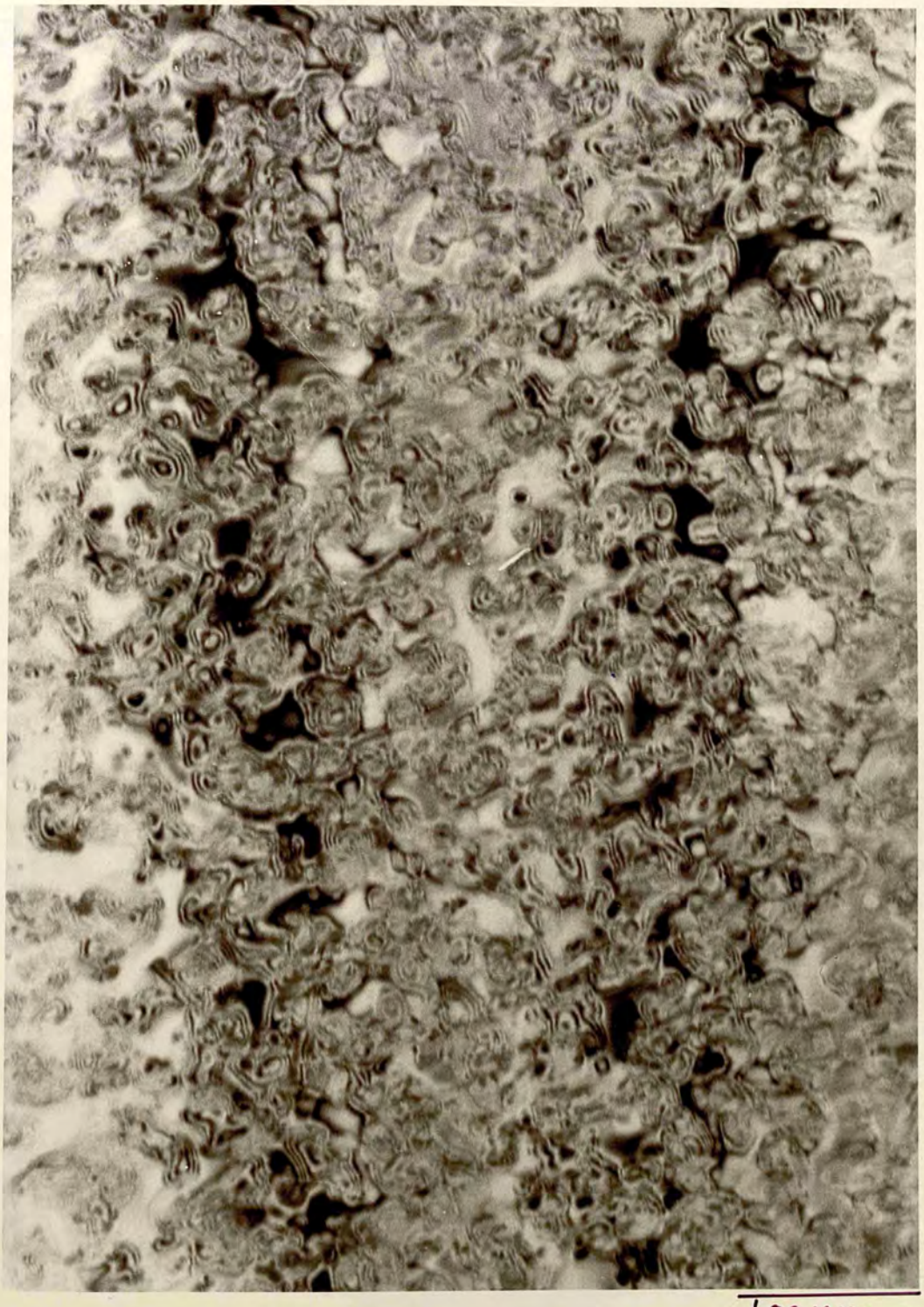
100nm

The natural specimens were investigated structurally by Hendricks and Jefferson (1939), Levinson (1953), Takeda and Donnay (1965) and Ross et al., (1966). The common polymorphs given by these workers are 1M, $2M_2$ and 3T. Levinson (1953) reported three polymorphs 1M, 6M and 3H but Smith and Yoder (1956) said that 6M cell can also be described as $2M_2$ with b_o = 0.53 nm, and the 3H is equivalent to 3T. Lepidolites do not crystallize with the $2M_1$ structure adopted by muscovites and the 3T specimens are comparitively rare. The essential features of lepidolite structure are those already described in the begining of this section but the way in which the tetrahedral and octahedral sites are occupied, shows it to be intermediate between the di-octahedral and tri-octahedral types.

The most common polymorphs 1M and $2M_2$ have following unit cell parameters.

1M:- a_o = 0.53 nm b_o = 0.92 nm

c_o = 1.02 nm β = 100°

Space group: Cm or C2/m

and

$2M_2$:- a_o = 0.92 nm b_o = 0.53 nm

c_o = 2.00 nm β = 98°

Space group: C2/c .

Fig. 6.22 (a) shows a micrograph of a thin sheet of lepidolite which represents a number of dislocation lines.

These dislocations are possibly due to the inclusion of impurities which indicated by dark regions in the micrograph. The white regions are due to the intergrowth of talc layers. Its diffraction pattern is shown in Fig. 6.22 (b) which indicates slightly misoriented grains in the crystal.

6.3 Application of Mica Thin Sheets as a Substrate.

The importance of electron-transparent substrates in the study of nucleation and growth by transmission electron microscopy has been explained in chapter 2. Mica is a well-investigated epitaxial substrate material. The deposition of metals on mica in particular has been studied in the past in consideable detail. Enrique Grunbaum (1975) has given a list of workers who used mica as a substrate.

Apart from the easy cleavage and electronic transparency, the mica substrate exhibits good adhesion for metal particles. To discuss the adhesion properties of mica at cleavage, let us consider the structure of mica and its perfect cleavage at $\{001\}$. With reference to Fig. 6.3, the cleavage occurs along (001) plane where a monolayer of potassium ions separates the sheets. These ions form a hexagonal array and upon cleavage it is believed that they are distributed equally between the newly-created surfaces, so that a cleaved face would contain half a monolayer of potassium ions on the average.

Fig. 6.22 (a)

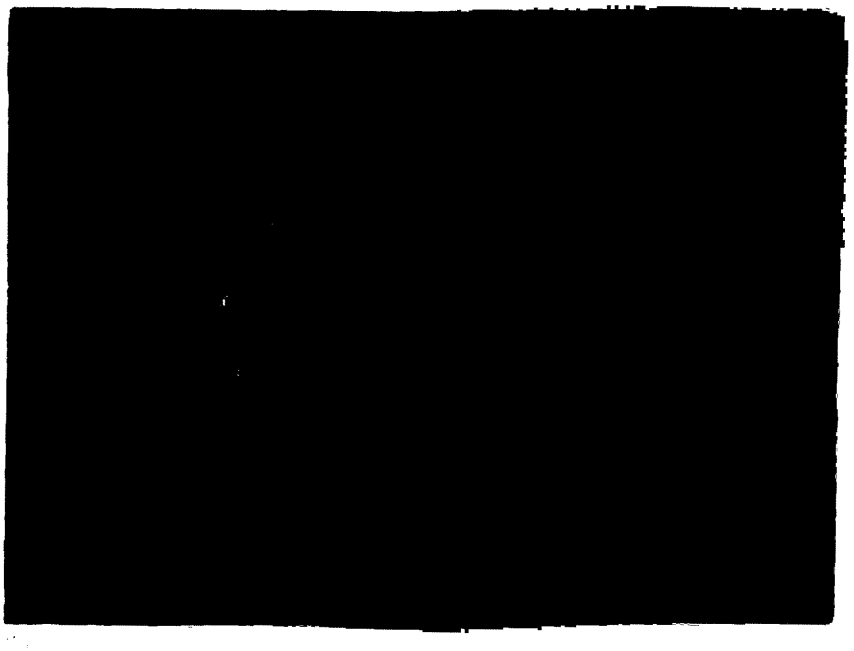

Fig. 6.22 (b)

Fig. 6.22. (a) Micrograph of thin sheet of lepidolite.

(b) Its diffraction pattern.


100nm

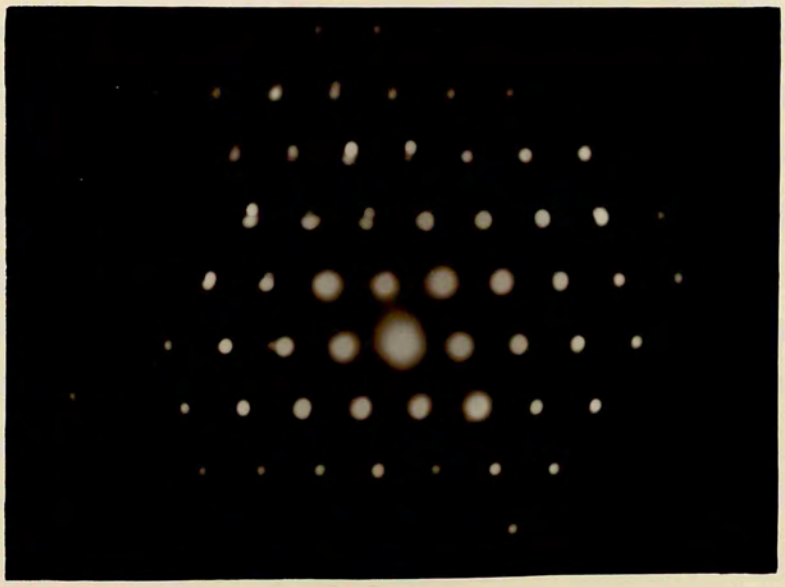

Because no extra spots are observed in the low energy electron diffraction patterns from cleaved mica surfaces, Muller and Change (1968) concluded that potassium must be distributed randomly. Beneath the surface potassium, lies a layer of negatively charged oxygen ions and ordered in an hexagonal fashion. These hexagons are somewhat distorted leading to a slightly puckered (001) surface. In the third layer from the surface potassium, a quarter of the sites are occupied by Al^{3+} ions and the remainder by Si^{4+} ions (the deficiency of positive charge being compensated by the potassium ions on the surface). No ordering of the aluminium ions in the hexagonal lattice positions associated with the third layer has been observed (Radoslovich, 1960).

The cleavage mechanism is particularly interesting for single crystal mica. When sheets are initially separated, positively and negatively charged sites lie opposite one another and there is a resulting electrostatic attraction, although each resulting section may be electrically neutral especialy macroscopically. Assuming that the major part of the surface energy arises from these coulomb interactions, Gaines and Tabor (1956) calculated that the surface energy of mica in vacuum would be 2875 erg cm^{-2}. Bryant (1962) measured a cleavage energy of 10250 erg cm^{-2} for mica in ultrahigh vacuum. However, if the surfaces were separated for the first time in air, the measured cleavage energy was only 300 erg cm^{-2} (Higginbotham, Williams and McEvoy, 1975).

Higginbotham, et al., (1975) in experiments on the adhesion of gold on mica, examined the cleaved mica surfaces using the potential probe, and established that the surface charge varies significantly from region to region. The sign could be positive or negative and they concluded that the regions with dense charge of either sign corresponded to the area of strong adhesion. The origin of the forces binding the metallic film to cleaved mica surfaces may be van der Waals interactions, chemical interactions and electrostatic forces. The chemical interactions include covalent, ionic and metallic bonding. The arrangements of atoms on a mica cleaved surface is shown in Fig. 6.24.

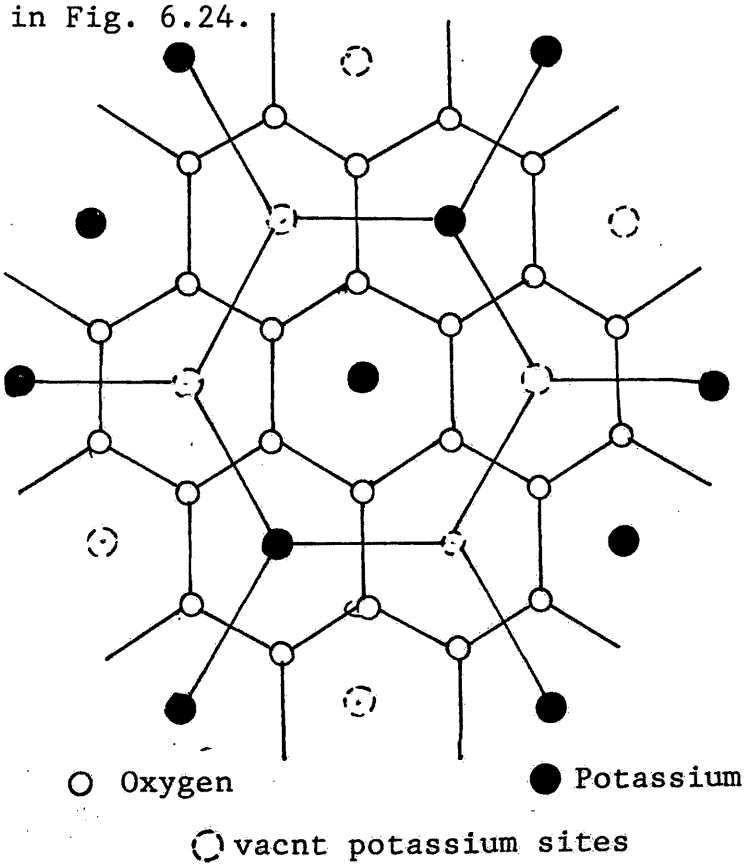

Fig. 6.24. The surface structure of cleaved (001) mica. The potassium ions are arranged randomly.

It is assumed that metal films (usually gold films because it was used by majority of the investigators) make intimate contact with thin surface and that the sites for the strongest adhesion of the metal ad-atoms are those situated between the potassium ions, i.e., oxygen sites and vacant potassium sites. Initial metallic nucleation has been discussed in this way by Allpress and Sanders (1967). Harrach (1974) has investigated theoretically the adsorption energies of gold ad-atoms on the various surface sites shown in Fig. 6.24. Taking into consideration van der Waals interaction and induction components he showed that the strongest adsorption occurs on vacant potassium sites.

Vacuum decoration provides a means of examining the relief and structure of crystal surfaces at the molecular level (Bassett, 1958). In the present work, very thin (less than 5 nm) gold film were evaporated on the cleavage faces of muscovite and biotite. Fig. 6.25 (a) shows a micrograph of evaporated gold on muscovite representing the oriented growth as indicated by its diffraction pattern in Fig. 6.25 (b). The size of gold nuclie in the micrograph is between 4 nm and 7 nm. Fig. 6.26 (a) shows the micrograph of gold decoration on biotite in vacuum. A few step decorations are observed otherwise the gold particles are distributed evenly on the mica surface. Its diffraction pattern is shown in Fig. 6.26 (b). The results of these experiments indicate that the mica surfaces are smooth and ideal for nucleation and growth studies.

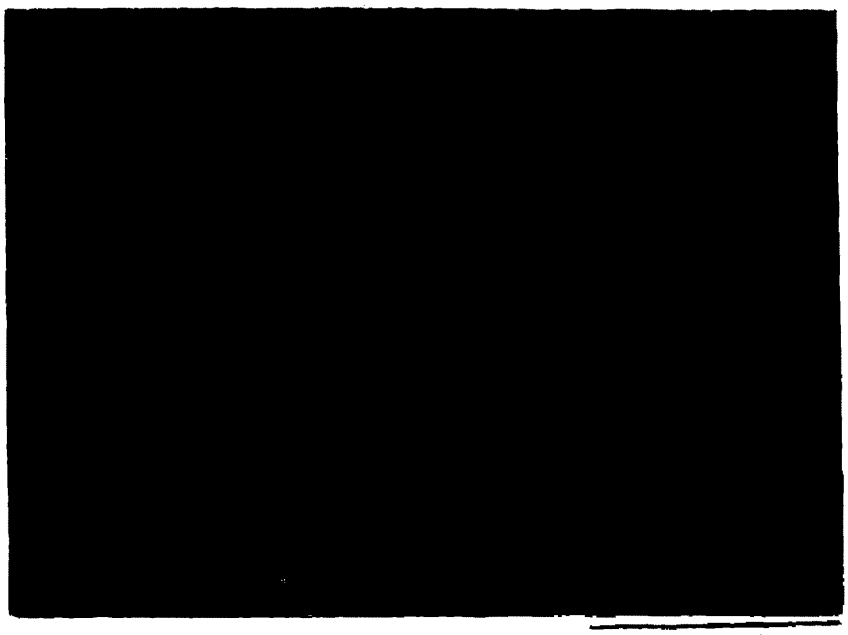

Fig. 6.25 (a)

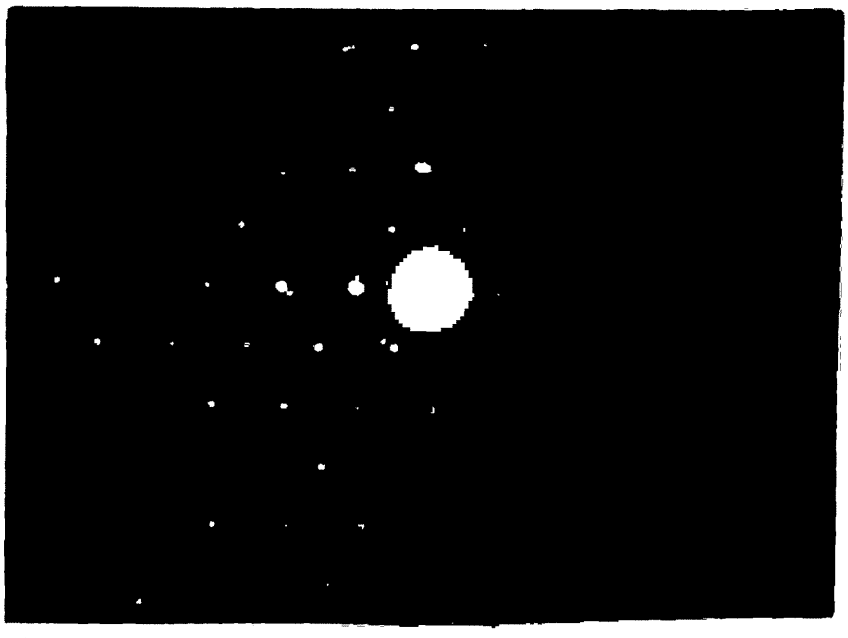

Fig. 6.25 (b)

Fig. 6.25. (a) Gold decoration on muscovite.

(b) The diffraction pattern of gold decoration on muscovite.


100 nm

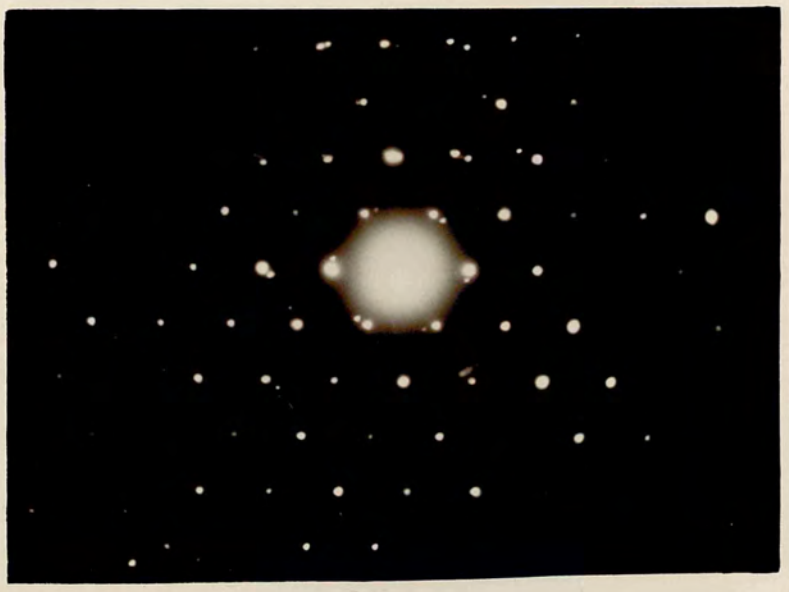

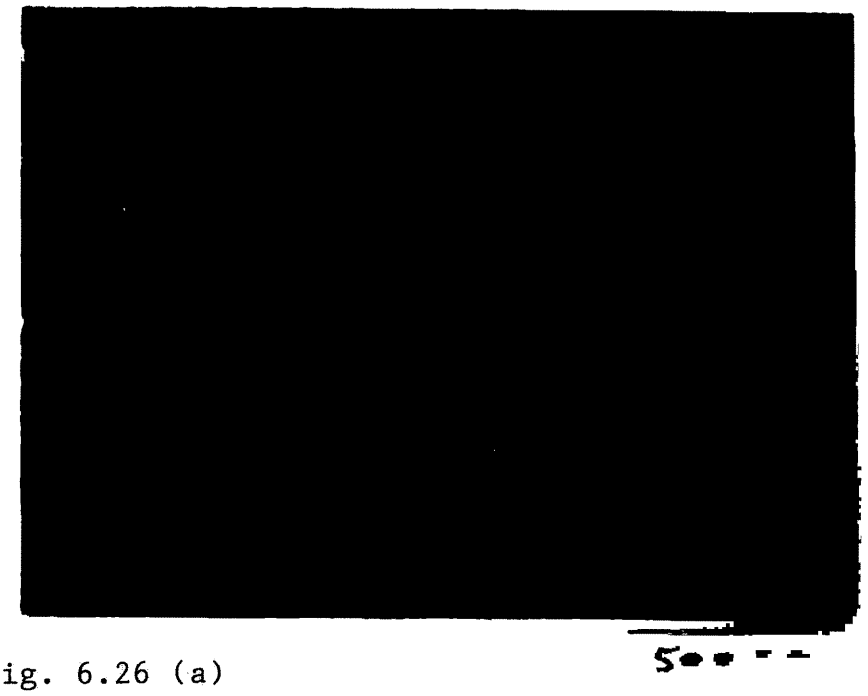

Fig. 6.26 (a)

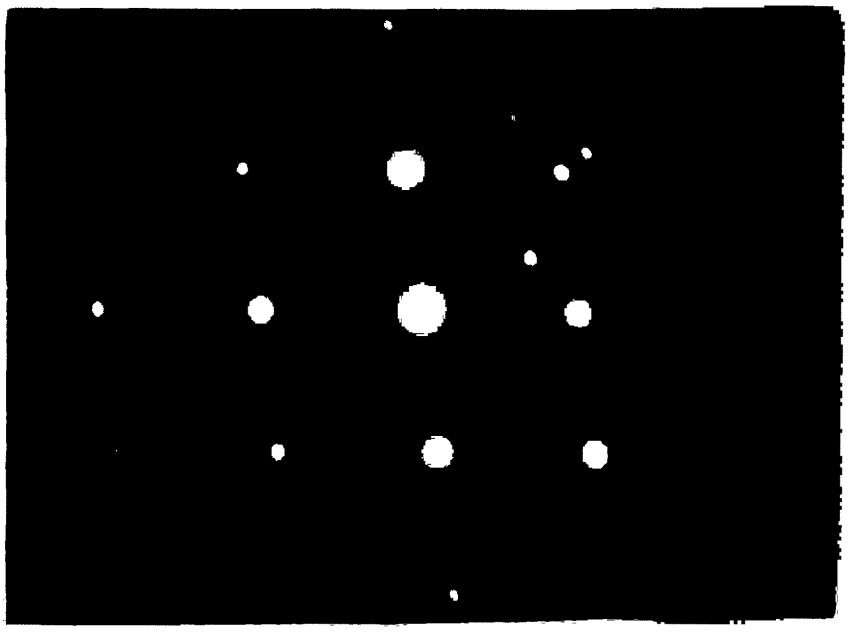

Fig. 6.26 (b)

Fig. 6.26. (a) Gold decoration on biotite.

(b) Its diffraction pattern.


500 nm

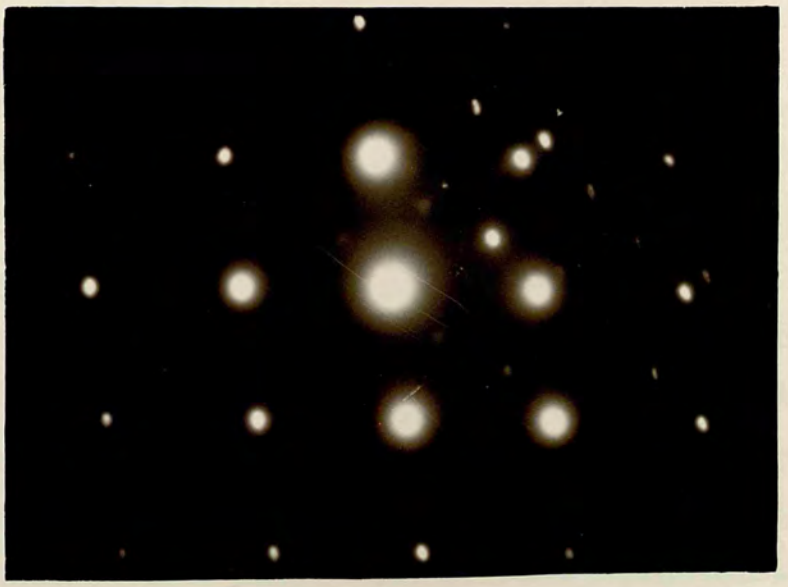

6.4 Experimental Preparation and Procedure.

Most of the alkali halides are hygroscopic, therefore, it is vital to avoid the effects of atmospheric water vapour when making transmission electron microscopical studies of the early stages of nucleation and growth of these materials. In the past a few investigators used the in situ technique for this purpose (Koch and Vook, 1972; and the reviews by Pashley, 1965a; Poppa, 1975; Butler,1979), but it has its own problems. In the present work the transport chamber, discussed in chapter 3, has been used and by the use of electron transparent substrate (thin sheet of mica), transmission electron microscopy of the alkali halides has been made possible.

The thin sheet of mica (muscovite and / or biotite), between a folded electron microscope grid, was prepared by the method described in section 6.2, and was carefully put inside the specimen holder which used with the transport chamber. The holder was then attached to the manipulating system in the transport chamber, inserted into the intermediate chamber (see chapter 3) and fixed on a stainless steel jar which is placed on the vacuum unit. The whole assembly is shown by a schemetic diagram in Fig. 4.1 in chapter 4. A simple boat of folded tungsten was used to evaporate the alkali halides under the following experimental conditions:

1. Residual gas pressure, during the deposition, less than 10^{-9} bar.
2. Temperature of the substrate is 20 °C (room temperature) or otherwise stated.
3. Deposition rate is nearly 1 nm sec^{-1}.

After deposition the sample was transferred into the electron microscope without exposure to the atmosphere. The detail of the transfer procedure has been given in chapter 3. The deposits of this kind are referred to as the growth from the vapour phase and called "unexposed deposits".

In the second series of experiments, the alkali halides deposits were exposed to the atmosphere or moist air before being observed in the electron microscope. A hygroscopic alkali halide deposit absorbs water from the atmosphere and forms drops of solution on the substrate surface. In side the electron microscope the water evaporates and recrystallization occurs. Therefore, the crystals form in this kind of experiment are referred to as crystals grown from solution. This method of preparing alkali halide crystals from solution was used by Schulz (1951) for the first time. The observations in the electron microscope were made by transmission electron microscopy and selected area electron diffraction at 100 X 10^3 volts, accelerating voltage. The materials used in the present work are CsI, CsCl, CsBr and CsF.

6.5 Observations and Discussion.

Examination in the electron microscope of the deposit of alkali halides used, on the substrate of mica with average thickness between 10 nm and 20 nm revealed that they grow with a veriety of orientations depending on the overgrowth-substrate combination and experimental conditions. In most cases, at room temperature unexposed deposits consist of small crystallites situated randomly in nearly continuous films. Their diffraction patterns show them to be mostly polycrystalline. At higher substrate temperature large clusters without any recognisable crystallographic shape, but with some internal ordering as indicated by their diffraction patterns, are formed.

In exposed deposits or growth from solution, large clusters with diferent sizes, depending on the thickness of unexposed deposits and the length of exposure, have been observed. They also have some definite orientation with the substrate surface. Island structure and some very large crystals are also observed in a few cases. Due to these variation in growth, it is necessary to discuss each deposit-substrate combination separately.

6.5.1 CsI on Biotite.

Fig. 6.28 shows a micrograph of evaporated CsI on biotite at room temperature and observed in the electron

microscope before exposure to the atmosphere. The deposit thickness is nearly 10 nm and consists of large number of crystallites with lateral dimensions between 5 nm and 40 nm. The small crystallites without any particular crystallographic shapes are likely to be stabilized nuclei and larger ones are due to the coalescence of these stable nuclei and multilayer condensation. The distribution of nuclei is not uniform on the substrate surface because the cleavage surface of mica contains some step structures as revealed by gold decoration. Initial nuclei migrate over the surface until they stop by a step on the surface. The uncovered areas caused by the migration are covered by further nucleation.

Another micrograph from a 20 nm thick unexposed deposit of CsI on biotite at room temperature is shown in Fig. 6.29 which shows the large clusters of overgrowth with dimensions from 40 nm to 80 nm. They are mainly due to the multilayer condensation and coalescence of the small nuclei. The micrograph in Fig. 6.30 (a) is also from an unexposed deposit of CsI on biotite and consists of large clusters which are randomly situated as indicated by its diffraction pattern. The rings in diffraction pattern show that the overgrowth is polycrystalline and there is no particular orientation between the substrate and overgrowth. The discontinuity in some rings indicate the presence of fewer and larger clusters or in other words some crystallites have a weak orientation. This orientation is [111] normal to the substrate surface and

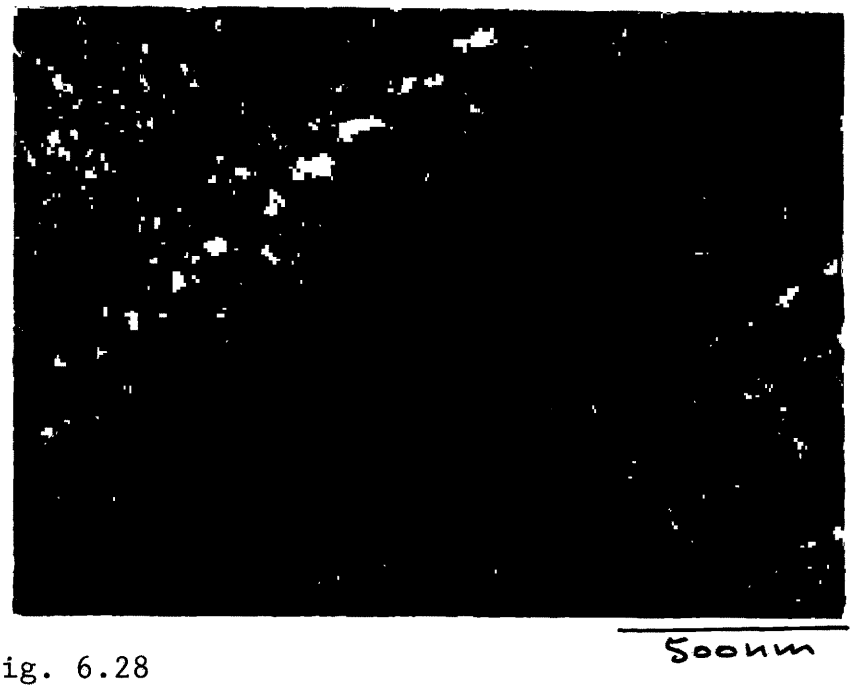

Fig. 6.28

Fig. 6.29

Fig. 6.28. and 6.29. Unexposed deposits of CsI grown on biotite at room temperature (thicknesses= 10 nm and 20 nm respectively).

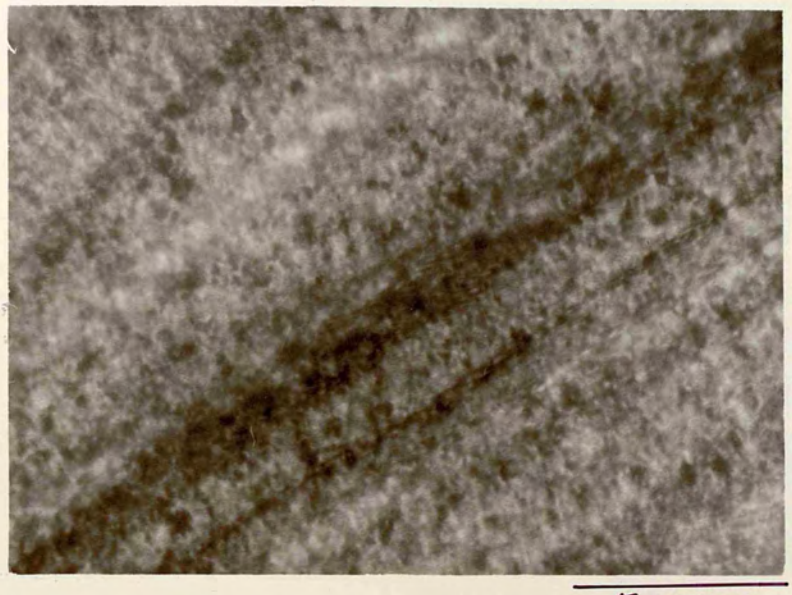

500nm

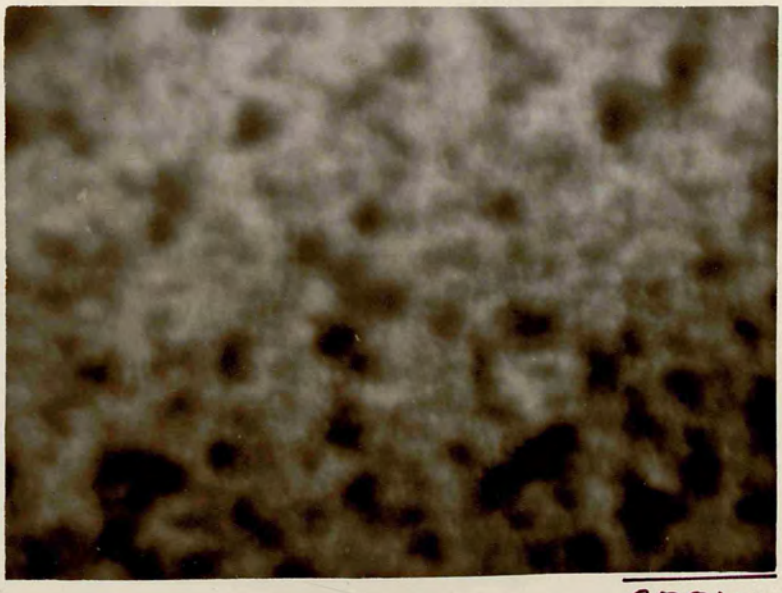

200nm

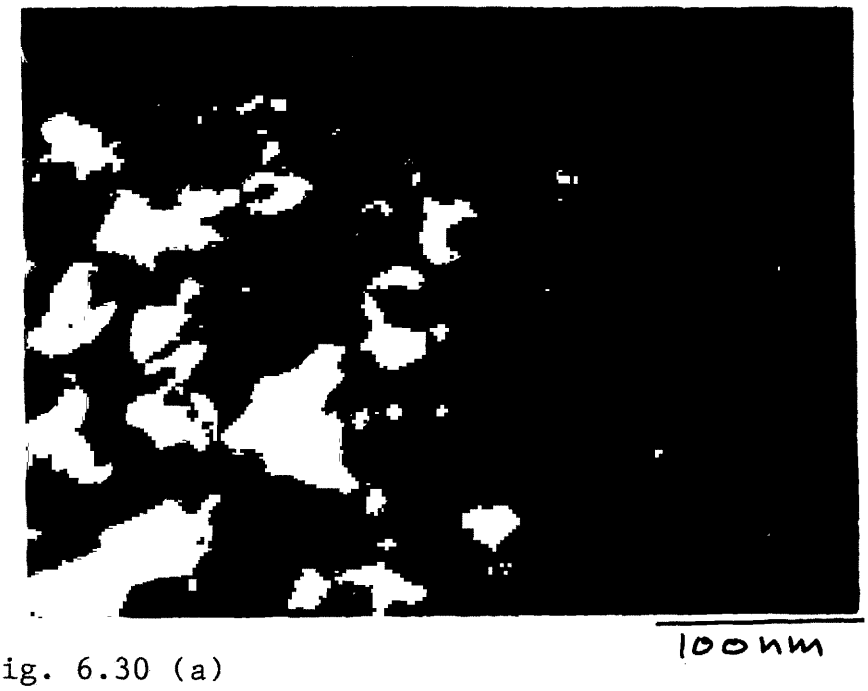

Fig. 6.30 (a)

Fig. 6.30 (b)

Fig. 6.30. (a). Micrograph of 20 nm thick unexposed deposit of CsI grown on biotite at room temperature. (b) Its diffraction pattern.

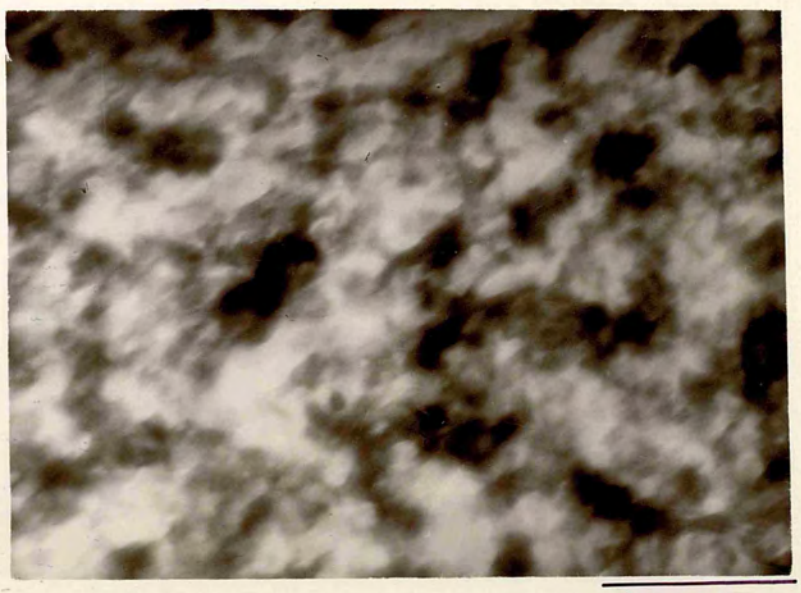

100nm

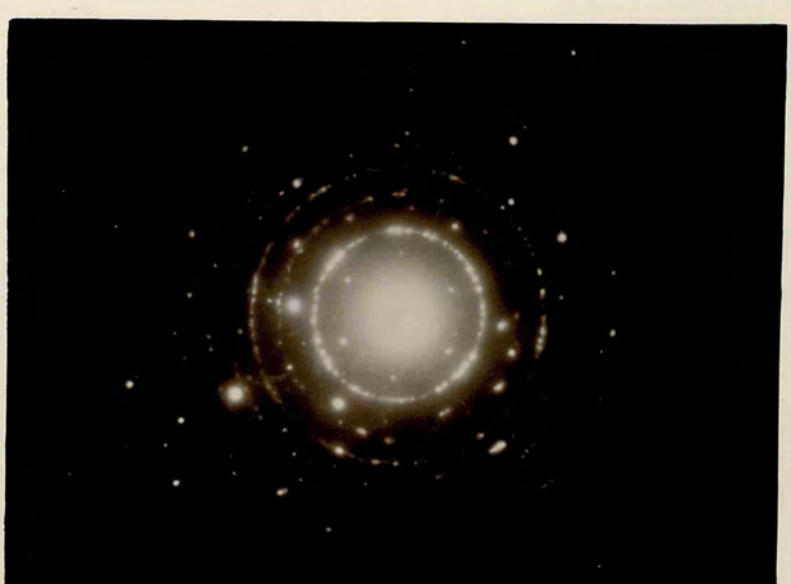

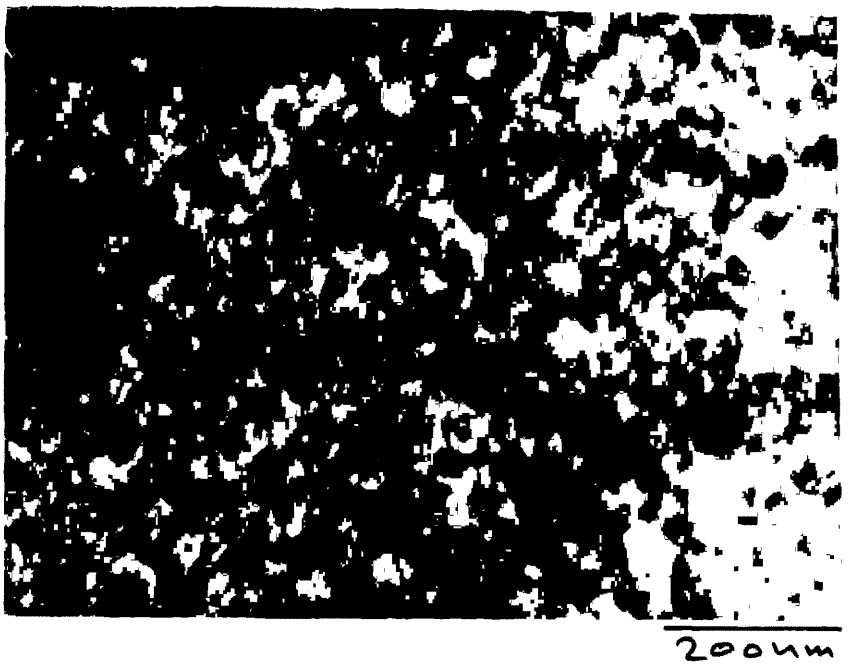

Fig. 6.31 (a)

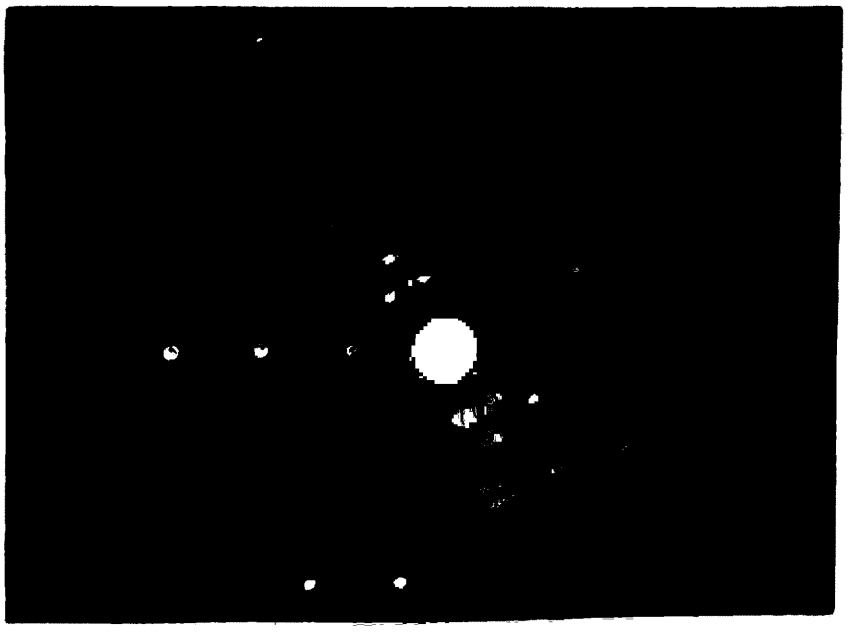

Fig. 6.31 (b)

Fig. 6.31. (a). Unexposed deposit of CsI grown on biotite at room temperature. (b) Its diffraction pattern.

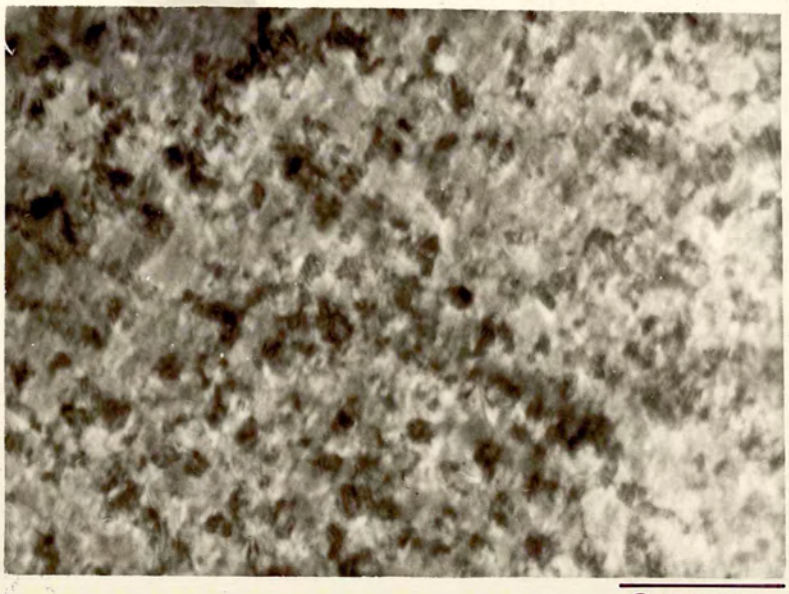

200nm

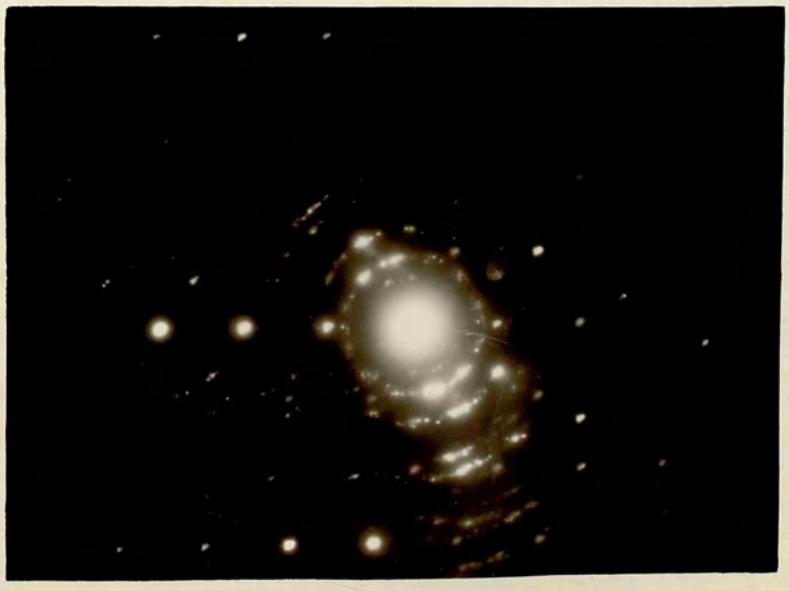

{110} and {211} planes of the crystallites in overgrowth produce strong reflections.

Similar observations were obtained from another sample of CsI, about 15 nm thick, grown on biotite when examined before exposure to the atmosphere (Fig. 6.31, a). This shows small crystallites with dimension between 7.5 nm and 25 nm, situated randomly on the substrate surface. As biotite gives strong reflections from certain planes such as (200), (400) and (600), the reflected beams from the substrate due to these planes act as primary beams with respect to the overgrowth which is on the bottom side of the substrate and produced secondary diffractions as shown in Fig. 6.31 (b).

When the substrate was heated up to 200 °C and then CsI evaporated on it, in the unexposed deposit, the overgrowth formed clusters without any particular crystallographic shapes. These clusters have sizes ranging from 25 nm to 100 nm as shown in the micrograph of Fig. 6.32 (a). Some of these clusters are linked to each other and form an island-like pattern on the substrate surface. The phenomenon of the growth of these clusters can be explained by the liquid-like coalescence of the initial nuclei as described by Pashley et al., (1964) for the growth of gold and silver deposits by evaporation inside the electron microscope. In the case of CsI deposited on biotite at 200 °C, the initial stable nuclie are nucleated themselves on preferred sites on the substrate surface. These preferred sites are provided by the K ions

(or lack of K ions) on the cleavage surface of mica as described in the cleavage procedure.

The orientation of the overgrowth can be determined from the diffraction pattern shown in Fig. 6.32 (b). This has two intense spots, marked A and B, corresponding to $\{110\}$ planes of overgrowth, on either side of the spot correspond to (130) of the substrate. This indicates two equivalent orientations usually known as double-positioning. The common factors of these two orientations is that the (111) planes of the overgrowth are parallel to the (001) plane of the substrate. Further explanation of these orientations and the atomic fitting between the contact planes of the CsI and biotite will be discussed later in this section.

After nucleation, the nuclei grow laterally until coalescence with the neighbouring nuclei commences. The coalescence occurs rapidly in a liquid-like manner and newly- formed nuclei cover less substrate area than the previous two (Pashley et al., 1964). In other words the liquid-like character of the coalescence leads to an increase in the uncovered area of the substrate. Secondary nucleation occurs either directly on the previous coalesced nuclei or between the two and coalesces with any one to form large clusters which may touch each other and form islands. These islands are not well-oriented. The diffraction pattern shows a large number of extra spots which do not indicate any recognizable orientation.

Fig. 6.32 (a)

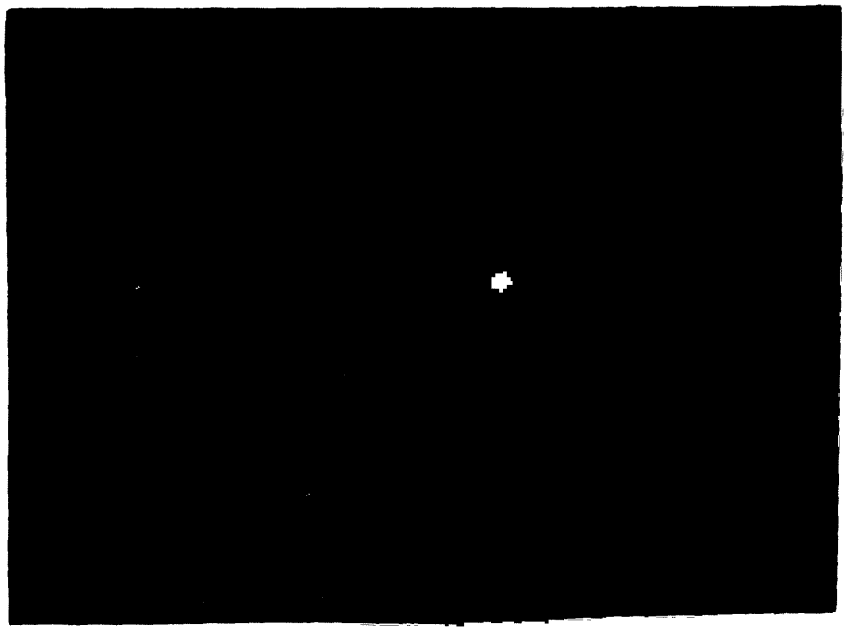

Fig. 6.32 (b)

Fig. 6.32. (a). Unexposed deposit of CsI grown on biotite at 200 °C. (b) Its diffraction pattern.

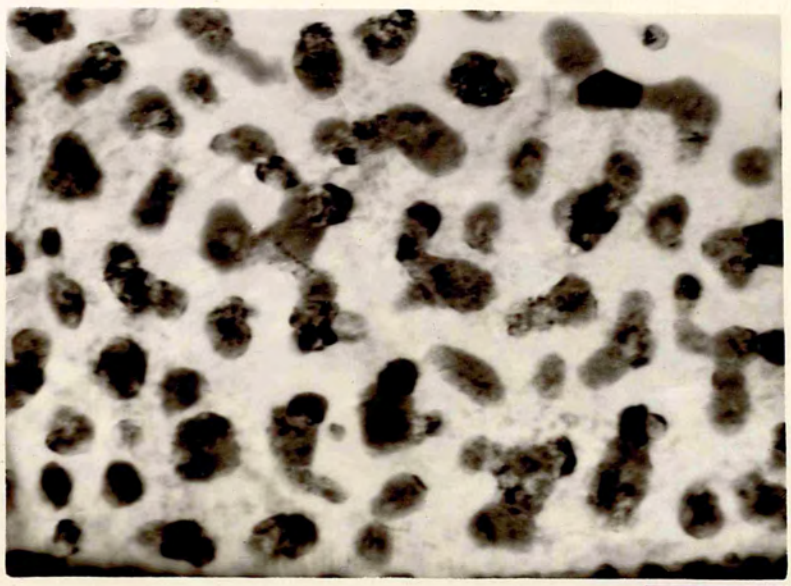

200nm

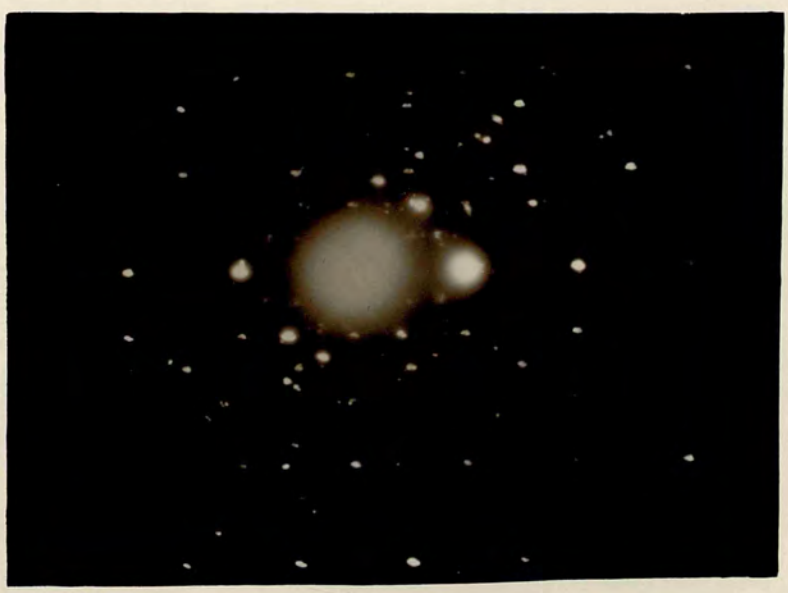

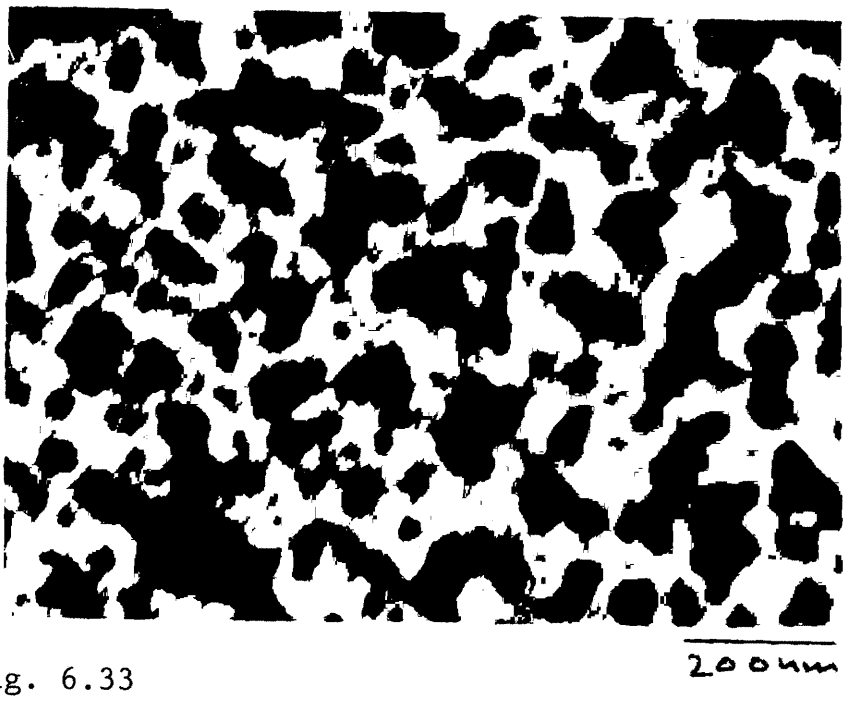

Fig. 6.33

Fig. 6.34

Fig. 6.33 and 6.34. Exposed deposits of CsI grown on biotite at room temerature. Deposit thickness = 10 nm and exposure times 10 minutes and 30 minutes respectively.

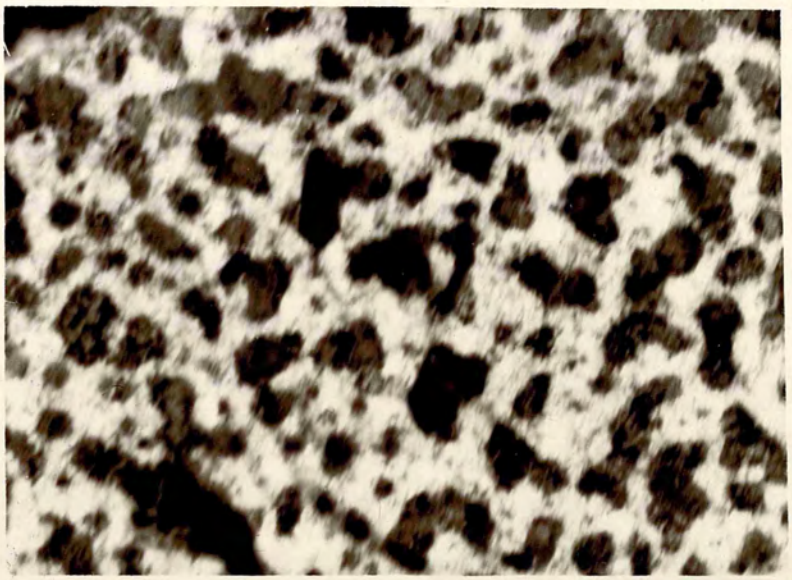

200nm

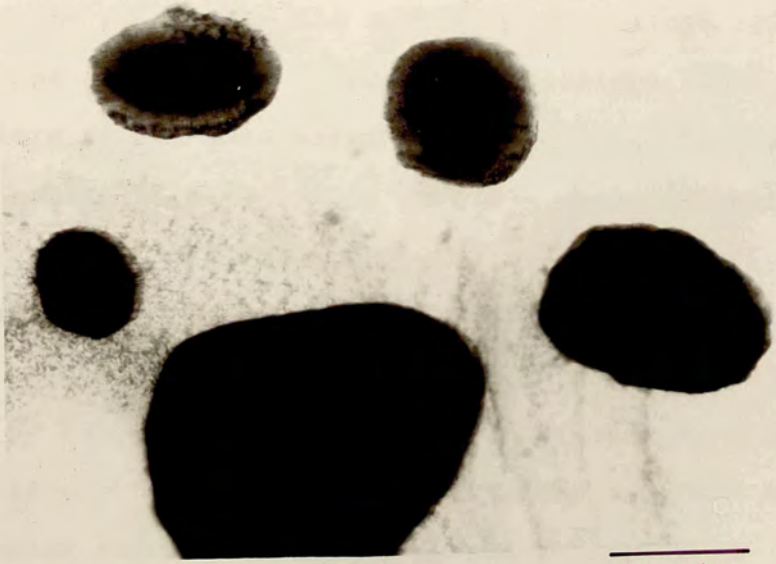

500nm

When a thin layer of CsI was deposited on biotite substrate and then exposed to the moist air, sufficient moisture condensed on the deposit to dissolve it. When the sample was transferred to the electron microscopethe water evaporated and the salt recrystallized. Fig. 6.33 shows the micrograph of a 10 nm thick deposit of CsI on biotite evaporated at room temperature and exposed to the atmosphere for 10 minutes. Three dimensional plate-like crystals without any recognizeable shape were formed allover the substrate surface. A possible objection to this method might be that all the original deposit formed from the vapour did not dissolve and therefore the growth from solution began around incompletely dissolved crystals acting as nuclei. When a deposit of the same thickness was exposed for 30 minutes and then observed in the electron microscope the resulting micrograph (Fig. 6.34) shows a few large round-shaped clusters. This length of exposure caused more water to be condensed on the deposit making it more likely that the whole deposit would be dissolved to form large drops of solution which, upon recrystallization form large clusters.

Fig. 6.35 (a) shows a micrograph of a 5 nm thick deposit of CsI grown at room temperature and exposed to the atmosphere for 5 minutes. Small round clusters are formed which are well-oriented on the substrate as indicated by the diffraction pattern in Fig. 6.35 (b). To determine the orientation from the diffraction pattern it is necessary to consider the diffraction pattern from

biotite alone (Fig. 6.14) and its indexed solution (Fig. 6.36).

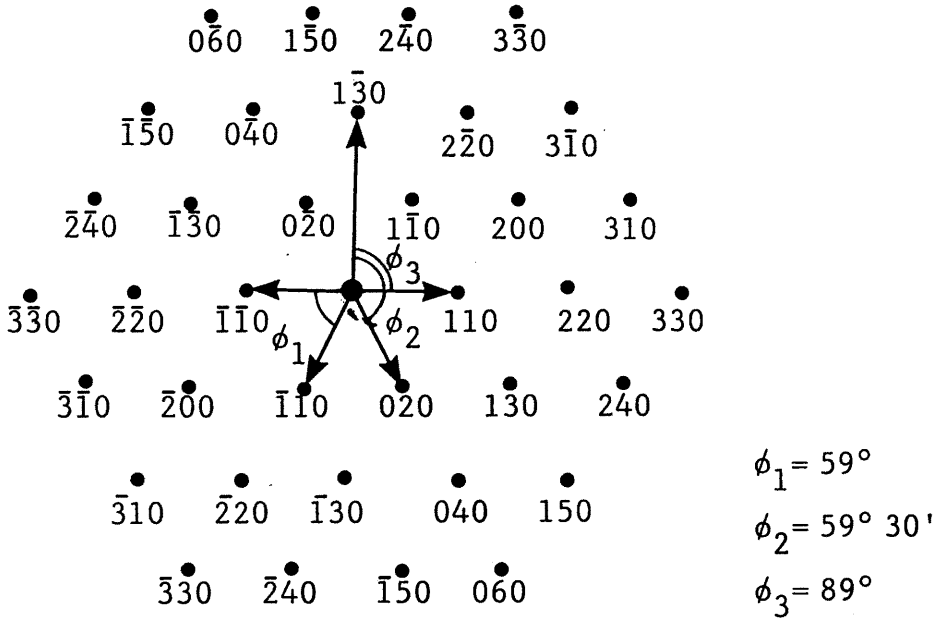

Fig. 6.36. Indexing of the diffraction pattern of biotite normal to [001].

Every spot of the diffraction pattern when connected to the centre of the diffraction pattern is a vector in the reciprocal space with the following properties:

a. It is perpendicular to a set of parallel and equidistant planes of the crystals in real space.
b. The length of the vector is inversely proportional to the distance between the planes responsible for the reflection.

The mica sheet is a hexagonal net of linked tetrahedral groups. Fig. 6.37 reproduces a projection on a plane parallel to $\underline{a}$ and $\underline{b}$.

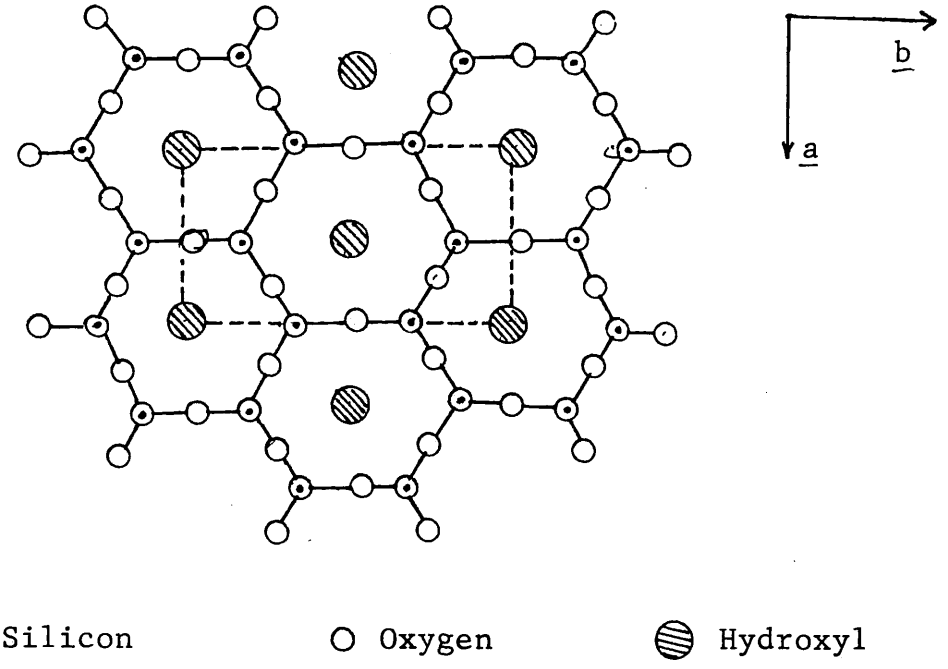

Fig. 6.37. The projection of a generated sheet of mica parallel to a and b plane. The unit cell is shown by broken lines.

The projections of the potassium ions on a plane parallel to a and b coincide with the projections of the hydroxyls. Since here we are concerned with the cleavage faces, the hexagonal net of Fig. 6.37 is repeated in Fig. 6.38, while hydroxyls are replaced by potassium atoms and oxygen atoms are omitted for convenience. In Fig. 6.38 two hexagonal nets can be distinguished: one large hexagon connects the potassium-atom sites in the cleavage plane. The other small hexagon network connects points located at the centres of the triangles of the large network and representing the projection of the silicon atom positions.

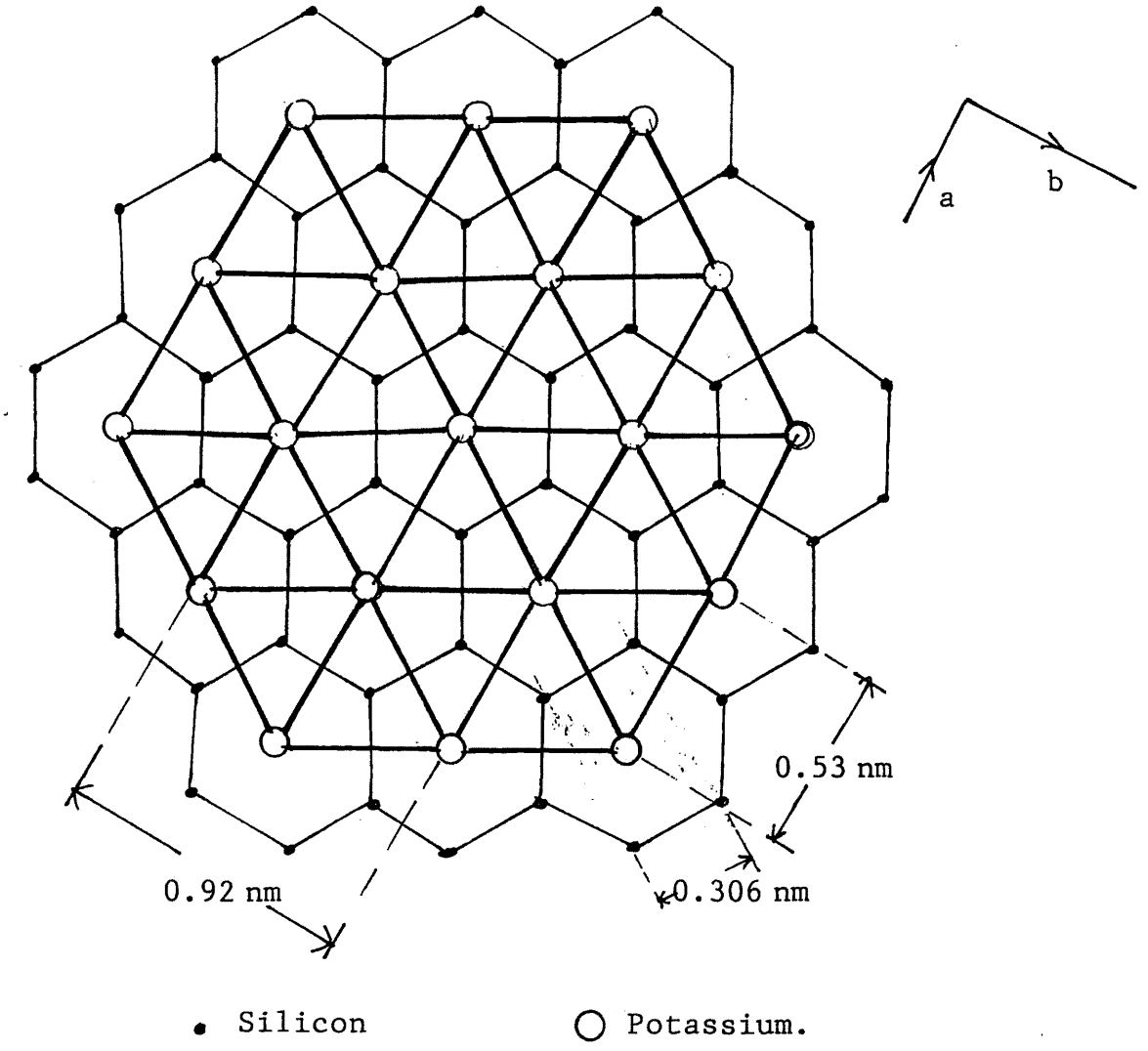

Fig. 6.38. The projection of potassium and silicon atoms of biotite on the cleavage plane.

This projection is from the cleavage surface of biotite i.e., sheet of linked tetrahedra upon which the structure of biotite is based. Although it has perfect hexagonal symmetry, this symmetry is lost when two are opposed to form a double sheet linked by Mg or Fe. The potassium atoms lie at the centre of each hexagon but since they are not opposite one another, owing to the close packing true hexad axes cannot be common to a pair of sheets. The staggering lowers the symmetry to monoclinic.

Fig. 6.35 (a)

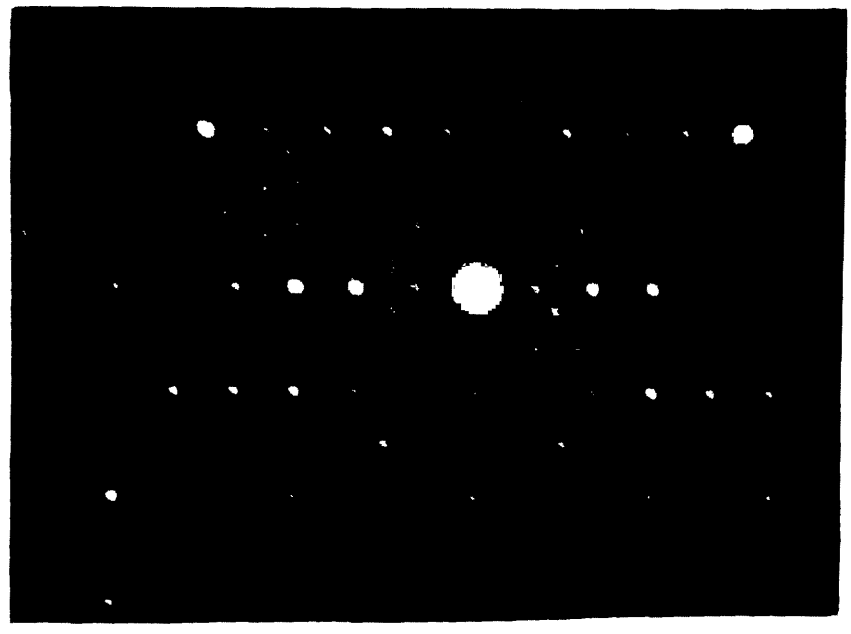

Fig. 6.35 (b)

Fig. 6.35 (a). Exposed deposit of CsI grown on biotite at room temerature. Deposit thickness = 5 nm and exposure time 5 minutes .

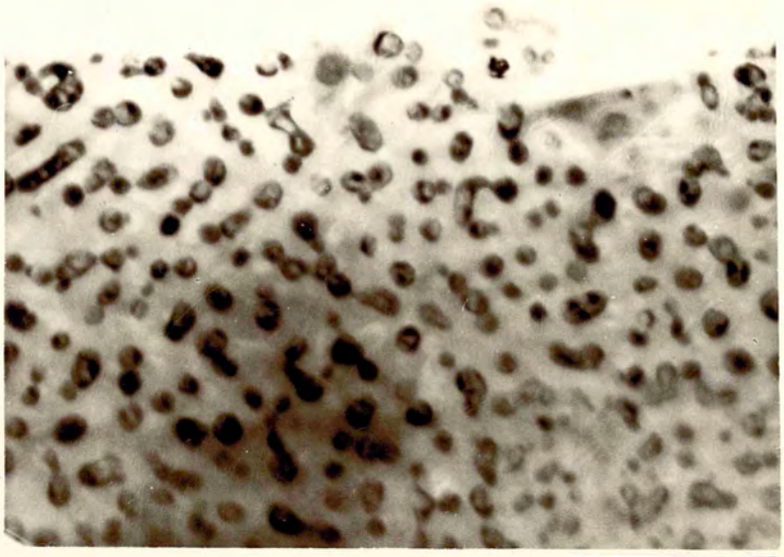
200нм

So in the diffraction pattern the nearest six spots are not at the same distance from the origin, two belong to the parallel planes with separation 0.46 nm in real space and four to those separated by 0.454 nm. The indices for these sets of planes are $\{020\}$ and $\{110\}$ respectively. These planes pass through the potassium atoms and perpendicular to the sides of silicon network i.e., the bases of the triangles in Fig. 6.38. Similarly the second nearest six spots with a separation of 0.264 nm for $\{130\}$ set of planes and 0.261 nm for $\{200\}$ set of planes. These planes pass through the silicon atoms and perpendicuar to the bases of the triangles formed by the sides of potassium network.

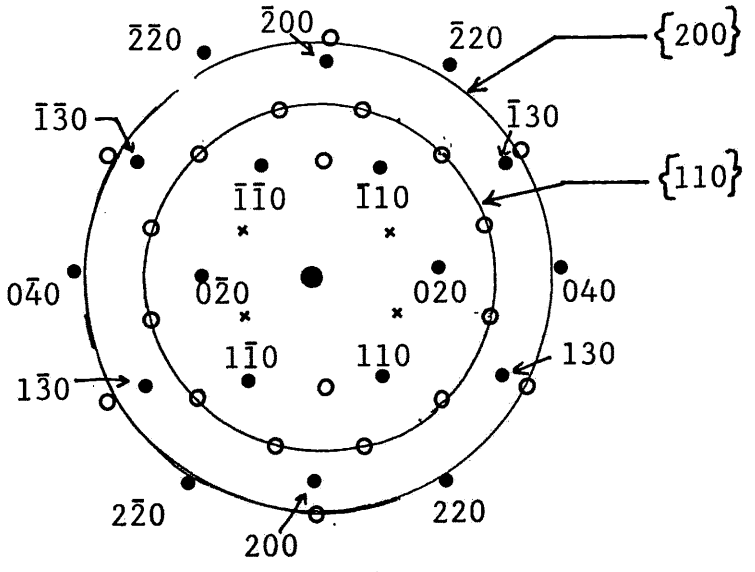

• Biotite o CsI * Prabably CsF

Fig. 6.39. Schematic representation of the diffraction pattern from exposed CsI on biotite (in Fig. 6.35 b).

In the light what has been said so for, it is possible to discuss the orientation of CsI on biotite. Fig. 6.39 shows the schematic representation of the diffraction pattern in Fig. 6.35 (b). In this diffraction pattern there are 12 spots on the $\{110\}$ ring reflected from the overgrowth and indicate double positioning of CsI with [111] normal to the substrate surface. This means (111) planes of the both positions are parallel to the (001) mica surface at the interface. The two positions are rotated with respect to each other by 30°. The distance between the nearest neighbours in (111) plane for CsCl-like structure is $a_o\sqrt{2}$. Thus for CsI with a_o = 0.4562 nm, this distance is 0.645 nm as shown in Fig. 6.40.

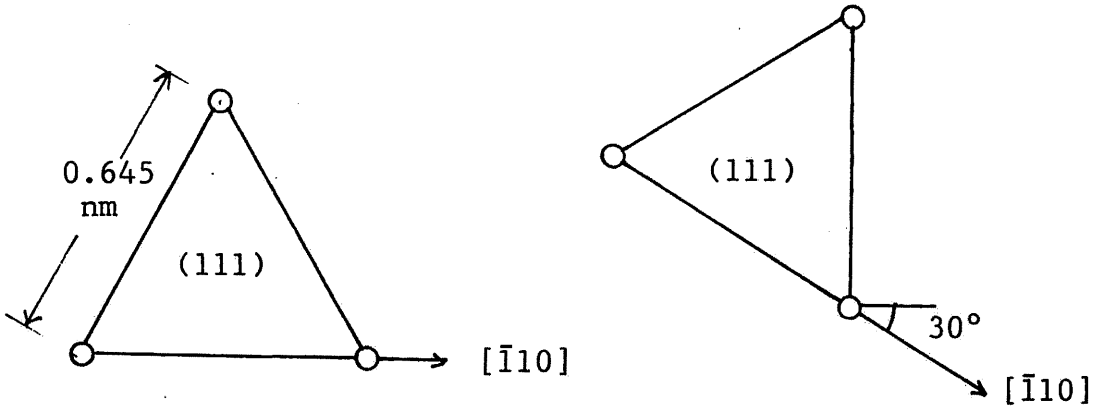

Position I Position II

Fig. 6.40. Plan view of two [111] orientations of CsI on biotite.

The network containing this length does not exist in the cleavage surface of biotite, so there is no exact-fit for all the overgrowth atoms on the atoms of the substrate.

In the diffraction pattern of Fig. 6.35 (b) there are two spots with separation 0.456 nm and six spots with separation 0.229 nm, which correspond to $\{100\}$ and $\{200\}$ sets of planes in CsI respectively. This indicates two orientations: one is (001) of CsI parallel to (001) of biotite with [100] of the overgrowth parallel to [100] direction in biotite and the second one (001) of the overgrowth parallel to (001) of the substrate with the [100] direction of the overgrowth parallel to [130] direction in substrate. The spacing of nearest neighbours in the (001) plane of CsI is 0.4562 nm, which is nearly half the spacing of the large network in the biotite surface network, so there should be some exact-fit between the atoms of the two materials. These orientation might occur during the recrystallization process.

There was also observed four very faint spots with separation 0.605 nm which do not correspond to any set of planes in CsI or biotite and are not observed in any individual diffraction pattern of either material. They probably belong to CsF, the unit cell of which has edge length 0.6008 nm. As biotite containes some fluorine, there could be a reaction with the overgrowth to form CsF, because at this scale of a few nanometers of deposit the chances of chemical reaction cannot be ignored.

Fig. 6.41 (a)

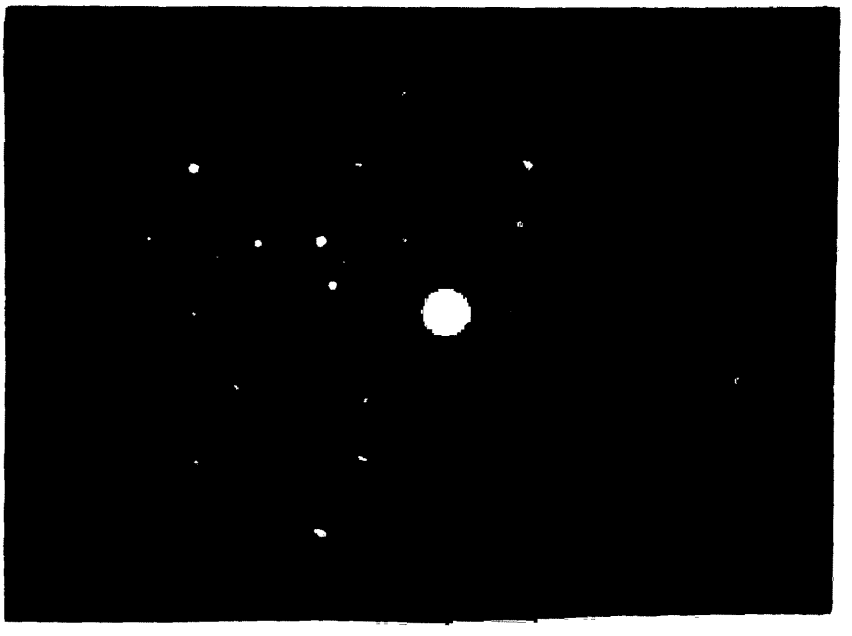

Fig. 6.41 (b)

Fig. 6.41 (a). Exposed deposit of CsI grown on biotite at 200 °C. Deposit thickness = 10 nm and exposure time 10 minutes. (b). Its diffraction pattern.

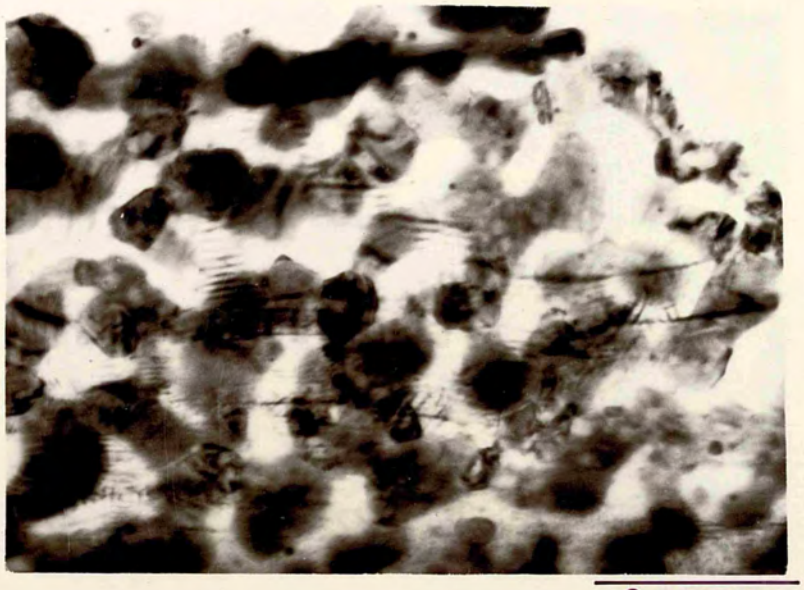
200nm

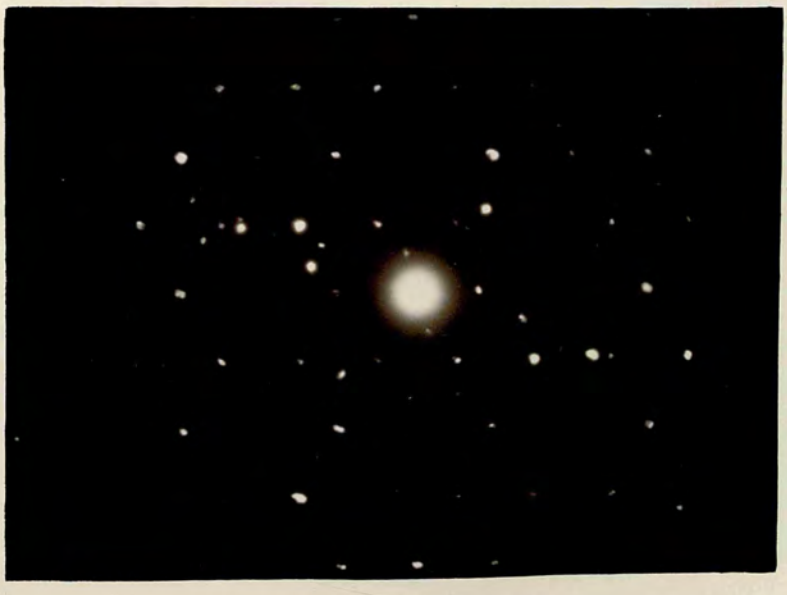

Fig. 6.43 (a)

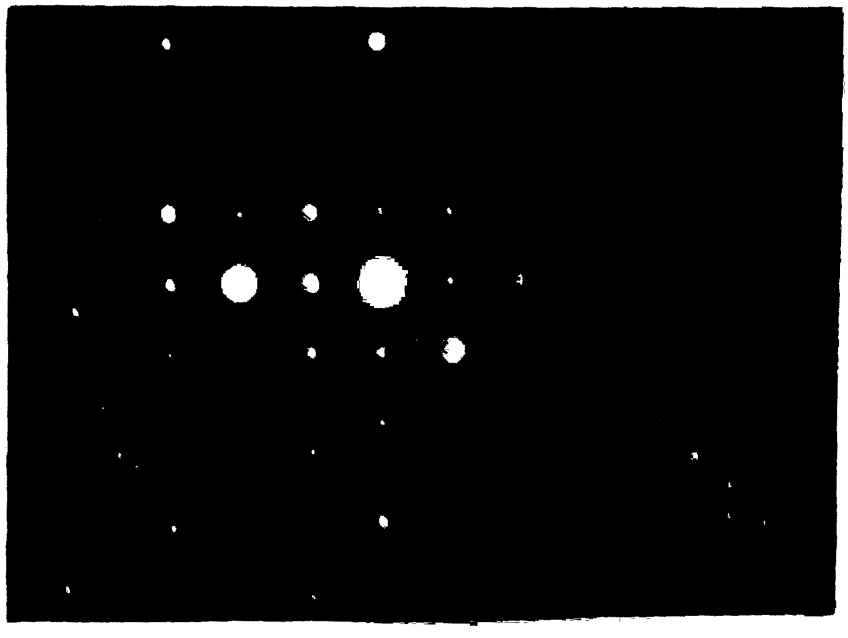

Fig. 6.43 (b)

Fig. 6.43 (a). Exposed deposit of CsI grown on biotite at 200 °C. Deposit thickness = 20 nm and exposure time 30 minutes. (b). Its diffraction pattern.

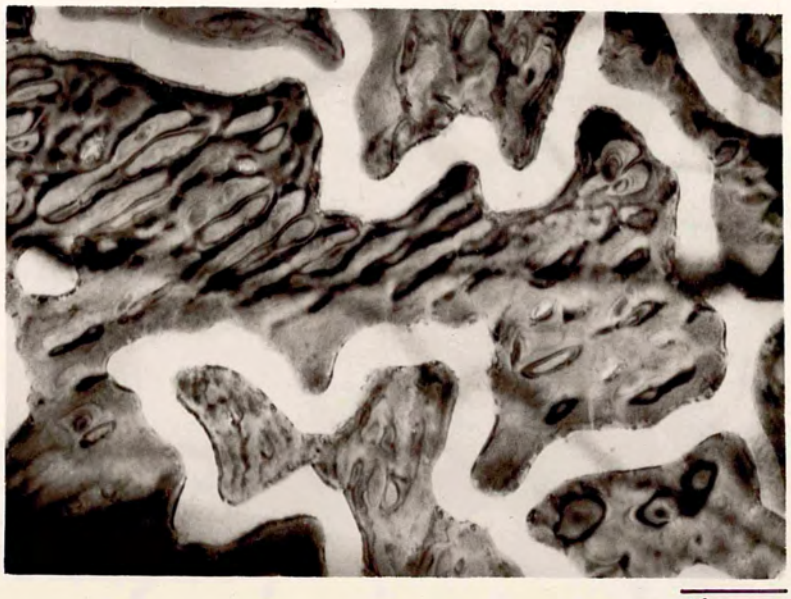

500nm

When a 10 nm film of CsI was deposited on biotite and exposed to the atmosphere for 10 minutes large clusters of deposit were formed. Most of them were linked to each other forming islands as shown in the micrograph of Fig. 6.41 (a). These clusters are well-oriented on the surface of biotite as indicated by its diffraction pattern shown in Fig. 6.41 (b) and projected in Fig. 6.42.

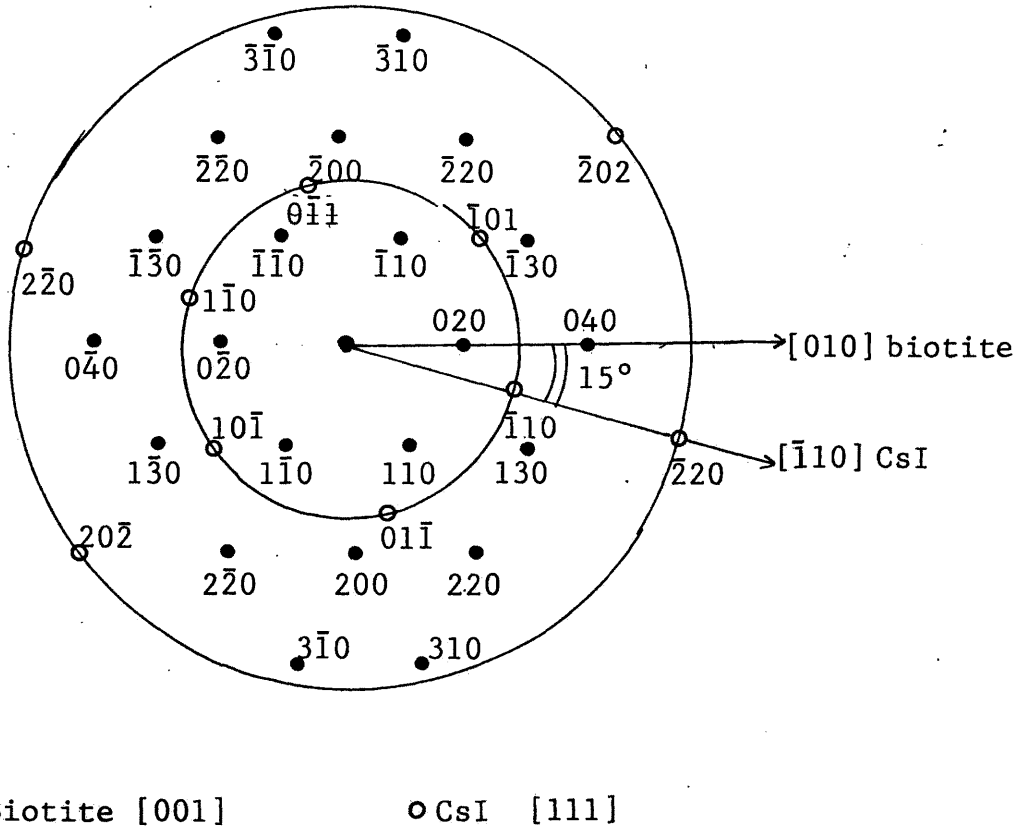

Fig. 6.42. Projection of the diffraction pattern from exposed CsI on [001] biotite grown at 200 °C.

As seen from the above diffraction pattern there is single orientation of CsI with [111] normal to the substrate

surface i.e., (111) plane of CsI is parallel to the (001) of the biotite with [$\bar{1}$10] of CsI making an angle of 15° with [010] of biotite.

In another experiment where a 20 nm film of CsI was deposited on biotite at 200 °C and exposed to the atmosphere for 30 minutes, the deposit formed large islands separated by channels and covering most of the substrate surface as shown in Fig. 6.43 (a). A number of lens-like loops were observed on the islands, some have fringes around them. The probable explanation of these loops is as follows: During exposure the deposit absorbed water from the atmosphere and form a solution. Although this water from the solution evaporates in the electron microscope, perhaps a small quantity of water, trapped between the deposit and the substrate surface, could cause lenticular flaws or bubbles in the film which are responsible for these loops. This island structure is also well-oriented on the surface of biotite as indicated by the diffraction pattern shown in Fig. 6.43 (b).

The orientation of the overgrowth is [001] normal to the substrate surface which can be stated as (001) plane of the deposit is parallel to (001) of the substrate with [100] of the deposit parallel to the [100] of the substrate. The likely exact-fit of the atoms of the overgrowth and the bstrate is given in Fig. 6.44. As shown in Fig. 6.38, in the biotite surface ther are two networks: potassium and silicon, and they are not on the same plane. So there is possibility that negatively

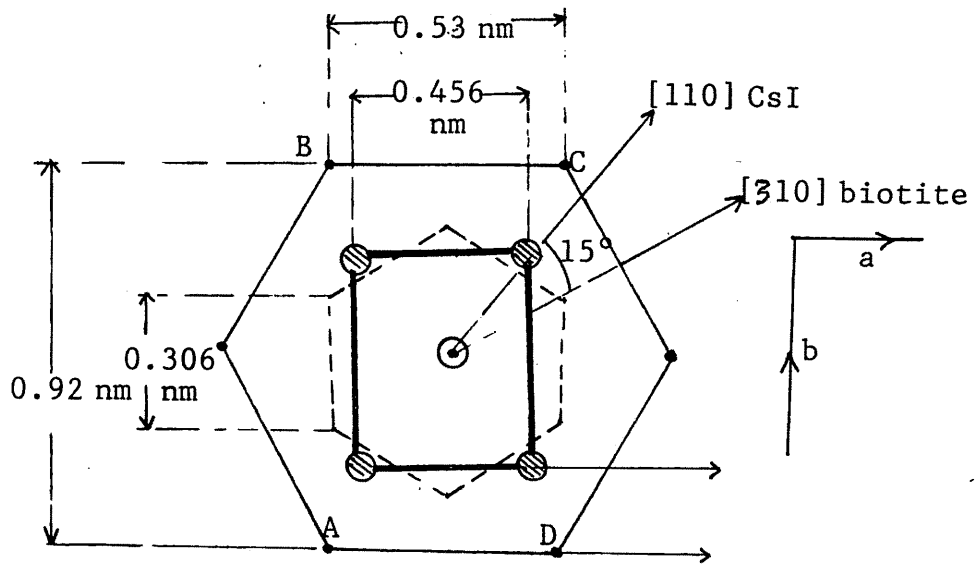

Fig. 6.44. A possible configuration of (001) plane of CsI with respect to the atomic arrangement of biotite.

charged I^- ion fit on the potassium ions above the potassium network plane and Cs^+ ions are locate beside the silicon atoms because it is possible that the potassium atoms on the sites marked A, B, C and D are vacant during cleavage process which allow the Cs^+ to place themselves near that sites. This orientation is confirmed, because the angle between [110] of biotite and [110] of CsI in the diffraction pattern and in the above configuration is the same.

Fig. 6.45 (a)

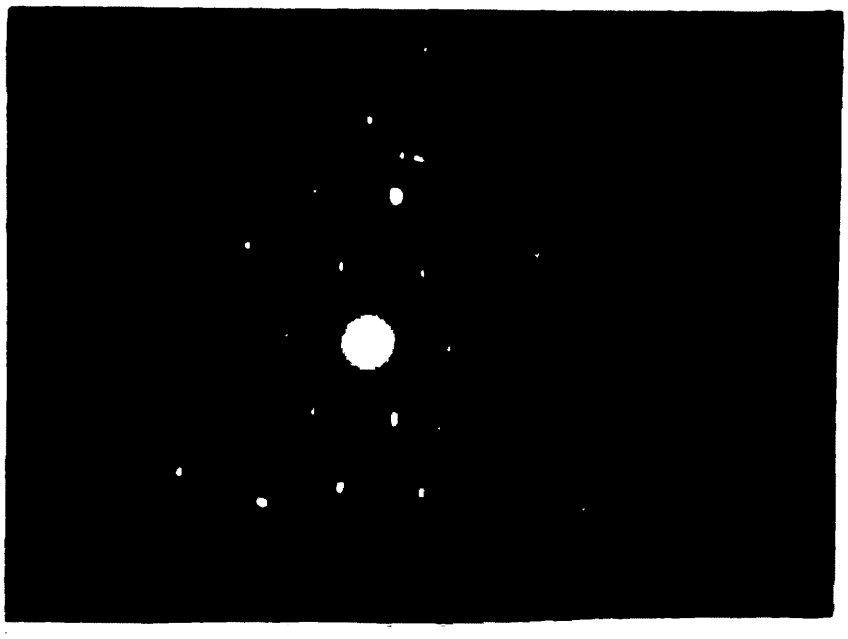

Fig. 6.45 (b)

Fig. 6.45 (a). Unexposed deposit of CsI grown on muscovite at room temperature (thickness = 15 nm).

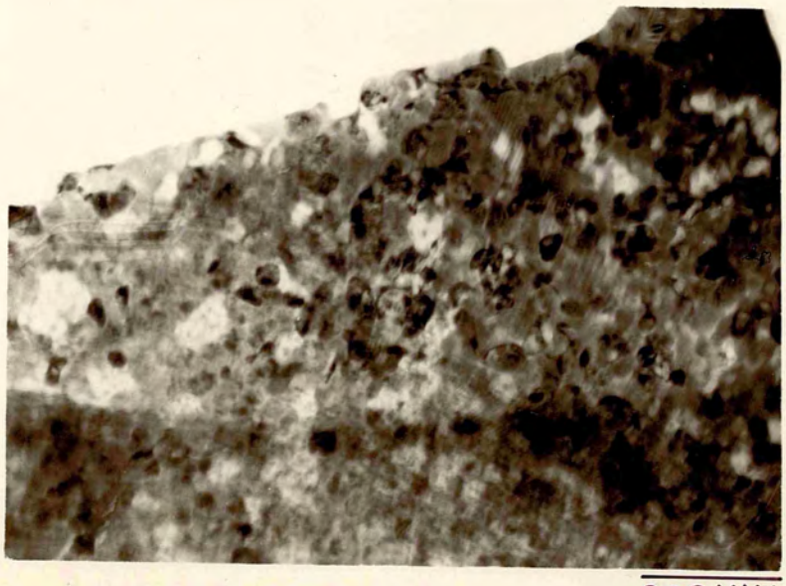

200 nm

Fig. 6.46

Fig. 6.47

Fig. 6.46 and 6.47. Unexposed deposits of CsI grown on muscovite at 150 °C (thickness = 1o nm and 15 nm respectively).

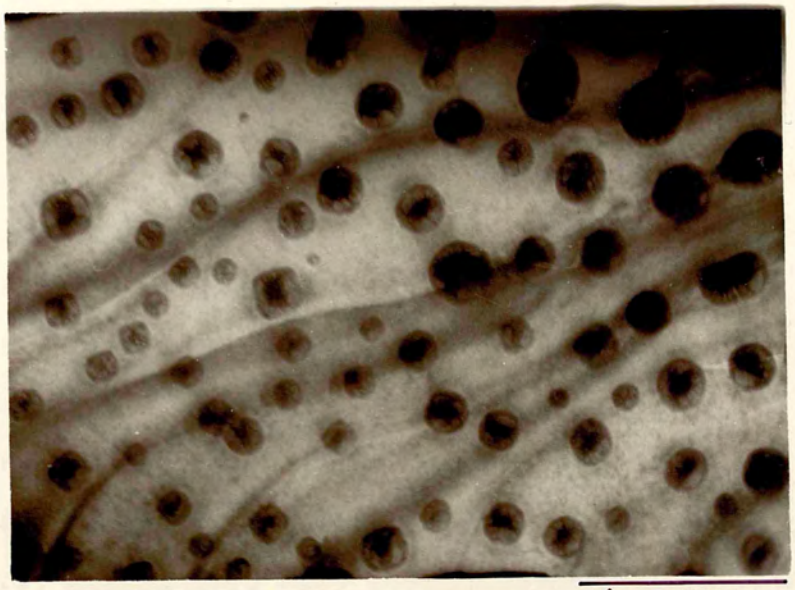
500 nm

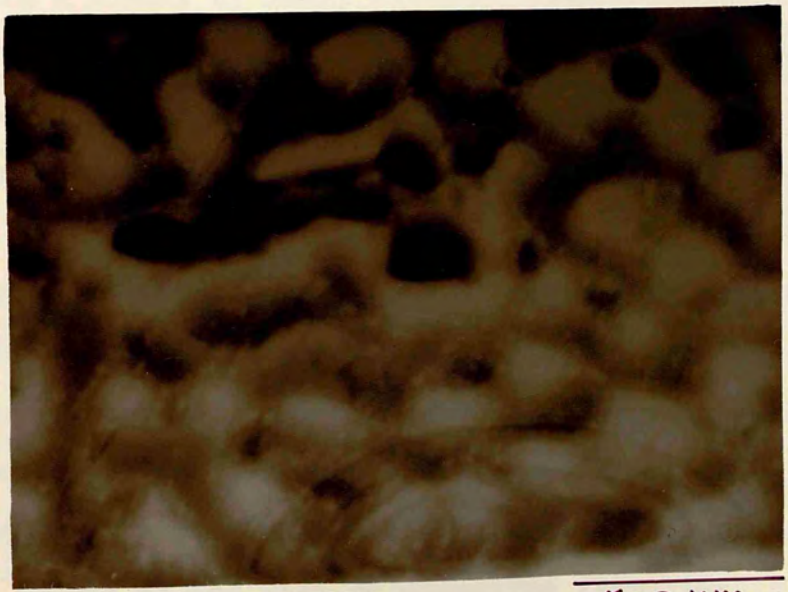
500 nm

6.5.2 CsI on Muscovite.

The difference between biotite and muscovite is not great so for as the (001) cleavage face is concerned. The lattice parameters along a and b are 0.53 nm, 0.92 nm and 0.519 nm, 0.904 nm in biotite and muscovite respectively. However the c-axis spacing in muscovite is nearly twice that in biotite because the most common polymorph of muscovite is $2M_1$. The growth of CsI on muscovite is nearly the same as that on biotite discussed in 6.5.1, differences only occurring when orientations other than [001] of muscovite are taken into account.

Fig. 6.45 (a) shows a micrograph of a 15 nm deposit of CsI on muscovite before atmospheric exposure. There are a number of small platelet-like crystallites formed in a nearly continuous layer of deposit. As observed by a number of investigators, alkali halides form a continuous film on mica for a deposit thickness between 5 to 10 nm (Tavassoli, 1978). The dark crystallites in the micrograph are either multilayer nucleation or the early nucleation on the vacant sites of potassium atoms due to the cleavge process. Some of these crystallites appear hexagonal in shape, indicating the probability of preferentional nucleation on the grooves in the muscovite surface formed by the lack of potassium atoms (Green, 1971; Koch and Vook, 1972). The diffraction pattern of this deposit is shown in Fig. 6.45 (b), the indexing of which indicates that the substrate is tilted through an

angle of 23° with respect to the electron beam, as the present orientation of muscovite is normal to [312], (The cleavage plane of mica is (001) and the angle between [001] and $[\bar{3}\bar{1}2]$ in monoclinic system is 23° 18'). The overgrowth does not show any specific orientation as there is only a few weak reflections corresponding to the overgrowth. Some intense spots on the {211} ring indicate that probably there is a [111] orientation.

When CsI was deposited on muscovite at above room temperature it formed clusters on the substrate surface. Fig. 6.46 shows the micrograph of a 10 nm thick deposit of CsI on muscovite grown at 150 °C and was observed before exposure to the atmosphere. A large number of clusters are formed all over the mica surface, some of these clusters are square shaped but most of them are circular. The sizes also vary between 25 nm and 200 nm. The 'square' crystals have side lenghs between 70 nm and 125 nm. The central parts of these crystals are thicker than the edges, which indicates that the nucleation started at the centre, on a preferred site on the substrate surface. The crystals are probably built up around the previous nuclei. These preferred sites are formed either by potassium atom vacancies formed during cleavage or by water molecules produced in the mica lattice by local reversible reaction of structural OH groups at higher temperature (Gaines and Vedder, 1964). These water molecules accomulate at defect sites and participate in the formation of lenticular flaws observed in some heated micas. When the deposit thickness

was increased from 10 nm the clusters coalesced due to further nucleation between the spaces of previous clusters, and formed island structures. This is observed in the micrograph of Fig. 6.47, which is from a deposit of CsI with thickness nearly 15 nm on muscovite grown at 150 °C and observed before atmospheric exposure.

Fig. 6.48 (a) shows a 10 nm thick CsI film deposited on muscovite at 150°C and examined before atmospheric exposure. The crystals formed on the surface of the substrate are mainly circular in shape and some of them are rectangular in shape. These crystals are well oriented on the substrate as shown in Fig. 6.48 (b). The orientation is rather complicated. The substrate is oriented normal to the [532] as indicated by its indexing. This mean the (001) cleavage plane is tilted 45° with respect to the electron beam (The angle between [001] and [532] in the monoclinic system is 44° 50'). The spots in the diffraction pattern corresponding to the overgrowth indicate a mixed orientations of [001] and [011]. The crystals with [001] orientation have {110} planes of the overgrowth parallel to the (001) plane of the substrate and those with [011] have {001} planes parallel to the (001) plane of the substrate. The first orientation is shown in Fig. 6.49 in which the iodide ion at the centre of the (110) plane lies on the potassium atom, and the corner Cs^+ ions which are on the same plane lie in between two potassium atoms (or potassium vacant sites). The second orientation with (001) of the deposit parallel to (001) of

the substrate is similar to that shown in Fig. 6.44 of CsI on biotite.

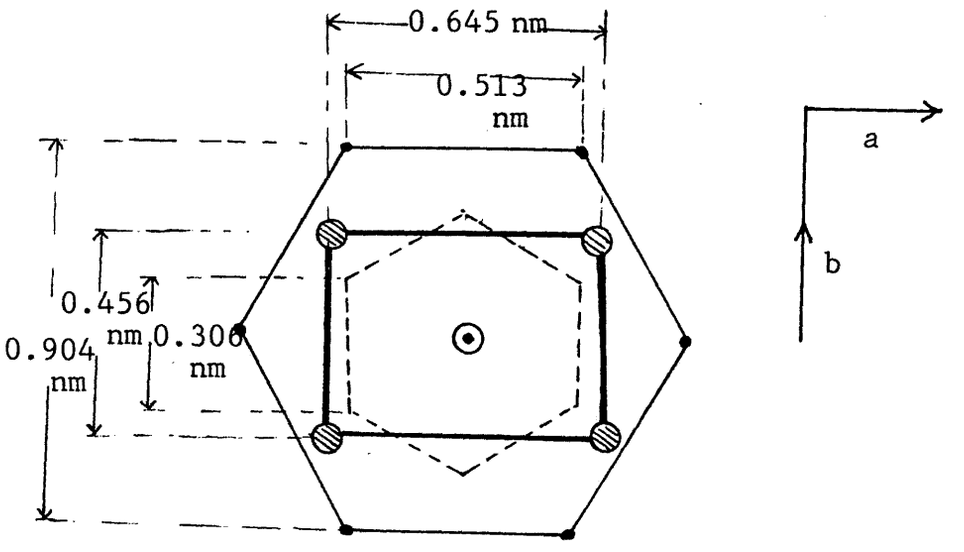

• Potassium sites ○ Iodide ion ◍ Cs ions

Broken lines represent the silicon network and thick lines show the(110) plane of CsI.

Fig. 6.49. A possible configuration of (110) plane of CsI with respect to atomic arrangement of muscovite.

When the deposit of CsI on muscovite was exposed to the atmosphere it absorbed water and made tiny droplets of solution. In the microscope, water evaporated leaving behind clusters of crystals. Fig. 6.50 shows the micrograph of a 20 nm deposit of CsI on muscovite grown at room temperature and exposed to the atmosphere for 30 minutes. Clusters of various sizes are formed, the larger clusters

Fig. 6.48 (a)

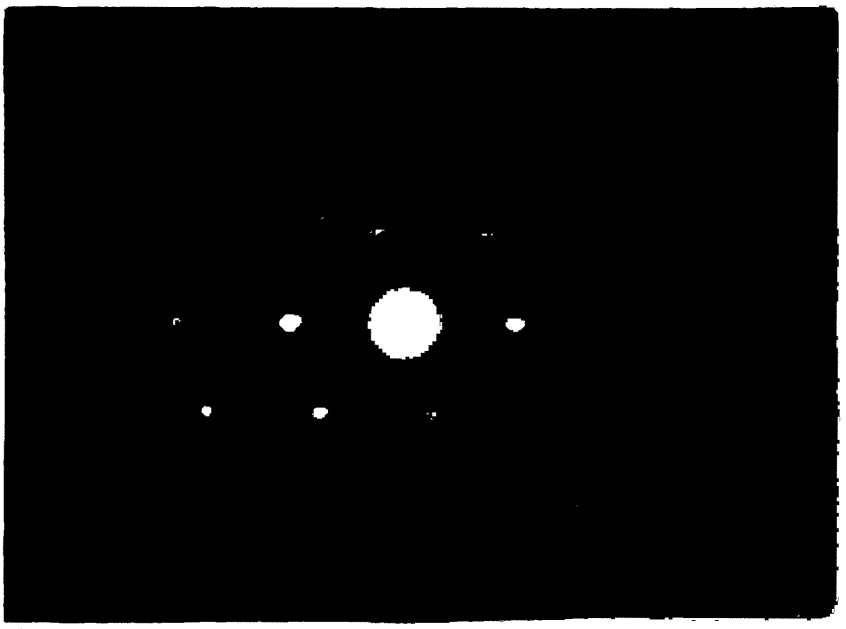

Fig. 6.48 (b)

Fig. 6.47 (a). Unexposed deposit of CsI grown on muscovite at 150 °C (thickness = 10 nm).
(b) Its diffraction pattern.

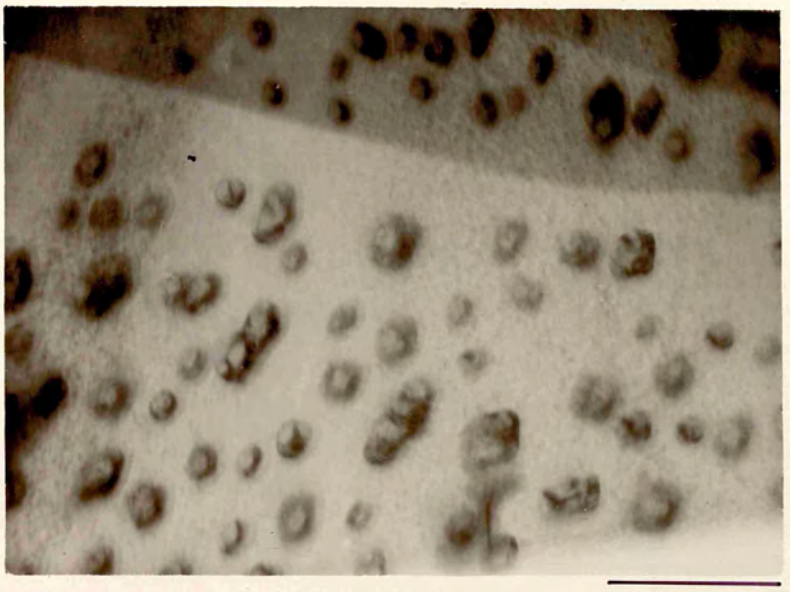

200nm

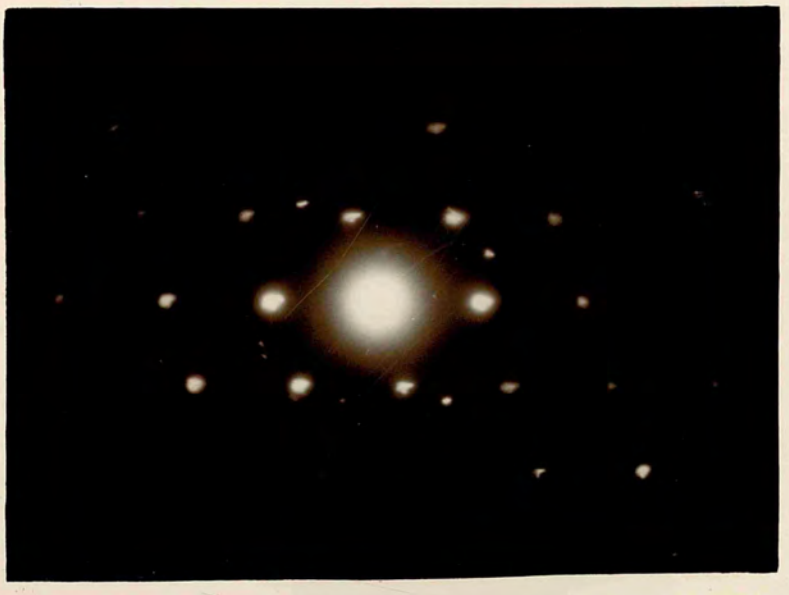

Fig. 6.50

Fig. 6.51

Fig. 6.50 and 6.51. Exposed deposits of CsI grown on muscovite at room temperature. Deposits thicknesses = 20 nm and 5 nm, and exposure time 30 minutes and 5 minutes respectively.

200nm

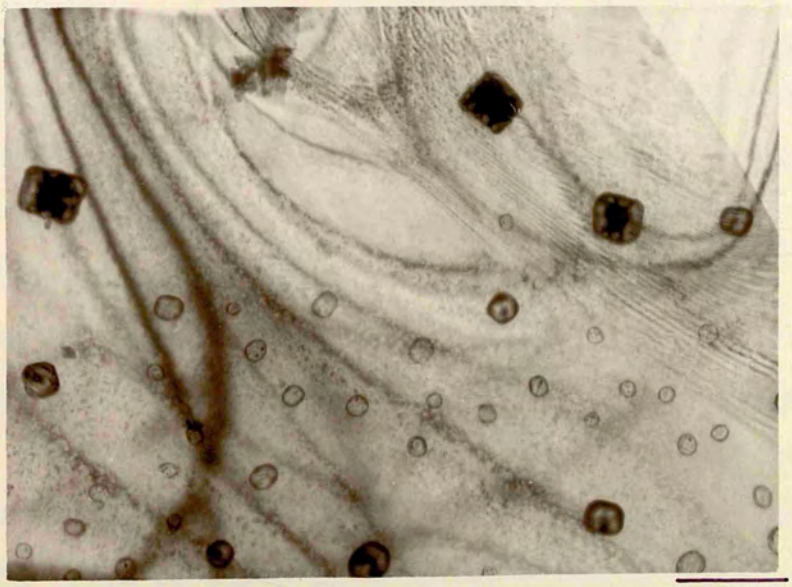

1000nm

apparently being formed by the coalescence of small clusters. Similarly when a 5 nm layer of CsI on muscovite exposed to the atmosphere for 5 minutes, small crystals with square shapes are formed as shown in Fig. 6.51.

Fig. 6.52 (a) shows a 10 nm layer of CsI on muscovite exposed to the atmosphere for 10 minutes, forming an island-structure film all over the substrate surface. The white areas in the islands are probably due to the re-evaporation of the material under electron bombardment in the microscope. The coalesced nuclei in the island structure have a variety of orientations as indicated by the diffraction pattern in Fig. 6.52 (b). There are 12 spots with separation 0.323 nm representing the two [111] orientations of CsI on muscovite surface rotated by 30° with respect to each other. The (111) planes with these two positions in CsI have been shown in Fig. 6.40 (section 6.5.1). As the cell size in the (111) plane of CsI differs considerably from any network length on the cleavage surface of muscovite, there is no exact fit between the atoms of overgrowth and of the substrate. This results in an angular orientation and $\{110\}$ sides of both [111] orientations make an angle of 15° with the sides of small and large networks on the surface of muscovite. In the diffraction pattern there are four spots with separation 0.456 nm which must be reflected from $\{100\}$ planes of CsI indicating [001] orientation with the (001) plane of the overgrowth parallel to the (001) of the substrate.

When the deposit of CsI on muscovite grown at 150 °C were exposed to the atmosphere, similar results were obtained. Fig. 6.53 shows a 10 nm thick deposit of CsI on muscovite grown at 150 °C after exposure to the atmosphere for 15 minutes. Some circular clusters and large number of square-shaped crystals are formed. These crystals have some regions thicker than others, usally the centres of the crystals. The likely explanation of this is that the nucleation in a drop of solution, formed by the water vapour condensation on the deposit, starts at a preferred site. This nucleation decreases the concentration of the solution and later-grown crystal is thinner. Fig. 6.54 shows the island-structure film formed when a 15 nm layer of CsI on muscovite grown at 150 °C is exposed to the atmosphere for 30 minutes.

In another experiment where a deposit of CsI of 10 nm thick was exposed to the atmosphere for 10 minutes, fewer large clusters were formed (Fig. 6.55 a). The small black specks are might be the undissolved nuclei of the overgrowth which are not oriented on the substrate and which give rise to very faint rings in the diffraction pattern shown in Fig. 6.55 (b). The observed orientation from this diffraction pattern of CsI is [001] normal to the substrate surface with the (001) plane of the overgrowth parallel to the (001) plane of the substrate and [100] direction in the overgrowth parallel to the [100] direction in the substrate. This orientation is shown in Fig. 6.56.

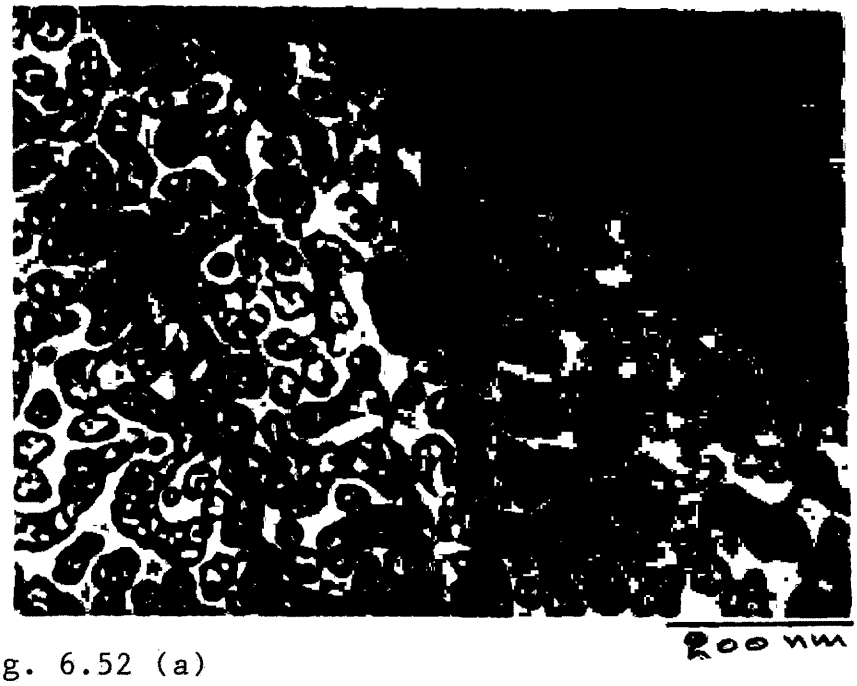

Fig. 6.52 (a)

Fig. 6.52 (b)

Fig. 6.52 (a). Exposed deposit of CsI grown on muscovite at room temperature (thickness = 10 nm and exposure time 10 minutes). (b) Its diffraction pattern.

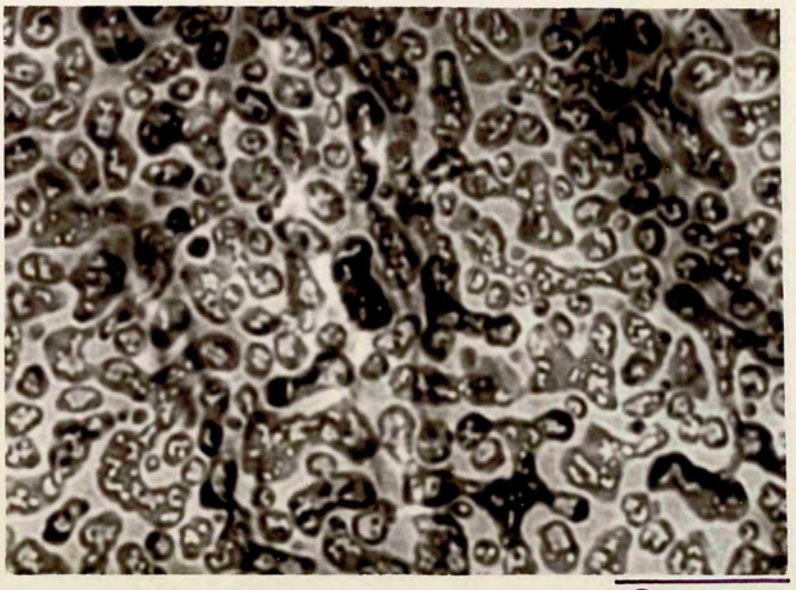
200 nm

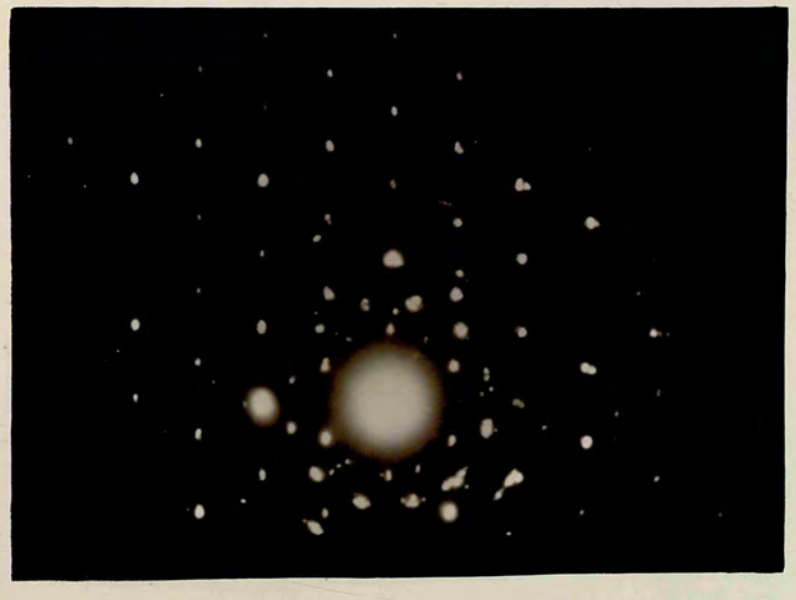

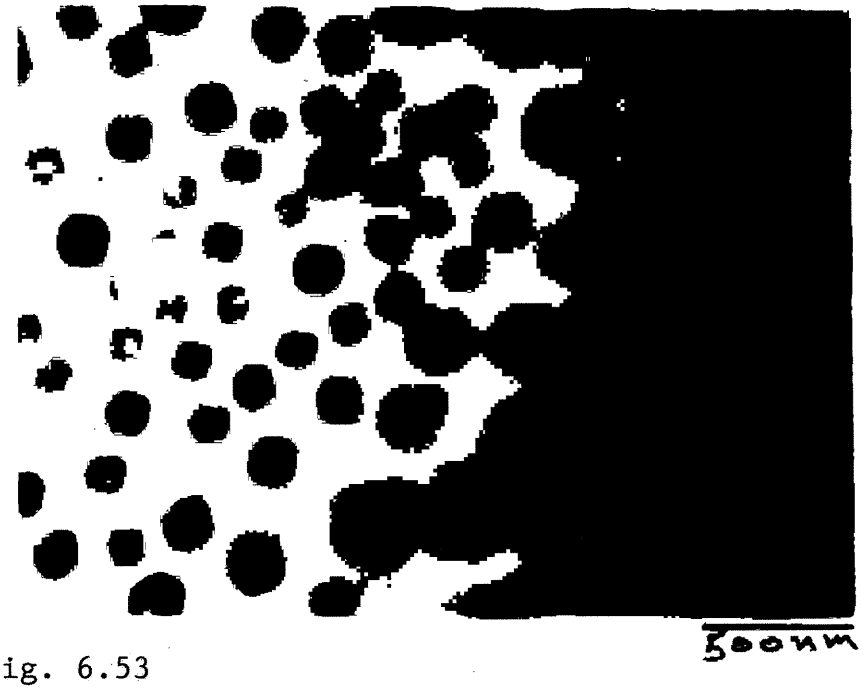

Fig. 6.53

Fig. 6.54

Fig. 6.53 and 6.54. Exposed deposits of CsI grown on muscovite at 150 °C. Deposits thicknesses = 10 nm and 15 nm, and exposure time 15 minutes and 30 minutes respectively.

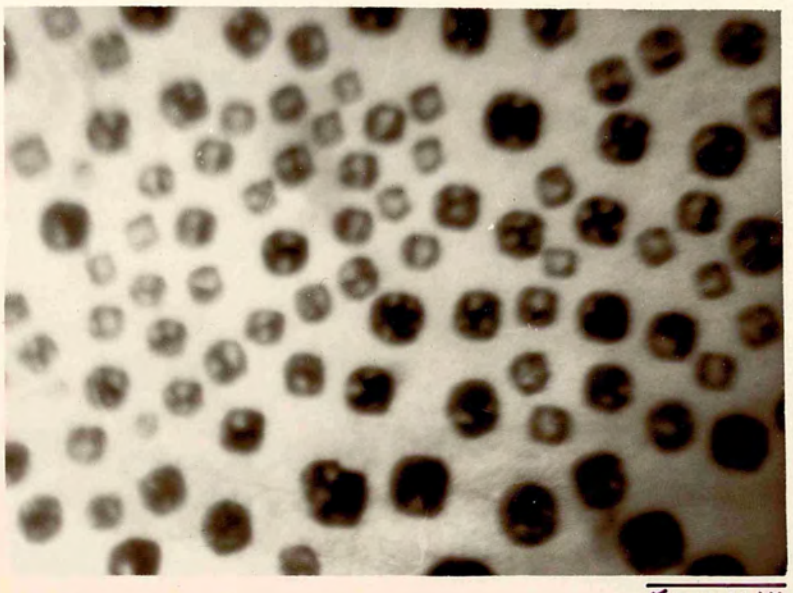
500nm

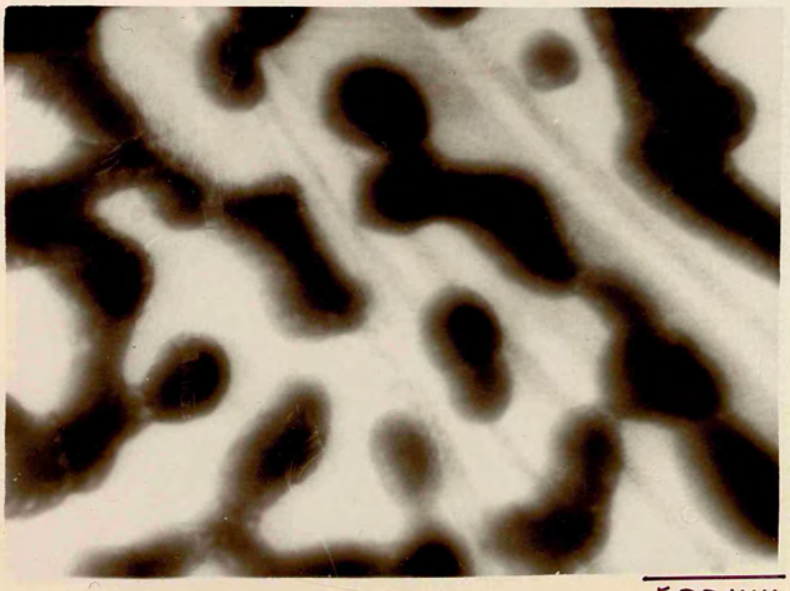
500 nm

Fig. 6.55 (a)

Fig. 6.55 (b)

Fig. 6.55 (a). Exposed deposit of CsI grown on muscovite at 150 °C (thickness = 10 nm and exposure time 10 minutes). (b) Its diffraction pattern.

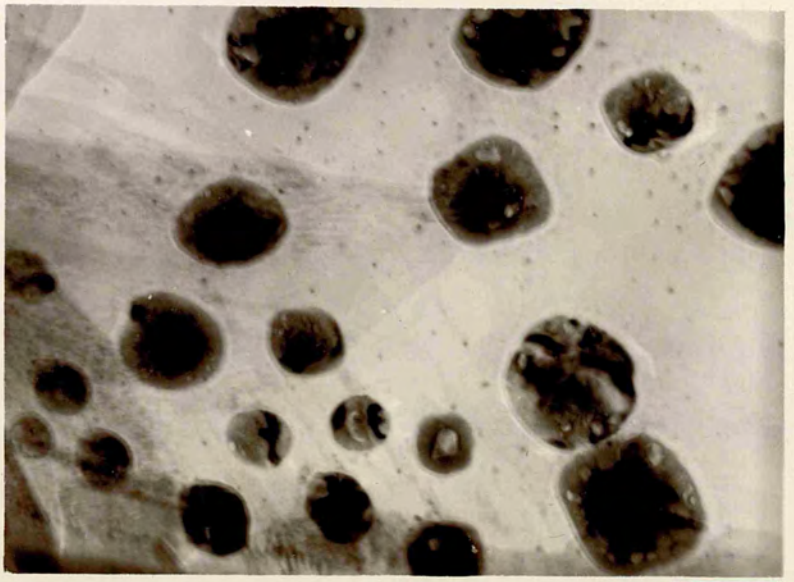
100nm

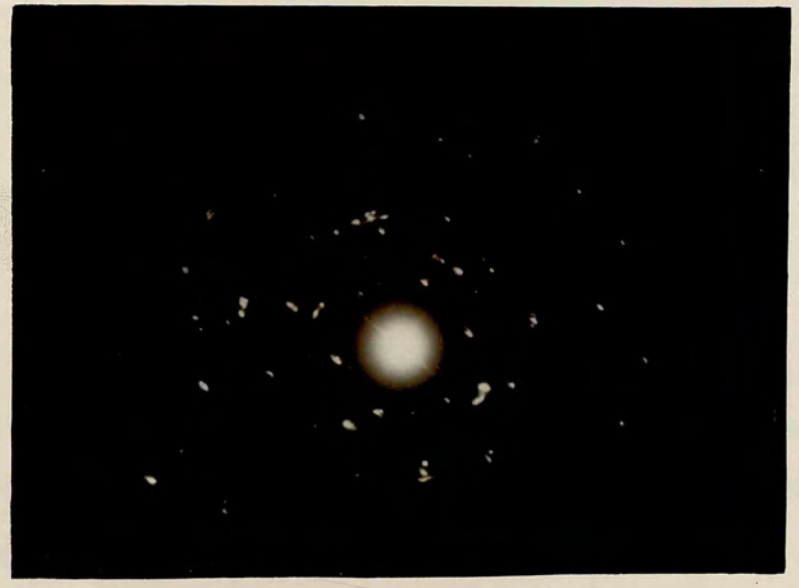

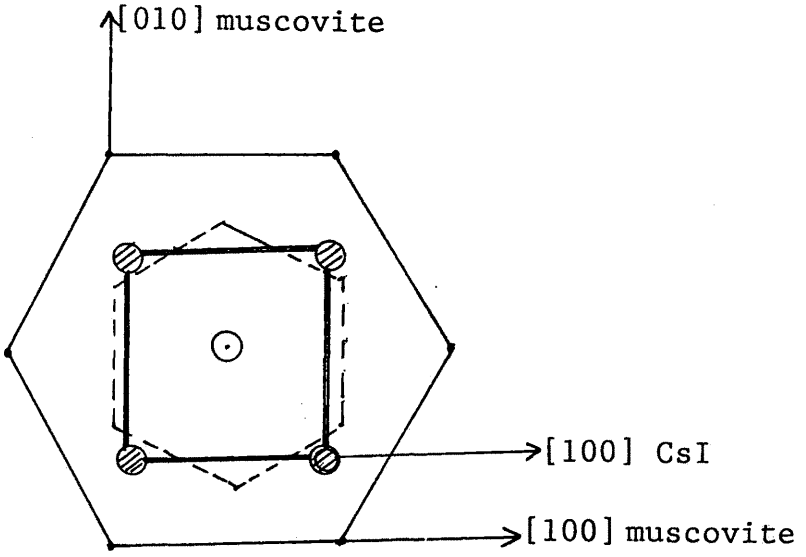

• Potassium sites ○ Iodide ion ▨ Cs ions

Broken lines show the silicon network and the heavy lines show the sides of the (001) plane of CsI.

Fig. 6.56. A possible configuration of [001] orientation of CsI on muscovite grown at 150°C (exposed deposit).

6.5.3 CsCl on Biotite.

Unexposed deposits of CsCl on biotite at room tenperature are similar to those of CsI on biotite i.e., they consist of small crystallites situated randomly on the substrate surface. However, the exposed deposits form clusters and sometime single crystals as shown in Fig. 6.57 and 6.58.

Fig. 6.57 shows a 15 nm deposit of CsCl grown on biotite at room temperature and exposed to the atmosphere for 10 minutes. Large clusters with average diameter 140 nm are formed, Some of these clusters have coalesced to form large clusters. Fig. 6.58 shows a single crystal of CsCl formed when a 10 nm deposit of CsCl on muscovite grown at room temperature was exposed to the atmosphere for 30 minutes. For this length of time the deposit absorbed sufficient water from the atmosphere to dissolve completely and form a single large drop of solution. In the electron microscope the water evaporated but due to the relatively greater quantity of water the time of evaporation is longer than that for a large number of small drops. The crystal formed in this process is similar to those formed from the solution on cotinuous carbon support films or in the holes of carbon support films as disscused in capter 2.

In another experiment when a deposit of CsCl nearly 10 nm in thickness was exposed to the atmosphere for 15 minutes, the clusters of the overgrowth formed all over the substate surface (Fig. 6.59, a). The spots reflected from the overgrowth in the diffraction pattern (Fig. 6.59, b) are either faint or not on any geometrical line corresponding to a cubic crystal pattern, which means there is no recognisable orientation occurs.

When CsCl is deposited on biotite at 200^{o}C and observed before atmospheric exposure, the result is different from that obtained from a similar deposit of CsI

Fig. 6.57

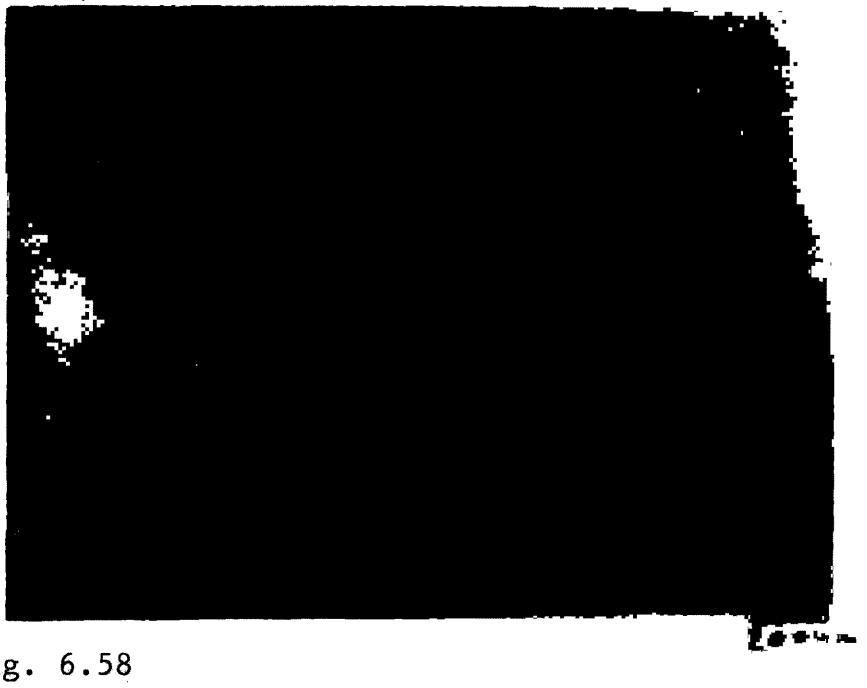

Fig. 6.58

Fig. 6.57 and 6.58. Exposed deposits of CsCl grown on biotite at room temperature. Deposits thicknesses = 15 nm and 10 nm, and exposure time 10 minutes and 30 minutes respectively.

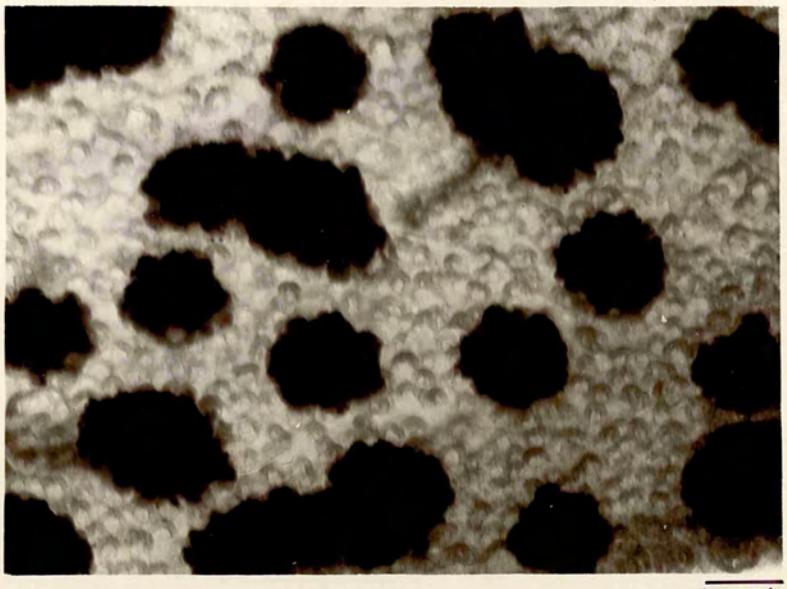

100nm

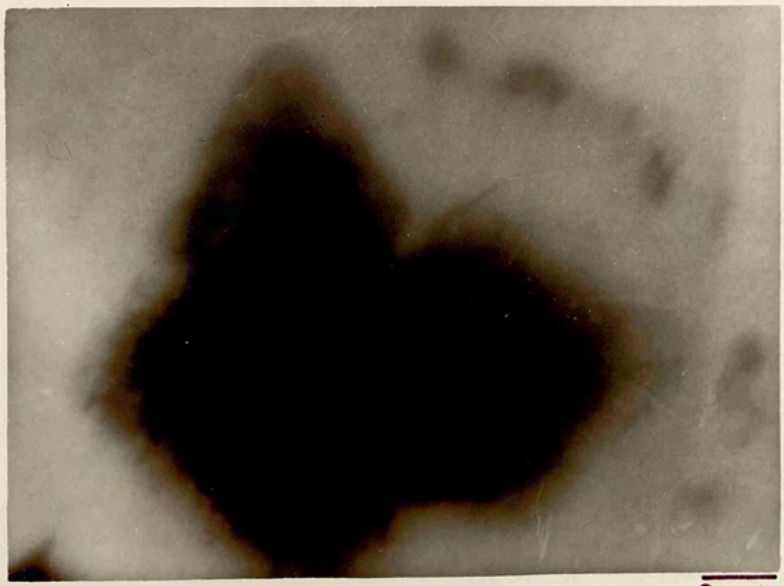

200nm

Fig. 6.59 (a)

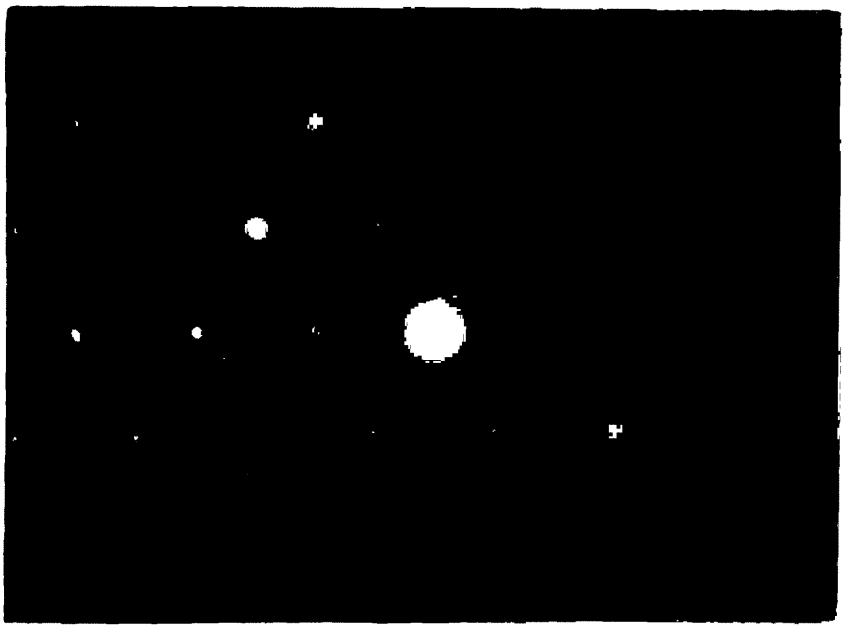

Fig. 6.59 (b)

Fig. 6.59 (a) Exposed deposit of CsCl grown on biotite at room temperature (thickness = 10 nm and exposure time 15 minutes). (b) Its diffraction pattern.

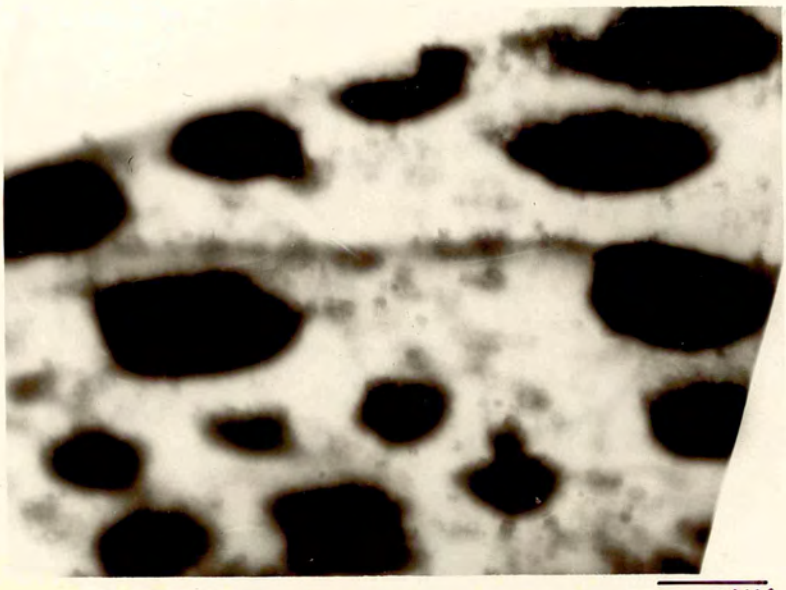

200nm

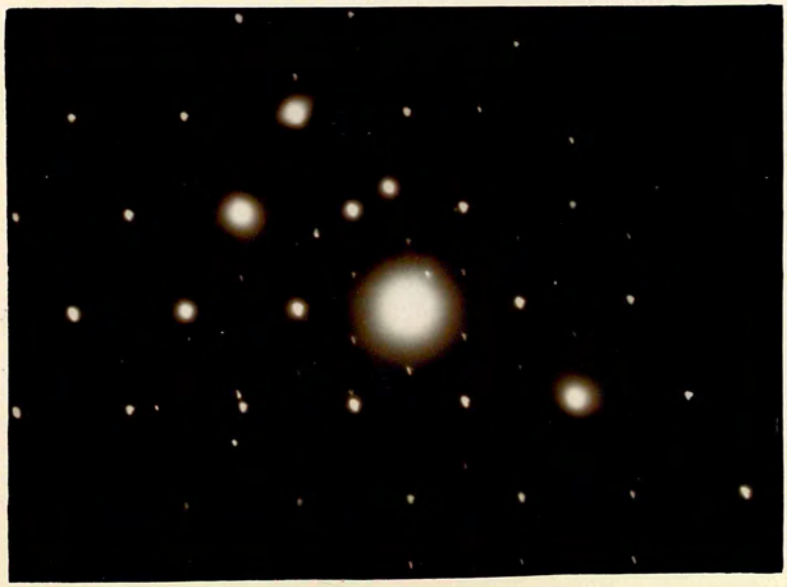

Fig. 6.60

Fig. 6.61

Fig. 6.60. Unexposed deposit of CsCl grown on biotite at 200 °C.

Fig. 6.61. Exposed deposit of CsCl grown on biotite at 200 °C.

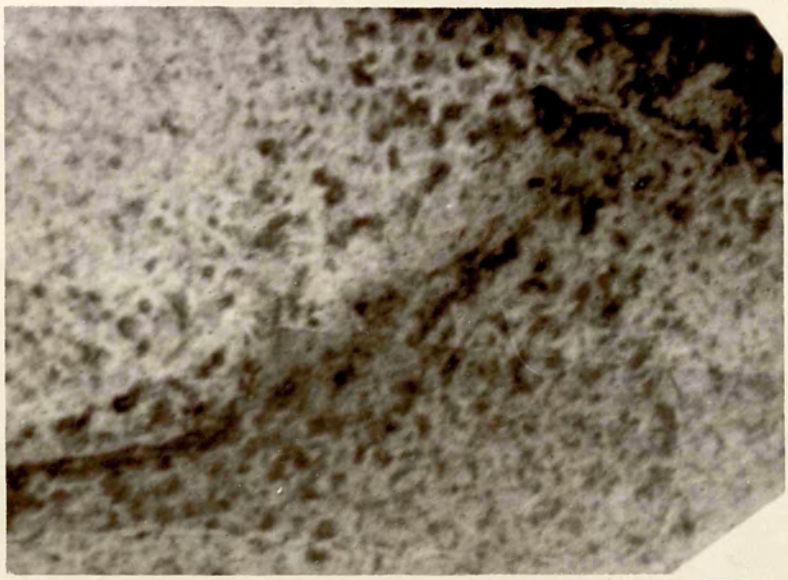

200nm

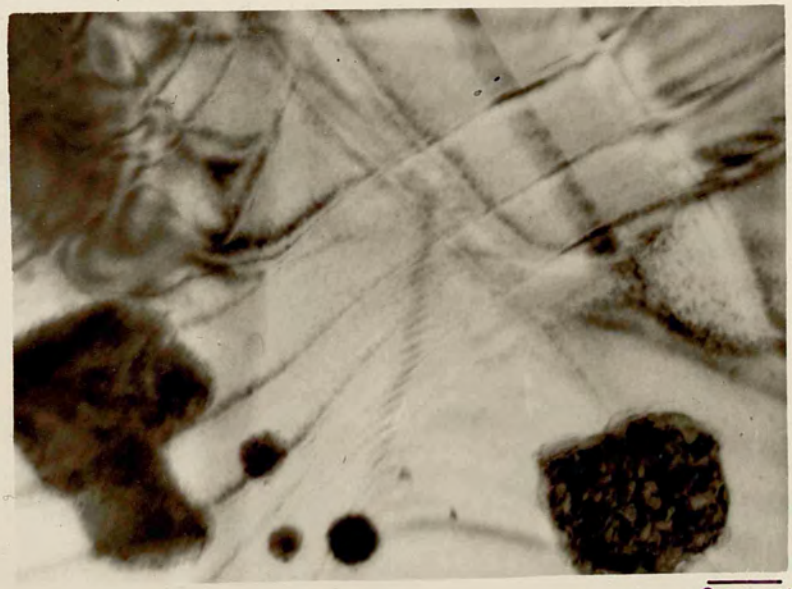

200nm

on biotite. For CsCl no clusters are formed but small nuclei situated randomly on the substrate (Fig. 6.60). However some nuclei are coalesced and form small clusters usually along the step structure on the substrate surface. The size of the smallest observed nucleus is 5 nm (deposit thickness is nerly 10 nm), and the largest coalesced nucleus is 80 nm. The higher density of nuclei at the step structure indicates that at higher substrate temperature than room temperature, the nuclei migrate on the surface until they are stopped by a step where coalescence occurs.

When this type of deposit was exposed to the atmosphere large clusters were formed. Fig. 6.61 shows a CsCl deposit with thickness less than 10 nm exposed to the atmosphere for 15 minutes. The diffraction pattern in Fig. 6.62 is from an exposed deposit of CsCl on biotite grown at 200 °C. The spots corresponding to the overgrowth do not indicate any particular orientation but as there is no ring observed in the diffraction pattern which means there are randomly oriented large crystals participating the diffraction pattern.

6.5.4 CsCl on Muscovite.

Unexposed deposits of CsCl on muscovite grown at room temperature consist of small crystallites randomly situated on the surface of the substrate as indicted by the diffraction pattern in Fig. 6.63. Here the substrate is normal to $[01\bar{1}]$, which means the (011) plane in the

substrate is normal to the electron beam. The mica cleavage surface is usually $(00\bar{1})$ and placed horizontally in the electron microscope where the electron beam is vertical. However, if the edges of the mica sheet are not clamped between the bars of folded grid properly, a loose edge might be bent due to heating in the electron microscope or uneven clamping. This kind of bend in mica sheet is also confirmed by the moving extinction contours usually observed during the imaging process. The angle between [001] and $[01\bar{1}]$ in the muscovite system is $24^{\circ}\,15'$, so the mica sheet in this experiment is tilted through the said angle as shown in Fig. 6.64. The rings in the diffraction pattern formed by the reflections from the overgrowth are very faint.

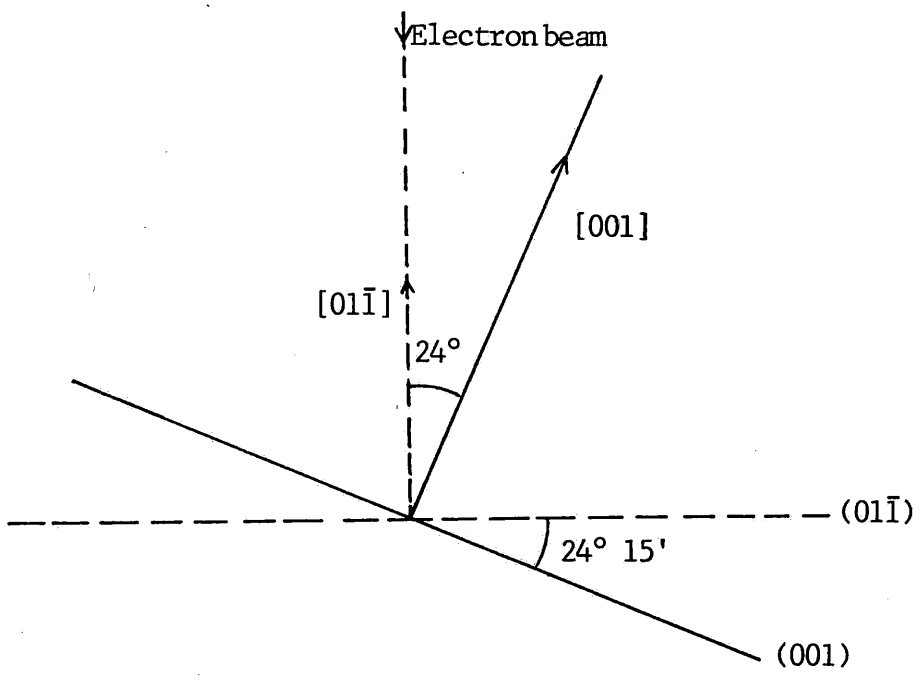

Fig. 6.64. Tilt in mica sheet with respect to the electron beam.

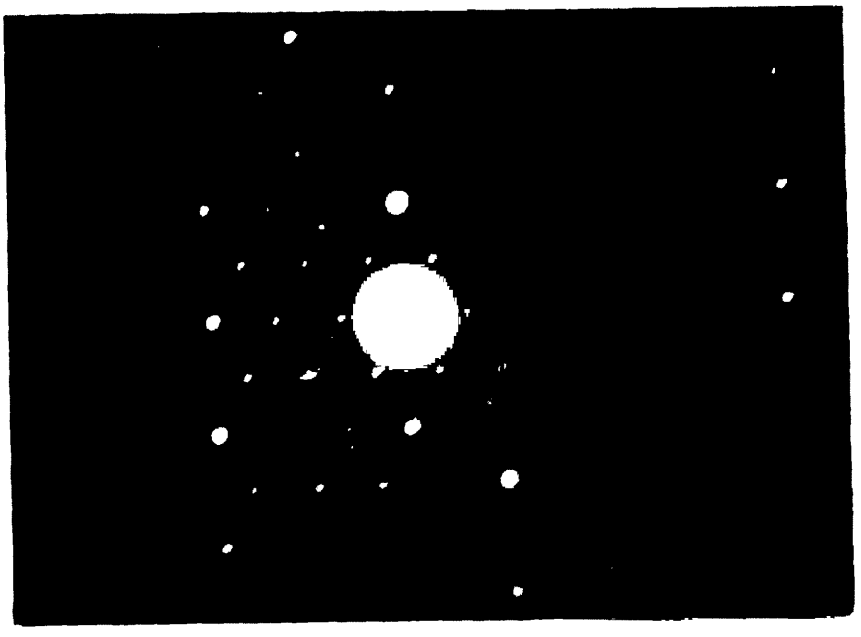

Fig. 6.62

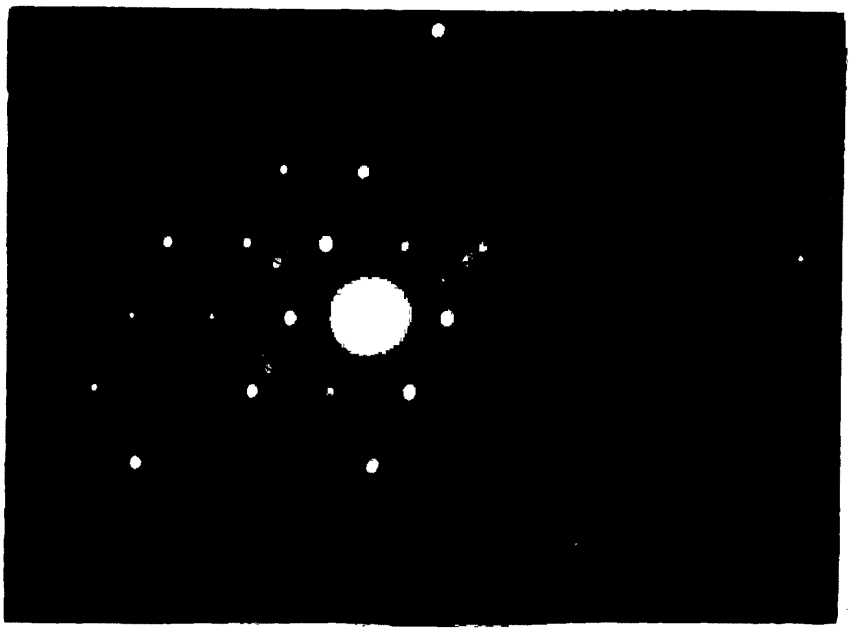

Fig. 6.63

Fig. 6.62. Diffraction pattern from an exposed deposit of CsCl grown on biotite at 200°C.

Fig. 6.63. Diffraction pattern from an unexposed deposit of CsCl grown on muscovite at room temperature.

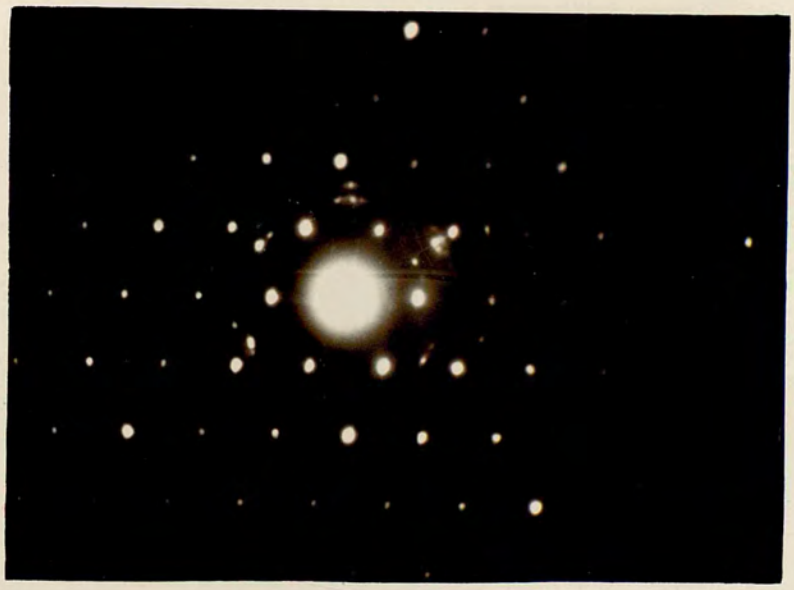

Fig. 6.65 (a)

Fig. 6.65 (b)

Fig. 6.65 (a). Unexposed deposit of CsCl grown on muscovite at 150 °C (thickness = 5 nm).

(b). Its diffraction pattern.

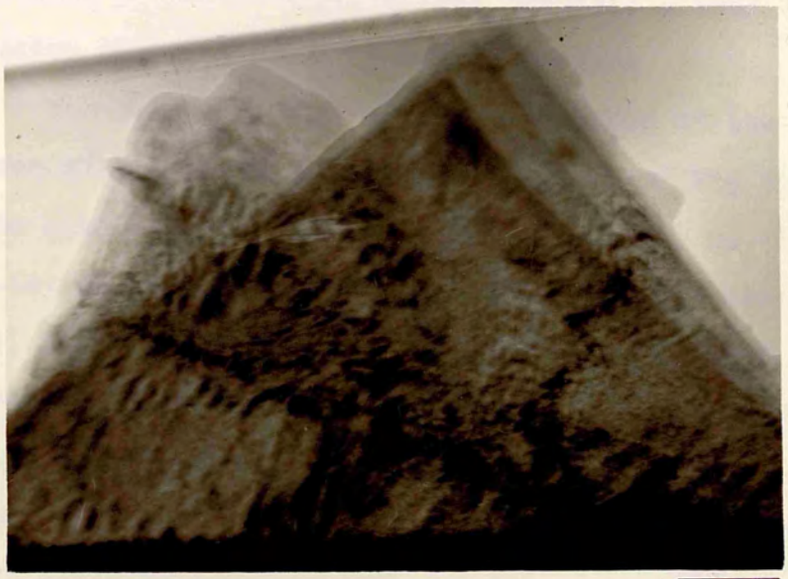

200nm

Some intense spots on the {110} ring indicate a weak [111] orientation normal to the substrate surface.

The length of the reciprocal vector of the innermost ring (in the diffraction pattern of Fig.6.63) and some other spots (which also do not belong to the substrate) do not correspond to any interplanar distance in CsCl. This indicates either the presence of other substances or a change in the lattice parameter of CsCl with some lattice trnsformation. The other substances could be impurities in the CsCl or compounds formed by the chemical reaction between CsCl and the surface atoms of the substrate. The possibility of lattice transformation is more likely because CsCl transforms from Cs-Cl structure to Na-Cl structure at higher temperature (below melting point) with a considerable increase in lattice parameter. This transformation was first reported by Wagner and Lippert (1936) from Cs-Cl structure to Na-Cl structure with an increase in lattice parameter from 0.412 nm to 0.702 nm. Schulz (1951) has also reported polymorphic transition in CsCl to NaCl structure in the experiments of growth from the vapour phase on substrates with Na-Cl structure, and increase in lattice parameter to 0.694 nm with decrease in interatomic distance from 0.356 nm in Cs-Cl structure to 0.347 nm in Na-Cl structure.

This kind of change in lattice parameter of CsCl has also been observed in an other experiment when an unexposed deposit of CsCl on muscovite grown at 150 °C was observed in the electron microscope. The micrograph and

diffraction pattern are shown in Fig. 6.65 (a) and (b). The deposit thickness in this experiment was nearly 5 nm and it formed small nuclei on the substrate surface, most of them coalesced into small clusters on the step structure. This is probably due to the migration of nuclei on the hot substrate surface. Some of these coalesced nuclei or clusters are situated randomly on the substrate surface and produced very faint ring in the diffraction pattern (Fig. 6.65, b). The diffraction pattern of Fig. 6.65 (b) is reproduced in Fig. 6.66.

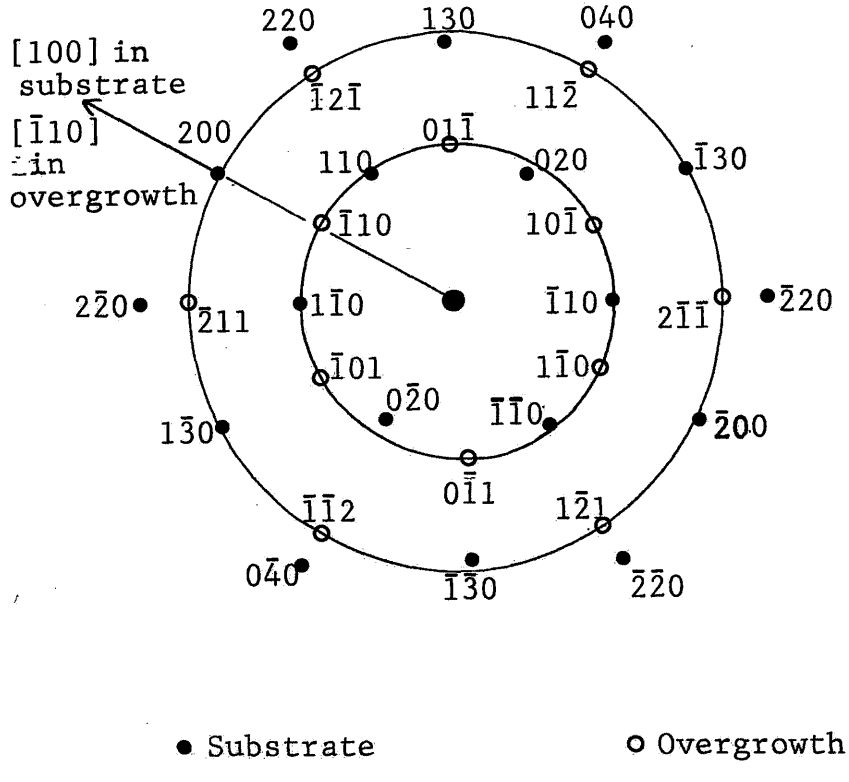

Fig. 6.66. Reproduction of the diffraction pattern of CsCl grown on muscovite at 150 °C.

The length of the reciprocal vector for the nearest ring was measured precisely and converted into interplanar spacing which is 0.45 ± 0.002 nm. As the largest interplanar spacing in CsCl is for $\{100\}$ set of planes which is 0.412 nm. This indicates the increase in the lattice parameter of CsCl by 9.22 %. The interplanar spacing for the second oberved ring is 0.26 ± 0.002 nm which corresponds to the $\{111\}$ set of planes of CsCl with lattice parameter 0.45 nm (the ratio between the vector lengths of second and first rings is 1.73 which is equal to $\sqrt{3}$). There are six equally distant spots on each ring which are not belong to the substrate. If we assume that these spots are formed by the reflections from the overgrowth then the spots on the first ring must be correspond to the $\{110\}$ set of planes and those on the second ring to the $\{211\}$ planes. This gives the lattice parameter of CsCl as 0.636 nm and [111] orientation of the overgrowth normal to the substrate surface. In [111] orientation the distance between nearest neighbour atoms in Cs-Cl type structure is $a_o\sqrt{2}$, which is in above case is 0.9 nm. Although this is equal to the distance between two potassium sites along [010] direction which gives an exact fit of the overgrowth ions to the surface atoms of the substrate. But the parallel directions in the substrate and overgrowth, indicated by the diffraction pattern, are not possible. The directions in a (111) plane of the overgrowth and in the surface network of muscovite are shown in Fig. 6.67 (a) and (b).

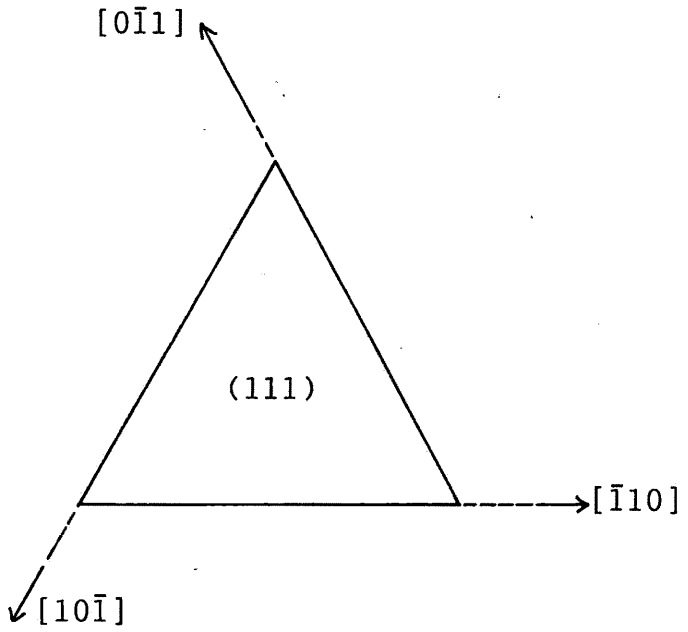

Fig. 6.67 (a). The directions in a (111) plane of CsCl.

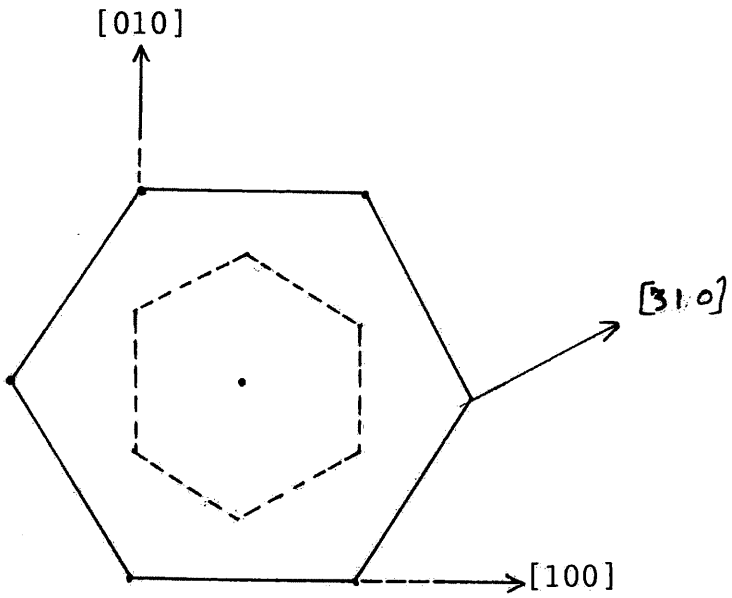

Fig. 6.67 (b). The directions in the surface network of muscovite.

It is unlikely that the lattice parameter of CsCl is changed so much while retaining its Cs-Cl structure, the previous assumption is therefore wrong. These six spots belong to another sheet of mica rotated 0^{o} with respect to each other. The indexing of the diffraction pattern with above consideration is given in Fig. 6.68.

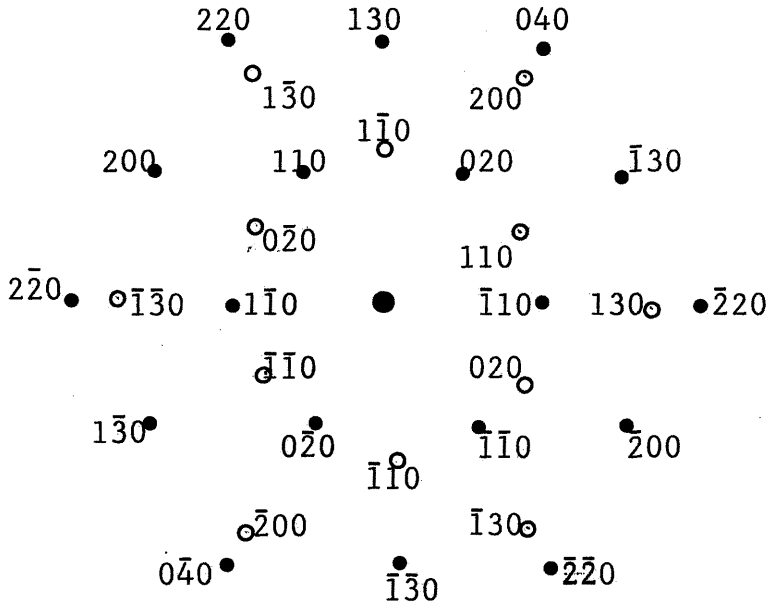

• Base sheet o Superimposed sheet

Fig. 6.68. Diffraction pattern of two superimposed muscovite sheets rotated by 0^{o} with respect to each other.

In the same diffraction pattern there are four very faint spots with separation 0.316 nm and equally spaced. If we assume the lattice parameter of CsCl is 0.45 nm then these spots are reflected from {110} set of planes in CsCl. This gives the [001] orientation of the overgrowth normal to the substrate surface and the spots due to the reflections from {100} set of planes in CsCl of

this orientation coincide with the spots rereflected from the substrate. The interplanar distances for $\{020\}$ and $\{110\}$ in muscovite are 0.452 nm and 0.448 nm respectively. So some nuclei of the deposit are well-oriented on the substrate surface with (001) of the overgrowth parallel to the (001) of the substrate and [010] of the overgrowth parallel to [010] of the substrate. The next nearest neighbour in the (001) plane of CsCl (assuming the lattice parameter of CsCl is 0.45 nm) is 0.45 nm which is half the distance between two potassium sites along the [010] direction on the surface network of muscovite. This orientation is shown in Fig. 6.69.

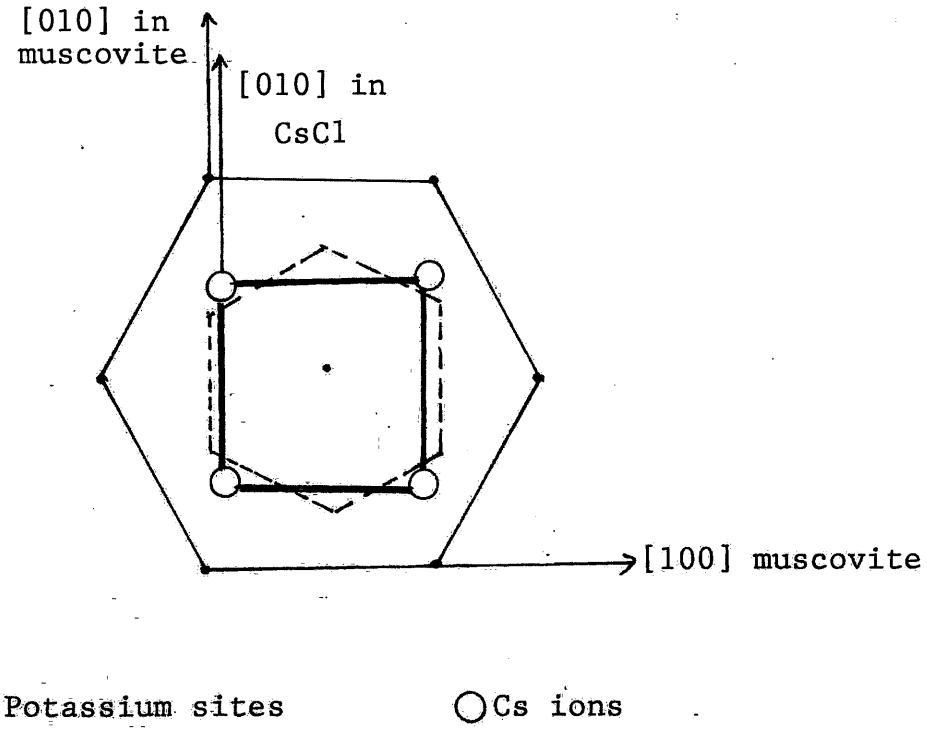

Fig. 6.69. A possible configuration of [001] orientation of CsCl on muscovite surface.

Fig. 6.70 (a)

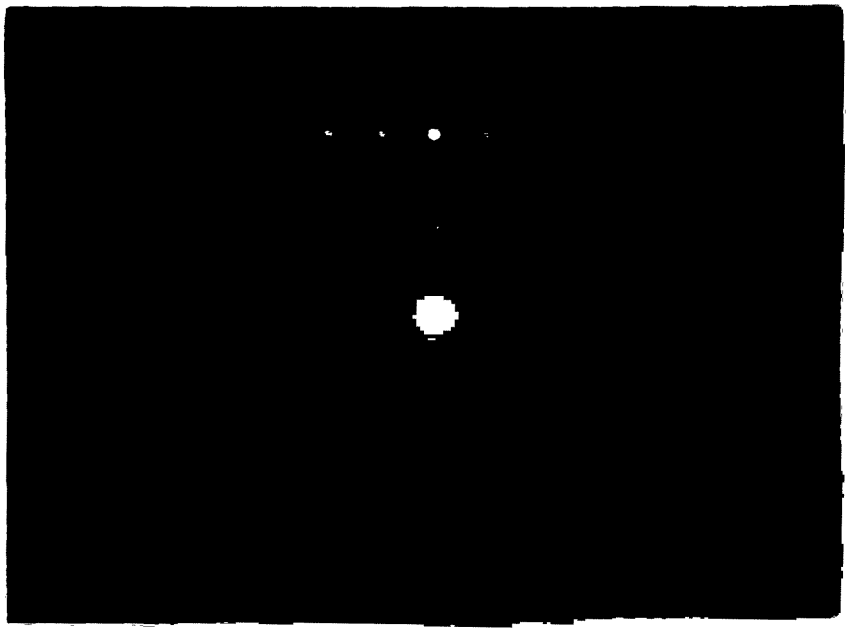

Fig. 6.70 (b)

Fig. 6.70 (a). Exposed deposit of CsCl grown on muscovite at room temperature.
(b) Its diffraction Pattern

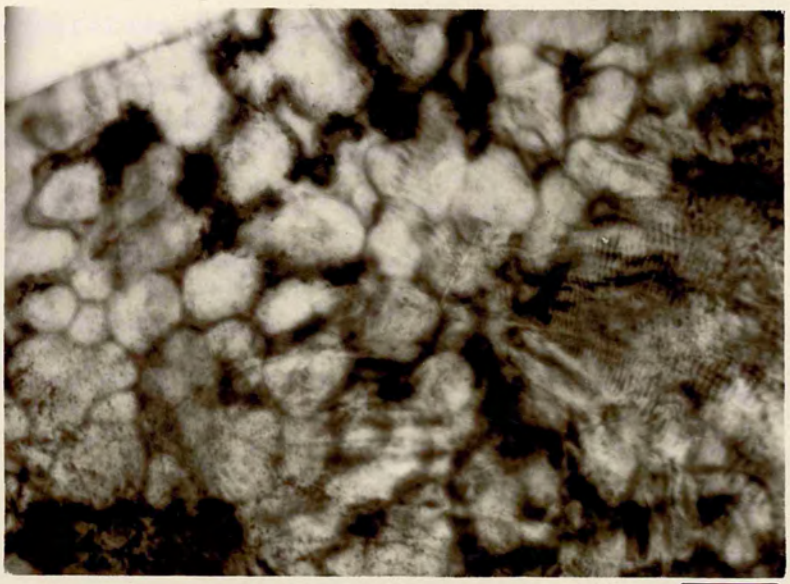

300nm

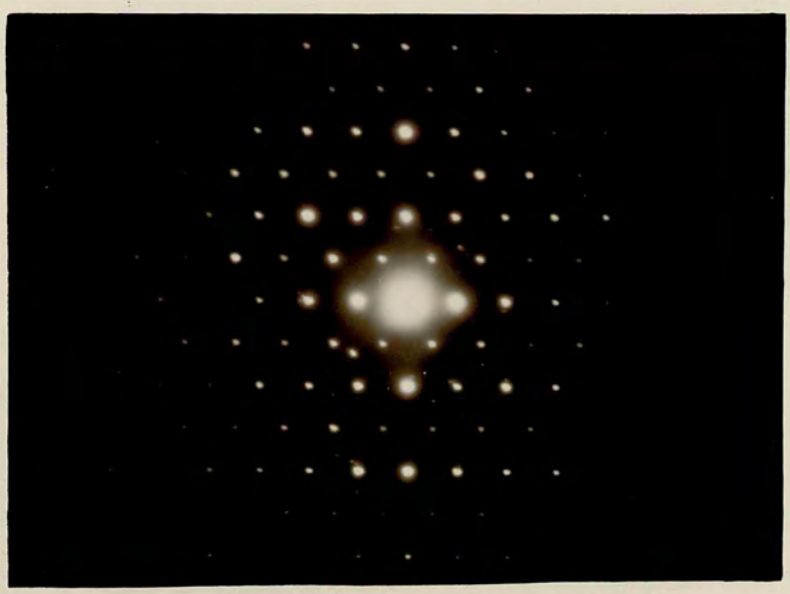

When the deposit of CsCl grown on muscovite at room temperature was exposed to the atmosphere and then examined in the electron microscope, it appear to form hexagonal-like network on the substrate surface (Fig. 6.70, a). During the cleavage process the potassium atoms which lie on the cleavage plane are randomly distributed to two separate sheets of mica. As these atoms are distributed in a hexagonal-like network on the surface, the deficiency may produce grooves on the surface. These grooves provide preferential sites for the overgrowth. There are large randomly oriented crystals of the overgrowth on the substrate surface as there is no ring observed in the diffraction pattern shown in Fig. 6.70 (b). There are few extra spots, it is difficult to determine a particular orientation.

6.5.5 CsBr on Biotite.

Fig. 6.71 shows a 10 nm thick deposit of CsBr grown on biotite at room temperature and examined in the electron microscope without exposure to the atmosphere. The deposit consists of very small nuclei situated randomly on the surface of the substrate, the size of the smallest nucleus being less than 5 nm. Most of these nuclei have coalesced and formed small clusters of average size between 10 nm and 30 nm. Some of these nuclei are square but they are not well-oriented on the substrate surface: its diffraction pattern shows a number of rings.

When the deposit of CsBr on biotite grown at room temperature is exposed to the atmosphere, it forms a large number of round clusters with sizes ranging from 250 nm to 750 nm (Fig. 6.72). These clusters are aligned in some pattern on the substrate surface, probably along steps or dislocation lines in the biotite which are not visible due to thicker substrate. Perhaps these clusters are formed on the lenticular flaws or bubles usually observed in the biotite (refer to Fig. 6.21 (a) and (b) in section 6.2). The thicker substrate produced high background intensity due to scatterd electrons in the diffraction pattern, it is difficult to locate any reflected spot. So the orientation of these clusters are not known.

The micrograph in Fig. 6.73 (a) is from a 10 nm deposit of CsBr grown on biotite at 200 °C and examined before the atmospheric exposure. The deposit consists of small clusters formed by the coalescence of nuclei and covering the whole substrate surface by forming a nearly polycrystalline continuous film as indicated by its diffraction pattern shown in Fig. 6.73 (b). Some double diffraction has also been observed around the more intense spots reflected from the substrate. This is due to the overgrowth on the bottom side of the substrate and reflected electron beams from the substrate act as primary beams with respect to the overgrowth. In the diffraction pattern the rings correspond to $\{110\}$ and $\{211\}$ sets of planes of the overgrowth are more intense which indicates a weak [111] orientation normal to the substrate surface.

Fig. 6.71

Fig. 6.72

Fig. 6.71. Unexposed deposit of CsBr grown on biotite at room temperature (thickness = 10 nm).

Fig. 6.72. Exposed deposit of CsBr grown on biotite at room temperature.

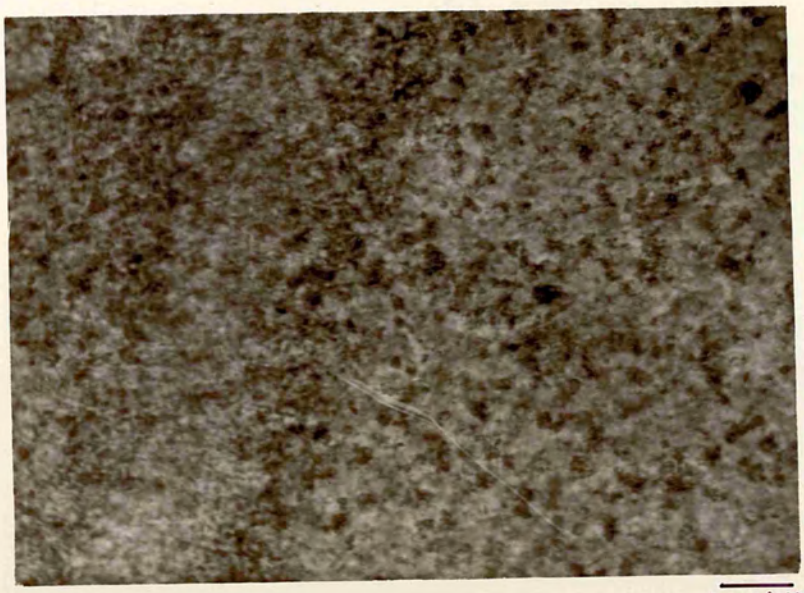

200nm

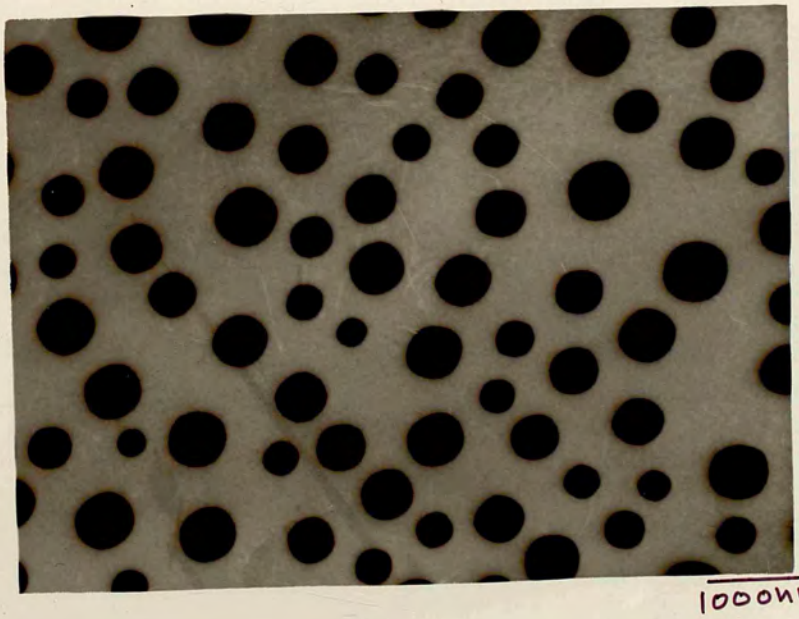

1000nm

Fig. 6.73 (a)

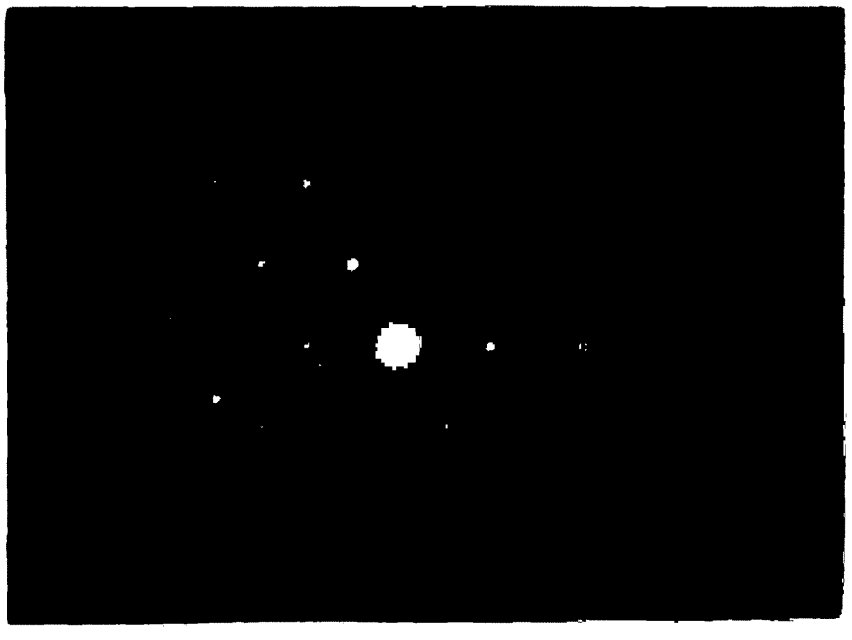

Fig. 6.73 (b)

Fig. 6.73 (a). Unexposed deposit of CsBr grown on biotite at 200 °C. Deposit thickness ≅ 10 nm.

(b). Its diffraction pattern.

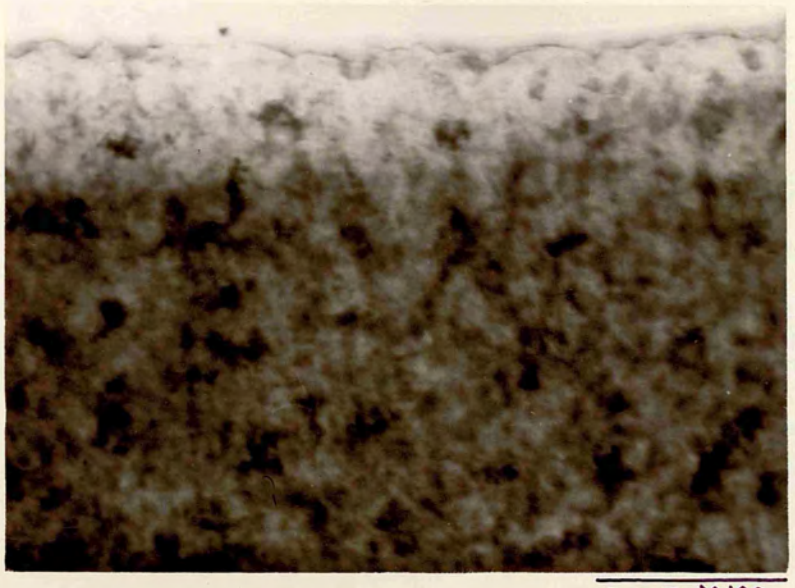
200 nm

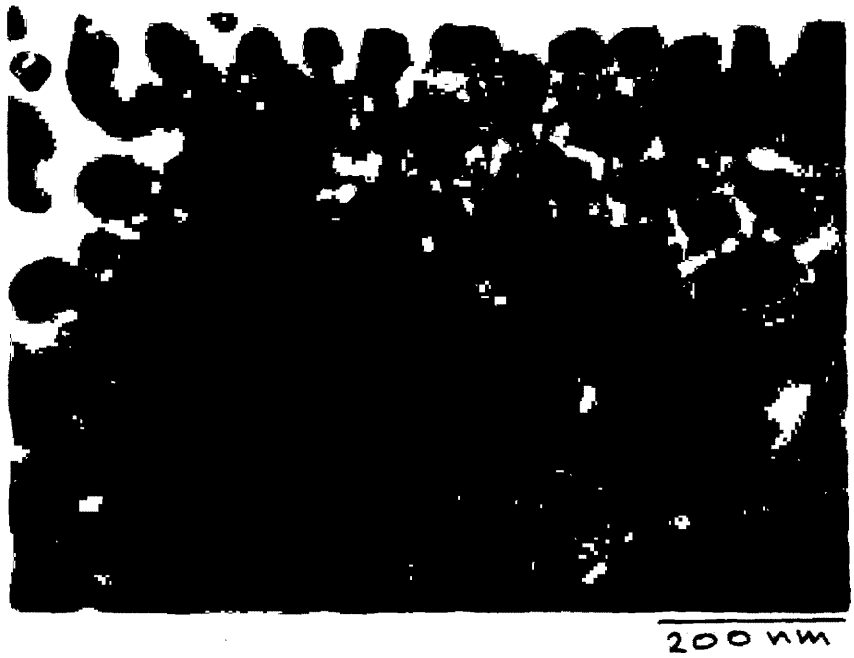

Fig. 6.74 (a)

Fig. 6.74 (b)

Fig. 6.74 (a). Exposed deposit of CsBr grown on biotite at 200 °C. Deposit thickness≅ 10 nm and exposure time 10 minutes. (b). Its diffraction pattern.

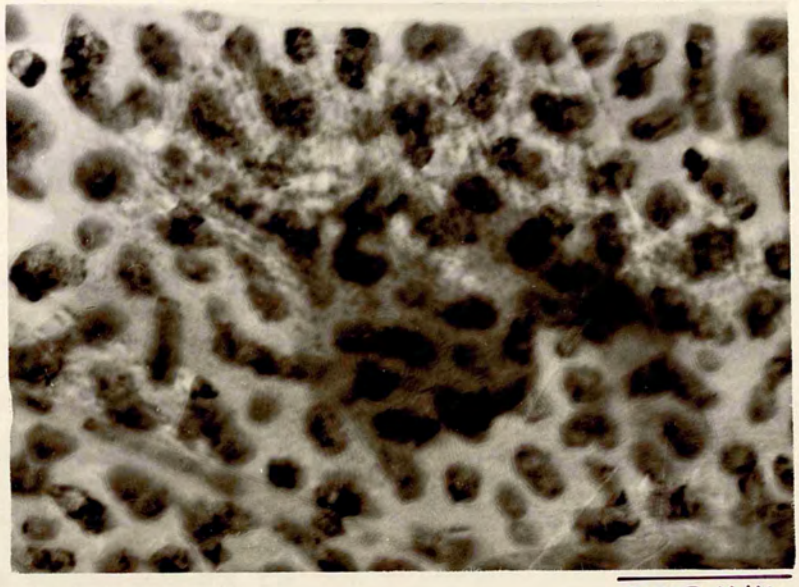
200 nm

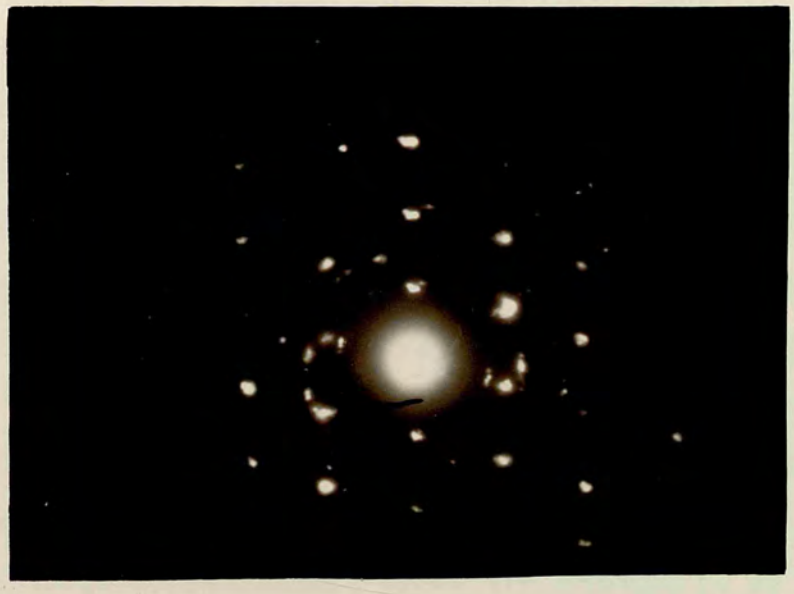

When a 10 nm deposit of CsBr on biotite grown at 200 °C was exposed to the atmosphere for 10 minutes, it formed a large number of clusters as shown in the micrograph of Fig. 6.74 (a). Most of these clusters have either square or rectangular shape and are oriented on the substrate surface. There are some extra spots along some rings in the diffraction pattern shown in Fig. 6.74 (b). They are probably due to the small nuclei which might be undissolved during exposure to the atmosphere. The possible orientation which observed by indexing the more intense spots belong to the overgrowth is [001] normal to the substrate surface.

6.5.6 CsBr on Muscovite.

The deposits of CsBr on muscovite are quite different from those of the other halides of caesium on muscovite and CsBr on biotite. Fig. 6.75 (a) shows a micrograph of a 10 nm thick deposit of CsBr, grown on muscovite at room temperature, before exposure to the atmosphere. The deposit consists of small crystallites with a veriety of shapes and sizes, and most of them aligned along the step structure on the substrate surface. The size of the smallest crystallite is less than 8 nm, and the large crystallites, which are assumed to be formed either by coalescence of the small crystallites or by multilayer condensation on the previous one, have dimensions ranging between 30 nm and 90 nm.

The shapes of these crystallites which have been observed in the micrograph are triangular, square and rectangular. Some of these crystallites have not possesed any particular shape, in other words they are deformed, probably due to the growth of two crystallites on each other with different shapes, because some parts of these crystallites are thicker than the others.

These crystallites are well-oriented on the substrate surface as there is no ring observed in the diffraction pattern shown in Fig. 6.75 (b). The substrate in this diffraction pattern is normal to $[3\bar{4}1]$ and nearest six spots to the centre have separations 0.428 nm, 0.430 nm and 0.434 nm, which are very near to the lattice parameter of CsBr, 0.429 nm. So it can be assumed that spots belong to the overgrowth coincide with the spots from the substrate.

When a 50 nm thick deposit of CsBr grown on muscovite at room temperature was exposed to the atmosphere for about 20 minutes, the deposit absorbed water from the atmosphere and formed solution. During recrystallization in the microscope the overgrowth formed large dendritic crystals as shown in Fig. 6.76. The dendrites are usually formed by rapid growth in a supersaturated solution as discussed in chapter 2. The deposit with 50 nm thickness has sufficient material to form a concentrated solution on the surface of the substrate during exposure to the atmosphere. During the evacuation of the electron microscope, water evaporated

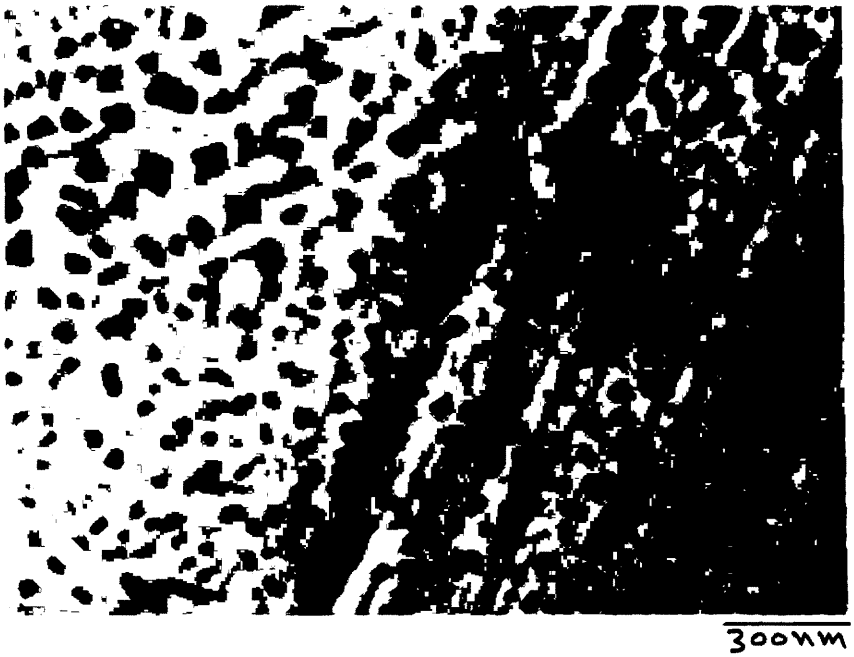

Fig. 6.75 (a)

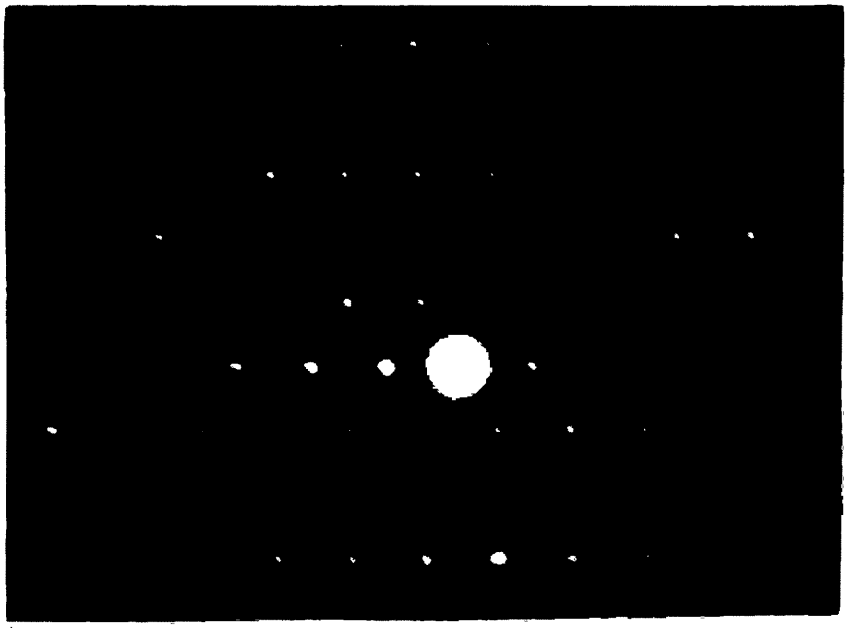

Fig. 6.75 (b)

Fig. 6.75 (a). Unexposed deposit of CsBr grown on muscovite at room temperature (thickness = 10 nm).

(b). Its diffraction pattern.

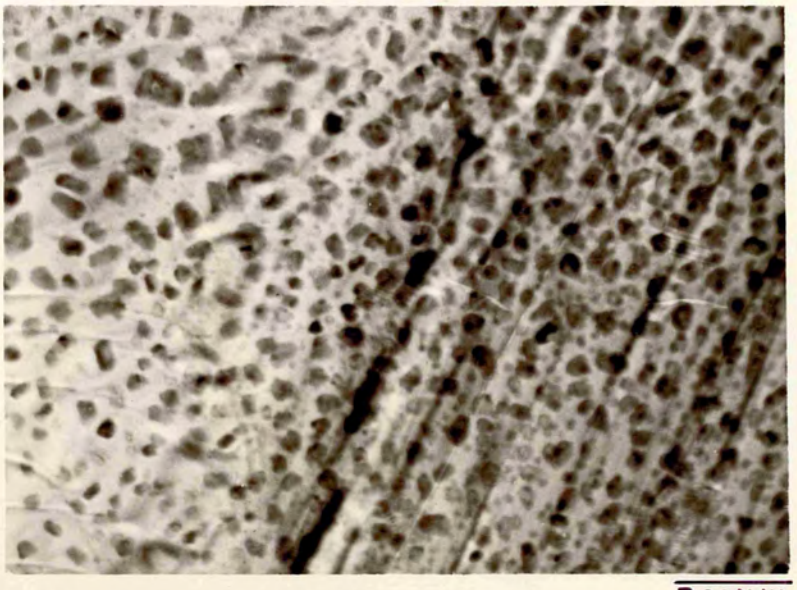

300nm

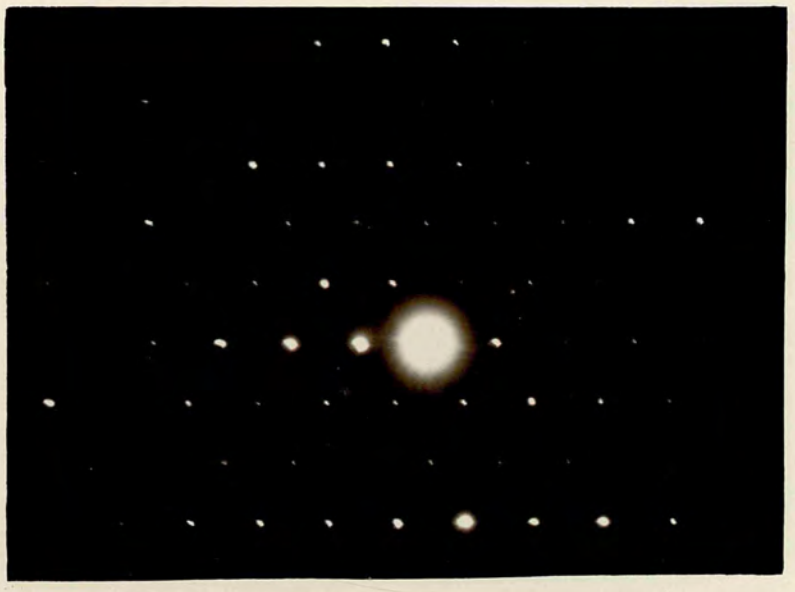

Fig. 6.76

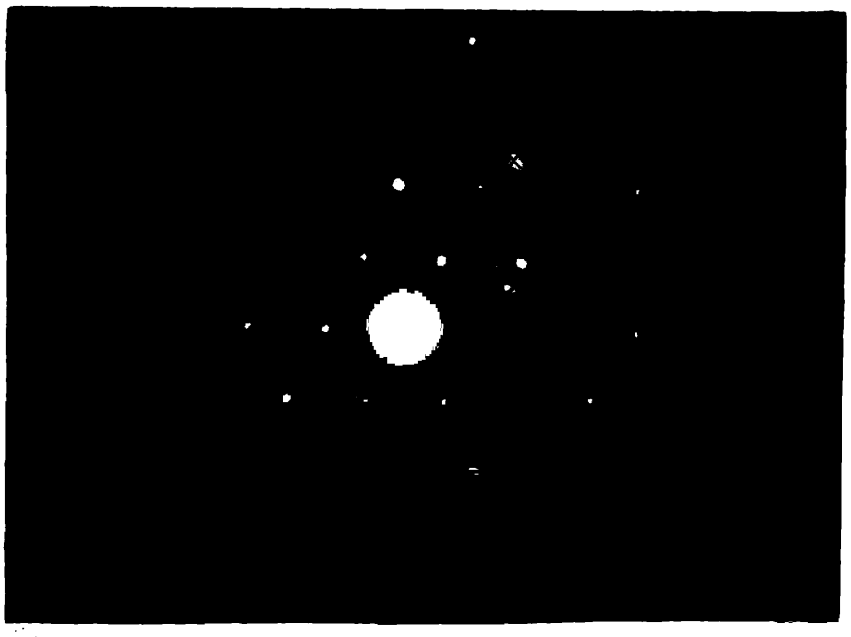

Fig. 6.77

Fig. 6.76. Dendritic crystals were formed when a 50 nm deposit of CsBr grown on muscovite at room temperature was exposed to the atmosphere for 20 minutes.

Fig. 6.77. Diffraction pattern from an exposed deposit of CsBr on muscovite at room temperature.


2000 nm

very rapidly and the substance crystallized in the form of dendrites. These crystals are very thick and opaque to the electrons, so it is nearly impossible to obtained a diffraction pattern in the transmission mode. Therefore their orientation is not known.

However, the crystals formed by recrystallization from evaporated CsBr on muscovite are oriented as indicated by the diffraction pattern in Fig. 6.77. This diffraction pattern is from a thin deposit of CsBr which was exposed to the atmosphere for 10 minutes. The spots belonging to the overgrowth are reflected by $\{110\}$ and $\{211\}$ planes so the orientation should be [111] normal to the substrate surface. Some extra spots in the diffraction pattern, which are not on any geometrical line, indicate that there are some misoriented fragments in the overgrowth, possibly might be the undissolved crystallites of the overgrowth.

Fig. 6.78 (a) shows a 20 nm thick deposit of CsBr grown on muscovite at 200 °C and examined without exposure to the atmosphere. The overgrowth formed large square and rectangular-shaped islands all over the substrate surface. The film of the overgrowth is damaged by the electron irradiation and shows granularity on the surface of the islands. This produces extra spots in the diffraction pattern as shown in Fig. 6.78 (b). Some intense spots belonging to the overgrowth indicate a weak [111] orientation of the overgrowth normal to the substrate surface.

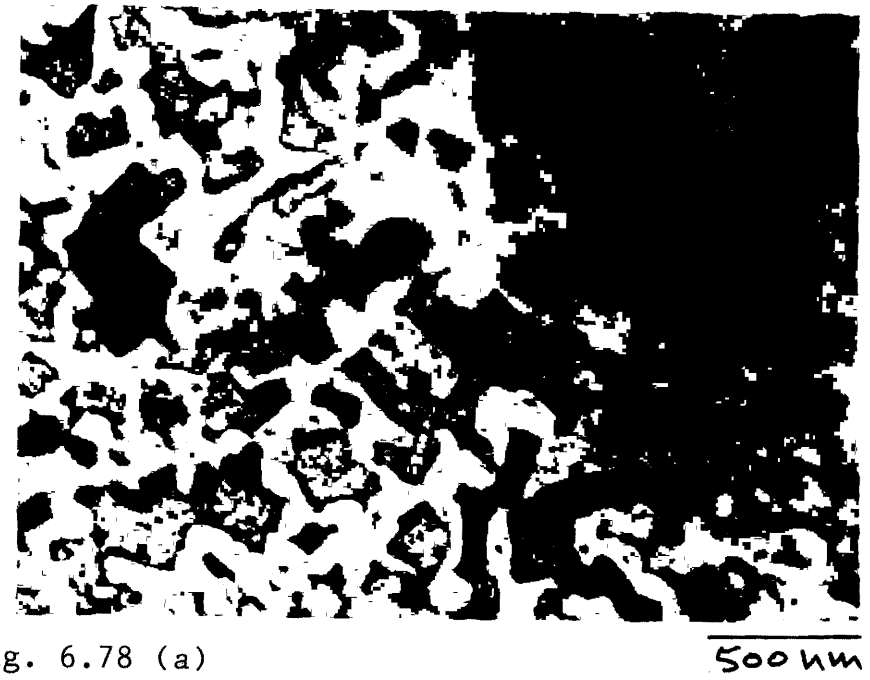

Fig. 6.78 (a)

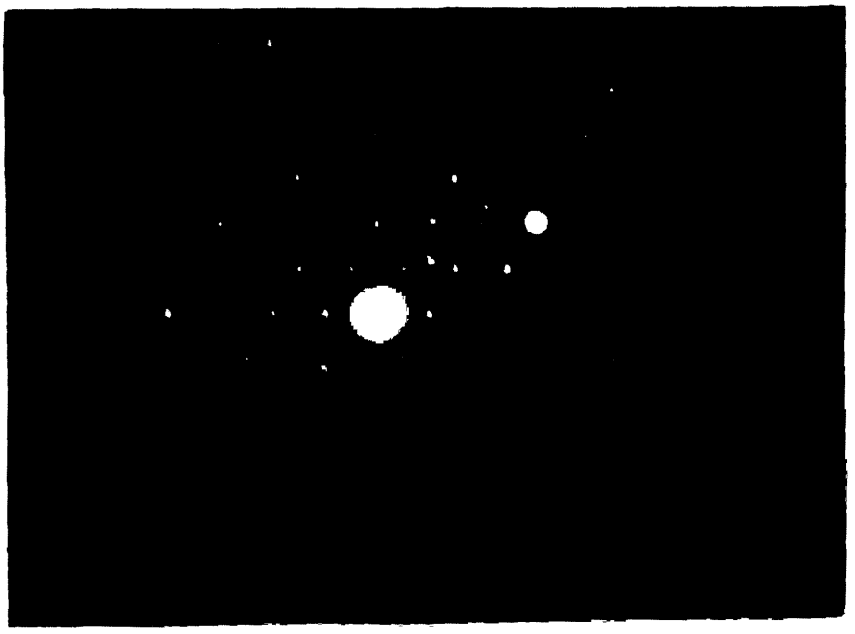

Fig. 6.78 (b)

Fig. 6.78 (a). Unexposed deposit of CsBr grown on muscovite at 200 °C (thickness = 20 nm). (b). Its diffraction pattern.

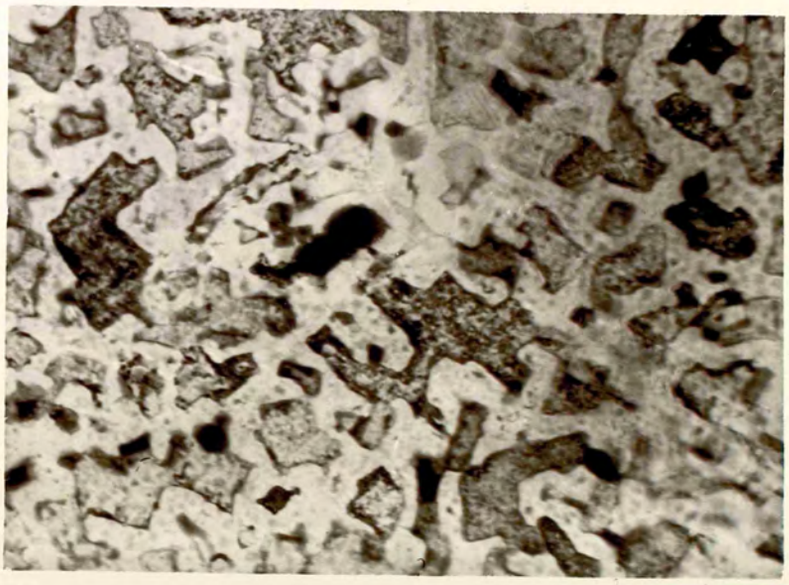

500 nm

6.5.7 CsF on Biotite.

CsF crystallizes with coordination number of six (NaCl structure) in contrast with the other caesium halides i.e., CsCl, CsBr and CsI, which adopt the CsCl structure with coordination number of eight. The lattice parameter of CsF is 0.601 nm with Cs-F contact distance is 0.300 nm. Fig. 6.79 (a) shows a thin deposit (thickness $\simeq$ 5 nm) of CsF grown on biotite at room temperature and observed before exposure to the atmosphere. The deposit consists of very small crystallites which seem to be oriented on the substrate surface as there are no rings observed in the diffraction pattern shown in Fig. 6.78 (b).

The micrograph in Fig. 6.80 (a) is from an unexposed deposit of CsF grown on biotite at 170°C. It consists of small clusters distributed over the substrate surface. Its diffraction pattern (Fig. 6.80, b) shows spots and arcs other than the reflections from the substrate. The pattern is reconstructed in Fig. 6.81. From indexing the pattern it is observed that the biotite is normal to [001] with nearest six spots to the centre have separation (interplanar distance) 0.46 nm and 0.454 nm which reflected from $\{020\}^*$ and $\{110\}^*$ planes respectively.

---

* $\{020\}$ set of planes in a monoclinic system has only (020) and $(0\bar{2}0)$ planes, and $\{110\}$ has (110), $(1\bar{1}0)$, $(\bar{1}10)$ and $(\bar{1}\bar{1}0)$ planes .

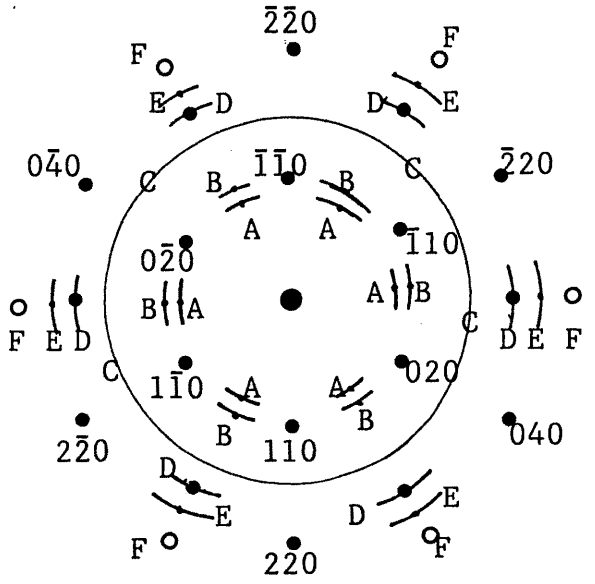

• Spots due to the reflection from the substrate,

{ arcs with spots in the middle,

o spots from the {220} set of planes of CsF.

Fig. 6.81. Reproduction of the diffraction pattern of Fig. 6.80 (b).

All the reflections from the substrate are marked with dots. All other arcs and spots should be reflected from the overgrowth. The nearest six arcs to the centre, A, are evenly spaced between the spots from the substrate and have a separation of 0.5 nm, while the second nearest six arcs, B, have 0.43 nm. The faint circle, C, which also has some intense arcs has a separation 0.31 nm. Faint arcs, D, coincident with the second nearest six spots of substrate, are separated by 0.26 nm. The arcs marked with E, indication interplaner distance of 0.23 nm and those spots marked with F, have less streak along them and indicate a

separation 0.21 nm. As stated earlier CsF with Na-Cl structure (fcc) has lattice parameter 0.601 nm: the d-spacing for some of the planes in a cubic system is given in Table 6.4.

Table 6.4

h k l	d-spacing (nm)
1 0 0 *	0.601
1 1 0 *	0.424
1 1 1	0.346
2 0 0	0.300
2 1 0 *	0.268
2 1 1 *	0.245
2 2 0	0.212

(The planes marked with, *, do not give reflection in fcc system)

From these calculations it is clear that the six spots marked with F in Fig. 6.82 are reflected from $\{220\}$ set of planes, they are evenly spaced (60° from each other) and more intense than other reflections from the overgrowth. This gives a strong [111] orientation of the overgrowth normal to the substrate surface with (111) plane of the overgrowth parallel to the (001) plane of the substrate and $[1\bar{1}0]$ of the overgrowth parallel to the [100] of the substrate. This orientation is shown in Fig. 6.82.

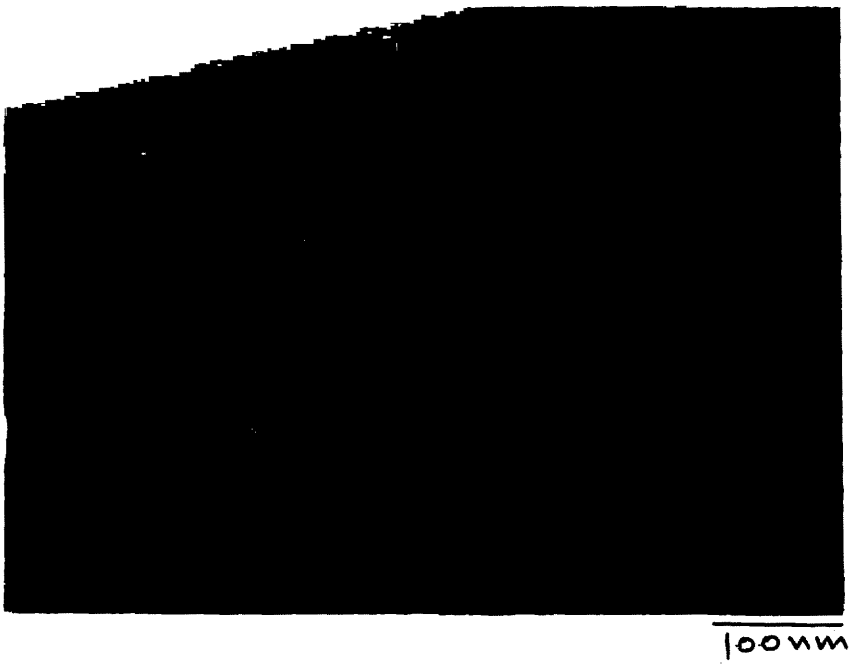

Fig. 6.79 (a)

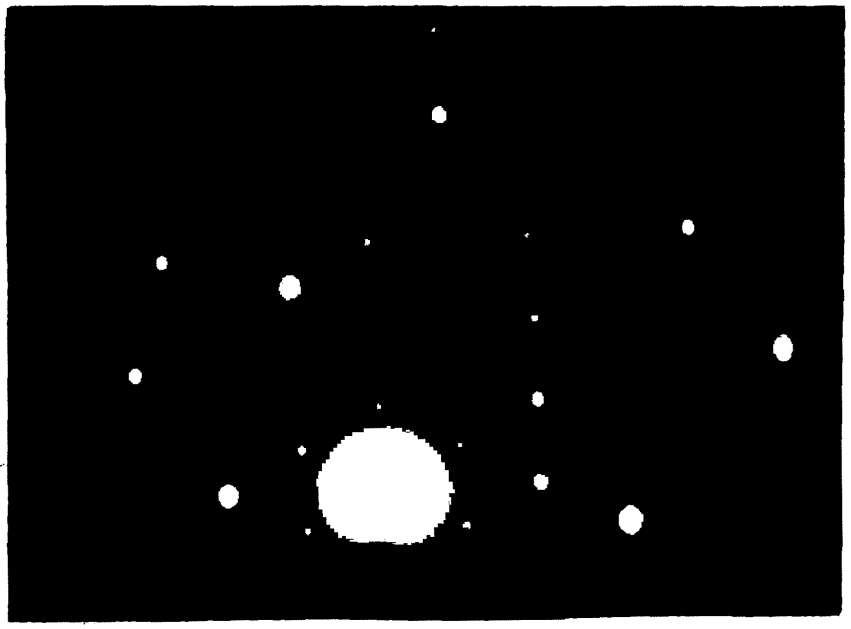

Fig. 6.79 (b)

Fig. 6.79 (a). Unexposed deposit of CsF grown on biotite at room temperature (thickness = 5 nm).
(b). Its diffraction pattern.

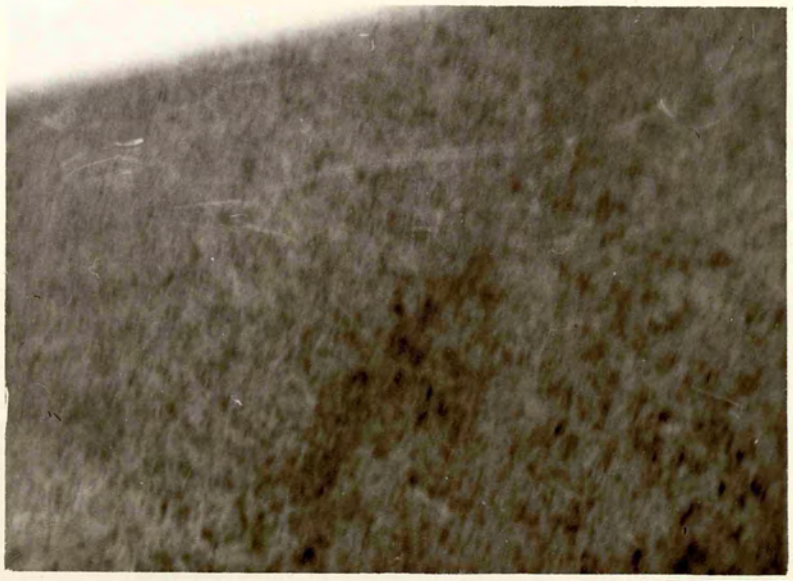

100nm

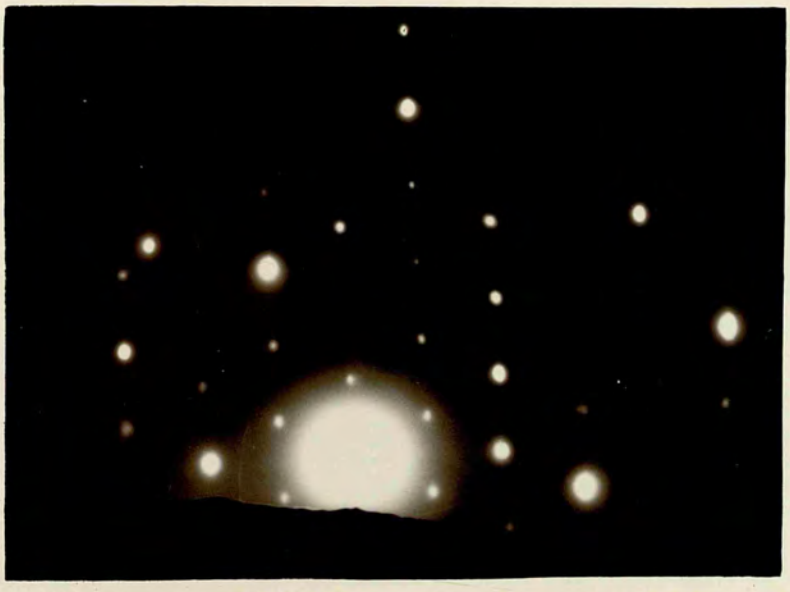

Fig. 6.80 (a)

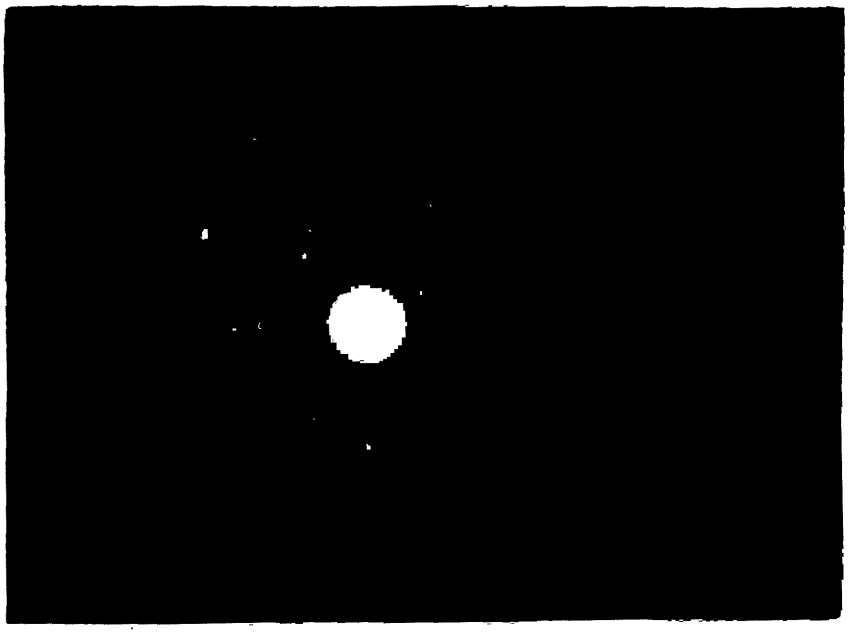

Fig. 6.80 (b)

Fig. 6.80 (a). Unexposed deposit of CsF grown on biotite at 170 °C (thickness = 10 nm).

(b). Its diffraction pattern.

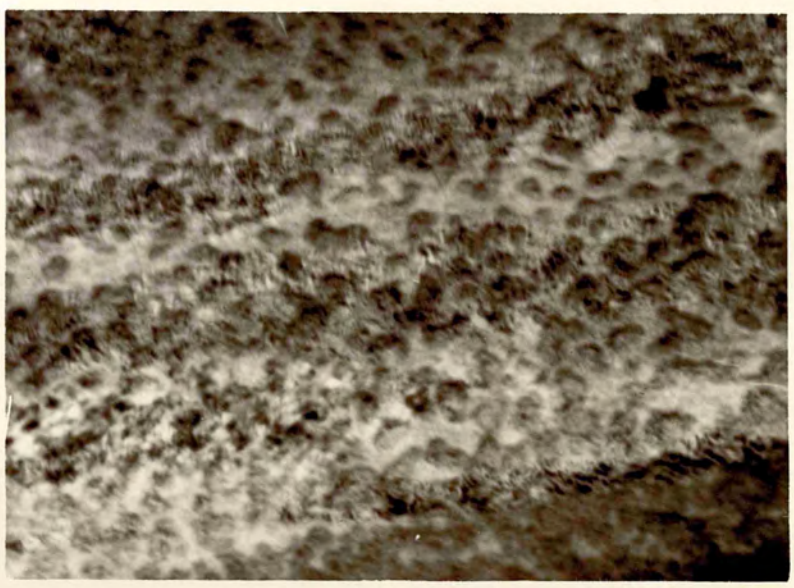

200 nm

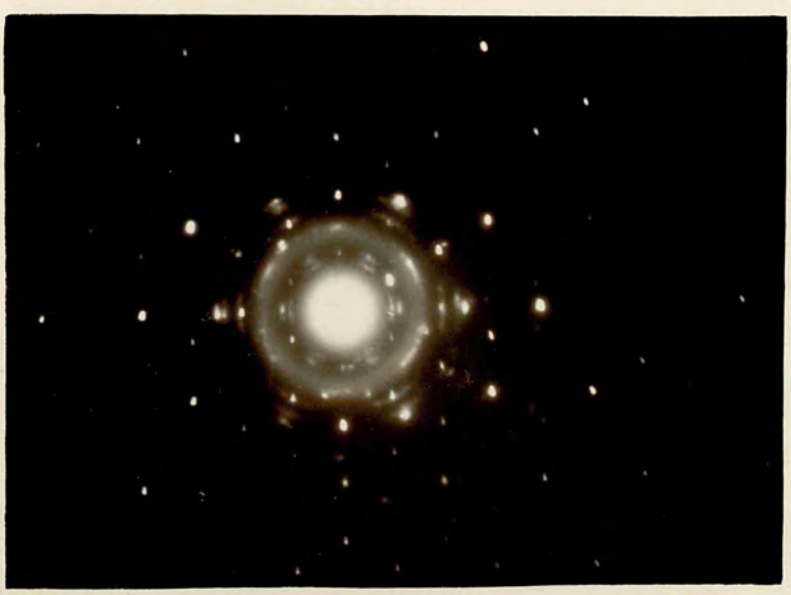

317

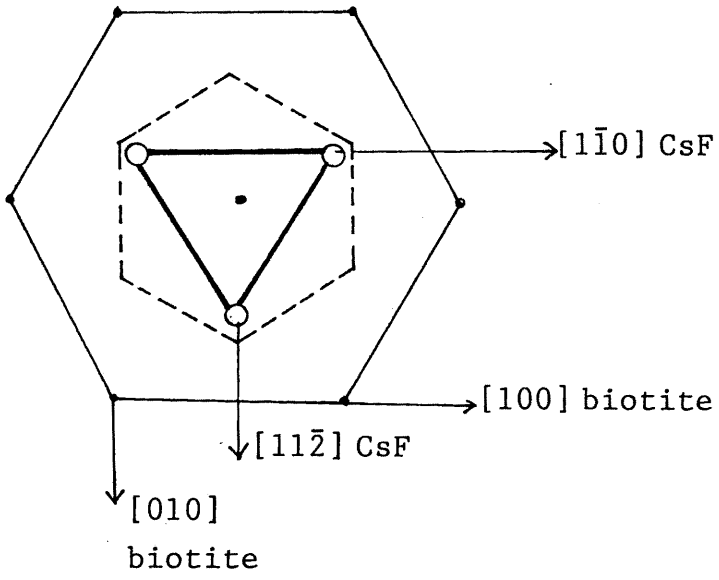

• Potassium sites ○ CsF ions

Broken lines show the silicon network and thick lines show the sides of CsF (111) plane.

Fig. 6.82. The possible configuration of [111] orientation of CsF on biotite.

The faint ring, C, due to the reflection from $\{200\}$ set of planes which indicates that there is some misoriented fragments of the overgrowth on the substrate surface. Other arcs do not correspond to any plane of CsF as fcc lattice structure; however, if CsF assumed to have a simple cubic lattice structure then arcs marked with B are from $\{110\}$ and those marked with E are from $\{211\}$ sets of planes. This gives the same [111] orientation as shown in Fig. 6.82.

The arcs marked with A and D do not belong to any possible plane in CsF, they are perhaps due to the presence of other material, formed by chemical reaction on the substrate surface. The (001) cleavage plane of mica consists potassium atoms which can react with the overgrowth and form KF.

Fig. 6.83 (a) shows a micrograph from a 10 nm deposit of CsF grown on biotite at 170 °C and exposed to the atmosphere for 5 minutes before being observed in the electron microscope. As CsF is highly hygroscopic, it dissolvesin the atmospheric moisture very rapidly. During exposure the deposit forms tiny droplets of solution on the substrate surface and recrystallizes in the electron microscope. The crystals formed during the recrystallization process look bright with dark edges and have a variety of shapes. The diffraction pattern (Fig. 6. 83, b) of this deposit is complicated so there is no recognizeable orientation. This means these crystals are randomly oriented on the substrate surface.

6.5.8 CsF on Muscovite.

Unexposed deposits of CsF grown on muscovite at room temperature consists of small clusters situated randomly on the substrate surface (Fig. 6.84). However, in its diffraction pattern some spots belonging to the overgrowth are reflected from $\{220\}$ set of planes and give a [111] orientation of the overgrowth normal to the substrate surface.

Fig. 6.83 (a)

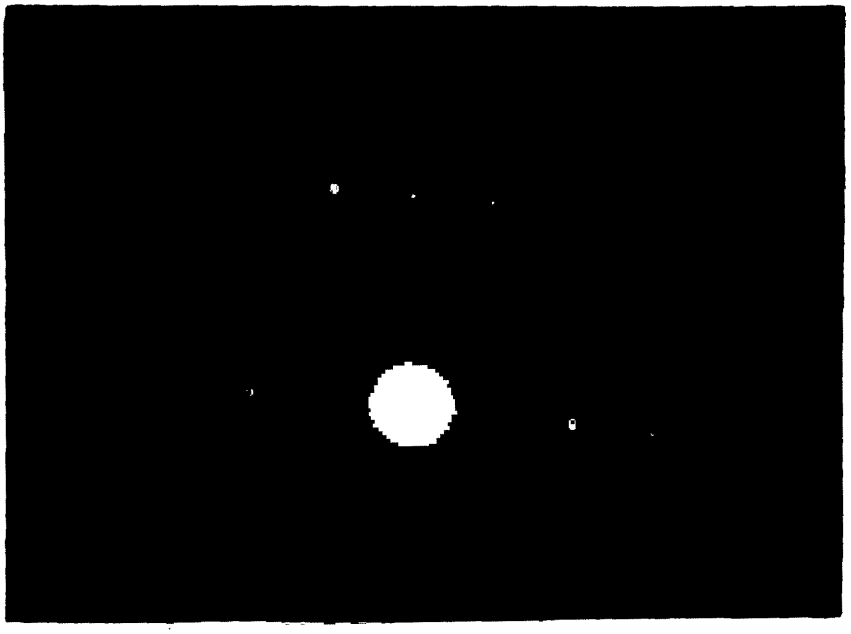

Fig. 6.83 (b)

Fig. 6.83 (a). Exposed deposit of CsF grown on biotite at 170 C. Deposit thickness ≅ 10 nm and exposure time 5 minutes. (b). Its diffraction pattern.

100 nm

Fig. 6.85 (a) shows an unexposed deposit of CsF grown on muscovite at 200 °C. It consists of very small crystallites or clusters situated randomly on the substrate surface as indicated by the diffraction pattern shown in Fig. 6.85 (b). Some intense spots along the rings are reflected from $\{111\}$, $\{220\}$ and $\{311\}$ sets of planes and give a [112] orientation of the overgrowth normal to the substrate surface. In this orientation the (112) plane of the overgrowth is parallel to the (001) plane of the substrate and $[\bar{1}10]$ of the overgrowth parallel to the [100] of the substrate.

The directions in a (112) plane of a cubic crystal is shown in Fig. 6.86 and the [112] orientation on the mica surface is shown in Fig. 6.87.

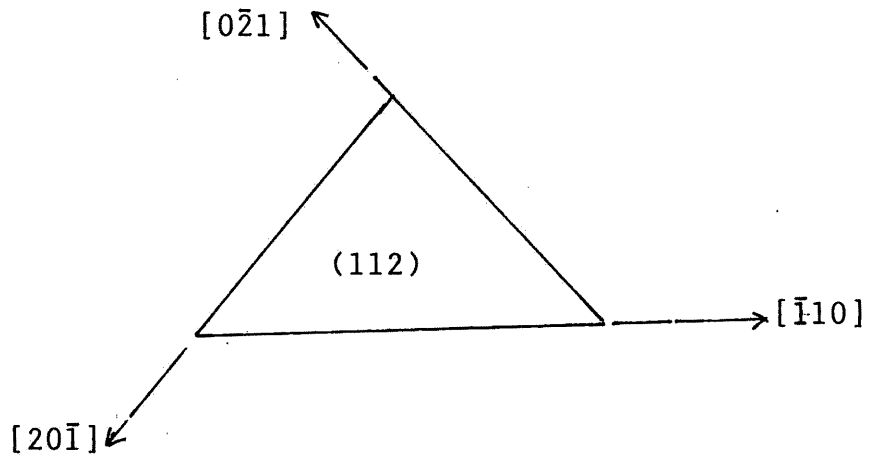

Fig. 6.86. Directions in a (112) plane of a cubic crystal.

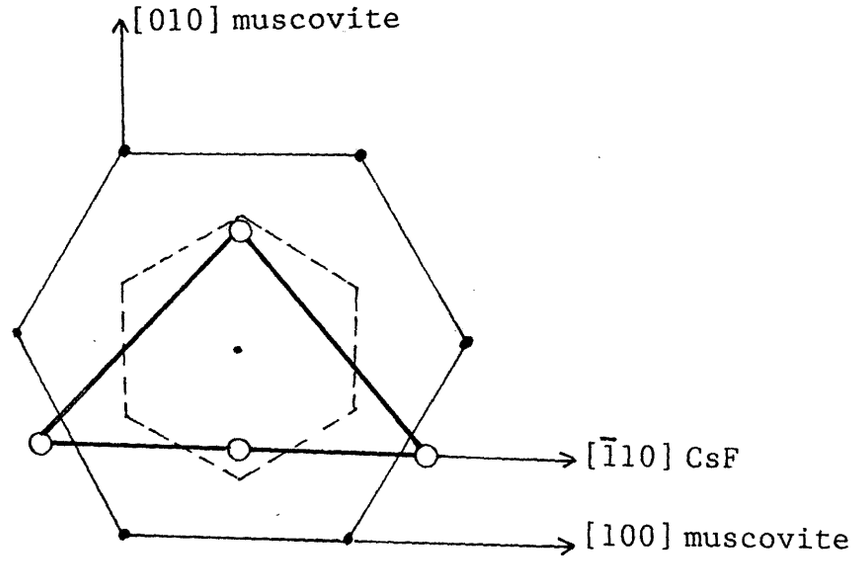

• Potassium sites O CsF ions

Broken lines show the silicon network and thick lines show the sides of (112) plane.

Fig. 6.87. The possible configuration of the [112] orientation of CsF on muscovite.

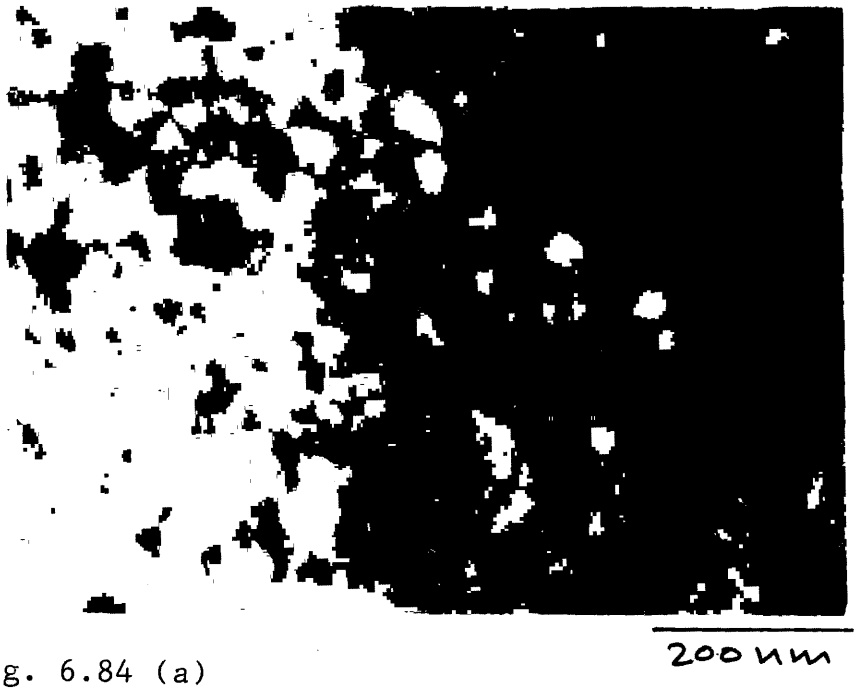

Fig. 6.84 (a)

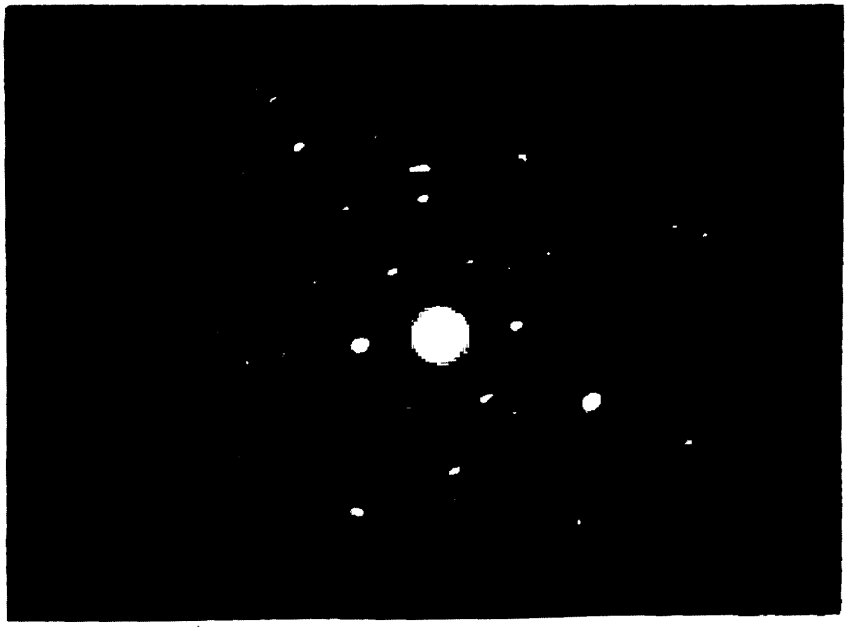

Fig. 6.84 (b)

Fig. 6.84 (a). Unexposed deposit of CsF grown on muscovite at room temperature.

(b). Its diffraction pattern.

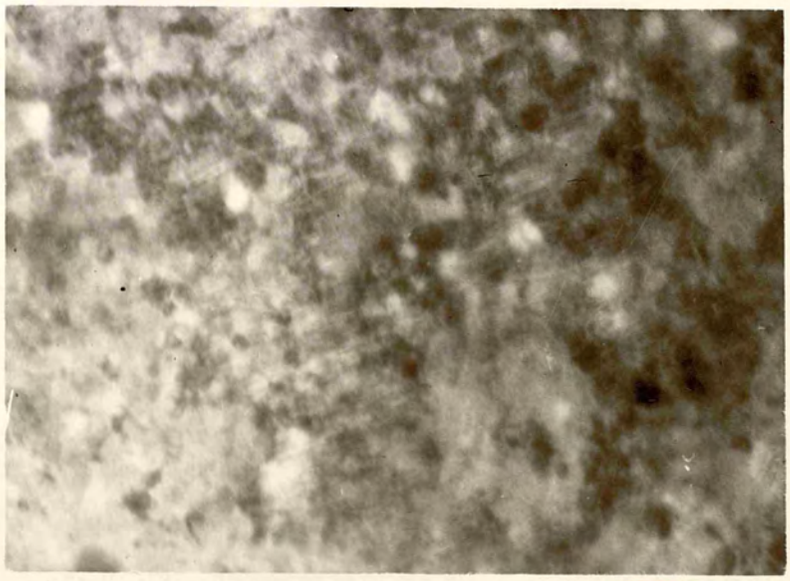

200 nm

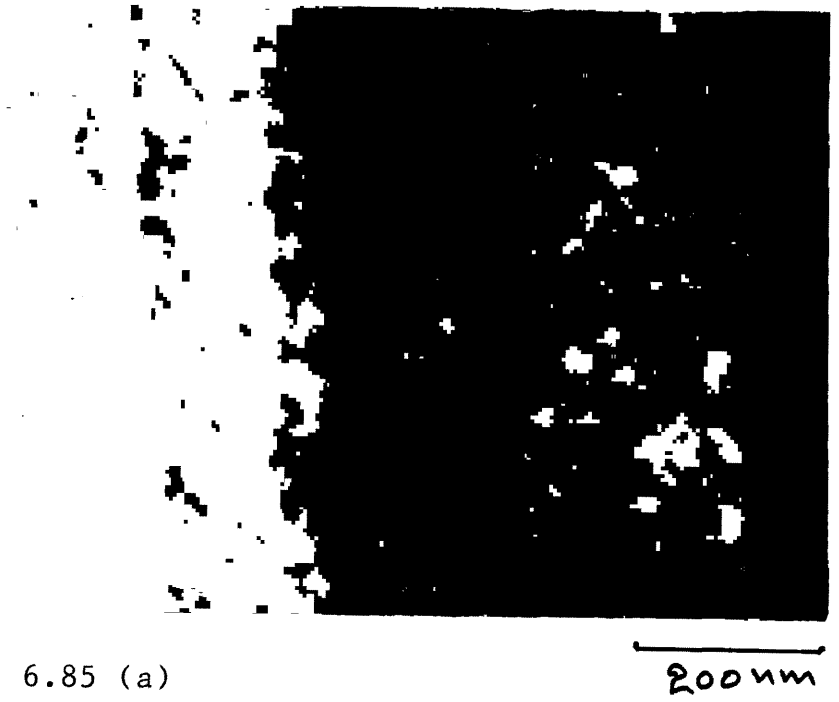

Fig. 6.85 (a)

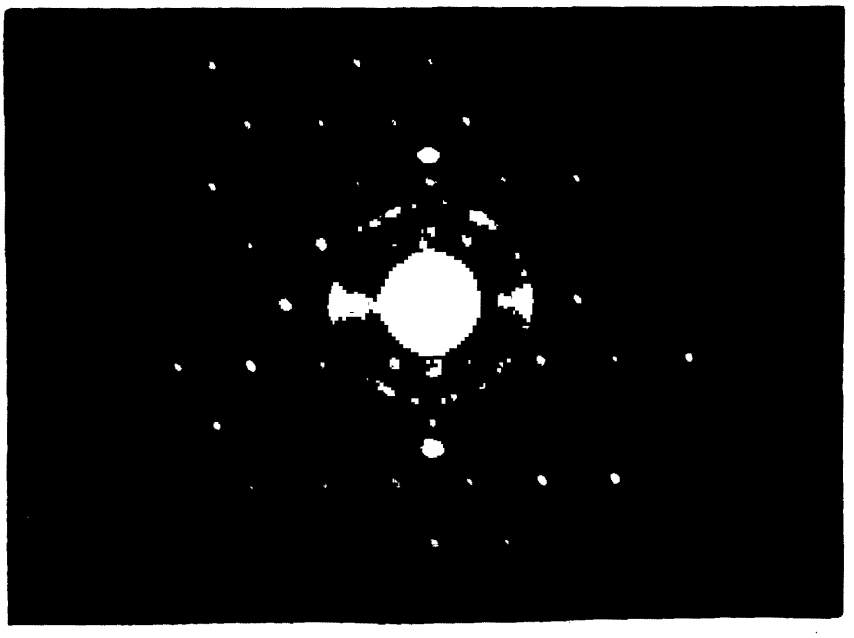

Fig. 6.85 (b)

Fig. 6.85 (a). Unexposed deposit of CsF grown on muscovite at 200 °C.

(b). Its diffraction pattern.

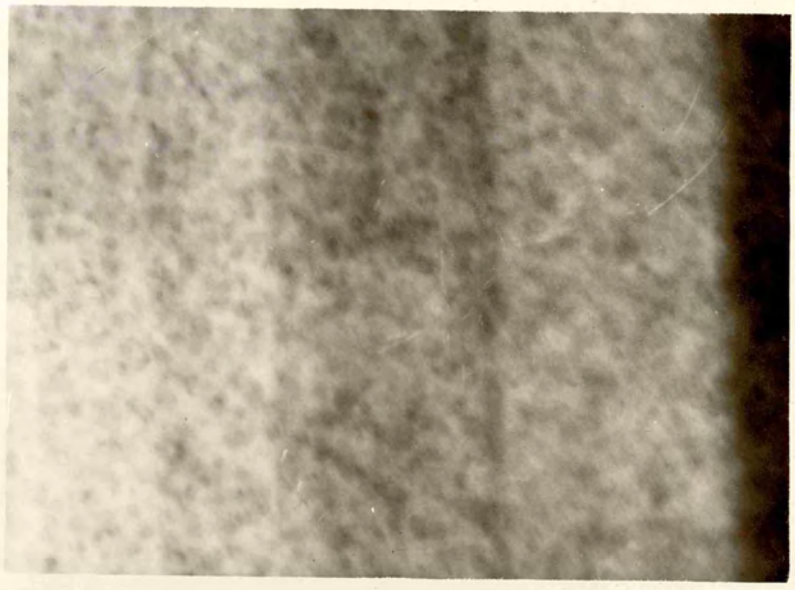

200nm

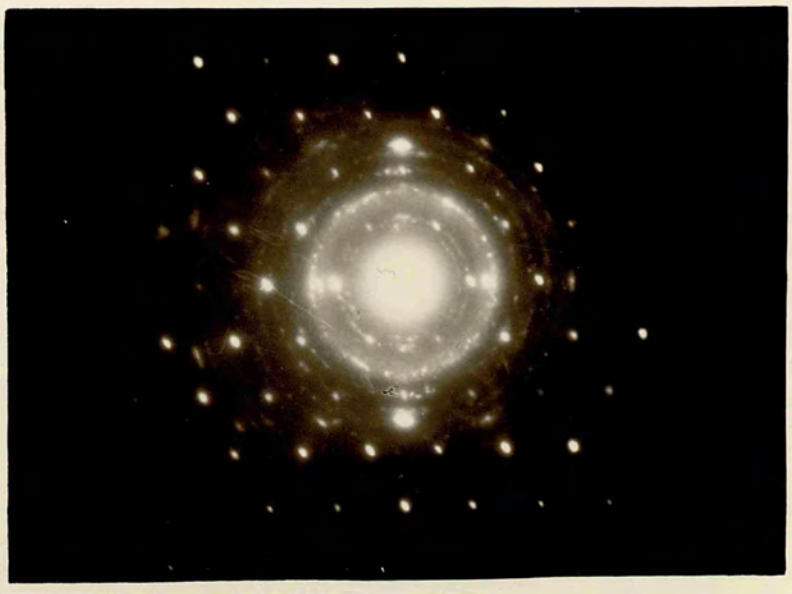

6.6 Conclusion.

The foregoing studies of the nucleation and growth of alkali halides from the vapour phase and from solution (exposed deposit) on to mica have produced the following conclusions:

1. Muscovite and biotite are good substrates for in situ studies of alkali halides due to their properties of perfect cleavage at {001}, transparency to electrons and smooth flat surfaces (as revealed by gold decoration).
2. The growth of alkali halides from the vapour phase on mica is similar to the growth of metals on alkali halides: they grow through the formation of small coalesced nuclei or clusters to produce an island-structured film.
3. Unexposed deposits of CsI, CsCl, CsBr and CsF grown on biotite at room temperature consist of small crystallites or clusters situated randomly on the substrate surface. Similar deposits on muscovite formed small clusters, some of which have crystallographic shapes. These clusters are usually randomly oriented but some intense spots on the rings in their diffraction patterns represent weak [111] orientations normal to the substrate surface.
4. Exposed deposits of CsI and CsBr grown on biotite at room temerature formed large clusters and CsCl formed large single crystals. Similarly exposed deposits of

CsI, CsCl and CsF on muscovite consist of small clusters some of which have square or triangle shapes. CsBr sometimes formed dendritic crystals.

5. Unexposed deposits of CsI grown on biotite at 200 °C consist of large clusters. CsCl, CsBr and CsF form small crystallites or clusters situated randomly on the substrate surface. Similar deposits on muscovite formed clusters of different sizes (from 10 nm to 70 nm) and shapes with some orientation.
6. Exposed deposits of CsI and CsBr grown on biotite and muscovite at 150 °C - 200 °C formed island structure films. CsCl and CsF formed large clusters.
7. The orientations of the overgrowths on the (001) surface of the substrate, as indicated by their diffraction patterns are summarized in Table 6.5 and 6.6.

Table 6.5

The orientations* of alkali halides grown on biotite

over-growth	substrate temperature during growth ≅ 20 °C		substrate temperature between 150 °C and 200 °C	
	unexposed deposits	exposed deposits	unexposed deposits	exposed deposits
CsI	random	double [111] weak [001]	random and weak [111]	[111] weak [001]
CsCl	random	not recog-nizable	random	not recog-nizable
CsBr	random	---	random and weak [111]	[001]
CsF	random	---	[111]	---

Table 6.6

The orientations* of alkali halides grown on muscovite

over-growth	substrate temperature during growth ≅ 20 °C		substrate temperature between 150 °C and 200 °C	
	unexposed deposits	exposed deposits	unexposed deposits	exposed deposits
CsI	random and weak [111]	double [111] weak [001]	[110]	[001]
CsCl	random and weak [111]	[111] weak [001]	[001]	---
CsBr	random	weak [111]	random and weak [111]	[001]
CsF	random and weak [111]	---	random and [112]	---

* All orientations are normal to the substrate surface. Random and weak [ ] orientation means that there are rings in the diffraction pattern with some intense spots.

8. From these orientations it has been concluded that there is no significant difference between the deposits on biotite and on muscovite except that CsI and CsF grown at higher temperature give different orientations.

9. Heating the substrate before deposition does not improve the epitaxy but exposure to the atmosphere (growth from solution) after deposition causes orientation.
10. Two different orientations in the same deposit may occur, possibly due to chemical reaction between the overgrowth and surface atoms of the substrate. In other words chemical interaction is likely to be one of the factor causing epitaxial growth.

References

ALLPRESS,J.G. and SANDERS,J.V. (1967). Surface Sci. 7, 1.

AMELINCKX,S. (1952). Comp. Rend. Acad. Sci., 234, 971.

AMELINCKX,S. (1952). Nature, 169, 580.

AMELINCKX,S. and DELAVIGNETTE,P. (1961). Electron Microscopic Observation of Dislocations in Silicate Layer Structures (Kriegel and Palmour eds.), Interscience New York.

AMELINCKX,S. (1964). In "Solid State Physics", Supplement 6, 'The Direct Observation of Dislocation' p. 123, Academic Press London.

BANOS,J.O., AMOURIC,M.A., FOUQUET,C.De. and BARONNET,A. (1983). Amer. Mineral, 68, 754.

BARONNET,A. (1972 a). C.R. Acad. Sci. Paris. 274, 785.

BARONNET,A. (1972 b). Amer. Min. 57, 1272.

BARONNET,A., AMOURIC,M. and CHABOT,B. (1975). J. crystal Growth 32, 37.

BARONNET,A. (1975). Acta Cryst. A31, 345.

BASSETT,G.A. (1958). Phil. Mag. 3, 1042.

BAUER,E., (1956). Z. Kristallogr., 107, 72.

BRINDLEY,G.W. and BROWN,G. (1980). Crystal Structures of Clay Minerals and Their X-Ray Identification. Mineroligical society Monograph No. 5.

BRYANT,P.J. (1962). Trans. 9th Vac. Symp. of the AVS , p. 331, Macmillan New York.

BUTLER,E.P. (1979). Rep. Prog. Phys., 42, 833.

CARTZ,L. and TOOPER,B. (1965). J. Appl. Phys. 36, 2783.

CASLAVSKY,J.L. and VEDAM,K. (1970). Phil. Mag., 22, 255.

CORNY,F., BARONNET,A. and JOURDAN,C. (1976). J. Crystal Growth 34, 304.

DEER,W.A., HOWIE,R.A. and ZUSSMAN,J. (1962). Rock Forming Minerals. Vol. 3, Sheet Silicates. John Wiley and Sons, Inc. New York.

DEICHA,G. (1946). C. R. Acad. Sci. 223, 1155.

DEMNY,J. (1963). Z. Naturforsch. 18a, 1088.

DEMNY,J. (1963). Z. Naturforsch. 18a, 1097.

EGERTON,R.F. (1970). Thin Solid Films 5, R41.

FOSTER,M.D. (1960). U.S. Geol. Surv. prof. Pap. 354-E, 115.

GAINES,G.L. and TABOR,D. (1956). Nature, 178, 1304.

GAINES,G.L. and VEDDER,W. (1964). Nature, 201, 495.

GREEN,M. (1971). Surface Sci. 26, 549.

GRUNBAUM,E. (1975). In "Epitaxial Growth" part B (Matthews ed.), p. 665, Academic Press New York.

von HARRACH,H. (1974). Thin Solid Films, 22, 305.

HEIDENREICH,R.D. (1949). J. App. Phys. 20, 993.

HEINRICH,E.W. and LEVINSON,A.A., (1953). Amer. Min., 38, 25.

HEINRICH,E.W., LEVINSON,A.A., LEVANDOWSKI,D.W. and HEWITT,C.H. (1953). University of Michigan Engineering Research Institute project M.978; final report.

HENDRICKS,S.B. and JEFFERSON,M., (1939). Amer. Min., 24, 729.

HIGGINBOTHAM,I.G., WILLIAMS,R.H. and McEVOY,A.J. (1975). J. Phys. D: Appl. Phys., 8, 1033.

IIJIMA,S. and BUSECK,P.R. (1978). Acta Cryst. A34, 709.

JACKSON,W.W. and WEST,J., (1930). Zeit. Krist., 76, 211.

JACKSON,W.W. and WEST,J., (1933). Zeit. Krist., 85, 160.

KOCH,F.A. and VOOK,R.W., (1971). J. Appl. Phys. 42, 4510

KOCH,F.A. and VOOK,R.W. (1972). Thin Solid Films 14, 231.

LEVINSON,A.A. (1953). Amer. Mineral. 38, 88.

LISGARTEN,N.D. (1954). Trans. Faraday. Soc. 50, 684.

MAUGUIN,C. (1927). Comp. Rend. Acad. Sci., 185, 288.

MAUGUIN,C. (1928). Bull Soc. Franc. Min., 51, 285.

METSIK,M.S. (1958). Sovit Phys. Cryst. 3, 92.

MISSIROLI,G.F. (1972). Thin solid Films 12, S35.

MULLER,K. and CHANG,C.C. (1968). Surface Sci. 8, 455.

PASHLEY,D.W. (1965 a). Advan. Phys. 5, 174.

PAULING,L., (1930). Proc. Nat. Acad. Sci., 16, 123.

RABBIT,L.I., HAMPSHIRE,M.J., TOMLINSON,R.D. and CALDERWOOD,J.H. (1971). Conduction in Low-Mobility matter., Proc. 2nd., Int. Conf. Eilat, Israel 1971 (Klein and Tannhauser eds.), 419. Taylor and Francis, London.

RADOSLOVICH,E.W., (1960). Acta Cryst., 13, 919.

RANGE,O. (1953 a). Optik 10, 90.

RANGE,O. (1953 b). Z. Phys., 136, 465.

ROSS,M. and WONES,D.R. (1965). Amer. Min. 50, 291.

ROSS,M., TAKEDA,H. and WONES,D.R. (1966). Science, 151, 191.

ROYER,L. (1928). Bull. Soc. Franc. Min. 51, 7.

SCHULZ,L.G., (1951). (B) Acta Cryst. 4, 483.

SCHULZ,L.G., (1951). (B) Acta Cryst. 4, 487.

SHIMAOKA,G. and Herold,J.F. (1967). 25th EMSA, 348.

SILK,E.C.H. and BARNES,R.S., (1961). Acta Met., 9, 558.

SMITH,J.V. and YODER,H.S., (1956). Min. Mag., 31, 209.

STEVENS,R.E., (1938). Amer. Min., 23, 607.

SUNAGAWA,I. (1964). Amer. Min., 49, 1427.

TAKEDA,H. and DONNAY,J.D.H. (1965). A.C.A. Program and Abstracts, Winter Meeting, Suffern, N. Y., 23.

TAKEDA,H. and DONNAY,J.D.H. (1966). Acta Cryst. 20, 638.

TAKEDA,H. (1967). Acta Cryst. 22, 845.

TOLANSKY,S. and MORRIS,P.G. (1947). Min. Mag., 198, 137.

TAVASSOLI,M.T. (1978). Ph.D. Thesis, University of London.

UPERETI,M.C. and WALTON,A.G. (1966). J. Chem. Phys. 44, 1936.

VAN DER MERWE,J.H. (1949). Faraday Soc. Discussions, 5, 201.

VEBLEN,D.R. (1983). Amer. Miner. 68, 566.

VEBLEN,D.R. (1983). Amer. Miner. 68, 1160.

WAGNER,G. and LIPPERT,L. (1936). Z. Phys. Chem. B,33, 297.

WEST,C.D. (1945). J. Opt. Soc. Amer. 35, 26.

WILLAIME,C. and AUTHIER,A. (1966). Bull. Franc. Mineral. Crist., 89, 269.

WINCHELL,A.N., (1927). Amer. Mineral., 12, 267.

WINCHELL,A.N., (1942). Amer. Min., 27, 114.

ZOUCKERMANN,R. (1961). 2nd., ERCEM 1, 316.

ZVYAGIN,B.B. (1962). Sov. Phys. Crystallogr. 6, 571.

chapter seven

CONCLUSION

The main conclusions to be drawn from the studies of nucleation and growth of alkali halides in general presented in this work are as follows:

1. The new technique developed for producing perforated carbon support film is simple and more effective. The sizes of the holes can be controlled by adding a suitable quantity of glycerol to the formvar solution.
2. The holes in the carbon support film are preferred sites for growth of single crystals of alkali halides from solution. As these crystals are very thin (ranging from 50 nm to 500 nm, depending on the concentration of the solution), they are very useful for studies of the defects in alkali halides crystals induced by electron irradiation in the electron microscope.
3. Crystals of CsI, CsBr and CsCl are dendritic if grown from a solution with concentration more than 10 %. CsF, which is highly hygroscopic, forms crystals in the electron microscope from solution. CsI crystals, formed from a solution with concentration less than 10 % are electron-transparent. Gold decoration reveals that their surfaces are smooth and flat (free from

step structures). These crystals are suitable substrates for electron microscope studies of the nucleation and growth of other alkali halides. The present work is the first study of the growth of alkali halides on CsI. The lattice structure of CsI is quite different from NaCl and KCl, which have been mostly used for this kind of study in the past. New information is therefor available for the understanding of epitaxy in general.

4. The transport chamber is a newly designed device for transferring specimens from a vacuum deposition unit to the electron microscope without exposure to the atmosphere. This eliminates the effect of atmospheric moisture on hygroscopic samples and overcomes the difficulties of preparing specimens in the electron microscope. The present work shows clearly that the use of electron-transparent crystalline substrates in conjunction with the transport chamber expands the range of application of the transmission electron microscopy in epitaxy studies.
5. Electron diffraction is very useful in determining crystal lattice structures. Knowledge of the relation between the camera constant and objective lens current is very useful in determining the camera constant for each diffraction pattern so as to calculate the separation of the planes producing the pattern. This avoids measuring the camera constant with a material of known lattice spacing each time.

6. The growth of alkali halides on a continuous carbon film from the vapour phase is similar to the growth of metals: they grow through the formation of small nuclei to an island-structure film by coalescence (Volmer-Veber mode of growth). Thin deposits of alkali halides form a solution when exposed to the atmosphere and recrystallization may occur in the electron microscope. Even LiF, which in bulk is insoluble in water, dissolves in the atmospheric moisture and form crystals in the electron microscope, when initially grown as a thin deposit.
7. Alkali halides grow epitaxially, parallel orientation, on substrates of CsI when deposited at room temperature from the vapour phase and from solution. CsF usually crystallizes with the Na-Cl lattice structure as bulk but when grown on CsI (Cs-Cl structure), it transforms from Na-Cl structure to Cs-Cl structure with an increase in its lattice parameter from 0.6008 nm to 0.649±0.004 nm.
8. Although mica has been used extensively as a substrate for thin film studies in the past, only one form of mica, muscovite, has been used before. Another variety of mica, biotite, has been used for the first time in the present work. The difference in the c-axes spacing and in the chemical composition produced different orientations in the overgrowth in some cases.

9. Chemical interaction between the ions of the overgrowth and the atoms of the mica surface plays a major role in epitaxial growth. Two different orientations may be obtained, especially when the growth takes place at an elevated temperature.

The following suggestions can be made for further study in this field.

As CsI has proved to be a suitable electron-transparent substrate with Cs-Cl lattice structure, the growth of other alkali halides with Na-Cl structure such as halides of potassium, sodium, lithium and rubidium would give interesting results which might improve our understanding of the overgrowth-substrate co-relation and factors influencing epitaxial growth.

Other varieties of mica as a substrate with different symmetry and chemical composition (glauconite and paragonite have sodium atoms on (001) surface), might produce different orientations in overgrowths which could shed light on the chemical interaction between the overgrowth and the substrate.

The transport chamber would be modified by attaching an auxiliary pump to further reduce the effects of residual atmosphere. With better quality vacuum sealing in the transport chamber it would be possible to transfer the specimen prepared in the ultrahigh vacuum to the electron microscope.

ACKNOWLEDGEMENTS

I am very grateful to Dr. R.F. Miller, who supervised and encouraged the work. His critical reading of the work and his help in the preparation of the thesis is deeply appreciated.

I would like to thank all the technical staff of the Department of Physics, for their help. I am especially grateful to Mr. M. Thyer and Mr. J. Taylor for their continuous assistance.

I am grateful to the Ministry of Education Pakistan and the authorities of Islamia University of Bhawalpur for their financial support.

I gratefully acknowledge the continuous assistance and encouragement of my wife, without who this work could have become very difficult.